Environmental Science and Engineering

Han-Yong Jeon *Editor*

Sustainable Development of Water and Environment

Proceedings of the ICSDWE2021

Springer

Environmental Science and Engineering

The ultimate goal of this series is to contribute to the protection of our environment, which calls for both profound research and the ongoing development of solutions and measurements by experts in the field. Accordingly, the series promotes not only a deeper understanding of environmental processes and the evaluation of management strategies, but also design and technology aimed at improving environmental quality. Books focusing on the former are published in the subseries Environmental Science, those focusing on the latter in the subseries Environmental Engineering.

More information about this series at http://www.springer.com/series/7487

Han-Yong Jeon
Editor

Sustainable Development of Water and Environment

Proceedings of the ICSDWE2021

Springer

Editor
Han-Yong Jeon
GeoSynthetics Research Laboratory (GSRL)
Division of Nano-Systems Engineering
Inha University
Incheon, Korea (Republic of)

ISSN 1863-5520 ISSN 1863-5539 (electronic)
Environmental Science and Engineering
ISBN 978-3-030-75277-4 ISBN 978-3-030-75278-1 (eBook)
https://doi.org/10.1007/978-3-030-75278-1

This Springer imprint is published by the registered company Springer Nature Switzerland AG
The registered company address is: Gewerbestrasse 11, 6330 Cham, Switzerland

Preface

Dear Distinguished Authors and Guests,

We are glad to introduce you to the proceedings of 2021 the 4th International Conference on Sustainable Development of Water and Environment (ICSDWE2021), which was successfully held on March 13, 2021. Different from the previous three times, ICSDWE2021 was carried out in the form of the virtual conference due to the impact of COVID-19. Because there is worldwide travel restriction, we held this flexible online conference to gather experts and scholars from China, Korea, Japan, Thailand, Malaysia, USA, Viet Nam, Germany etc. with the aim to continue disseminating the latest advanced research in the field of sustainable development of water and environment and developing the academic exchange among researchers.

The aim of ICSDWE2021 is to present the latest research and results of scientists (professors, students, Ph.D. students, engineers, and post-doc scientists) related to the sustainable development of water and environment. The key goal of the conference provides opportunities for academic scientists, engineers, and industry researchers to exchange and share their expertise, experience, new ideas, or research result and discuss the challenges and future in their expertise. ICSDWE2021 also provides a platform for the students, researchers, and engineers to interact with experts and specialists on the technical matters and future direction of their research area.

The papers were selected after the peer-review process by conference committee members and international reviewers. The submitted papers were selected on the basis of originality, significance, and clarity for the purpose of the conference. The papers should provide the reader an overview of many recent advances in the field related to the Sustainable Development of Water and Environment. The conference program is extremely rich, featuring high-impact presentation. We hope that the conference results constituted a significant contribution to the knowledge in these up-to-date scientific field.

On behalf of the organizing committee, we would like to express our sincere gratitude to the distinguished keynote speakers, as well as all the participants. We also want to thank the publisher for publishing the proceedings. May the readers could enjoy the gain some valuable knowledge from it.

We are expecting more and more experts and scholars from all over the world to join the 5th ICSDWE2022.

With our warmest regards

Incheon, Korea (Republic of) Han-Yong Jeon

Contents

Chapter 1
Solar Thermal Energy Production in DSF Applied in the Human Comfort Improvements

Eusébio Conceição, Ma Inês Conceição, Ma Manuela Lúcio, João Gomes, André Ramos, and Hazim Awbi

Abstract This work presents a numerical study of solar thermal energy production in DSF applied in the human comfort improvements, in winter conditions. The study considers a solar thermal energy production made in a DSF system placed in the outdoor environment and the improvement of human comfort conditions, namely the thermal comfort and the indoor air quality in a virtual office provided with impinging jets ventilation and occupied by eight occupants seated around the table with eight seats. This study uses a Building Dynamic Response numerical model and coupling of the Computational Fluids Dynamics and Human Thermal Response numerical models. The impinging jets ventilation is built with an inlet system and an outlet system. The inlet system integrates 4 vertical ducts, installed near the corner of the walls, whose airflow direction is descendent, at 0.5 m from the floor. The outlet system integrated six vertical ducts, located above the head level, with ascendant airflow direction. The study considers a solar thermal energy production in DSF during all day and the detailed evaluation of comfort condition in the middle of the morning and afternoon. The indoor air quality, thermal comfort, Draught Risk and Air Distribution Index are evaluated. The results show that the energy production ensures acceptable indoor air quality and thermal comfort conditions.

E. Conceição (✉) · M. M. Lúcio · A. Ramos
FCT - Universidade do Algarve, Campus de Gambelas, 8005-139 Faro, Portugal
e-mail: econcei@ualg.pt

A. Ramos
e-mail: aframos@ualg.pt

M. I. Conceição
Instituto Superior Técnico, Av. Rovisco Pais, 1049-001 Lisboa, Portugal
e-mail: ines.conceicao@tecnico.ulisboa.pt

J. Gomes
CINTAL, Campus de Gambelas, 8005-139 Faro, Portugal
e-mail: jgomes@ualg.pt

H. Awbi
School of Built Environment, University of Reading, Reading RG6 6AW, UK
e-mail: h.b.awbi@reading.ac.uk

H.-Y. Jeon (ed.), *Sustainable Development of Water and Environment*,
Environmental Science and Engineering,
https://doi.org/10.1007/978-3-030-75278-1_1

Keywords Energy · DSF · Impinging jets ventilation · Indoor air quality · Thermal comfort · Draught risk · Air distribution index

1.1 Introduction

A DSF, double skin façade, is frequently used in the solar thermal energy production, see Ghaffarianhoseini et al. (2016), Pasut and Carli (2012), Hazem et al. (2015) and Poirazis (2004). This equipment is built by an air cavity between two transparent glasses. The control of the cavity air ventilation can be performed by natural process, mechanical process or hybrid processes. The DSF is dependent on the characteristics of the skin coverage, the air ventilation topologies used, the eventual use of shading devices, its location in the building, among other details.

Several authors have investigated ventilation systems based on impinging jets in the last years. Example of this kind of study can be analysed in Karimipanah et al. (2008), Karimipanah and Awbi (2002), Cao et al. (2014), and Karimipanah et al. (2000). This study considers vertical ducts with descendent airflow. The ducts can be localized in the corner of the walls or in other placed.

The human comfort is evaluated by the thermal comfort level and the indoor air quality level (IAQ). The performance of the Heating, Ventilation and Air Conditioning (HVAC) system is evaluated by the Air Distribution Index (ADI). However, the local thermal discomfort eventually promoted by HVAC system is evaluated by the Draught Risk (DR).

The Predicted Mean Vote (PMV) index and the Predicted Percentage of Dissatisfied people (PPD) index are used to evaluate the occupants thermal comfort level. The PMV and PPD indexes, parameters developed by Fanger (1970), are applied to assess the thermal comfort conditions in spaces with HVAC system and they are presented in ISO 7730 (2005).

The carbon dioxide concentration is used in the IAQ evaluation (Conceição et al. 2008a). The carbon dioxide concentration, release by the occupants, can be used as reference of IAQ in occupied spaces (ANSI, ASHRAE Standard 2016).

ADI is used to assess simultaneously the air quality, thermal comfort, contaminants removal efficiencies and heat removal efficiencies. ADI was presented in detail in the work of Awbi (2003), for uniform environments, and in the work of Conceição et al. (2013), for non-uniform environments.

DR is used to assess the level of local thermal discomfort of occupants of an air-conditioned space. DR was developed by Fanger et al. (1988) and it is depending of air temperature, air velocity and air turbulence intensity.

The numerical software used in this work is based on a coupling between two numerical models, Computer Fluid Dynamics (CFD) and Human Thermal Response (HTR). This methodology can be seen in the studies of Conceição and Lúcio (2001, 2016), Conceição (2000), and Conceição et al. (2010a). The coupling methodology need inputs obtained from Buildings Dynamics software. Examples of this kind of

software can be analysed in the studies of Yan et al. (2014), Sailor (2008), and Balaji et al. (2013).

In this study the inputs of the coupling methodology came from a Building Dynamic Response numerical model developed by the authors. Examples are shown in Conceição et al. (2000, 2008b), Conceição and Lúcio (2009, 2010a). The assessment of the air temperature distribution, surfaces temperature distribution and energy consumption was carried out. The surrounding building bodies, as tree, and others external details, can be see analysed in Conceição and Lúcio (2010b). This software considers the evaluation of thermal comfort through the PMV/PPD indexes (Conceição et al. 2018), the adaptive thermal comfort (Conceição et al. 2010b), and the temperature preferred control model (Conceição et al. 2009).

The main objective of this numerical work is to develop a new situation where the production of energy is made in a DSF system using the solar renewable energy. The human comfort, in this work, is made by an impinging jet system. In the numerical simulation, made in winter conditions, it is used a coupling of the CFD, HTR and Building Dynamic Response numerical models to evaluate the thermal comfort, IAQ and DR levels, and the ADI.

1.2 Numerical Methodology

This work is made in a virtual office with $4.5 \times 2.55 \times 2.5$ m^3. The office is equipped with an internal impinging jets ventilation system and an external DSF system.

The impinging jets ventilation system is built with an inlet system and an outlet system. The inlet system integrates four ducts placed in the wall corners. The inlet airflow, with descendent direction, enters at 0.5 m from the floor. The outlet system uses six vertical ducts, located above the table level.

The numerical methodology used in grid generation of the CFD model is presented in Fig. 1.1. Figure 1.1a represents eight occupants, a table and eight chairs. Figure 1.1b includes the inlet ventilation and the outlet ventilation system. Figure 1.1c represents the inlet (light green arrows) and outlet (light blue arrows) airflow.

Figure 1.2 shows the numerical methodology used in the grid generation of the HTR model. Figure 1.2a represents eight occupants and a table. Figure 1.2b also includes the impinging jets ventilation, namely the incoming and exit system. The occupant location and identification number are presented in Fig. 1.3.

In Fig. 1.4 the scheme of the DSF system used in the energy production is presented. Figure 1.4a represents the office space equipped with a DSF system and Fig. 1.4b represents the DSF detailed.

In the numerical simulation is important to consider the occupation and the ventilation cycle.

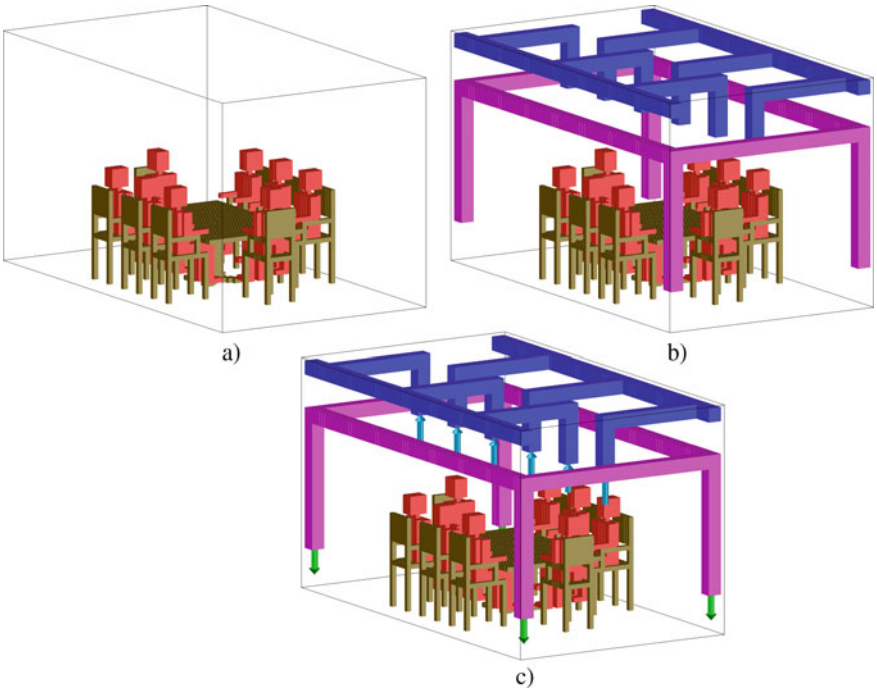

Fig. 1.1 Numerical methodology used in the CFD model grid generation: **a** Representation of eight occupants, a table and eight chairs. **b** Including the inlet ventilation and the outlet system. **c** With inlet (light green arrows) and outlet (light blue arrows) airflow used

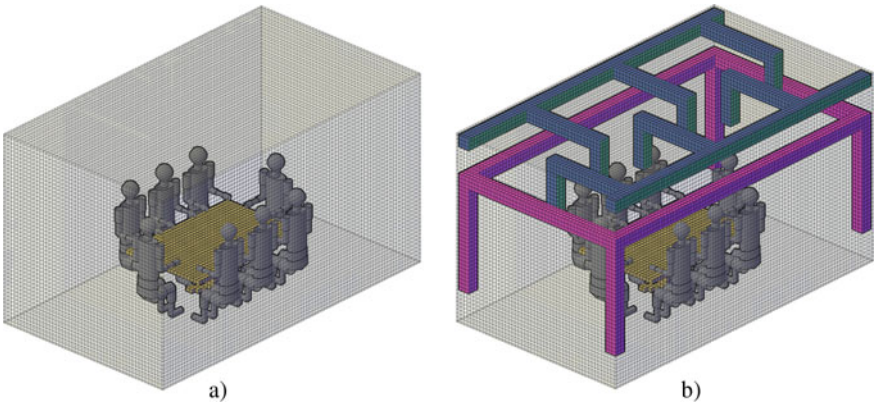

Fig. 1.2 Numerical methodology used in the grid generation of the HTR model: **a** Representation of eight occupants, a table and eight chairs. **b** Including the impinging jets ventilation

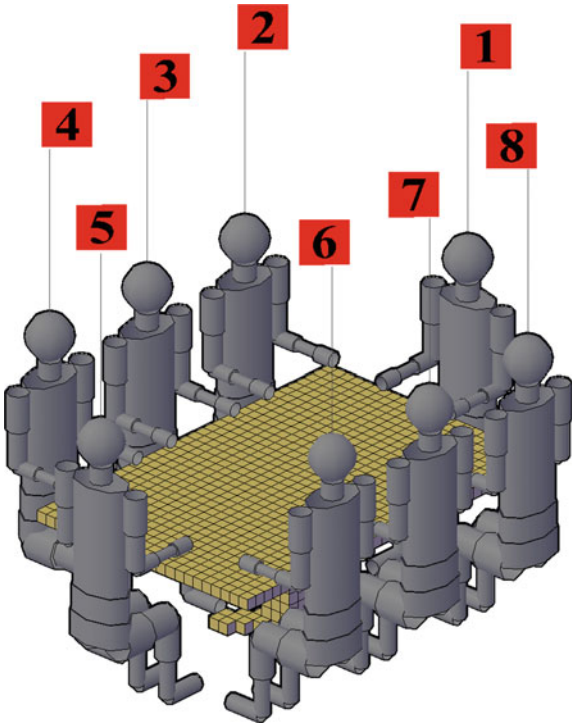

Fig. 1.3 Location of the occupants and identification number of each occupant

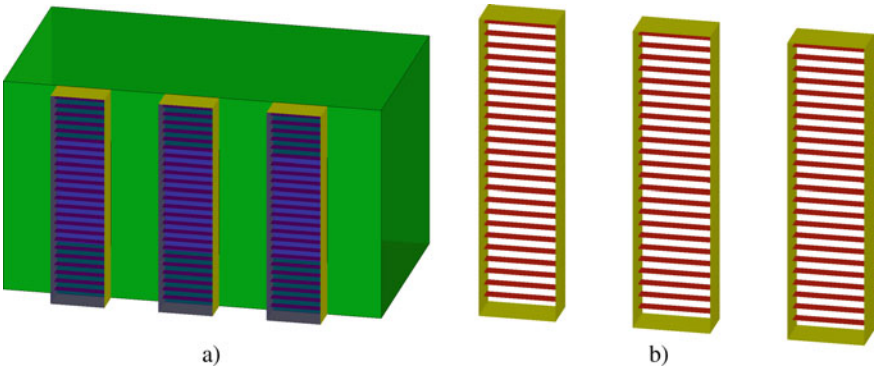

Fig. 1.4 Design of the DSF system used in the production of energy: **a** Office space equipped with a DSF system. **b** DSF detailed

The occupation cycle of the virtual chamber is the following:

- 8h00 to 12h00, during the morning time, is occupied by eight persons;
- 12h00 to 14h00 is not occupied (lunch time);
- 14h00 to 18h00, during the afternoon time, is occupied by eight persons.

The ventilation cycle, that is used to transfer the energy from the DSF system to the office space and to improve IAQ and thermal comfort levels, namely:

- 0h00 to 8h00, one air renovation;
- 8h00 to 12h00, airflow rate acceptable for eight occupants;
- 12h00 to 14h00 one air renovation;
- 14h00 to 18h00, airflow rate acceptable for eight occupants.
- 16h00 to 24h00 one air renovation.

In order to evaluate the thermal comfort and indoor air quality, the coupling numerical software as used at 10:00 h and 16:00 h, namely:

- 10 h, evaluation of human comfort conditions at morning;
- 16 h, evaluation of human comfort conditions at afternoon.

1.3 Results and Discussion

In this point, the results obtained of the DSF numerical simulation and of the occupants and environment variables determination are presented.

1.3.1 Energy Production in the DSF System

In Fig. 1.5, the DSF system indoor air temperature and outdoor environment temperature evolution is presented.

In accordance with the results, the three DSF system presented the same internal temperature and the DSF air temperature increases during the morning and decreases during the afternoon. This fact is associated with the solar radiation.

The Building Dynamics Response numerical model calculates the results presented in the Fig. 1.5. The obtained results at 10:00 h and at 16:00 h are transferred to the coupling system, in order to be used in the thermal comfort and IAQ evaluation.

1.3.2 Air Velocity

The distribution of the air velocity around the sections of the human body is depicted in Fig. 1.6. At 10 and 16 h, the evolution is presented, respectively, in Fig. 1.6a and b.

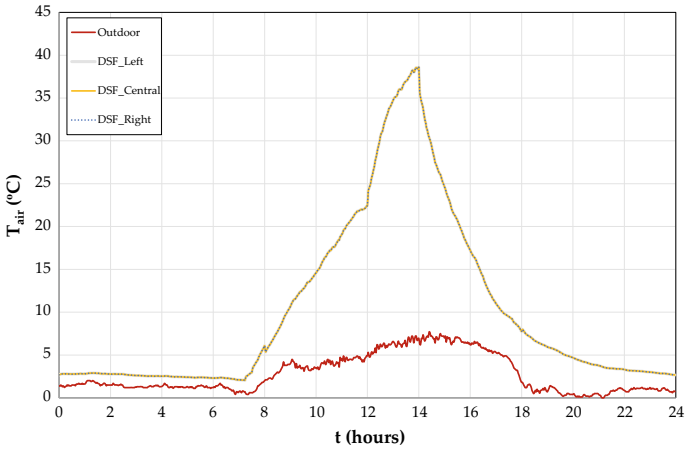

Fig. 1.5 Evolution of DSF system indoor air temperature and of outdoor air temperature

According to the obtained results, the air velocity is higher in the lower human body sections than in the upper human body sections.

1.3.3 Air Temperature

In Fig. 1.7 is possible to verify the evolution of the air temperature distribution around the human body sections at 10 h, in Figure a), and at 16 h, in Figure b). The air temperature is higher in the upper body sections than in the lower body sections.

1.3.4 Draught Risk

In Fig. 1.8, it is shown the DR distribution around the human body sections at 10:00 h and at 16:00 h, respectively in figures a and b.

DR is higher in the lower sections than in the upper sections. The DR is slightly highest in the lower sections for the occupants located in the top of the table than for the occupants located in the side of the table. The DR level is acceptable, regarding to ISO 7730 (ISO 2005).

1.3.5 Air Distribution Index

ADI values are presented in Tables 1.1 and 1.2. The Table 1.1 is associated with 10:00 h, while Table 1.2 is associated with 16:00 h.

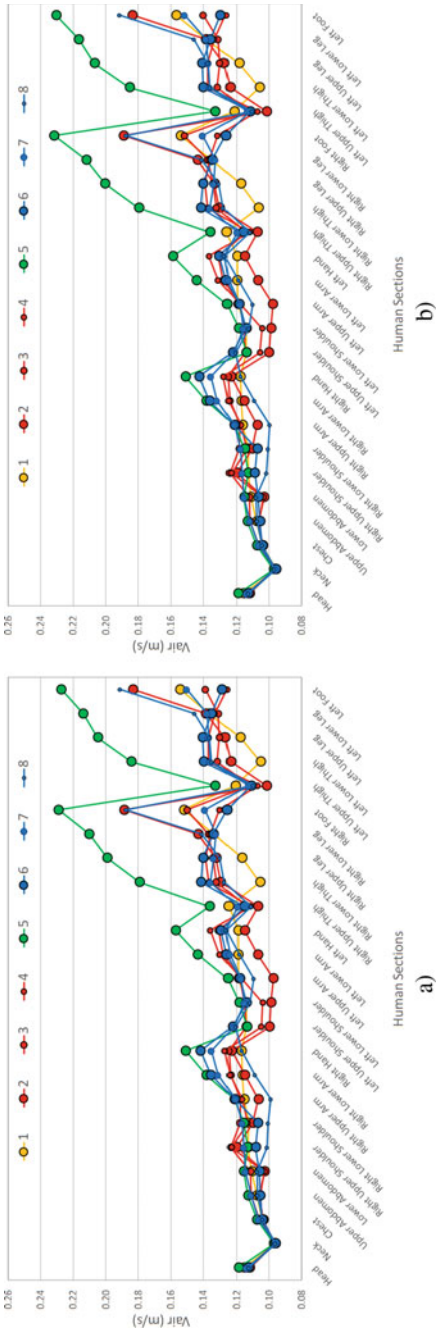

Fig. 1.6 Air velocity distribution around the human body sections at **a** 10 h, and **b** 16 h

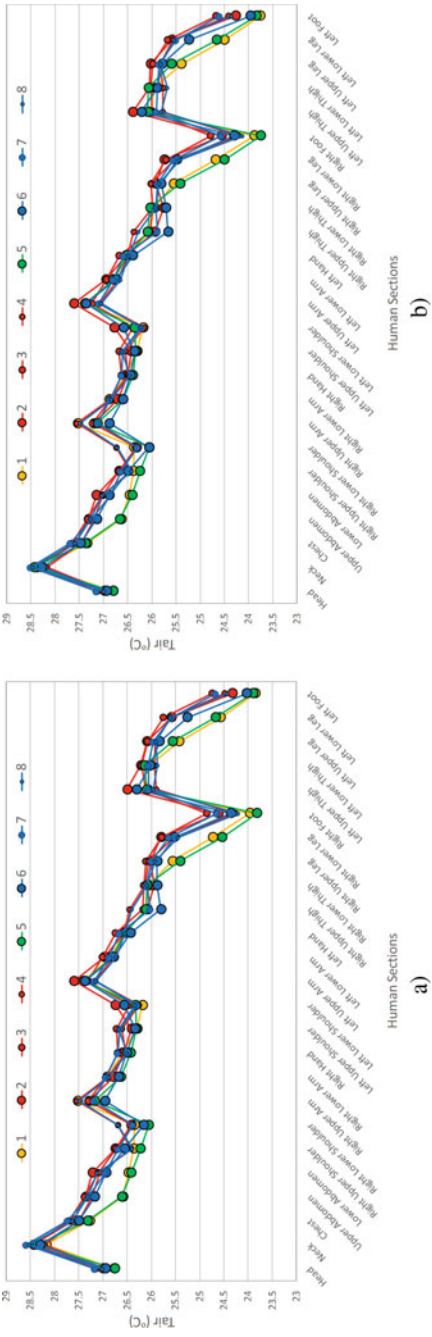

Fig. 1.7 Air temperature distribution around the human body sections at **a** 10 h, and **b** 16 h

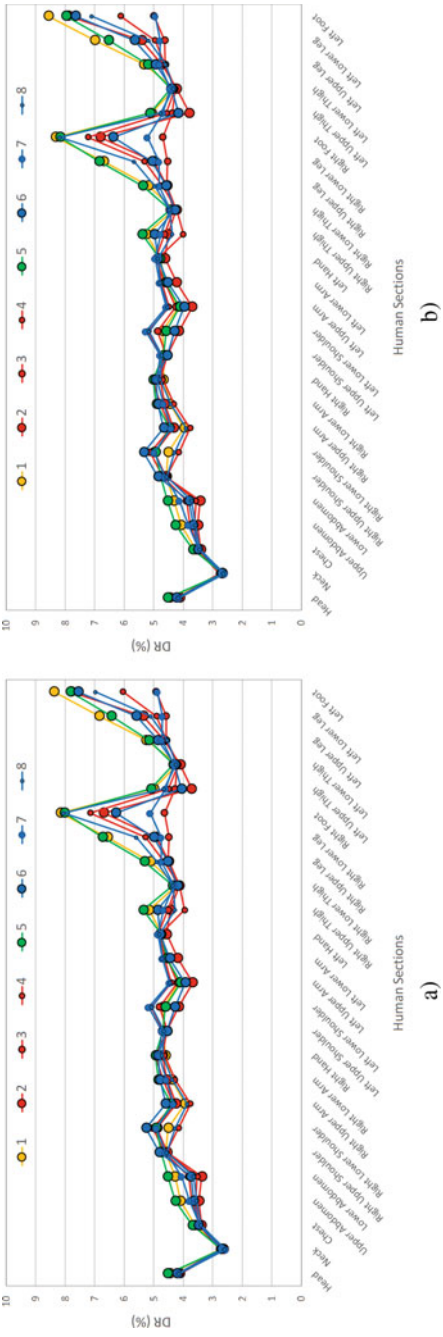

Fig. 1.8 DR distribution around the human body sections at **a** 10 h, and **b**) 16 h

Table 1.1 ADI value obtained at 10 h

People number	1	2	3	4	5	6	7	8	Mean
Body mean temperature (°C)	26.4	26.8	26.8	26.7	26.4	26.6	26.8	26.7	26.6
Effectiveness for heat removal (%)	79.2	76.0	75.6	76.8	79.3	77.5	76.1	76.5	77.1
PPD (%)	15.0	17.5	17.7	17.1	14.1	16.8	17.4	17.2	16.6
Thermal comfort number	5.3	4.3	4.3	4.5	5.6	4.6	4.4	4.5	4.7
CO_2 in the respiration area (mg/m^3)	1524.2	1642.8	2023.1	1704.7	1510.3	2050.2	2296.3	1808.9	1820.1
Effectiveness for contaminant removal (%)	36.6	32.8	24.6	31.1	37.1	24.2	20.9	28.6	29.5
Air quality number	2.5	2.2	1.7	2.1	2.5	1.6	1.4	1.9	2.0
Air Distribution Index (ADI)	3.6	3.1	2.7	3.1	3.8	2.7	2.5	2.9	3.0

Table 1.2 ADI value obtained at 16 h

People number	1	2	3	4	5	6	7	8	Mean
Body mean temperature (°C)	26.4	26.7	26.7	26.6	26.4	26.5	26.7	26.6	26.6
Effectiveness for heat removal (%)	79.9	77.3	77.0	78.0	79.8	78.6	77.5	77.8	78.2
PPD (%)	15.0	17.2	17.4	17.0	14.1	16.6	17.1	16.9	16.4
Thermal comfort number	5.3	4.5	4.4	4.6	5.7	4.7	4.5	4.6	4.8
CO_2 in the respiration area (mg/m^3)	1538.3	1652.1	2054.7	1720.6	1526.4	2105.5	2354.0	1840.3	1849.0
Effectiveness for contaminant removal (%)	36.2	32.6	24.2	30.8	36.6	23.4	20.3	28.0	29.0
Air quality number	2.4	2.2	1.6	2.1	2.5	1.6	1.4	1.9	2.0
Air Distribution Index (ADI)	3.6	3.1	2.7	3.1	3.7	2.7	2.5	2.9	3.1

In general. all variables and parameters are similar both at 10:00 h and 16:00 h. The thermal comfort and IAQ levels are acceptable regarding to the international standards. The level of the thermal comfort is near the Category C (ISO 2005), and the value of carbon dioxide concentration is near the acceptable limit (ANSI, ASHRAE Standard 2016).

The results of the production of energy in the DSF system reveals that this system can promote acceptable thermal comfort and IAQ conditions, in accordance with the international standards.

1.4 Conclusion

In this work a numerical study of solar thermal energy production in DSF applied in the human comfort improvements, in winter conditions, is developed and presented. This DSF system, located in the office space outdoor environment and used in the energy production, uses solar renewable energy. The HVAC system, founded in an impinging jet system, is used to improve the human comfort conditions.

A coupling of CFD and HTR and a Building Dynamic Response numerical models were used in the numerical simulation to evaluate the human comfort and discomfort conditions. ADI was used to evaluate the performance of the HVAC system.

In accordance with the obtained results, the energy production guarantees acceptable thermal comfort and IAQ conditions. The HVAC system, applied in this work, promotes, inclusively, low DR levels to the occupants.

Acknowledgements The authors would like to acknowledge to the project (SAICT-ALG/39586/2018) from Algarve Regional Operational Program (CRESC Algarve 2020), under the PORTUGAL 2020 Partnership Agreement, through the European Regional Development Fund (ERDF) and the National Science and Technology Foundation (FCT).

References

ANSI/ASHRAE Standard 62–1 (2016) Ventilation for acceptable indoor air quality, american society of heating, refrigerating and air-conditioning engineers: Atlanta, GA, USA

Awbi H (2003) Ventilation of buildings. Taylor & Francis, London, UK

Balaji N, Mani M, Venkatarama B (2013) Thermal performance of the building walls. In: Proceedings of building simulation applications BSA 2013. BU press, Bozen-Bolzano, pp 151–159

Cao G, Awbi H, Yao R, Sirén K, Kosonen R, Zhang J (2014) A review of the performance of different ventilation and airflow distribution systems in buildings. Build Environ 73(3):171–186

Conceição E (2000) Evaluation of thermal comfort and local discomfort conditions using the numerical modelling of the human and clothing thermal system. In: Proceedings of 7th international conference on air distribution in rooms, ROOMVENT 2000, Elsevier, Amsterdam, pp 131–136

Conceição, E., Lúcio, M.: Numerical and subjective responses of human thermal sensation. In: Proceedings of the 6th portuguese conference on biomedical engineering, Faro, Portugal, 11–12 June (2001)
Conceição E, Lúcio M (2009) Numerical study of the thermal efficiency of a school building with complex topology for different orientations. Indoor Built Environ 18(1):41–51
Conceição E, Lúcio M (2010a) Numerical simulation of passive and active solar strategies in building with complex topology. Build Simul 3:245–261
Conceição E, Lúcio M (2010b) Numerical study of the influence of opaque external trees with pyramidal shape on the thermal behaviour of a school building in summer conditions. Indoor Built Environ 19(6):657–667
Conceição E, Lúcio M (2016) Numerical simulation of the application of solar radiant systems, internal airflow and occupants' presence in the improvement of comfort in winter conditions. Buildings 6(3):38
Conceição E, Silva M, André J, Viegas D (2000) Thermal behaviour simulation of the passenger compartment of vehicles. Int J Veh Des 24(4):372–387
Conceição E, Lúcio M, Vicente V, Rosão V (2008a) Evaluation of local thermal discomfort in a classroom equipped with crossed ventilation. Int J Vent 7(3):267–277
Conceição E, Lúcio M, Lopes M (2008b) Application of an indoor greenhouse in the energy and thermal comfort performance in a kindergarten school building in the south of Portugal in winter conditions. WSEAS Trans Environ Dev 4:644–654
Conceição E, Lúcio M, Ruano A, Crispim E (2009) Development of a temperature control model used in HVAC systems in school spaces in Mediterranean climate. Build Environ 44(5):871–877
Conceição E, Rosa S, Custódio A, Andrade R, Meira M, Lúcio M (2010a) Study of airflow around occupants seated in desks equipped with upper and lower air terminal devices for slightly warm environments. HVAC&R Res 16(4):401–412
Conceição E, Nunes A, Gomes J, Lúcio M (2010b) Application of a school building thermal response numerical model in the evolution of the adaptive thermal comfort level in the Mediterranean environment. Int J Vent 9(3):287–304
Conceição E, Lúcio M, Awbi H (2013) Comfort and airflow evaluation in spaces equipped with mixing ventilation and cold radiant floor. Build Simul 6:51–67
Conceição E, Gomes J, Ruano A (2018) Application of HVAC systems with control based on PMV index in university buildings with complex topology. IFAC PapersOnLine 51(10):20–25
Fanger P (1970) Thermal comfort: analysis and applications in environmental engineering. Danish Technical Press, Copenhagen, Denmark
Fanger P, Melikov A, Hanzawa H, Ring J (1988) Air turbulence and sensation of draught. Energy Build 12(1):21–39
Ghaffarianhoseini A, Ghaffarianhoseini A, Berardi U, Tookey J, Li D, Kariminia S (2016) Exploring the advantages and challenges of double-skin façades (DSFs). Renew Sustain Energy Rev 60:1052–1065
Hazem A, Ameghchouche M, Bougriou C (2015) A numerical analysis of the air ventilation management and assessment of the behavior of double skin facades. Energy Build 102:225–236
ISO 7730 (2005) Ergonomics of the thermal environments—analytical determination and interpretation of thermal comfort using calculation of the PMV and PPD indices and local thermal comfort criteria. International Standard Organization, Geneva, Switzerland
Karimipanah T, Sandberg M, Awbi H (2000) A comparative study of different air distribution systems in a classroom. In: Proceedings of 7th international conference on air distribution in rooms, ROOMVENT 2000, Elsevier, Amsterdam, pp 1013–1018
Karimipanah T, Awbi H (2002) Theoretical and experimental investigation of impinging jet ventilation and comparison with wall displacement ventilation. Build Environ 37(12):1329–1342
Karimipanah T, Awbi H, Moshfegh B (2008) The air distribution index as an indicator for energy consumption and performance of ventilation systems. J Hum-Environ Syst 11(2):77–84
Pasut W, De Carli M (2012) Evaluation of various CFD modelling strategies in predicting airflow and temperature in a naturally ventilated double skin façade. Appl Therm Eng 37:267–274

Poirazis H (2004) Double skin façades for office buildings – literature review. In: Report EBD-R–04/3. Department of construction and architecture, Lund University, Lund, Sweden

Sailor D (2008) A green roof model for building energy simulation programs. Energy Build 40(8):1466–1478

Yang L, Yan H, Lam J (2014) Thermal comfort and building energy consumption implications - a review. Appl Energy 115:164–173

Chapter 2
Hydraulics Geometry Analysis of UPNM Channel

Zuliziana Suif, Saiful Syazwan Wahi Anuar, Nordila Ahmad, Maidiana Othman, and Siti Khadijah Che Osmi

Abstract Depth, width, velocity and suspended load are essential hydraulic features that are determined mainly in the form of the river cross-section. The objective of this study is to measure the hydraulic geometry parameters at station and investigate the relationship between hydraulic geometry parameters with suspended sediment concentration of the Universiti Pertahanan Nasional Malaysia (UPNM) channel. In the analyses on the channel, three stations were selected. All of these stations have sediment discharge, flow discharge and cross-sections measured data. Result shows that at relationship of discharge and hydraulic geometry parameters b, f, m, a, c and k were obtained to be −0.0440, 0.1386, 0.3305, 1.4948, 0.3670 and 0.4868 respectively. While the average hydraulic geometry sediment rating at every station found to be 0.2728, 0.3765, 0.3745, 3.9596, 1.9478 and 1.4601 respectively. Moreover, suspended sediment discharge and flow discharge shows a good average correlation coefficient and exponent of 0.0112 and 2.7031 exponent, respectively. Overall, the results of this research should be useful for watering the basin, management and resource planning projects.

Keywords Depth · Width · Velocity · Hydraulic geometry · Suspended sediment concentration · UPNM

2.1 Introduction

Research on hydraulic geometry and hydraulic characteristic has been started long ago to improve the management of water, as it is great importance in the watershed. The measurable hydraulic characteristics that constitute the form of rivers such as depth, width and velocity are achieve by expressing these values as a power function of flow discharge. The river has a capacity to transport large volume of sediment while conveying water.

Z. Suif (✉) · S. S. Wahi Anuar · N. Ahmad · M. Othman · S. K. Che Osmi
Department of Civil Engineering, Faculty of Engineering, National Defence University of Malaysia, Kuala Lumpur, Malaysia
e-mail: zuliziana@upnm.edu.my

H.-Y. Jeon (ed.), *Sustainable Development of Water and Environment*,
Environmental Science and Engineering,
https://doi.org/10.1007/978-3-030-75278-1_2

The hydraulic geometry in a station scale describes the difference between mean depth and width of the water when discharging in a river. Hence, the ability to understand and anticipate the shape of such fluvial geometry relations is a powerful tool for river managers. The term is introduced at-a-station hydraulic geometry of the relationship between (Leopold et al. 1964) between depth, flowrate (velocity) and surface width and discharge of water. Hydraulic geometry at-a-station produces mean values at certain period. For example, such as one week, one month, one season or one year. Analysis that carried out at a certain flow measurement station for a given cross section of the river or stream. A line that is compared to the plot of monthly dumping values cross- sectional field characteristics of a station presents a hydraulic geometry parameter power function.

Theoretically, after rain the amount of sediment will increase the amount of sediment, too much sediment will cause damage to water quality, algal bloom, and deposition build up. However, sediment is important to aquatic life but excessive amount of it will cause more damage than create. However, too little sediment also become a main trouble to environmental. Starvation of sediment often made by human in construction field but natural barrier also can limit sediment transportation. That is why this problem has to put priority to find solution and avoid future environmental issue.

Hydraulic geometry parameters show variations, Alluvial channels depending on bed content (Kolberg and Howard 1995). As it is costly and inefficient to collect actual Channel Information, it is proposed that the planning level model should be subject to hydraulic geometry relations and that the approach of evaluating other models should be merged (Allen et al. 1994). Hydraulic geometry represents changes made by the stream, both on a cross section and downstream, due to release changes. Changes in width, mean depth, mean velocity, tilt, friction, suspended load and water surface pitch are made. The relation between releases and changes is transmitted as power work: $y = aQb$, with y being the changing parameter, Q releasing, a and b being coefficients.

Hydraulic geometry similar to the hydraulic slope and bank strength (manning) (Huang and Warner 1995). Dense vegetation produces smaller channels, while bed vegetation enhances flow resistance and generates broader channels, decreases flow speed and no major changes in depth (Huang and Nanson 1998). The hydraulic geometry of a river flow channel refers to the relationship between flow and some hydraulic properties of the channel, such as distance, depth and speed. In comparison to hydraulic geometry downstream, which deals with spatial variations in channel properties at some reference load, the hydraulic geometry of one station deals with temporal variations in flux variables as fluctuates at a cross section for uncommon discharges to bank full ranges. Hydraulic geometry at stations uses a variety of discharges for single transverse geometry to be bankrupt.

The main objective of this study were following (1) To measure the flow discharge, suspended sediment concentration and hydraulic geometry at selected station, (2) To investigate the relationship between hydraulic geometry with suspended sediment concentration.

2.2 Study Area

Universiti Pertahanan Nasional Malaysia (UPNM) is a military university located in Sungai Besi Camp, Kuala Lumpur, Malaysia. There are few construction has been conducted in UPNM currently to fulfil current needs so UPNM will be the new study area of this research. Three sediment and flow stations were used in this analysis. The sediment and discharge data of all these stations is available. Every week, cross-sectional data on the channel were collected and sediment measurements were taken. The cross-sectional area data with the related regular discharge values were used for evaluating each station. The study will be cover in channel and small stream at UPNM only.

2.3 Methodology

In this study, the instalment of apparatus is to investigate the value of suspended sediment concentration and hydraulic geometry parameters at different station in UPNM area. The different type of station will tell the different condition of suspended sediment concentration. In this experimental phase there will be one laboratories involve that is Environmental Laboratory. In Environmental Laboratory, the field sample will undergo the Total Suspended Solid (TSS) test. Then the Flow Tracker will be used to determine the discharge (Q), velocity (V), depth (D) and surface width (B) at different station in UPNM area. All the mentioned data will be measured at the field during the uses of Flow Tracker.

2.3.1 Collecting Water Sample

The water sample used in this research was measured from three (3) station selected in area of UPNM as shown in the Fig. 2.1 under study area. There will be three (3) water sample all together and each of them taken every week to be tested the quantity of suspended sediment concentration. The first station is a natural type. While, the second and third station is human made channel which is trapezoidal shape channel. The point of sample that collected is shallow so the procedure of collecting the sample does not face many challenge. The sample taken at center of the channel and at the mid from the base of the channel. To analyse suspended sediment concentration, the sample that have been collected will be carry to the Environmental Laboratory to be tested using TSS testing.

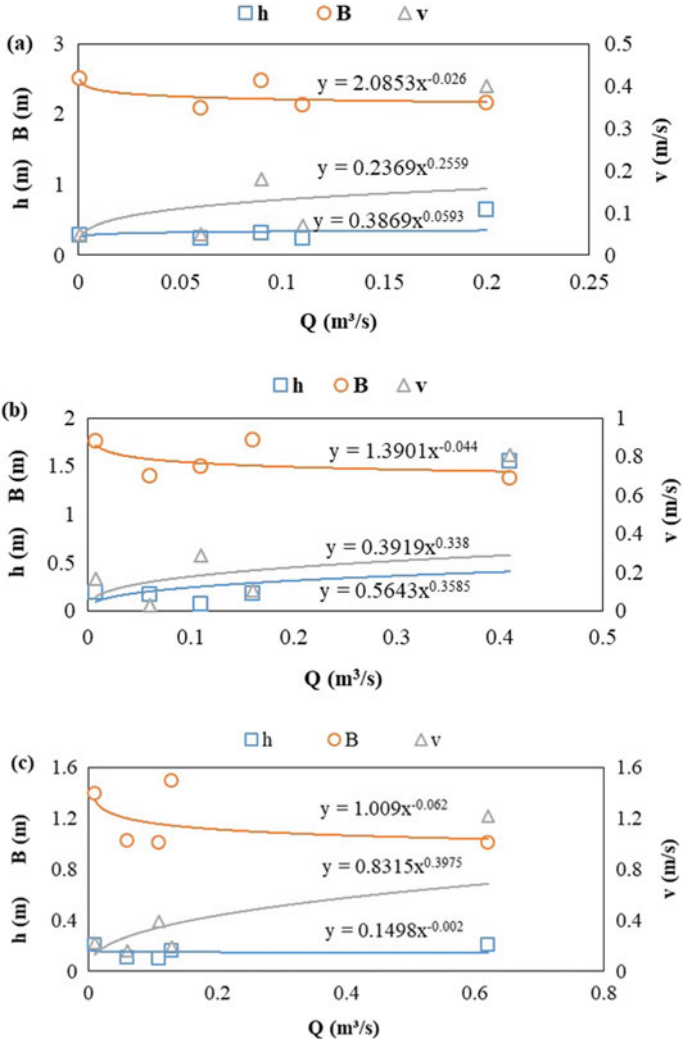

Fig. 2.1 Relationship between hydraulic geometry parameters and discharge at Station 1 (**a**), Station 2 (**b**) and Station 3 (**c**)

2.3.2 Measurement of Hydraulic Geometry

Measurement of hydraulic geometry parameters using a device named Flow Tracker2. The instalment of this device is to measure and determine the hydraulic geometry of the channel that has been specifically determined. The device will be setup at the field and all data will be collect on the spot. The hydraulic geometry parameters that collected at different station in UPNM was recorded. The Flow Tracker2 able to detect velocity, water discharge, depth, coordinate, temperature and

many more of it function it is easy to handle and used. For this research, data was collected such as water discharge, velocity and depth of stream at different location using the device.

2.3.3 Suspended Sediment Concentration

The water sample used in this research was from three (3) selected station in the UPNM area. The sample was collected once a week from all station in 1.5 L container. Then the water sample will be carry to Environment Laboratory to be tested TSS experiment. Firstly, weigh the filter paper, filter disc, and record the data on a paper. Then pick a volume of samples to yield not more than 200 mg of total suspended solids. Next, place the filter on the rim, squeeze it to the funnel, and vacuum. Wet the filter to screen the pipe against the base with a small amount of distilled water. Pass 100 ml sample to the filter with a broad, volumetric pipette orifice vigorously and quantitatively. Clear all water traces after samples have passed through continuing to apply the vacuum. Further rinse the pipette with small amount of distilled water on the filter and start it. Lastly, carefully remove the disc filter from the base. Dry for at least (1) hour at 103 °C– 105 °C. Cool in an oven and weigh.

2.4 Results and Analysis

2.4.1 Relationship Between Hydraulic Geometry and Discharge

Graph in the Fig. 2.1a–c shows a relationship discharge and hydraulic geometry (width, depth, velocity) for three (3) UPNM flow-testing stations. Using a tool to derive empirical equations analysis of function. The exponents average values of b, f and m are −0.0440, 0.1386, and 0.3305 while the coefficient average values a, c, and k were register for at-a-station hydraulic geometry to be 1.4948, 0.3670, and 0.4868 respectively. As to comply the theory introduced hydraulic geometry theory by analyzing the cross-sectional data of 20 rivers and found b, f and m values to be 0.26, 0.40 and 0.34, respectively for at-a-station hydraulic geometry (Leopold and Maddock 1967).

From the value of m, station 1 shows a low value m. As for station 1 is natural type channel as it is at the water opening so the velocity is lower than station 2 and 3 as it man-made channel and have trapezoidal shape so the velocity is high because it is surface is wider and less sediment. That is because along with the channel there are some plant and grass that living along the channel. It observed to be make the channel become narrower and make the flow of water is unstable. The smaller the sediment size and load, and the lower the flow velocity and stream power, the more

Table 2.1 The exponents and coefficients of relationship between hydraulic geometry parameters and discharge

Sta	Exponents			Coefficient			b + f + m	a × c × k
	b	f	m	a	c	k		
1	−0.026	0.0593	0.2559	2.0853	0.3869	0.2369	0.2892	0.1911
2	−0.044	0.3585	0.3380	1.3901	0.5643	0.3919	0.6525	0.3074
3	−0.062	−0.002	0.3975	1.0090	0.1498	0.8315	0.3335	0.1257
Ave	−0.044	0.1386	0.3305	1.4948	0.3670	0.4868	0.4251	0.2081

stable the stream. The depth at station 2 and 3 is lower than station 1. Along with increasing discharge the mean depth decreased marginally, indicating shallow and small transversals.

Table 2.1 shows the summary of the exponents and coefficients of relationship of flow discharge and hydraulic geometry parameters. The coefficients a at station 1 is higher which is 2.0853 than station 2 and 3 which is 1.3901 and 1.0090 respectively. This is because the natural channel is not vulnerable and always affected by water flow or when heavy rain. It will widen the channel because the wall of the channel having corrosion.

2.4.2 Relationship Between Hydraulic Geometry and Sediment Concentration

Graph in the Fig. 2.2a–c shows a relationship between suspended sediment concentration and hydraulic geometry (width, depth, velocity) for three (3) selected flow-testing stations. From the result analysis it can be see that at station 1 which is natural channel brings out value of b, f, m, a, c and k of 0.0048, 0.5358, 0.5289, 2.3134, 3.9005, 1.2182 respectively. While for station 2 are -0.0870, 0.5411, 0.7037, 1.1200, 1.7600 and 2.3800 respectively. The b value given is very low due to unstable wall of channel which is very easily to break down. White et al. (1982) presented an approach which is variation in principle and which assumes that an alluvial channel adjusts its slope and geometry to maximize its transport capacity.

For all station mean flow velocity were observed to increase with increasing flow discharge and the mean depth seems not changing much due to the man-made channel at station 2 and station 3, the surface width station 2 and 3 was observed to decrease slightly and keep stable at station 1.

Table 2.2 Show the summary of the exponent and coefficients of the suspended sediment concentration hydraulic geometry parameters. The results of a, c and k shows a different between natural and man-made channel. At station 3 the coefficient a shows the highest, because at station 3 the flow water is the highest and the widest channel among man-made channel. Most of discharge from building is flowing through it, so the width and flow can be considered highest. The c value at

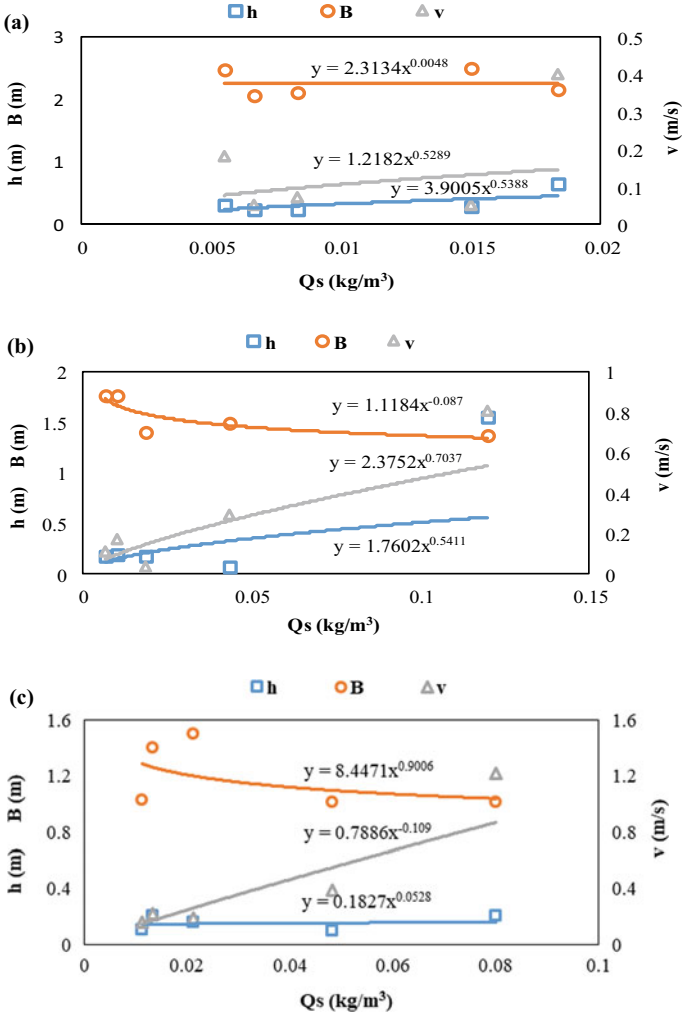

Fig. 2.2 Relationship hydraulic geometry parameters and suspended sediment concentration at Station 1 (**a**), Station 2 (**b**) and Station 3 (**c**)

Table 2.2 The exponent and coefficient of the hydraulic geometry and suspended sediment concentration

Sta	Exponents			Coefficient			b + f + m	a × c × k
	b	f	m	a	c	k		
1	0.0048	0.5358	0.5289	2.3100	3.9000	1.2200	1.0695	10.9923
2	−0.0870	0.5411	0.7037	1.1200	1.7600	2.3800	1.1578	4.6758
3	0.9006	0.0528	−0.1090	8.4500	0.1827	0.7890	0.8444	1.2171
Ave	0.2728	0.3765	0.3745	3.9596	1.9478	1.4607	1.0239	5.6284

station 1 show the highest value because it is containing and transport the most of sediment as it is natural channel. Moreover, at station 3 it shows a good and efficient c value due it efficiency transporting of sediment.

2.4.3 Suspended Sediment

The analyses were conducted in the form of a power function and was utilised to determine the relationship between the channel flow discharge and the sediment discharge. Where Qs (kg/m^3) is the river sediment discharge, Q (m^3/s) is the river flow discharge; p and j are the coefficient and the exponent of a power function, respectively. For the selected six flow measurement stations, the $Qs = pQj$ scale sediment rating curves (Q–Qs relation) are graphically presented in Fig. 2.3.

Graph in the Fig. 2.3 is a relationship between suspended sediment concentration and hydraulic geometry (width, depth, velocity) for three (3) UPNM flow-testing stations. In the analysis, it was observing that the sediment discharge is increasing with increasing flow discharge in station 2 and 3 and slightly decrease in station 1.

In the analysis, at natural channel station 1 brings out p and j value of 0.0076 and −0.0740. Station 2 has 0.0103 and 5.410. It was observed that the sediment discharge is increasing with increasing flow discharge in all stations except at station 1 that is decreasing. This is due to low amount of sediment than other stations. From an examination of published data on bed forms, channels with artificial roughness elements, meandering channels and bed armouring, the deformation will cease when the shape of the boundary is that which gives rise to a local maximum friction factor. Thus, the equilibrium shape of a non-planar self-deformed flow boundary or channel corresponds to a local maximum friction factor.

The calculated coefficients, exponents, and correlations of the power function are given in Table 2.3. Table 2.3 indicates the association factors between water release and canal flow release for the three flow and sediment measurement stations on the UPNM system. Station 2 and station 3 are most closely related to these variables. In the study of coefficients all, the correlation values are positive, so it can be assumed that there is a strong correlation between flow discharge and sediment discharge. The results of the study can also be used to forecast the transversal characteristics of the UPNM channel and can be useful in food security, hydropower planning and management.

In addition to power function analysis, the relationship between the flow discharge and the sediment discharge was examined by performing the correlation analyses. R^2 were utilised to determine the correlation coefficients. While station 2 and station 3 show the strong relationship between these variables. In general, the other stations indicate a meaningful relationship between the flow discharge and the sediment discharge with power function analysis. As the coefficients are examined, it is clearly seen that all correlation values are positive. Then, one can say that there is a positive correlation between the flow discharge and the sediment discharge. The amount of sediment in UPNM channel can be determined according to this relationship.

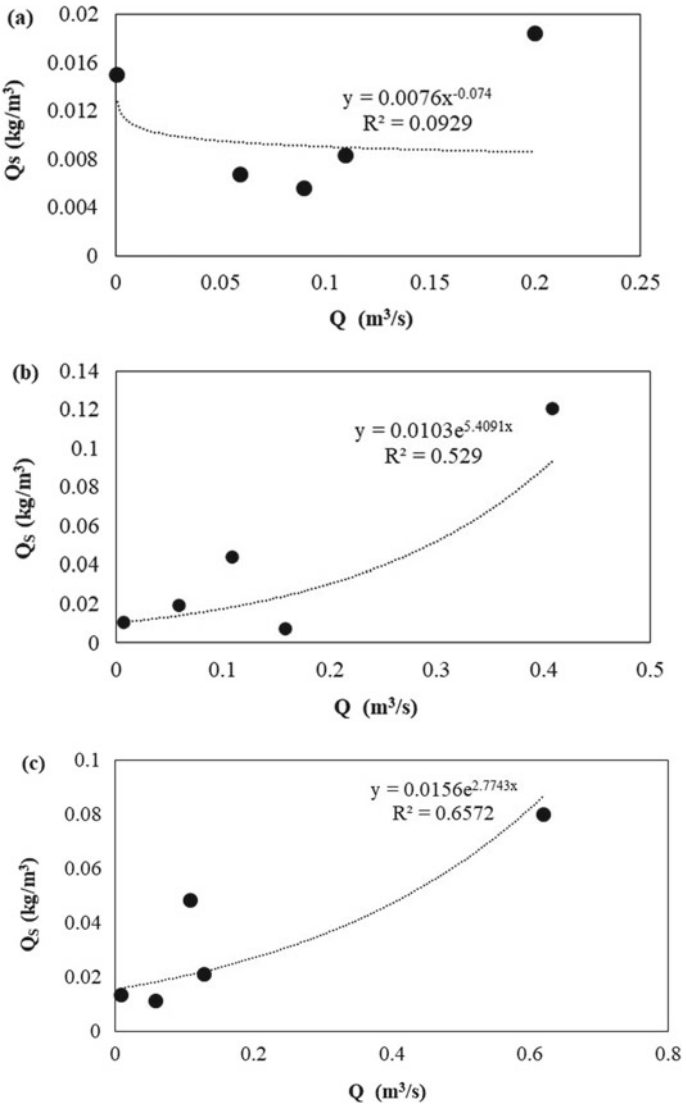

Fig. 2.3 Sediment rating curves (Qs–Q) for 3 stations, Station 1 (**a**), Station 2 (**b**), Station 3 (**c**)

Table 2.3 Coefficients and exponents of the relationship between flow discharges and sediment

Station	P	J
1	0.0076	−0.0740
2	0.0103	5.4100
3	0.0156	2.7700
Average	0.0112	2.7031

2.5 Conclusion

For water resources, hydraulic geometry and transit of sediments on river are relevant extreme hydrological conditions (food and drought) management, planning and control. Based on the experiment conducted to investigate the relationship between hydraulic geometry and suspended sediment concentration at every station, there are several significant conclusions could be obtaining:

i. Because of the various geology, physiography, and morphology environments that apply the basic hydraulic geometry method, the number of exponents and coefficients of the relation between hydraulic geometry and suspended sediment concentration are considerable.
ii. The relationship between discharge and hydraulic geometry at every station is observe to increase in velocity and depth but keep constant at surface width.
iii. In addition to hydraulic geometry studies, sediment discharge, flow discharge relationship has also been study. The findings have shown that relationships of natural and man-made channel are more important in terms of correlation coefficients relative to other stations. The amount of sediment borne in UPNM channel can be calculate according to this relationship.

Acknowledgements This research work was supported by Ministry of Higher Education (MOHE) through Fundamental Research Grant Scheme (RACER/1/2019/TK01/UPNM/1). A part of this research was funded by Short Term Grant of Universiti Pertahanan Nasional Malaysia under grant UPNM/2019/GPJP/TK/9.

References

Allen PM, Arnold JG, Byars BW (1994) Downstream channel geometry for use in planning-level models. Water Resour Bull 30(4):663–671

Huang HQ, Nanson GC (1998) The influence of bank strength on channel geometry: an integrated analysis of some observations. Earth Surf Proc Land 23(10):865–876

Huang HQ, Warner RF (1995) The multivariate controls of hydraulic geometry: a casual investigation in terms of boundary shear distribution. Earth Surface Land 20:115–130

Kolberg FJ, Howard AD (1995) Active channel geometry and discharge relations of U.S. piedmont and midwestern streams: the variable exponent model revisited. Water Resour Res 31(9):2353–2365

Leopold LB, Maddock T (1967) The hydraulic geometry of stream channels and some physiographic implications: by Luna B. Leopold and Thomas Maddock. Washington: U.S. Govt. Print. Off

Leopold LB, Wolman MG, Miller JP (1964) Fluvial processes in geomorphology. W.H. Freeman and Company, San Francisco, p 522

White WR, Bettess R, Paris E (1982) Analytical approach to river regime. J Hydraul Div (Proceedings of ASCE) 108(HY10):1179–1193

Chapter 3
Productivity Enhancement of Solar Still Distillation System Using Immersion-Type Water Heater

Nordila Ahmad, Norhasirah Mohd Isa, Zuliziana Suif, Maidana Othman, Jestin Jelani, and Jaafar Adnan

Abstract Water is importance to Earth and living things. Human can survive for a few weeks without food but only a few days without water. Clean and safe water is particularly needed as a source of drinking water. It also needs to be used for various purposes, such as domestic and drinking purposes. Solar distillation process is one of the purification technologies that is sustainable and green technology which can be used to resolve the current problem. This paper presents the efficiency of solar still distillation system integrated with 1000 and 2000 W alternating current (AC) immersion water heater to optimize clean water output. Comparison of the amount of water output between the solar still distillation system with 1000 W immersion water heater (SSA) and the solar still distillation system with 2000 W immersion water heater (SSB) was made. The productivity increased about five times when SSB was used compared to SSA. A numerical analysis was performed to verify the results of the experiment. The water production was expected to increase up to 7.50 L/m^2 per 24 h when using SSB. Therefore, SSB is more effective than SSA to produce distilled water.

Keywords Immersion water heater · Solar energy · Solar still distillation system

3.1 Introduction

Water is substances that are vital on earth. There would be no life on earth if there was no water. 71% of the surface of the Earth is covered by water. Approximately 96.5% of all Earth's ocean holding water (USGS 2014). Ground water and spring water are common source used for drinking purposes by human. Most water sources are clean and safe for daily use but can also be contaminated by leakage of landfills, excessive fertilizer or pesticide use. Contaminated water sources can damage human, flora and fauna.

N. Ahmad (✉) · N. Mohd Isa · Z. Suif · M. Othman · J. Jelani · J. Adnan
Faculty of Engineering, National Defence University, Sungai Besi Camp, 57000 Kuala Lumpur, Malaysia
e-mail: nordila@upnm.edu.my

H.-Y. Jeon (ed.), *Sustainable Development of Water and Environment*,
Environmental Science and Engineering,
https://doi.org/10.1007/978-3-030-75278-1_3

Solar water distiller or solar still is one of the water purification technology that most widely used to produce drinking water. Solar energy is used in this process to separate the contaminants from the fresh water. Untreated water is evaporated in this process, hence the water vapor is then isolated and purified as fresh water from dissolved substances and contaminants. Solar still distillation system is comprised of two categories that are active and passive. Active system uses additional technology applied to the solar still to enhance the solar efficiency. In the other hand, solar energy is mainly used in passive system for the processing of distilled water. The advantage of passive system is that there is no problem with electricity breakdown and generally more efficient, easier to handle and potentially have long life time than active system. Therefore, the efficiency performance for active system is higher than passive system but it is costly (Gugulothu et al. 2015). In general, solar still efficiency is depending on the internal and external parameters such as incident solar radiation, water depth, addition of dye (Al-Hayeka and Badran 2004), cover material, thickness of cover (Panchal and Patel 2017), inclination angle of cover (Aljubouri 2017; Aybar et al. 2005) and etc.

Many attempts have been made by researcher to improve the productivity of solar distillation system (e.g. Al-Hayeka and Badran 2004; Aybar et al. 2005; Al-Garni 2012, 2014; Gugulothu et al. 2015, Riahi et al. 2016; Panchal and Patel 2017 and Aljubouri 2017). Riahi et al. (2016) have made a comparative research between conventional solar still and conventional solar (CSS) still equipped with 500 W photovoltaic modules alternating current (PV-AC) heater system (CSSPVH). It was found that the CSSPVH was more effective and contributes about six to ten times the production of water by the CSS. A theoretical analysis was done in order to verify the experimental result.

In Saudi Arabian, a research was being carried out by Al-Garni (2012) using water heater and cooling ventilator to analyze solar still efficiency. Two immersion water heaters used for double sloped solar still with optimum output power of 500 W each was examined. It has been found that the productivity was found to improve by 370% for the still with the heater. Due to that, the wind speeds efficiency of 7 and 9 m/s were decreased by 4 percent and 8 percent, respectively when the solar still glass surface was cool down by using external cooling ventilator.

In year 2014, Al-Garni (2014) was made an improvement for single slope solar still. Based on the study, a single slope solar was suggested by using immersion water heater and external cooling ventilator. It was found that when a 500 W heater was used in the base tank, the productivity increased by 250 percent. The efficiency also improved when using an external cooling fan to cool the outer glass surface of solar still which was 5.2 and 10.3 percent with wind speeds of 7 and 9 m/s, respectively.

A comprehensive literature review reveals that the uses of the still active solar with an AC heater are reliable. Thus, this study focuses on solar efficiency still being the renewable and sustainable energy with specific 1000 and 2000 W AC immersion heaters.

3.2 Experimental Set-Up and Data Collection

3.2.1 Experimental Set Up

A double slope solar still system was developed at the weather station, National Defence University of Malaysia (NDUM). This system employs the concept of evaporation and condensation based on the natural phenomenon to remove dissolved particles and produce distilled water. Figures 3.1 and 3.2 illustrate the photos and schematic model of experimental setup of the solar still at site. Spring water was collected in NDUM to fill up the insulated box up to 7 cm depth. The water depth in the box was maintained at 7 cm for the both experiment by using water sensor level. The internal dimension of insulated box was 84 cm length, 49 cm width and 50 cm height. A double slope glass cover was designed for the solar still with an inclined angle of 40°. A metal trunking with coated surface was used to collect condensing water vapor from the glass cover. The glass cover used as condensing surface has a thickness of 4 mm. Two AC heater immersion each having 1000 W were used in this study. The handle of the heaters was hanging in the box while the heaters were constantly immersed in the water when the test was running. Both heaters were powered electrically by solar panel with the maximum output of 4.3 kW. Solar panel power was regulated by a charge regulator. The solar panel charged 12 V batteries with capacity of 100 Ah each. By an inverter, the DC power was converted from the batteries into AC power. The two type of solar still distillation was solar still distillation system integrated with 1000 W immersion AC water heater (SSA) and solar still distillation system integrated with 2000 W immersion AC water heater (SSB). The experiment was conducted for two days which were on 17th August 2020 and 18th August 2020. Water temperature, inner solar still cover, and volume

(a). Distilled water was collected in the glass beaker

(b). Heaters were submerged in water

(c). Double slope glass cover with inclination angle of 40º

(d). Black bin used to supply water

Fig. 3.1 Experimental set up at site

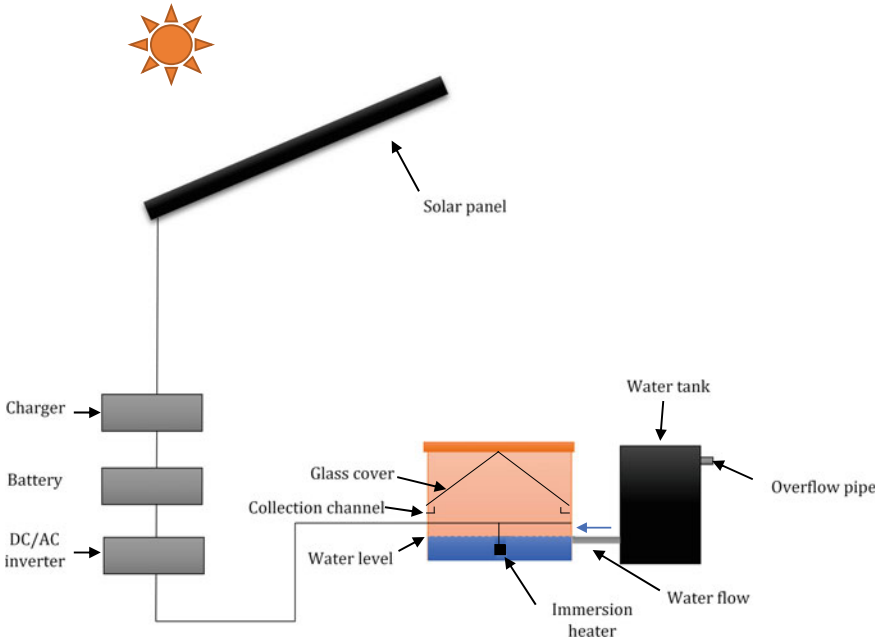

Fig. 3.2 Schematic model of solar still

of collected distillate water were measured for nine hours. A digital thermometer was used to measure water and inner glass cover temperature on an hourly basis, while the collected distilled water was measured using a measuring beaker and a measuring cylinder. For find analysis, numerical calculation from Tiwari and Suneja (1998) and Elkader et al. (1999) will be used to compare the water productivity between experimental and numerical results.

3.3 Results and Discussion

3.3.1 Evaluation of AC Power

Figure 3.3 shows the AC power required for SSA and SSB. It was observed that both AC power required increased directly proportional to the time. The maximum AC power required for SSA is 11.4 kWh while 20.4 kWh for SSB.

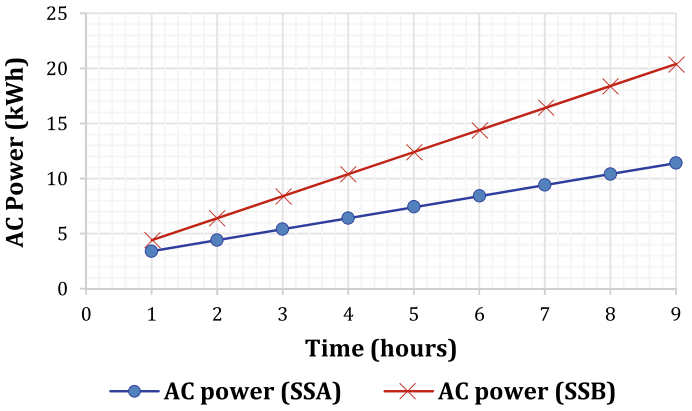

Fig. 3.3 AC power used for SSA and SSB

3.3.2 Temperature of Water and Inner Glass Cover for SSA and SSB

Two type of temperature were measured in this study were temperature of water (tw) and temperature of inner glass cover (tc). Figure 3.4 shows the comparison between temperature of water (tw) and temperature of inner glass cover (tc) for SSA and SSB. Water temperature was found to increase significantly with increasing with time. The maximum temperature of water for SSB is 98.4 °C while the inner glass cover peak value is identified 67.0 °C. The maximum temperature of water and inner glass cover found to be 79.0 °C and 62 °C respectively for SSA. The temperature of water was increasing abruptly for the first 4 h and then it reached equilibrium until at the 9th hours for SSB. The temperature of inner glass cover for SSB was

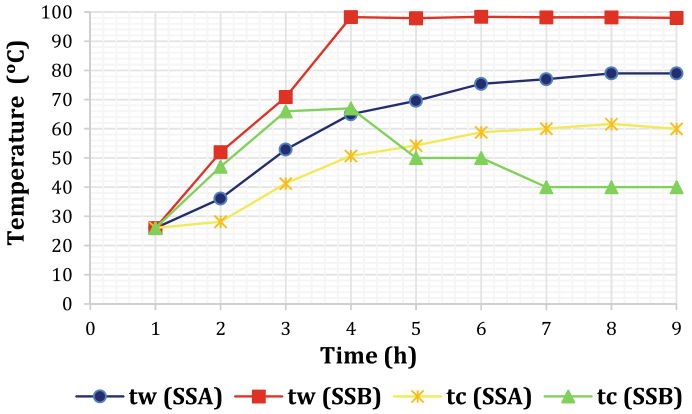

Fig. 3.4 Temperature of water and inner glass cover for SSA and SSB

decreasing with time at the 5th hour as shown in Fig. 3.4. This might be due to heat loss to surrounding. It was found that the temperature of water for SSA was increase 22% for 2nd hour until 6th hour and then slowly increase until 8th before achieve equilibrium at 9th hour. The temperature of inner glass cover for SSA also have the same pattern with the water temperature of SSA but it is slightly lower than water temperature.

3.3.3 Distilled Water Productivity of SSA and SSB with Temperature

The distilled water productivity of both solar still from the first hour to 9th hour are shown in Fig. 3.5. Based on Fig. 3.5, the curves show temperature of water for both SSA and SSB. The maximum distilled water productivity for SSA and SSB were 0.14 l/m^2 occurred at 9th hour and 0.36 l/m^2 at 5, 7, 8 and 9th hour duration. A significant increase in distilled water productivity for SSB. However, the distilled water productivity for SSA were quiet slowly increase with time. The distilled water productivity for nine hours for SSA was 0.44 l/m^2, while the total productivity of distilled water for SSB was 2.02 l/m^2. It was showed the distilled water productivity of SSB was about five times higher compared to SSA. This difference occurred due to different power output of immersion heater used in SSA and SSB.

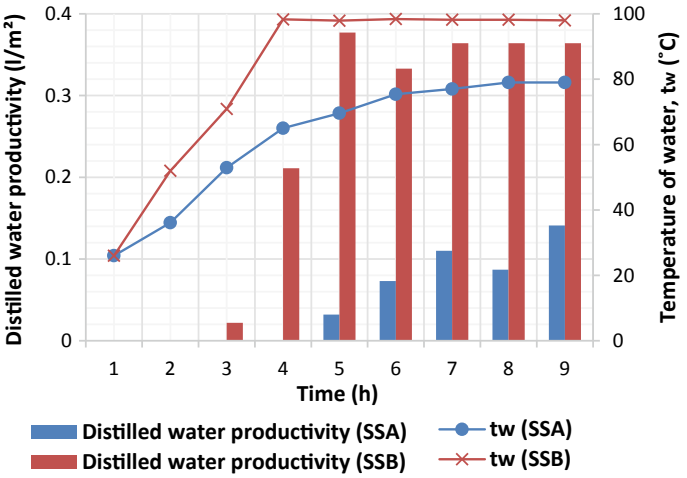

Fig. 3.5 Distilled water productivity of solar still and temperature of water for SSA and SSB

3.3.4 *Experimental and Numerical Distilled Water Productivity for SSA and SSB*

Figures 3.6 and 3.7 show the comparison between experimental and numerical productivity of distilled water for SSA and SSB respectively. It was observed that the productivity of distilled water increases by adding the power output of immersion water heater. The total distilled water productivity produced experimentally by SSA for 9 h was 0.44 l/m^2 while for SSB is 2.02 l/m^2 while the productivity of distilled water for SSA and SSB produced by numerical for 9 h were 0.435 l/m^2 and 1.92 l/m^2

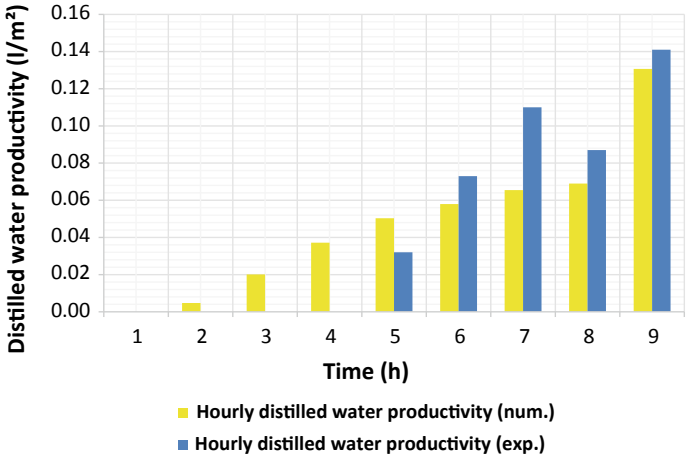

Fig. 3.6 Comparison between experimental and numerical distilled water productivity of SSA

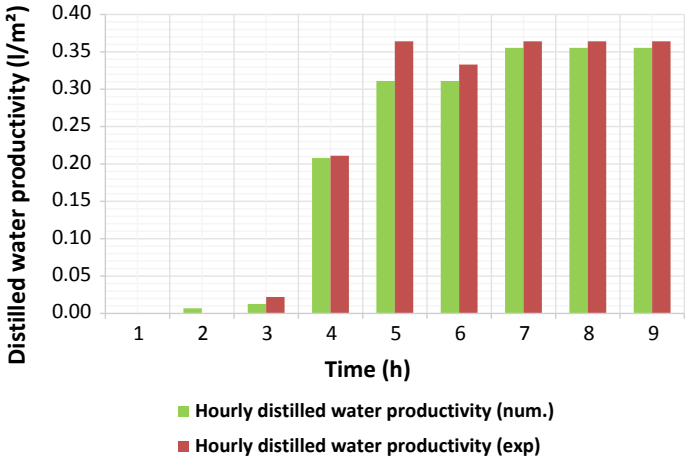

Fig. 3.7 Comparison between experimental and numerical distilled water productivity for SSB

respectively. The production of distilled water by experiment and numerical for SSB were constant at 7–9 th h.

3.3.5 *Analysis of Error Between the Hourly Distilled Water Productivity of Numerical and Experimental for SSA and SSB*

Tables 3.1 and 3.2 show the error analysis for both SSA and SSB hourly productivity of distilled water between numerical and experimental. The Root Mean Squared Error (RMSE) obtained for SSA and SSB were 0.0286 and 0.0201 respectively. The correlation for SSA was high which is 0.915 with $R^2$of 0.837 while SSB, the high correlation of 0.996 with R^2 of 0.992. The relationship hourly distilled water

Table 3.1 Error analysis (RMSE) between experimental and numerical output for SSA

Time (h)	Mh_e (l/m^2)	Mh_n (l/m^2)	Residual	RMSE	Correlation	Coefficient of determination (R^2)
1	0.00	0.00	0.00	0.0286	0.915	0.837
2	0.00	0.00	0.00			
3	0.02	0.00	0.02			
4	0.04	0.00	0.04			
5	0.05	0.03	0.02			
6	0.06	0.07	−0.02			
7	0.07	0.11	−0.04			
8	0.07	0.09	−0.02			
9	0.13	0.14	−0.01			

Table 3.2 Error analysis (RMSE) between experimental and numerical output for SSB

Time (h)	Mhe (l/m^2)	Mhn (l/m^2)	Residual	RMSE	Correlation	Coefficient of determination (R^2)
1	0.00	0.00	0.00	0.0201	0.996	0.992
2	0.00	0.01	−0.01			
3	0.02	0.01	0.01			
4	0.21	0.21	0.00			
5	0.36	0.31	0.05			
6	0.33	0.31	0.02			
7	0.36	0.36	0.01			
8	0.36	0.36	0.01			
9	0.36	0.36	0.01			

production between numerical and experimental of SSA and SSB are shown in Figs. 3.8 and 3.9 respectively. The R^2 value for SSA and SSB were 0.837 and 0.992 and the result were closed to 1. It shows that the numerical performance was in good agreement with experimental productivities.

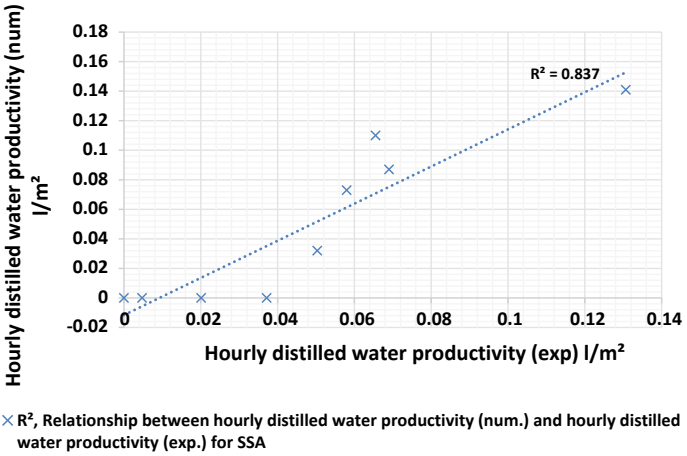

Fig. 3.8 Relationship between hourly productivity (num.) and hourly productivity (exp.) of SSA

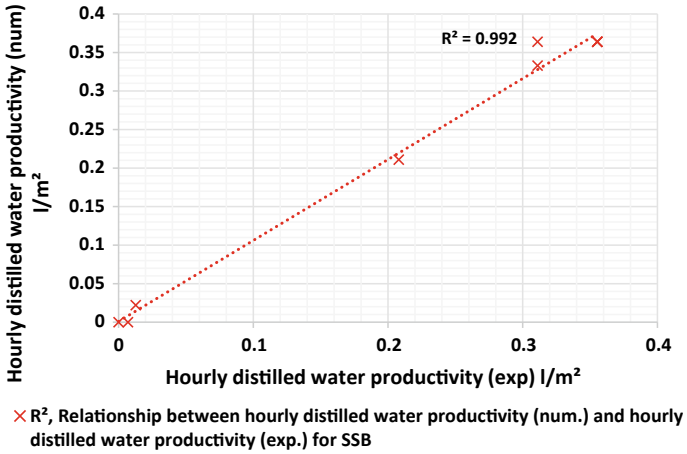

Fig. 3.9 Relationship between hourly productivity (num.) and hourly productivity (exp.) of SSB

3.4 Conclusions

In summary, solar energy for the production of alternative water can be efficiently developed, generated and converted to electrical energy using the double-slope solar still attached with 4.3 kW solar panel, 12 V batteries with capacity of 100 Ah and two 1000 W AC heaters each. Throughout that research, the solar still with 1000 W immersion AC heater (SSA) generated 0.44 l/m^2 of distilled water, and the solar still with 2000 W immersion AC heater (SSB) generated 2.02 l/m^2 for 9 h. SSB output approximately 4–5 times more than SSA water production. A numerical simulation was also driven for both solar systems using mathematical equation by Tiwari and Suneja (1998). The model showed numerical performance is in good agreement with experimental productivities. Solar still with immersion AC heater is a sustainable design due to the use of solar panels to produce energy and store it using batteries to ensure that the device can run 24 h. Thus, the system potentially can produce distilled water for a long period of time with low maintenance cost even in areas with very low daily solar radiation intensity. The system also can be applied in arid, remote, rural and coastal areas and also can be commercialize. commercialize.

Acknowledgements The authors are grateful to the National Defence University of Malaysia management, research and innovation office for providing fund (Project code: UPNM/2019/GPJP/TK/10) for this research.

References

Al-Garni AZ (2012) Productivity enhancement of solar still using water heater and cooling fan. J Sol Energy Eng Trans ASME 134(3):1–8. https://doi.org/10.1115/1.4005760

Al-Garni AZ (2014) Productivity enhancement of single slope solar still using immersion-type water heater and external cooling fan during summer. Desalin Water Treat 52(34–36):6295–6303. https://doi.org/10.1080/19443994.2013.822151

Al-Hayeka I, Badran OO (2004) The effect of using different designs of solar stills on water distillation. Desalination 169(2):121–127. https://doi.org/10.1016/j.desal.2004.08.013

Aljubouri AA (2017) Design and manufacturing of single sloped solar still: study the effect of inclination angle and water depth on still performance. J Al-Nahrain Univ-Sci 20(2):60–70. https://doi.org/10.22401/juns.20.2.08

Aybar H, Egeliofglu F, Atikol U (2005) An experimental study on an inclined solar water distillation system 180:285–289. https://doi.org/10.1016/j.desal.2005.01.009

Elkader MA., Nafy AS, Elmotalip AA, Mabrouk AA (1999) Experimental evaluation of solar still mathematical models. Fourth International Water Technology Conference IWTC 99, Alexandria, Egypt. Pp. 197–205

Gugulothu R, Sarada N, Vilasagarapu D, Bindu H (2015) Solar water distillation using three different phase change materials. Mater Today: Proc 2(4–5):1868–1875. https://doi.org/10.1016/j.matpr.2015.07.137

Panchal HN, Patel S (2017) An extensive review on different design and climatic parameters to increase distillate output of solar still. Renew Sustain Energy Rev 69: 750–758. https://doi.org/10.1016/j.rser.2016.09.001

Riahi A, Wan Yusof K, Mahinder Singh BS, Isa MH, Olisa E, Zahari NAM (2016) Sustainable potable water production using a solar still with photovoltaic modules-AC heater. Desalin Water Treat 57(32):14929–14944. https://doi.org/10.1080/19443994.2015.1070285

Tiwari GN, Suneja S (1998) Performance evaluation of an inverted absorber solar still. Energy Convers Manage 39(3–4):173–180. https://doi.org/10.1016/s0196-8904(96)00227-0

USGS (2014) How much water is there on earth? In the USGS water science school (p 1). https://doi.org/10.1021/acs.joc.6b01497

Chapter 4
Stability Analysis of a Man-Made Slope: A Case Study on the UPNM Campus, Sg Besi, Kuala Lumpur

Jestin Jelani, Mohamad Saiful Adli Hah, Mohd Nazrin Mohd Daud, Nordila Ahmad, Maidiana Othman, and Wan Mohamed Syafuan Wan Mohamed Sabri

Abstract This study performs a stability analysis to evaluate the performance of man-made slopes constructed on the UPNM campus. One of the slopes has a steep slope angle and is selected for investigation in this case study to re-examine its stability and prevent any potential hazard to people and nearby structures. The factor of safety (FOS) of the slope is determined using the ordinary method of slices and SlopeW, where the computed FOS is 0.64 and 0.88, respectively. This study did not take into account groundwater level or rock layer and hence it is recommends using soil nailing to enhance the stability of the slope. The results of this study will help local authorities identify the potential failure zone and implement possible remedial measures.

Keywords Slope stability · Safety factor · Method of slices · SlopeW

4.1 Introduction

Slope failure is a natural hazard that involves the movement of soil and rocks under the influence of gravity (Budhu 2008). Several factors contribute to reducing the shear strength of a slope and causing landslides. The factors influencing slope stability are includes geological, physical and human factors (Zaki et al. 2014; Lacasse and Nadim 2009; Lee et al. 2011; Wieczorek and Snyder 2009). The factor of safety (FOS) of a slope is the ratio of the shear strength of the soil to shear stress and is defined by Eq. (4.1), where τ_s is the shear strength of the soil and τ_f is the shear stress. Slopes with FOS less than 1 are likely to fail (Spencer 1967; Das and Sobhan 2013).

J. Jelani (✉) · M. S. A. Hah · M. N. Mohd Daud · N. Ahmad · M. Othman · W. M. S. Wan Mohamed Sabri
Department of Civil Engineering, Faculty of Engineering, National Defense University of Malaysia, Kuala Lumpur, Malaysia
e-mail: jestin@upnm.edu.my

H.-Y. Jeon (ed.), *Sustainable Development of Water and Environment*,
Environmental Science and Engineering,
https://doi.org/10.1007/978-3-030-75278-1_4

$$FOS = \frac{\tau_s}{\tau_f} \tag{4.1}$$

This study used two methods to determine the FOS of the slope. The first method is the ordinary method of slices, which was developed by Fellenius in 1927. This method assumes a circular slip surface and that the sliding of the soil mass above the failure line is divided into several vertical slices (Fredlund et al. 1981). The second method is the limit equilibrium method using SlopeW simulation software.

4.1.1 Description of the Study Area

The study was conducted on the UPNM campus located on the Sungai Besi Camp, Kuala Lumpur. There are five completed man-made slopes on the new road infrastructure. This study analysed only one of the slopes, as shown in Fig. 4.1. Although there is no prior record of slope failure in the study area, there is still a need to ensure the safety of the road users and nearby structures since the new road is constructed on steep terrain. The original slope has an approximate height of about 22 m and an angle of inclination of about 70°. The slope has nine berms, and turfing by hydroseeding protects the slope surface from excessive erosion.

The data from site investigation showed that the study area consists of two different layers of soil underlain by fractured igneous rock. Table 4.1 shows the soil classification and physical properties of the slope that were obtained from a previous site investigation report. These values were converted from the Standard Penetration Test (SPT) number.

Previous research conducted by the author (Jelani et al. 2020) showed that there is a high groundwater table in this study area approximately 2 to 9 m below the ground surface. Spring water is seen seeps through soil and fractured igneous rock at several

Fig. 4.1 Location of the study area

Table 4.1 Soil properties of the slope

Approximate depth, m	Type of soil	Average cohesion, (kPa)	Average friction angle, (°)	Average density, (kN/m^3)
0–13	Sandy silt	10	30	26
13–22	Silty sand	9	27	19

locations. The stability of the slope is influenced by the fluctuation in the groundwater table, which suggests that remedial actions should be taken. However, this study did not take into account the effect of groundwater and rock layer existence.

4.2 Methodology

4.2.1 Ordinary Method of Slices

The ordinary method of slices is a simplified method for determining slope stability. Because the method ignores all inter-slice forces and satisfies only the moment equilibrium, slope stability can be calculated manually (Burman et al. 2015a). The FOS of the slope is given by Eq. 4.2, where c' is effective cohesion, b is the width of the slice, α is the angle of inclination, W is the weight of a slice within the slices, and φ is the internal friction angle of the soil. The slope is divided into 17 slices, and Table 4.2 shows the width and inclination angle of each slice. This study assumes that the water table is far below the ground.

$$FOS = \frac{\sum (c' b \sec\alpha + W \cos\alpha \tan\Phi)}{\sum W \sin\alpha} \tag{4.2}$$

4.2.2 SlopeW Simulation Software

SlopeW is a modern limit equilibrium software that can perform more complex analyses of highly irregular and non-linear problems. This study used the Morgenstern-Price method because it employs a rigorous mathematical formulation that takes into account all inter-slice forces and satisfies all equations of static (Krahn 2004; Morgenstern and Price 1967). The inter-slice shear force formulation is given by Eq. 4.3, where X is the inter-slice shear force, E is the inter-slice normal force, λ is the percentage of the function used.

$$X = E \lambda f(x) \tag{4.3}$$

Table 4.2 The width and angle of inclination of each slice

Number of slice	Width, b (m)	Angle of inclination, α (°)
1	1	0
2	1.5	0
3	0.5	31
4	1.5	32
5	0.5	42
6	1.5	44
7	0.5	46
8	1.5	46
9	0.5	49
10	1.5	49
11	0.5	50
12	1.5	51
13	0.5	53
14	1.5	56
15	0.5	58
16	1	58
17	1	58

Figure 4.2 shows the SlopeW model setup, which comprises sandy silt and silty sand modelled in yellow and orange, respectively. The igneous rock layer is not considered in this study. This program constructed 17 vertical slices and nine berms to replicate the actual slope geometry condition at the study site.

4.3 Results and Discussion

Figure 4.3 shows the results of the slope stability analysis produced by SlopeW. The calculated global factor of safe of 0.882 indicates that the slope is unstable as the value is less than 1. The slip plane, indicated in green, is the soil above the weak surface and is also known as the failure surface. This failure surface extends from the crest and intersects the slope above the toe, and is classified as face failure. The slip surface also found lies close to the slope surface, and the line is non-circular. The non-circular failure surface is expected as it is the most common type of failure in heterogeneous slope, as mentioned by Zolfaghari et al. (2005).

Table 4.3 shows the results of the ordinary method of slices and SlopeW. The computed FOS is less than 1, which indicates that slope failure is likely to occur even though the analysis did not take into account the effect of groundwater fluctuation and pore water pressure due to rainfall infiltration. The two factors are critical in

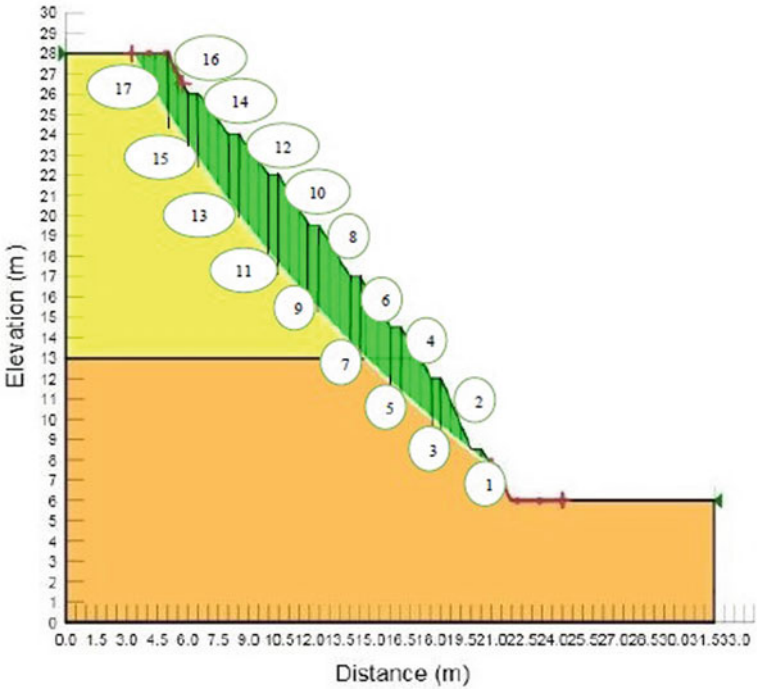

Fig. 4.2 The model setup in SlopeW

reducing the FOS of a slope. Even though there is no report of slope failure thus far, the results indicate that the slope is unstable.

The ordinary method of slices able to predict FOS with a good degree of accuracy with a percentage difference of about 24% compared to the prediction by SlopeW. The difference is due to the simplified assumptions in the ordinary method of slices that ignores all inter-slice forces and only considers the moment equilibrium (Burman et al. 2015b).

Further analysis was conducted to enhance the stability of the slope. The result of the analysis showed that the installation of nine soil nails at each berm and extension of the soil nails beyond the failure surface, as shown in Fig. 4.4, increased the slope's FOS by 36% to 1.194. The soil nailing also increased soil confinement and resistance to movement. Soil nailing is the most effective method for enhancing slope stability and is often used by geotechnical engineers to improve slope stability.

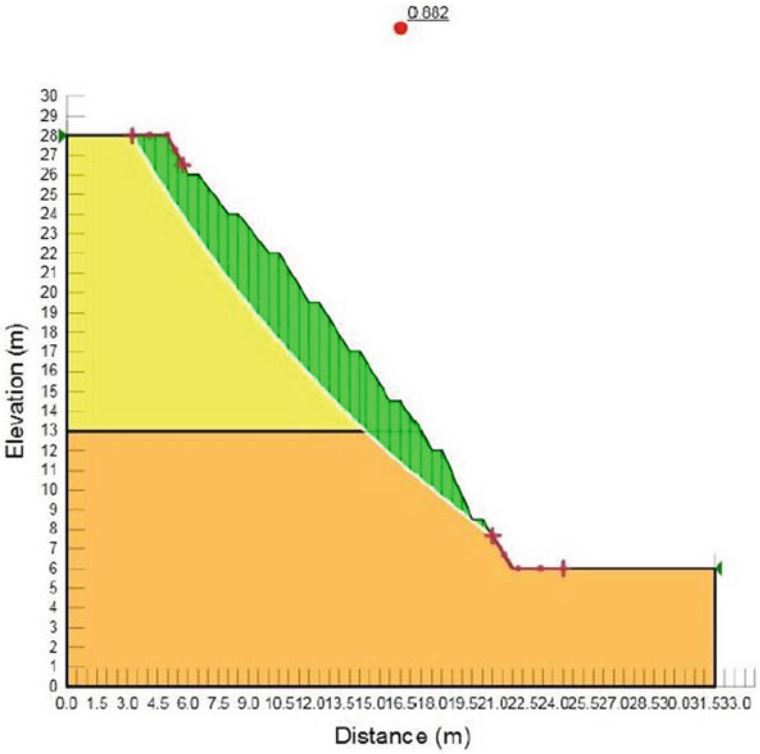

Fig. 4.3 The results of slope stability analysis using SlopeW

Table 4.3 Result of slope analysis

Method	Computed factor of safety
Ordinary method of slices	0.64
SlopeW	0.88

4.4 Conclusion

This paper presents the result of the stability analysis of a man-made slope constructed on the UPNM campus. The factor of safety of the slope was determined using the ordinary method of slices and SlopeW software. The FOS of less than 1 indicates an insufficient factor of safety. However, it should be noted that this study did not take into account groundwater level and rock layer existence. This research proposed increasing the slope's stability, confinement, and resistance to sliding through soil nailing. Local authorities can use the data from this study to identify the potential failure zone and develop possible remedial measures.

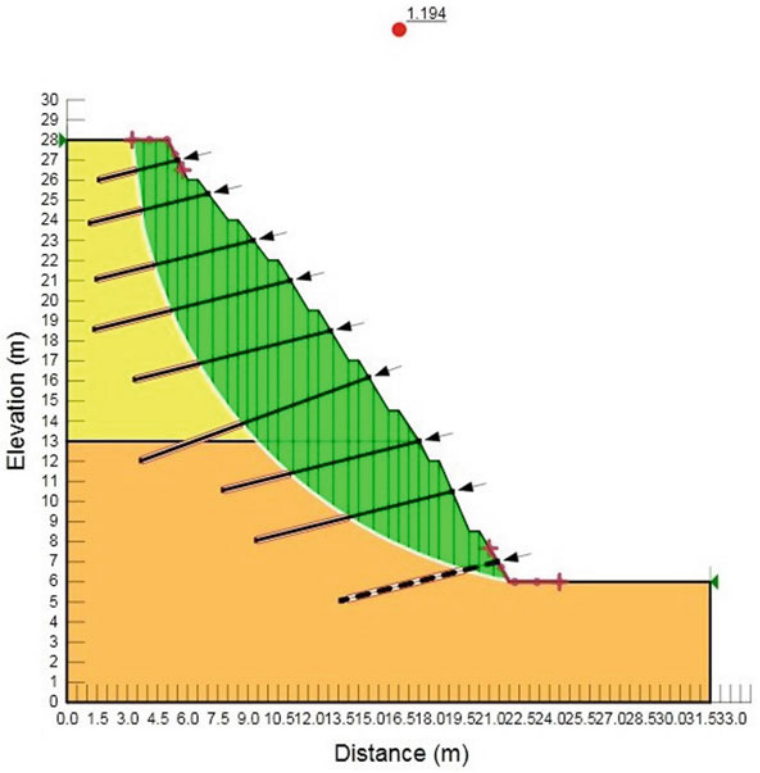

Fig. 4.4 Proposed soil nailing

Acknowledgements The authors wish to thank the National Defence University of Malaysia for providing financial support for this research under grant no. UPNM/2019/GPJP/TK/5. The authors appreciate the cooperation provided by the Development and Maintenance Department, UPNM.

References

Budhu M (2008) Soil mechanics and foundation. Wiley India Pvt. Limited. https://books.google.com.my/books?id=RY9YZ9h5zAoC

Burman A, Acharya SP, Sahay RR, Maity D (2015a) A comparative study of slope stability analysis using traditional limit equilibrium method and finite element method

Burman A, Acharya SP, Sahay RR, Maity D (2015b) A comparative study of slope stability analysis using traditional limit equilibrium method and finite element method. Asian J Civ Eng 16(4):467–492

Das BM, Sobhan K (2013) Principles of geotechnical engineering. Cengage learning

Fredlund DG, Krahn J, Pufahl DE (1981) The relationship between limit equilibrium slope stability methods. In: Proceedings of the international conference on soil mechanics and foundation engineering, vol 3, pp 409–416

Jelani J, Adnan NA, Husen H, Mohd Daud MN, Sojipto S (2020) The effects of ground water level fluctuation on slope stability by using slopeW. Def Sci Eng Technol 3(1):1–7

Krahn J (2004) Stability modeling with SLOPE/W: an engineering methodology. GEOSLOPE/W International Ltd., Calgary, Alberta, Canada

Lacasse S, Nadim F (2009) Landslide risk assessment and mitigation strategy. Landslides–disaster risk reduction. Springer, Berlin, pp 31–61

Lee LM, Kassim A, Gofar N (2011) Performances of two instrumented laboratory models for the study of rainfall infiltration into unsaturated soils. Eng Geol 117(1–2):78–89

Morgenstern NR, Price VE (1967) A numerical method for solving the equations of stability of general slip surfaces. Comput J 9(4):388–393

Spencer E (1967) A method of analysis of the stability of embankments assuming parallel inter-slice forces. Geotechnique 17(1):11–26

Wieczorek GF, Snyder JB (2009) Monitoring slope movements. In: Young R, Norby L (eds) Geological monitoring. Geological society of America, Boulder, Colorado.

Zaki A, Chai HK, Razak HA, Shiotani T (2014) Monitoring and evaluating the stability of soil slopes: a review on various available methods and feasibility of acoustic emission technique. Comptes Rendus-Geosci 346(9–10):223–232. https://doi.org/10.1016/j.crte.2014.01.003

Zolfaghari AR, Heath AC, McCombie PF (2005) Simple genetic algorithm search for critical non-circular failure surface in slope stability analysis. Comput Geotech 32(3):139–152. https://doi.org/10.1016/j.compgeo.2005.02.001

Chapter 5
Comparison of the Full-Scale Municipal Wastewater Treatment Plant Designs Consisting of Modified Bardenpho Process with and Without Membrane Bioreactor for Nutrient Removal: Cost Analysis

Shahryar Jafarinejad

Abstract Cost estimating for wastewater treatment plant (WWTP) construction/upgrade projects is a worldwide priority and is useful for forecasting its future economic needs. On the other hand, sensitivity analysis can provide valuable information about design decisions. Nowadays, there is an increasing interest to use membrane bioreactor (MBR) for wastewater treatment. This study intends to analyze and compare the total project construction, operation labor, maintenance labor, material, chemical, energy and amortization costs of the proposed full-scale municipal WWTP configurations consisting of modified Bardenpho (5-stage biological nutrient removal) process with and without MBR for different average influent wastewater flow rates. The designs, theoretical effluents quality and costs comparison of the two WWTP configurations were reported. Results demonstrated that the application of MBR system in WWTP could result in not only higher capital cost but also higher operation and maintenance costs than conventional processes for the same average influent wastewater flow rate. In addition, the costs were enhanced with increasing the average influent wastewater flow rate.

Keywords Nutrient · Treatment · Modified bardenpho process · Membrane bioreactor · Cost

S. Jafarinejad (✉)
Department of Chemical Engineering, College of Engineering, Tuskegee University, Tuskegee, AL, USA

H.-Y. Jeon (ed.), *Sustainable Development of Water and Environment*,
Environmental Science and Engineering,
https://doi.org/10.1007/978-3-030-75278-1_5

5.1 Introduction

Ground water contamination and eutrophication in the natural surface water can be caused by discharging nutrients (phosphorus and nitrogen) from municipal wastewater into the environment (Dube et al. 2016; Vu et al. 2019; Jafarinejad 2021). In other words, it can result in problems such as depletion of the stream's dissolved oxygen content, adverse effect on fish life under certain environmental conditions, etc. It is obvious that elevated nutrient levels in waters can be a major factor for harmful algal blooms occurrence. It can be harmful to the environment and threaten animal and human health (Heisler et al. 2008; United States Environmental Protection Agency 2015). Thus, many countries have established/adopted strict rules for control of nutrient discharges into environment to protect waters from its over-enrichment (Jafarinejad 2021; United States Environmental Protection Agency 2009; Liu et al. 2011; Xue et al. 2015; Jafarinejad et al. 2019; Jafarinejad 2019).

To remarkably decrease the nutrients release from wastewater treatment plants (WWTPs) to waterbodies, their effluent levels should be less than 1–3 mg N/L and 0.1 mg P/L, respectively (Jafarinejad 2021; Fowler et al. 2013; Yan et al. 2018). The term limit of treatment technology (LOT) was introduced in North America as the lowest economically attainable effluent quality, which is less than 1.5–3 mg/L and 0.07 mg/L for total nitrogen (TN) and total phosphorus (TP), respectively (Oleszkiewicz and Barnard 2006). WWTPs attaining these standards are not widespread (Jimenez et al. 2007). For instance, in the USA, some states with lowest TP permit limits for one or more publicly owned treatment works (POTWs) are Massachusetts, New Hampshire, Michigan and Maryland which their TP permit limits are 0.1, 0.2, 0.3, and 0.3, respectively (Bashar et al. 2018; United States Environmental Protection Agency 2017). The TP limit in most WWTPs is in the range of 0.5–1.5 mg/L. It is clear that more strict effluent permit levels should be complied in the future. Because conventional WWTPs usually do not remove TN and TP to the extent required to protect receiving waters, it is necessary to implement processes that reduce effluent nutrient concentrations to standard levels. This will unavoidably exert a remarkable financial burden on the wastewater treatment facilities because it usually involves major process modifications/upgrades to the WWTPs (Bashar et al. 2018; Headworks International 2018).

Biological nutrient removal (BNR) processes use microorganisms under different environmental conditions to remove nutrients from aqueous waste streams (Tchobanoglous and Burton 1991; United States Environmental Protection Agency 2007a). Some BNR technologies can remove only TN or TP, whereas, others are able to remove both. Modified Ludzack-Ettinger (MLE) process, A^2/O process, step feed process, Bardenpho process (4-stage), modified Bardenpho process (5-stage), sequencing batch reactor (SBR) process, modified University of Cape Town (UCT) process, rotating biological contactor (RBC) process and oxidation ditch are common BNR systems (United States Environmental Protection Agency 2007a). If the BNR system has an aerobic zone for nitrification and an anoxic zone for denitrification it can remove TN; whereas, the BNR system that has an anaerobic zone free of

dissolved oxygen and nitrate, can remove TP (United States Environmental Protection Agency 2007a; Water Environment Federation (WEF) and American Society of Civil Engineers (ASCE)/Environmental and Water Resources Institute (EWRI) 2006).

Target effluent concentrations, cost and other factors should be considered in choosing the most appropriate system/process for a particular facility. Cost estimating for WWTP construction/upgrade projects is a worldwide priority and is useful for forecasting its future economic needs (Jafarinejad 2017, 2019, 2020; Arif et al. 2020). On the other hand, nowadays, there is an increasing interest for application of membrane bioreactor (MBR) to treat wastewater. Studies on full-scale MBRs demonstrate that the MBR-based systems can efficiently/stably treat wastewater (Xiao et al. 2019). Limited information can be found in the literature on integration of modified Bardenpho (5-stage BNR) process with MBR in a full-scale municipal WWTP. In addition, to the best of author's knowledge, there is no information in the literature on the effect of different average influent wastewater flow rates on the total project construction, operation labor, maintenance labor, material, chemical, energy and amortization costs of the full-scale municipal WWTPs consisting of modified Bardenpho process with MBR. This study intends to analyze and compare the costs of WWTP configurations consisting of modified Bardenpho with and without MBR for different average influent wastewater flow rates.

5.2 Materials and Methods

5.2.1 The Characteristics of Influent Wastewater

Wastewater characteristics of an advanced wastewater treatment facility in Florida (Sedlak 1991) was used to base the research on an actual case for economic analysis. The characteristics of influent wastewater are listed in Table 5.1. Note that the influent biochemical oxygen demand (BOD), influent suspended solids (SS) and total Kjeldahl nitrogen (TKN) were obtained from Sedlak (1991). The author considered/assumed reasonable values for the other parameters to analyze the costs. The average observed mixed liquor suspended solids (MLSS) concentration in the facility was 4,090 mg/L (Sedlak 1991), which 4,000 mg/L was used as the design value in this study.

5.2.2 Description of WWTP Consisting of Modified Bardenpho Process

The modified Bardenpho process (5-stage) is similar to the Bardenpho process (4-stage) with the addition of an anaerobic zone ahead of the 4-stage process to achieve

Table 5.1 The characteristics of influent wastewater

Parameter	Unit	Value
Average, minimum and maximum influent flow	m^3/d (MGD)	15,142 (4)
Suspended solids (SS)	mg/L	250
Volatile solids	%	75
Biochemical oxygen demand (BOD)	mg/L	270
Soluble BOD	mg/L	95
Chemical oxygen demand (COD)	mg/L	600
Soluble COD	mg/L	360
Total Kjeldahl nitrogen (TKN)	mgN/L	43
Soluble TKN	mgN/L	28
Ammonia	mgN/L	25
Total phosphorus (TP)	mgP/L	8
pH	Standard units	7.6
Settleable solids	mL/L	10
Nitrite	mgN/L	0
Nitrate	mgN/L	0
Non-degradable fraction of VSS	%	40
Average summer temperature	°C	28
Average winter temperature	°C	17

phosphorus removal. In other words, this biological process consists of five distinct stages: anaerobic/first anoxic/first aerobic/second anoxic/second aerobic. A nitrate-rich liquor is recycled from the first aerobic zone, designed for complete nitrification, to the first anoxic zone. The return activated sludge (RAS) is recycled from the secondary clarifier to the beginning of the anaerobic zone/stage. The modified Bardenpho process is used to remove both TN and TP (United States Environmental Protection Agency 2009; United States Environmental Protection Agency 2007a; United States Environmental Protection Agency 2008; Esfahani et al. 2018) and its performance in TN and TP removals is respectively excellent and good (Esfahani et al. 2018).

The schematic process flow diagram (PFD) of the proposed WWTP consisting of modified Bardenpho (WWTP-A) is demonstrated in Fig. 5.1. The wastewater processing train consists of preliminary treatment (screening and grit removal), primary clarification, modified Bardenpho process (5-stage BNR), secondary clarifier, filtration, and ultra-violet disinfection; whereas, the sludge processing train includes sludge flotation thickening, anaerobic digestion, belt-filter press, and hauling and land filing. It has been reported that waste activated sludge (WAS) can be thickened in dissolved air flotation units, can be mixed with the primary sludge or gravity thickened primary sludge, and then can be stabilized in anaerobic digesters (Sedlak 1991; Zahreddine 2018). In this study, WAS and primary sludge are mixed and

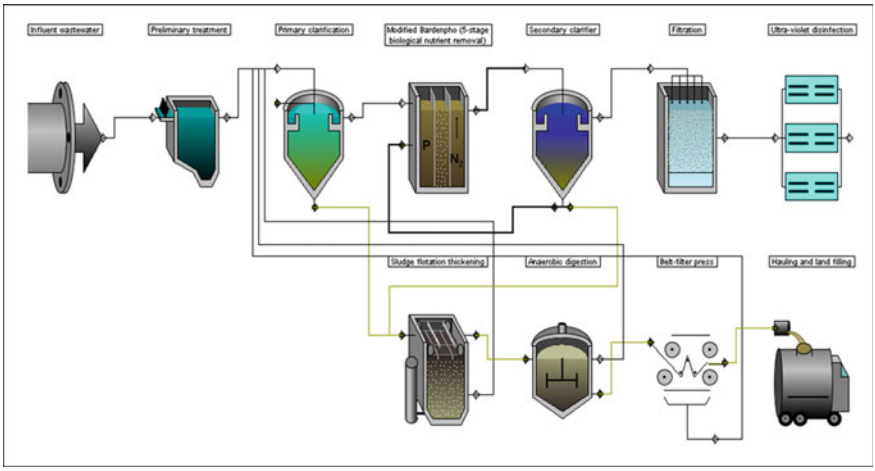

Fig. 5.1 The simplified PFD of the WWTP consisting of modified Bardenpho process (5-stage BNR) (WWTP-A)

thickened in flotation unit, digested anaerobically, and then dewatered using belt-filter press. The design criteria and process parameters applied in the research for several treatment units in the WWTP are listed in Table 5.2.

5.2.3 Description of WWTP Consisting of Modified Bardenpho Process with MBR

The MBR is a wastewater treatment system in which membrane filtration is used as a solid–liquid process instead of traditional secondary clarifier. The MBR-based systems can be operated at significantly higher MLSS concentration as compared to conventional separation processes, thus reducing the foot-print of the WWTP. The MBRs can be utilized to produce effluent of much higher quality (e.g., for reuse), for on-site upgrade of WWTPs, to enhance capacity and treatment efficiency, to reduce land use in densely populated areas, etc. The MBR system not only needs provisions of filtration membranes and associated coarse bubble scouring air arrangements to control membrane fouling but also physical and chemical cleaning at regular interval for smooth operation of the plant. The cost of membrane and additional membrane cleaning requirements usually makes this process more expensive than the conventional technologies. In other words, higher cost-effectiveness is a challenge for the full-scale application of MBRs, however there is still room to reduce their capital and operating costs (Xiao et al. 2019).

Table 5.2 The design criteria and process parameters for units of WWTP consisting of modified Bardenpho (5-stage BNR)

Process/unit	Design criteria and process parameters/operational conditions
Screening	Mechanically cleaned depth: 0.60 m; Width of bars: 1 cm; and other assumed process parameters can be found in Jafarinejad (2019)
Grit removal	Design basis: depth: 3 m; and other assumed process parameters can be found in Jafarinejad (2019)
Primary clarification	Circular clarifier; Sidewater depth: 3 m; and other assumed design criteria and process parameters can be found in Jafarinejad (2017, 2019)
Modified Bardenpho (5-stage BNR)	Number of stages: 5 stage; Internal recycle from oxic to anoxic zone: yes; Aeration type: diffused aeration; Effluent TN: 10 mgN/L; Effluent TP: 1 mgP/L; Design basis: temperature sensitive growth rate; Safety factor for calculated solids retention time (SRT): 1.5; Maximum heterotrophic specific growth rate: 6 1/d; heterotrophic decay rate: 0.24 1/d; Maximum autotrophic specific growth rate: 0.75 1/d; autotrophic decay rate: 0.08 1/d; Biomass yield: 0.5; Minimum influent BOD to P ratio: 20; Fraction of influent RB COD used by PAOs: 0.7; Total P content of PAOs: 0.1 mg P/mg PAO VSS; Bubble size: fine; Alpha factor for oxygen transfer in wastewater: 0.7; Beta factor for oxygen saturation in wastewater: 0.95; Coarse bubble minimum air flow: 0.33 L/s/m^2; Fine bubble minimum air flow: 0.61 L/s/m^2; Standard oxygen transfer efficiency: 20%; and Mixed liquor suspended solids (MLSS): 4,000 mg/dm^3
Secondary clarifier	Circular clarifier; Surface overflow rate: 20.37 $m^3/(m^2 \cdot d)$; Sidewater depth: 3.7 m; and other assumed design criteria and process parameters can be found in Jafarinejad (2019)
Filtration	Number of layers: 4; and details of the assumed design criteria and process parameters in filtration can be found in Jafarinejad (2017)
Ultra-violet disinfection	Total coliform: 250 MPN/100 mL; Unfiltered transmittance: 55%; Number of spare channels: 1; Disinfection season length: 12 month; UV lamp output: 26.7 W; Lamp power requirement: 85 W; Reduction of UV light by fouling: 30%; Reduction of UV light by aging: 30%; and Area of quartz sleeve: 0.00041 m^2
Sludge floatation thickening	Air pressure: 413,660 Pa; Detention time in float tank: 3 h; Solids loading: 48.82 kg/(m^2.d); Hydraulic loading: 146.69 $m^3/(m^2.d)$; Recycle time in pressure tank: 2 min; Removals of solids: 80%; Air/solids ratio: 0.02; Float concentration: 4%; and Polymer required: 0.5 g/kg (Jafarinejad 2017)

(continued)

Table 5.2 (continued)

Process/unit	Design criteria and process parameters/operational conditions
Anaerobic digestion	Location: warm-winter >10 °C; and other assumed design criteria and process parameters can be found in Jafarinejad (2017, 2019)
Belt-filter press	The assumed design criteria and process parameters can be found in Jafarinejad (2017, 2019)
Hauling and land filling	Disposal cost basis: annual charge of land fill; and other assumed design criteria can be found in Jafarinejad (2019)

The simplified PFD of the proposed WWTP consisting of modified Bardenpho with MBR (WWTP-B) is demonstrated in Fig. 5.2. The wastewater processing train consists of preliminary treatment (screening and grit removal), primary clarification, modified Bardenpho (5-stage BNR), MBR, and ultra-violet disinfection; whereas, the sludge processing train includes sludge flotation thickening, anaerobic digestion, belt-filter press, and hauling and land filing. The design criteria and process parameters of preliminary treatment (screening and grit removal), primary clarification, modified Bardenpho (5-stage BNR), ultra-violet disinfection, sludge flotation thickening, anaerobic digestion, belt-filter press, and hauling and land filing for this WWTP are the same as that of WWTP consisting of modified Bardenpho process.

There are several commercial MBR membrane module products: ZeeWeed (GE Zenon), PURON (Koch Membrane Systems), Microza (Asahi Kasei), SuperMAK (ENE Co., Ltd.), KSMBR (Korea Membrane Separations), MEMSUB (MEMOS

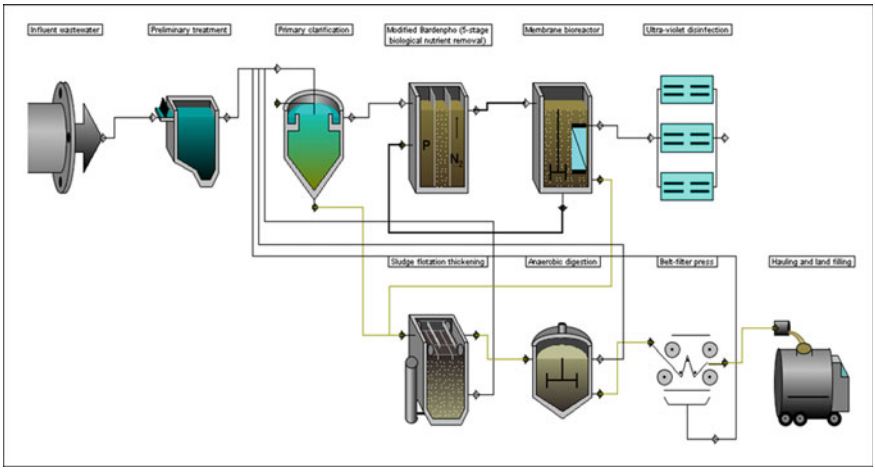

Fig. 5.2 The simplified PFD of the WWTP consisting of modified Bardenpho (5-stage BNR) with MBR (WWTP-B)

Membranes Modules Systems), Micronet (Micronet Porous Fibers S.L.), SENUOFIL (SENUO Filtration Technol. Co., Ltd.), POREFLON (Sumitomo Electric Industries), SuperUF (Superstring MBR Technol. Corp.), etc. (Santos and Judd 2010; Judd 2011). Most of the municipal WWTPs worldwide have adapted ZeeWeed hollow fiber membrane provided by GE Zenon (Park et al. 2015). Therefore, this study also suggests Zeeweed 500d (made of polyvinylidene fluoride (PVDF), membrane surface area per module of 31.6 m^2, nominal pore size of 0.04 μm, maximum number of modules per cassette of 48, and packing density of 228 m^2/m^3) (Judd 2011). In the design and cost analysis of MBR system, specific scour air demand based on membrane area of 0.54 N $m^3/(m^2.h)$ (Judd 2011; Park et al. 2015), physical cleaning interval of 10 min, physical cleaning duration of 45 s, chemical cleaning interval of 84 h (Cashman et al. 2018), membrane packing density of 228 m^2/m^3 (Judd 2011) were used; whereas, average net flux of 20 LMH, peak net flux of 30 LMH, scour air cycle time of 20 s, scour air on time of 10 s, backflush flow factor of 1.25, specific gravity of 1.03, effluent SS of 1 mg/L, and underflow concentration of 1.2% (default values in CapdetWorks) were assumed by author.

5.2.4 Cost Analysis Procedure

In this study, CapdetWorks software version 4.0 (developed by Hydromantis Environmental Software Solutions, Inc., Ontario, Canada) was used to estimate the costs to build, operate and maintain the proposed WWTP configurations (Hydromantis Environmental Software Solutions, Inc., 2020). CapdetWorks software is an enhancement of the CAPDET model (United States Environmental Protection Agency 1982) which Hydromantis has added a number of unit operations (e.g., sequencing batch reactor, ultra-violet disinfection, etc.) not originally included in the CAPDET model. The software designs each unit operation in a given WWTP layout according to the influent characteristics and then calculates the cost of the design (Hydromantis Environmental Software Solutions, Inc., 2018).

As the aim of the research is to compare costs of the treatment alternatives, the default cost data (the unit costs, cost indices, site-specific costs, and equipment costs) in the software was applied for the cost analysis. "Hydromantis 2014, (USA Avg.)" database was used for costing all types of treatment equipment. To account for changing costs over time in the costing algorithms, Hydromantis Equipment Cost Index (HECI), Hydromantis Construction Cost Index (HCCI) and Hydromantis Pipe Cost Index (HPCI) were updated to the current values (September 2020).

It is necessary to note that the costing algorithms take into consideration the replacement period for mechanical and structural parts of each unit process. The assumed replacement schedule (default values in CapdetWorks) is shown in Table 5.3.

Table 5.3 The assumed replacement period for mechanical and structural parts of each unit process

Process/unit	Replacement
Grit removal	Capital cost: 40 years
Primary and secondary clarification	Mechanical: 20 years; Structural: 40 years, and Pump: 25 years
Modified Bardenpho	Mechanical aerator: 20 years; Fine bubble diffuser: 10 years; Coarse bubble diffuser: 20 years; Swing arm diffuser: 20 years; Turbine mixer: 20 years; Pump: 25 years; and Structural: 40 years
Membrane bioreactor	Membrane: 10 years; Coarse bubble diffuser: 20 years; Swing arm diffuser: 20 years; Pump: 25 years; and Structural: 40 years
Filtration	Filter unit: 20 years and Structural: 40 years
Ultra-violet disinfection	Lamps: 2 years; Ballast: 10 years; Quartz sleeves: 5 years; and Structural: 30 years
Sludge floatation thickening	Air flotation unit: 20 years and Structural: 40 years
Anaerobic digestion	Floating cover: 20 years; Gas circulation unit: 20 years; Heating unit: 20 years; Gas safety equipment; Sludge pump: 25 years; Filter unit: 20 years and Structural: 40 years
Belt-filter press	Belt-filter: 20 years and Structural: 40 years
Hauling and land filling	Vehicle: 6 years and Structural: 40 years

5.2.5 Produced/Suggested Designs

CapdetWorks software utilizes the influent characteristics and the process parameters to design the applicable system. The designs produced by CapdetWorks (estimated/suggested values) based on influent wastewater flow rate of 15,142 m^3/d or 4 MGD for the two treatment alternatives are listed in Table 5.4.

5.2.6 Effluents Quality of the WWTPs

Theoretical effluents quality of the WWTP-A (consisting of modified Bardenpho with secondary clarifier and four-layer filter) and WWTP-B (consisting of modified Bardenpho with MBR) based on the CapdetWorks software results are listed in Table 5.5. The cost comparison of the two WWTP configurations was considered based on these final treated effluent parameters. TP concentration in treated water from the WWTP-B is 0.01 mgP/L which achieves the LOT effluent quality (Oleszkiewicz and Barnard 2006).

Table 5.4 Suggested designs for the two WWTPs

Process/unit	WWTP-A	WWTP-B
Primary clarification	Diameter of 15.54 m, excavation depth of 1.21 m, one battery, and two tanks per battery	Diameter of 15.54 m, excavation depth of 1.21 m, one battery, and two tanks per battery
Modified Bardenpho	Anaerobic volume of 2,074.8 m^3, anoxic volume of 4,841.2 m^3, aerobic volume of 6,916 m^3, tank width of 10 m, tank depth of 5 m, pipe gallery width of 6.59 m, excavation depth of 1.3 m, one battery, four tanks per battery, required air flow of 19.45 N m^3/min/1000m^3, and two mixers per unaerated tank	Anaerobic volume of 2,074.6 m^3, anoxic volume of 4,840.7 m^3, aerobic volume of 6,915.3 m^3, tank width of 10 m, tank depth of 5 m, pipe gallery width of 6.59 m, excavation depth of 1.3 m, one battery, four tanks per battery, required air flow of 19.45 N m^3/min/1000m^3, and two mixers per unaerated tank
Secondary clarification	Diameter of 23.77 m, excavation depth of 1.21 m, one battery, and two tanks per battery	
Membrane bioreactor		One battery, four tanks per battery, one standby tank per battery, length of 4.32 m, width of 2.16 m, depth of 5 m, and excavation depth of 1.3 m
Filtration	One unit and 68.75 m^2 total surface area required	
Ultra-violet disinfection	Four lamps per module, five modules per bank, four banks per channel, and two channels	Two lamps per module, three modules per bank, six banks per channel, and three channels
Sludge floatation thickening	One unit, diameter of 12.16 m, and sidewater depth of 2.62 m	One unit, diameter of 12.16 m, and sidewater depth of 2.62 m
Anaerobic digestion	One primary digester tank, one secondary digester tank, one battery, diameter of 16.74 m, and sidewater depth of 7.71 m	One primary digester tank, one secondary digester tank, one battery, diameter of 16.74 m, and sidewater depth of 7.71 m
Belt-filter press	One belt-filter and 235.51 m^2 building size requirement	One belt-filter and 235.51 m^2 building size requirement

5.2.7 Sensitivity Analysis

Sensitivity analysis can provide valuable information about design decisions. Estimations of the project construction, operation labor, maintenance labor, material, chemical, energy, and amortization costs of the proposed WWTP configurations were analyzed as a function of the average influent wastewater flow rate. The average influent flow rate of 3,785.4–83,280 m^3/d (1–22 MGD) were studied because these rates represent the majority of WWTPs in the USA.

Table 5.5 Theoretical effluents quality of the two WWTPs

Parameter	Unit	WWTP-A	WWTP-B
SS	mg/L	8	1
BOD	mg/L	1.36	1.45
COD	mg/L	2.03	3.09
TKN	mgN/L	0.18	0.25
Ammonia	mgN/L	0.18	0.18
TP	mgP/L	0.28	0.01
Nitrite	mgN/L	0	0
Nitrate	mgN/L	8.59	8.62
pH	Standard units	7.6	7.6

5.3 Results and Discussion

5.3.1 Costs Comparison of the WWTP Configurations for the Average Influent Flow of 4 MGD

The total project construction costs or capital construction costs for the two WWTP configurations were estimated using CapdetWorks software which includes three categories: (i) unit process construction costs; (ii) other direct construction costs; and (iii) other indirect construction costs (Fig. 5.3). Other direct construction costs includes mobilization, site preparation, site electrical, yard piping, instrumentation and control, and lab and administration buildings costs; whereas, indirect construction costs consist of land cost, miscellaneous cost, legal cost, engineering design fee, inspection cost, contingency, technical, interest during construction, and profit. The total project construction cost of the WWTP-B was higher than that of the WWTP-A by about 17.36% under the used design criteria and process parameters in this study. In other words, as the WWTP-B consists of the MBR system, its unit process construction and other indirect construction costs were higher than those of the WWTP-A (consisting of secondary clarifier plus four-layer filter instead of

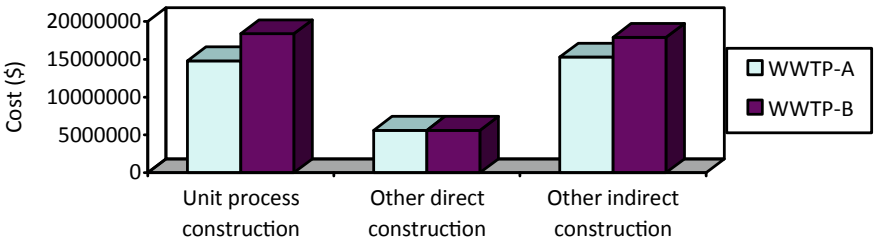

Fig. 5.3 The total project construction costs categories of the two WWTP configurations for the influent wastewater flow rate of 15,142 m^3/d or 4 MGD

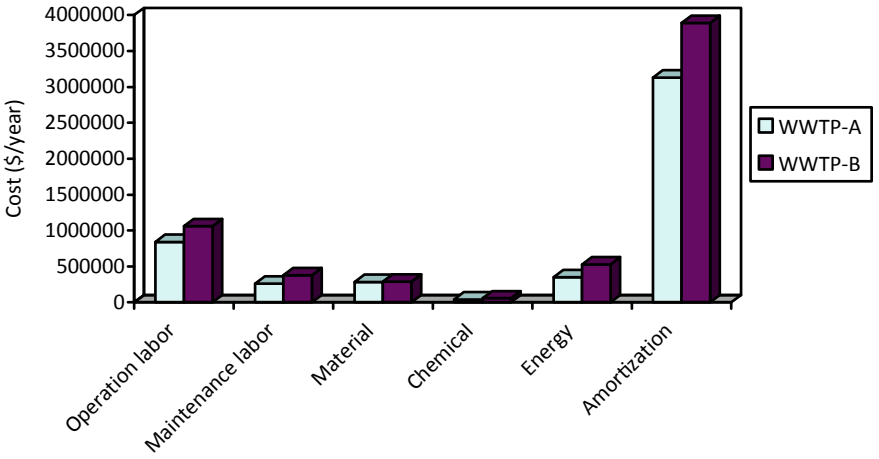

Fig. 5.4 The annual operation labor, maintenance labor, material, chemical, energy, and amortization costs ($/year) of the two WWTP configurations for the influent wastewater flow rate of 15,142 m^3/d or 4 MGD

MBR system). This may be attributed to the costs associated with the MBR system including the price of membrane, pumps, blowers, etc.

In the CapdetWorks, the operation and maintenance (O&M) costs for a WWTP are divided into several major categories: operation labor, maintenance labor, materials, chemicals, and energy required for operation (United States Environmental Protection Agency 1982). The annual operation labor, maintenance labor, material, chemical, energy, and amortization costs ($/year) of the two WWTP configurations are shown in Fig. 5.4. All these costs for the WWTP-B were higher than those of the WWTP-A. This can be because of the following reasons: (1) higher administration labor, laboratory labor, and operation labor costs due to the operational complexity of the MBR that may require trained personnel; (2) influence of possible aggressive environments and fouling on the membrane life; (3) membrane replacement cost; (4) chemical cleaning at regular interval for smooth operation of the MBR; and (5) higher energy use for the MBR pumps and/or the air-scouring blowers to reduce membrane fouling (Arif et al. 2020; Xiao et al. 2019; United States Environmental Protection Agency 2007). The results of this study were consistent with those of the previous studies related to MBR systems (Arif et al. 2020; Xiao et al. 2019; Judd 2011; United States Environmental Protection Agency 2007; Rachmani 2013; Verrecht et al. 2010).

It is necessary to note that the application of MBR system in WWTPs could result in higher capital and O&M costs than conventional processes for the same average influent wastewater flow rate; however, this system can produce higher quality effluent and require smaller space in comparison with the conventional processes. Membrane life and membrane guarantees can be important in determining the cost-effectiveness of the system. Generally, regular use of mild cleaners and

appropriate pre-treatment processes upstream of the MBR to protect the membranes from physical damage and reduce fouling may increase the membrane life (United States Environmental Protection Agency 2007b).

5.3.2 *Effect of the Influent Flow Rate on Costs*

The sensitivity analysis was used to calculate the impact of the average influent wastewater flow rate change (3,785.4–83,280 m^3/d or 1–22 MGD) on the project construction costs, annual operation labor, maintenance labor, chemical, and energy costs of the two WWTP configurations which are shown in Figs. 5.5, 5.6, 5.7, 5.8 and 5.9. All the costs were enhanced with increasing the average influent wastewater flow rate. In addition, all the costs for the WWTP-B were higher than those of the WWTP-A.

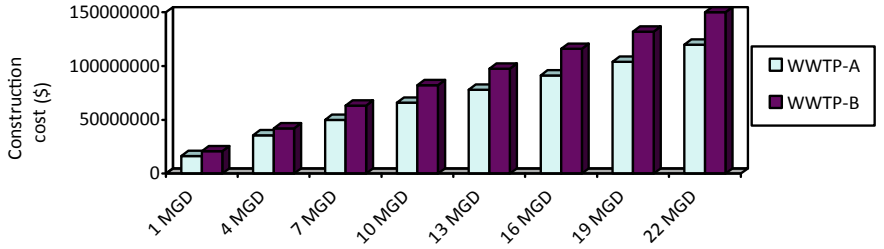

Fig. 5.5 The project construction costs ($) of the two WWTP configurations versus average influent wastewater flow rate

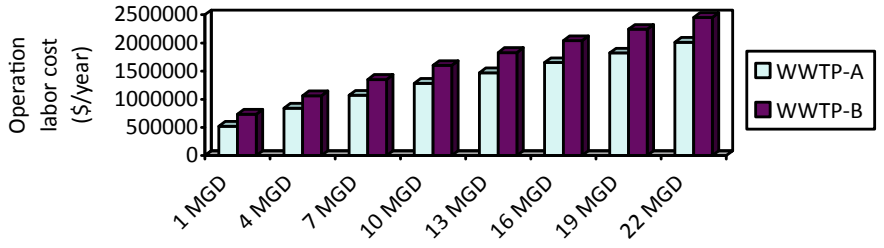

Fig. 5.6 The annual operation labor costs ($/year) of the two WWTP configurations versus average influent wastewater flow rate

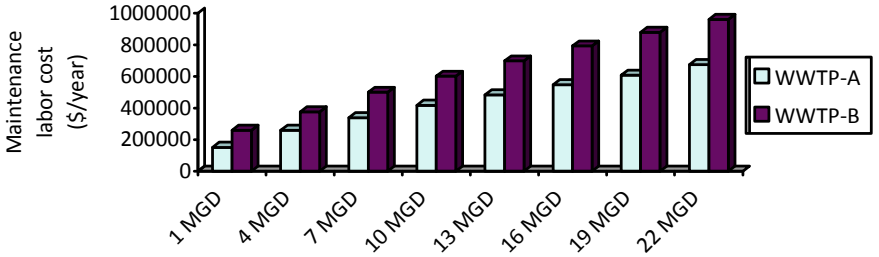

Fig. 5.7 The annual maintenance labor costs ($/year) of the two WWTP configurations versus average influent wastewater flow rate

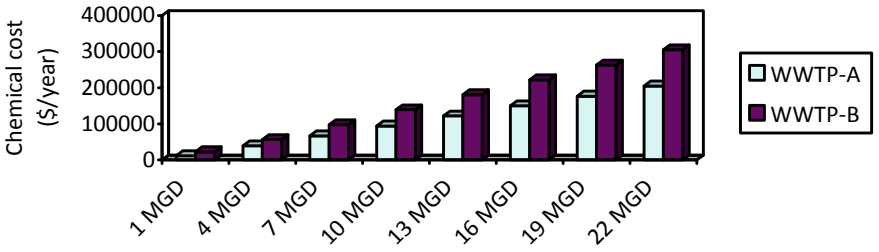

Fig. 5.8 The annual chemical costs ($/year) of the two WWTP configurations versus average influent wastewater flow rate

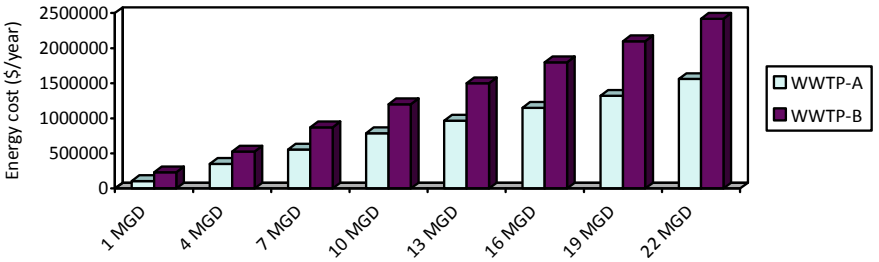

Fig. 5.9 The annual energy costs ($/year) of the two WWTP configurations versus average influent wastewater flow rate

5.4 Conclusion

The study analyzed and compared the capital and O&M costs of the WWTP configurations consisting of modified Bardenpho with and without MBR for different average influent wastewater flow rates.

For influent wastewater flow rate of 15,142 m^3/d or 4 MGD, the total project construction cost of the WWTP-B was higher than that of the WWTP-A by about 17.36%. In addition, all the annual operation labor, maintenance labor, material,

chemical, energy, and amortization costs for the WWTP-B were higher than those of the WWTP-A. Furthermore, all the costs were enhanced with increasing the average influent wastewater flow rate.

Acknowledgements The author gratefully acknowledges support from the UNCF - Henry C. McBay Faculty Research Fellowship award and the ORAU Events Sponsorship Program.

References

Arif AUA, Sorour MT, Aly SA (2020) Cost analysis of activated sludge and membrane bioreactor WWTPs using CapdetWorks simulation program: case study of Tikrit WWTP (middle Iraq). Alex Eng J (In Press) (2020). https://doi.org/10.1016/j.aej.2020.08.023

Bashar R, Gungor K, Karthikeyan KG, Barak P (2018) Cost effectiveness of phosphorus removal processes in municipal wastewater treatment. Chemosphere 197:280–290

Cashman S, Ma X, Mosley J, Garland J, Crone B, Xue X (2018) Energy and greenhouse gas life cycle assessment and cost analysis of aerobic and anaerobic membrane bioreactor systems: Influence of scale, population density, climate, and methane recovery. Bioresour Technol 254:56–66

Dube PJ, Vanotti MB, Szogi AA, García-Gonzalez MC (2016) Enhancing recovery of ammonia from swine manure anaerobic digester effluent using gas-permeable membrane technology. Waste Manage 49:372–377

Esfahani EB, Zeidabadi FA, Bazargan A, McKay G (2018) The modified Bardenpho process. In: Hussain CM (ed) Handbook of environmental materials management. Springer International Publishing AG, part of Springer Nature

Fowler D, Coyle M, Skiba U, Sutton MA, Cape JN, Reis S, Sheppard LJ, Jenkins A, Grizzetti B, Galloway JN (2013) The global nitrogen cycle in the twenty-first century. Phil. Trans. r. Soc. b. 368:20130164

Headworks International: BNR Biological Nutrient Removal (2018). https://www.headworksinternational.com/product/bnr-biological-nutrient-removal/#. Accessed 12 Oct 2020

Heisler J, Gilbert PM, Burkholder JM, Anderson DM, Cochlan W, Dennison WC, Dortch Q, Gobler CJ, Heil CA, Humphries E, Lewitus A, Magnien R, Marshall HG, Sellner K, Stockwell DA, Stoecker DK, Suddleson M (2008) Eutrophication and harmful algal blooms: a scientific consensus. Harmful Algae 8:3–13

Hydromantis Environmental Software Solutions, Inc.: CapdetWorks (2020). https://www.hydromantis.com/CapdetWorks.html. Accessed 12 Oct 2020

Hydromantis Environmental Software Solutions, Inc.: CapdetWorks V4.0: State-of-the-art software for the design and cost estimation of wastewater treatment plants. User's Guide. (2018)

Jafarinejad S (2017) Cost estimation and economical evaluation of three configurations of activated sludge process for a wastewater treatment plant (WWTP) using simulation. Appl Water Sci 7:2513–2521

Jafarinejad S (2019) Economic analysis: trickling filter/activated sludge or nitrifying trickling filter/activated sludge? Ecol Chem Eng S 26(2):345–356

Jafarinejad S (2020) A framework for the design of the future energy-efficient, costeffective, reliable, resilient, and sustainable full-scale wastewater treatment plants. Curr Opin Environ Sci Health 13:91–100

Jafarinejad S (2021) Forward osmosis membrane technology for nutrient removal/recovery from wastewater: recent advances, proposed designs, and future directions. Chemosphere 263:128116

Jafarinejad S, Park, H, Mayton H, Walker SL, Jiang SC (2019) Concentrating ammonium in wastewater by forward osmosis using a surface modified nanofiltration membrane. Environ Sc.: Water Res Technol 5:246–255

Jimenez J, Madhanagopal T, Schmidt H, Bratby J, Meka H, Parker D (2007) Full-scale operation of large biological nutrient removal facilities to meet limits of technology effluent requirements: the florida experience, In: CD ROM Proceedings WEFTEC 2007, water environment federation, Alexandria, Virginia (2007)

Judd S (2011) The MBR book - principles and applications of membrane bioreactors for water and wastewater treatment, 2nd ed. Elsevier

Liu Y, Kwag JH, Kim JH, Ra C (2011) Recovery of nitrogen and phosphorus by struvite crystallization from swine wastewater. Desalination 277(1):364–369

Oleszkiewicz JA, Barnard JL (2006) Nutrient removal technology in North America and the European Union: a review. Water Qual Res J Canada 41(4):449–462

Park HD, Chang IS, Lee KJ (2015) Principles of membrane bioreactors for wastewater treatment. CRC Press, Taylor & Francis Group

Rachmani A (2013) Cost and performance comparison of a membrane bioreactor (MBR) plant and a Bardenpho plant for wastewater treatment (Thesis, Master of Engineering (ME)). University of Waikato, Hamilton, New Zealand

Santos A, Judd S (2010) The commercial status of membrane bioreacters for municipal wastewater. Separation Sci Technol 45(7):850–857

Sedlak RI (1991) Sedlak Rl (ed) Phosphorus and nitrogen removal from municipal wastewater: principles and practice, 2nd ed. The soap and Detergent Association, NY

Tchobanoglous G, Burton FL (1991) Wastewater engineering, treatment, disposal and reuse. In: Tchobanoglous G, Burton FL (eds) Water resources and environmental engineering, 3rd edn. Mc Graw-Hill, Metcalf and Eddy Inc., New York

United States Environmental Protection Agency: Process design and cost estimating algorithms for the computer assisted procedure for the design and evaluation of wastewater treatment systems (CAPDET Design Manual). Cullinane Jr. Harris, editor. Sun, U.S. EPA, Office of Water Program Operations, Washington, D.C (1982)

United States Environmental Protection Agency: Biological nutrient removal processes and costs. EPA-823-R-07–002 (2007a)

United States Environmental Protection Agency: Wastewater management fact sheet, Membrane bioreactors. September (2007b). https://www.epa.gov/sites/production/files/2019-08/documents/membrane_bioreactor_fact_sheet_p100il7g.pdf

United States Environmental Protection Agency: Municipal nutrient removal technologies reference document. Office of Wastewater Management, Municipal Support Division, Municipal Technology Division, EPA 832-R-08–006, September (2008)

United States Environmental Protection Agency: Nutrient control design manual, State of Technology Review Report, Office of research and development, National risk management research laboratory, Water supply and water resources division, EPA/600/R-09/012 (2009)

United States Environmental Protection Agency: A Compilation of Cost Data Associated with the Impacts and Control of Nutrient Pollution. EPA 820-F-15–096 (2015)

United States Environmental Protection Agency: Discharge monitoring report (DMR) Pollutant Loading Tool (2017). https://cfpub.epa.gov/dmr/

Verrecht B, Maere T, Nopens I, Brepols C, Judd S (2010) The cost of a large-scale hollow fiber MBR. Water Res 44:5274–5283

Vu MT, Price WE, He T, Zhang X, Long D, Nghiem LD (2019) Seawater-driven forward osmosis for pre-concentrating nutrients in digested sludge centrate. J Environ Manag 247:135–139

Water Environment Federation (WEF) and American Society of Civil Engineers (ASCE)/Environmental and Water Resources Institute (EWRI): Biological nutrient removal (BNR) operation in wastewater treatment plants. McGraw Hill, New York (2006)

Xiao K, Liang S, Wang X, Chen C, Huang X (2019) Current state and challenges of full-scale membrane bioreactor applications: a critical review. Biores Technol 271:473–481

Xue W, Tobino T, Nakajima F, Yamamoto K (2015) Seawater-driven forward osmosis for enriching nitrogen and phosphorous in treated municipal wastewater: effect of membrane properties and feed solution chemistry. Water Res 69:120–130

Yan T, Ye Y, Ma H, Zhang Y, Guo W, Du B, Wei Q, Wei D, Ngo HH (2018) A critical review on membrane hybrid system for nutrient recovery from wastewater. Chem Eng J 348:143–156

Zahreddine P (2018) Innovative nutrient removal technologies: case studies of intensified or enhanced treatment. ACWA Nutrients Permitting Workshop, Columbus, OH, EPA Office of Wastewater Management

Chapter 6
Analysis of the Influence of Wax Precipitation and Paraffin Control Technology on Environmental Protection

Deyin Zhao, Yi Zhao, Rongqiang Zhong, Lirong Yao, and Gaojie Liang

Abstract With the rapid development of deepwater petroleum engineering, the waxing characteristics of waxy crude oil have attracted more and more attention. In order to obtain a more accurate wax precipitation point of waxy crude oil, the test methods of wax precipitation point are summarized and compared. The test methods are classified into conventional and unconventional methods. In terms of test conditions and applicability to gas-bearing crude oil, three conventional methods (microscopic observation method, rheometer method, and differential scanning calorimetry method) were compared. It is pointed out that the test conditions should be formulated according to the actual working conditions when the wax precipitation point is determined, and the test method should be selected according to the wax crystal type and wax content. Wax deposition will block the pipeline, thus reducing the transmission efficiency of the pipeline; the residual paraffin deposit in the scrapped pipeline will penetrate into the earth and pollute the environment. Before the pipeline is scrapped, wax removal measures should be taken to remove the paraffin deposit inside, so as to protect the environment. Therefore, the research on paraffin removal and prevention of crude oil is of great significance to the normal production and environmental protection of oil wells.

Keywords Waxy crude oil · Wax precipitation point · Wax removal · Environmental protection · Pollution prevention

D. Zhao · Y. Zhao · R. Zhong · L. Yao
Sinopec Northwest Oil Field Company, Wulumuqi city, China

G. Liang (✉)
School of Civil and Engineering, Northeast Petroleum University, Daqing 163318, China
e-mail: lljdqpi@126.com

H.-Y. Jeon (ed.), *Sustainable Development of Water and Environment*,
Environmental Science and Engineering,
https://doi.org/10.1007/978-3-030-75278-1_6

6.1 Introduction

The wax content of crude oil in my country is very high, most of the oilfields have a wax content of more than 20% (Ye 2016), and some even reach 40% to 50%. Crude oil with a wax content of more than 10% accounts for almost 90% of the output oil fields. The internal factors that affect the waxing of crude oil are the wax, gum and asphaltene content in crude oil. In the process of crude oil pipeline transportation, the pipeline transportation method of mixed transportation is often used, which greatly changes the composition and properties of crude oil, which may directly affect the stable operation of the crude oil pipeline (Xuanfeng and Cheng 2019).

Crude oil is a mixed liquid composed of many components. It is mainly composed of a large amount of hydrocarbons and a small amount of nitrogen, sulfur, and oxygen compounds. In addition, most crude oils also contain a certain amount of asphaltenes and gums. Among them, the hydrocarbons contained in crude oil are mainly:alkanes, aromatic hydrocarbons, and cycloalkanes (Jiaying 2006). The oxygen-containing compounds mainly include: fatty acid, benzoic acid, etc. The asphaltenes and gums are mainly composed of heterocyclic compounds containing nitrogen, sulfur, and oxygen. Asphalt has the highest molecular weight in crude oil, and its molecular weight is more than 1,000, and it may even be as high as 100,000. Molecular weight, and the molecular weight of gum is about 800 to 1200. A large number of research results show that there are many cycloalkane rings, aromatic rings, heterocycles, etc. in asphaltenes and gums.

When waxy crude oil encounters a low temperature environment during pipeline transportation, the wax dissolved in the crude oil will precipitate and deposit on the pipe wall, resulting in a decrease in the circulation area of the pipeline, an increase in transportation pressure, and a decrease in the transportation capacity of the pipeline. If the pigging is not timely, it may cause serious blockage of the pipeline or even the pipeline scrap (Nan 2018). Lead to the leakage of residues in the pipeline, polluting the environment.

6.2 The Wax Precipitation Mechanism of Crude Oil

As the mining conditions continue to change, the phase state of the various components in the crude oil will also change accordingly. The phase state may be a liquid phase, or a gas–liquid two-phase coexistence, or even a gas–liquid-solid phase. Three-phase. The wax in crude oil usually exists in liquid form at the bottom of the well. As the pressure and temperature are reduced and some light components escape in the form of gas, the solubility of wax in crude oil becomes smaller, and some waxes will become The form of crystals gradually precipitates, and continuously aggregates, grows, and deposits, causing wax formation. The changes in the microstructure and quantity of wax crystals in waxy crude oil significantly affect the changes in macro rheological parameters such as the storage modulus and

energy consumption modulus of crude oil (Teng 2013; Wang 2011; Liu 2014; Gao 2007; Lin 2010,1982; Peng 2007).

6.2.1 Composition of Wax Deposits

Paraffin wax is one of the natural components present in crude oil. Paraffin wax is mainly a mixture of a series of normal alkanes. In addition, there are a small amount of aromatic hydrocarbons and paraffinic hydrocarbons in paraffins, but under normal circumstances, the content of these isomeric hydrocarbons is only less than 10%, but it should not be ignored that these isomeric hydrocarbons will be very large. To the extent it affects the physical and chemical properties of paraffin wax.

Pure paraffin wax is a white solid at room temperature, and its crystal lattice shape is mainly diamond-shaped flakes or needles. The proportion of wax deposits in the crude oil is Probably between 40 and 60%. Paraffin entering water source will pollute it, and paraffin volatilizing into atmosphere will pollute the atmosphere. If people inhale high concentration paraffin vapor, they will have headache, dizziness, loss of appetite, cough and other symptoms. Paraffin can accumulate in organisms, especially in fish and seaweed, thus causing damage to the respiratory system of aquatic organisms.

More than 80% of the crude oil mined in China is waxy crude oil, which has a high freezing point and poor fluidity at room temperature, which brings many problems to the production, transportation and storage of crude oil (Wenchao 2019). In order to ensure the normal and efficient exploitation of crude oil in waxy oilfield and the environmental protection treatment of abandoned pipelines, wax removal and control is a very important measure in oilfield exploitation. In China, most of the oil field waste pipeline treatment method is to clean up the residues in the pipeline, and then take on-site burial, so as to reduce the environmental pollution caused by the residues in the pipeline. In order to ensure the safe and economical operation of pipelines, waxy crude oil must be treated with wax prevention and viscosity reduction (Yang 2012).

6.2.2 Waxing Process in Oil Wells

During the flow of waxy crude oil in the pipeline, when the temperature is lower than the wax precipitation point, the paraffin wax crystallites in the crude oil continue to precipitate and aggregate into particles. The particles adsorb each other so that the paraffin wax grows and adheres to the pipe wall, causing The reduction of the pipeline flow area reduces the pipeline transportation capacity, and even blocks the pipeline in severe cases, affecting the safe operation of the pipeline. Therefore, the crude oil pipeline needs to be pigged regularly.

Generally speaking, the waxing process can be composed of three stages: (1) The waxing stage. When the temperature of the crude oil is slightly higher than the cloud

point, wax crystals begin to precipitate from the crude oil; (2) The wax crystal growth stage. When the temperature of crude oil is near the cloud point, the precipitated wax crystals continue to combine with each other, and the aggregation becomes larger, and the speed of their combination will become faster as the temperature decreases; (3) The wax deposition stage. When the temperature of the crude oil is lower than the cloud point, increasing wax crystals gradually deposit on the surface of the tubing, causing wax formation (Guosi 2015).

At the same temperature, the amount of wax crystals precipitated, the number of wax crystals and the area ratio decreased with the increase of the cooling rate. This is because as the cooling rate increases, the wax in the oil is supersaturated but is too late to precipitate, leading to the precipitation of wax crystals and the formation of wax crystal structure lag, that is, the wax precipitation phenomenon of crude oil exhibits "hysteresis". In the case of the same pipe wall temperature, the higher the temperature of the crude oil, that is, the greater the temperature difference between the crude oil and the pipe wall, the wax deposition rate will gradually increase due to the formation of a radial temperature gradient that is conducive to wax deposition (Lilin 2016). At higher temperatures, the wax crystals are dispersed in the crude oil, making the crude oil behave as a Newtonian fluid; as the temperature decreases, the wax crystal concentration increases and the size increases, and the crude oil changes from a sol to a gel state. Its storage modulus and energy consumption the modulus also changes accordingly (Chuanxian 2000; Ming Zhen 2008; Coutinho 2004; Visintin 2005). Therefore, the quantitative description of the relationship between the storage modulus, energy consumption modulus and cumulative wax precipitation of waxy crude oil is very important to further understand the elastic change mechanism of waxy crude oil (Lorge 1997; Kané 2004; Coutinho 2004).

6.3 Crude Oil Wax Precipitation Point Test Method

There are three main methods for testing the wax separation point: microscopic observation method (often using polarizing microscope CPM), viscometer/rheometer method, differential scanning calorimetry (DSC), laser method and ultrasonic method, etc. This article mainly summarizes the test methods of wax precipitation point (Wei 2018), and compares and analyzes three common methods.

6.3.1 Introduction to Conventional Methods

Microscopic observation method. The oil sample is heated until the wax is completely melted, and the temperature at which the wax crystals first appear under the observation of the polarizing microscope during the cooling process is regarded

as the wax precipitation point. The microscopic observation method is the most sensitive and intuitive for the determination of wax precipitation point. With the development of microscopic image acquisition and processing technology, in recent years, the analysis of wax crystal microscopic images has focused on quantitative characterization research, using the first step temperature of the increase in the number of particles to determine the wax-out point; image processing technology enables microscopy The result of observation method is more accurate and reliable.

Viscometer/rheometer method

Rotational viscometer method. After heating the oil sample until the solid wax turns into liquid, record the shear stress or viscosity-temperature curve. When the temperature drops to the precipitation of wax crystals in the crude oil, it will cause a turning point in the viscosity-temperature curve, and the turning point corresponds to the wax precipitation temperature.

Activation energy method. According to the principle that the wax crystals in the dispersed phase appear in the crude oil after waxing, the activation energy of viscous flow is increased, and the waxing temperature is determined by the increase of activation energy.

Differential scanning calorimetry. The oil sample begins to cool down from a certain temperature below its waxing point, and the differential heat flow between the oil sample and the reference substance at each temperature point is drawn into a differential scanning calorimetry curve (DSC curve). The temperature at which wax crystals begin to precipitate in crude oil, that is, when the DSC curve deviates from the baseline to form an exothermic peak, the corresponding starting temperature is defined as the wax precipitation point. DSC method has the characteristics of easy operation, less time-consuming and less sample consumption, fast response and good reproducibility, and is widely used in the wax precipitation point test.

Wax deposition is an important factor affecting the safety and economic operation of crude oil pipelines. It is of great significance to accurately predict the wax content of crude oil and the wax deposition law of the pipeline (Qiyu 2011). Compared with the method of calculating the wax content by the thermodynamic model, the DSC test method is simple and efficient. At present, a large number of experimental studies have proved that the wax content measured by DSC is consistent with the results obtained by other methods. The influence of DSC cooling rate on wax precipitation of waxy oil samples is analyzed here, and the optimal cooling rate is determined to ensure the accuracy of the test results (Nan 2018).

6.3.2 Comparison of Test Conditions

Scholars at home and abroad have conducted a lot of comparative studies on the three conventional methods for testing wax precipitation points (microscopic observation method, viscometer/rheometer method, and differential scanning calorimetry).

Ronningsen, Pedersen, Hansen, Cazaux, etc. all believe that the results measured by the microscopic observation method are more accurate than the viscometer method and the DSC method, but the measurement results depend on the thickness of the test piece and the cooling rate. It is found that when the wax precipitation rate of the measured crude oil is large, the results measured by the three methods are almost the same; the microscopic observation method and the viscometer method are not suitable for measuring the wax precipitation point of the crude oil with a small wax precipitation rate.

6.3.3 Introduction to Unconventional Methods

Unconventional methods include laser method, ultrasonic method, in addition, filter screen pressure difference method and infrared spectroscopy, which can also be used to measure the waxing point.

6.4 Crude Wax Removal and Wax Prevention

The wax in crude oil usually exists in liquid form at the bottom of the well. As the pressure and temperature are reduced and some light components escape in the form of gas, the solubility of wax in crude oil decreases, and some waxes will be The form of crystals gradually precipitates, and continuously gathers, grows, and deposits. Paraffin will deposit on downhole equipment, production casing, around the well wall and oil pipelines and other equipment, causing wax clogging. After the tubing is waxed, the diameter of the tubing is reduced, thereby increasing the oil flow resistance, reducing the production efficiency of the oil well, and having a great impact on oil transportation. In severe cases, it may even block the oil well and stop the exploitation of crude oil. Therefore, in order to ensure the normal extraction of crude oil in waxy oilfields, wax removal and wax prevention are a very important measure in oilfield exploitation (Jiguo 2017).

To ensure the safe and economical operation of pipelines, waxy crude oil must be treated with wax prevention and viscosity reduction. Among them, the advantages of magnetic treatment technology are simple equipment installation, convenient use, non-polluting, low cost, and long duration, which can reduce the viscosity of crude oil and improve the fluidity of crude oil in gathering pipelines (Dirand 1998; Xiubo 2005). At present, in the actual application process, it is found that the viscosity reduction effect of the magnetic processor is unstable, which is due to the insufficient understanding of the key factors that affect the magnetic treatment effect and the viscosity reduction law of the magnetic treatment (Tung 2001; Zhang 2013).

6.4.1 General Rules of Wax Deposition in Oil Wells

Light crude oil group. The wax-dissolving ability in crude oil increases as the light fractions increase, and the lower the wax precipitation temperature, the less likely it is to wax. When natural gas is separated under the bubble point pressure, the wax dissolving ability of crude oil is reduced, the wax precipitation temperature rises, and the wax deposition is intensified. In other words, the wax precipitation temperature changes with the change of the crude oil composition during the mining process (Duntong 2017).

The influence of colloid. The increase in crude oil gum and asphaltene content will change the initial temperature during wax precipitation and the wax properties after condensation. In order to facilitate the study of the influence of gums and asphaltenes on paraffin in crude oil, experiments can be carried out in a kerosene-paraffin system (The research of acoustic wave anti-wax technology has reached the international advanced level 2000).

The influence of temperature and pressure. When the pressure does not change, if the temperature rises above the wax precipitation temperature, the wax in the crude oil will not precipitate. On the contrary, when the temperature drops below the wax precipitation temperature, the wax begins to crystallize. Among the wax prevention technologies used in oil fields around the world today, there are mainly: lined tubing wax prevention, cable wax prevention, strong magnetic wax prevention, ultrasonic composite wax prevention, and chemical wax prevention (Gang 2018).

6.4.2 Wax-Proof Lined Tubing

There are two types of anti-wax technologies for lining tubing: glass tubing and coating tubing (Hongjing 2017). The wax-proof method of glass tubing is to line a layer of about 0.5 to 1.0 mm of industrial glass on the wall of the tubing, and then lower the tubing into the waxing section of the oil well.

The main wax-proof effects of the wax-proof technology for lining tubing are: (1) The lining layer has a good smoothness, and it is difficult for wax crystals to deposit on the pipe wall. (2) The inner lining layer has strong hydrophilicity, and water can form a water film when adsorbed on the surface of the pipe wall. This water film will prevent wax crystals from depositing on the pipe wall surface.

6.4.3 Cable Wax Prevention

The function principle of the cable wax prevention is that the cable is energized to release heat, and the tubing that goes into the well with the cable is heated, and

the temperature of the crude oil in the tubing increases. When the temperature of the crude oil in the tubing rises above the cloud point, the wax in the crude oil the crystals are difficult to precipitate, and they will not be deposited on the wall of the tubing, but will be taken out with the flowing oil, so as to achieve the purpose of wax prevention.

According to the wax-proof effect of the cable wax-proof in the field application: the oil well is obtained under normal production conditions, from the 1000 m section downhole to the wellhead, the cable wax-proof can keep the temperature of the flowing oil above 40 °C, which can achieve good the anti-wax effect.

6.4.4 Ultrasonic Compound Wax-Proof Technology

The combination of ultrasonic oscillator wax-proof and solid wax-removing and wax-proofing agent has formed a new wax-proof technology-ultrasonic compound wax-proof technology (Ying 2013). The theoretical basis of ultrasonic oscillator design is derived from the principle of ultrasonic. When the sonication of oscillation occurs when the oil flow passes through, it can send an effective effect to delay and destroy the crystallization of paraffin, and it can also reduce the surface tension of the crude oil. In addition, it can also make the crude oil and solid wax preventive. The agent can be fully stirred and mixed to improve the wax-proof effect.

6.4.5 Chemical Wax Prevention Technology

(1) The method of surfactant aqueous solution to achieve wax prevention is to adsorb on the surface of the wax crystal or the surface of the wax to make the polarity reversal and form a water film to prevent wax deposition on the surface.
(2) When the wax molecules have not yet precipitated, the wax inhibitor molecules will first precipitate from the crude oil, and a large number of fine and small crystal centers will be produced. At this time, the crystallites formed by the wax crystal modifier will adhere Adding paraffin alkane makes the wax crystals in a dispersed state that cannot be coalesced and increased, so the wax deposition on the surface of the equipment is greatly reduced.

The problems of chemical paraffin inhibitors in paraffin control are: Chemical wax inhibitors have relatively poor adaptability. Due to the different properties of crude oil and wax and the influence of external factors such as temperature and pressure, the choice of wax inhibitors will also change accordingly. Some paraffin removers pollute oil wells and some wax removers have high pour point, which is not suitable for winter use.

Thermal wax removal and anti-wax technology Self-energy hot washing (Hongyan 2016): From 2013 to 2015, this unit has a total of hundreds of wells with self-energy hot washing. After hot washing, the average maximum load of the well decreased by 1.43 kN, and the minimum load increased by 0.52 kN. Reduced by 1.95 kN, the effect of hot washing to remove wax is better.

6.4.6 Acoustic Viscosity Reduction and Wax Prevention Technology

Under the action of the formation pressure of oil well, the velocity of fluid accelerates through the nozzle to excite the reed to vibrate and produce the sound wave with certain frequency and amplitude. With the action of fluid, the device continuously generates sound waves and acts on the fluid. This kind of hydraulic acoustic wave generated by the spring plate by the fluid jet establishes the vibration wave field in the fluid and the surrounding medium, acts on the fluid, achieves the purpose of viscosity reduction and wax prevention, and prolongs the hot washing period of oil wells. Acoustic wax control technology is a new type of advanced technology with high efficiency and low cost. It has the characteristics of simple process, convenient management, strong adaptability, good wax prevention effect and no pollution to the formation. It is a practical technology worthy of promotion.

6.5 Conclusions

By consulting the literature, we know that when testing the wax removal point, special attention should be paid to the choice of test conditions and the choice of test methods. This is due to the close relationship between wax precipitation characteristics and temperature drop rate, and the wax precipitation point can be considered as a conditional parameter. Therefore, there is no need to stick to the specifications for the choice of test conditions. In the choice of test method, a suitable test method should be selected according to the type of wax crystal and wax content, supplemented by other methods for verification. For the problem of paraffin control in oil wells, we should choose the wax prevention and removal methods with the characteristics of simple process, convenient management, strong adaptability, good wax prevention effect and no pollution to the formation according to different geographical, climatic and economic conditions. In order to prevent pollution and protect the environment, the ultrasonic anti wax technology and magnetic treatment anti wax technology have better effect.

References

Chuan Xian L (2000) A new method to characterize the change of rheological structure of crude oil with temperature. J Univ Petrol 24(5):76–79
Coutinho JA (2004) Dynamic rheological analysis of the gelation behaviour of waxy crude oils. Rheologica Acta 43(5):433–441
Dirand M (1998) Multicomponent paraffin waxes and petroleum solid deposits: structural and thermodynamic state. Fuel 77(12):1253–1260
Duntong X (2017) Study on the wax deposition law and wax removal and prevention process of crude oil. Petrochemical Technol 24(02):15
Gang P (2018) Development and performance evaluation of chemical wax removal and anti-wax agent for oil wells. Huazhong Univ Sci Technol
Gao P (2007) Studies and studies on the relationship between viscoelasticity and microstructure of waxy crude oil. J Oil Gas 29(1):136–139
Guosi J (2015) A brief talk on the research status and development direction of oil well wax removal and inhibitors. Technol Enterp (09)233
Hongjing Y (2017) Research and application of wax removal and prevention technology. Surf Technol 46(03):130–137
Hongyan B (2016) Research and application of wax removal and control technology in ultra-low permeability oilfields. Petrochemical Ind Appl 35(12):1–5
Jiaying C (2006) Research on the technology of anti-waxing of crude oil magnetization. Harbin Institute of Technology
Jiguo D (2017) Development of a new water-based wax remover. Xi'an Shiyou University
Kané M (2004) Rheology and structure of waxy crude oils in quiescent and under shearing conditions. Fuel 83(11–12):1591–1605
Lilin Z (2016) Analysis of wax deposition characteristics of waxy crude oil pipelines. Petrochemical Technol 23(12):122
Lin S (1982) Polymer chemistry. Beijing Science Press
Lin M (2010) Characteristics and mechanism of mutual conversion between non-Newtonian waxy crude sol and gel. China University of Petroleum, Qingdao
Liu R (2014) Study on viscoelasto-plastic failure of gelatinized crude oil. China University of Petroleum, Qingdao
Lorge O (1997) Crystallisation and gelation of waxy crude oils under flowing conditions. Oil Gas Sci Technol 52(2):235–239
Ming Zhen L (2008) Studies on the gelation characteristics of waxy crude oil. Chem J Chin Univ 29(11):2239–2244
Nan L (2018) The effect of DSC cooling rate on the wax precipitation characteristics of waxy oil samples. Oil Gas Storage Transp 37(03):281–284
Nan L (2018) Numerical simulation of the temperature field of waxy crude oil in the model loop. J Beijing Inst Petrochemical Technol 26(03):46–50
Peng G (2007) Study on the relationship between the rheological properties of waxy crude oil and wax crystal morphology, structure and composition of crude oil. China University of Petroleum, Beijing
Qiyu H (2011) Wax deposit erosion experiment. Oil Gas Storage Transp 30(04):312–313
Teng H (2013) Modeling the Thixotropic behavior of waxy crude. Ind Eng Chem Res 52(23):079–8089
The research of acoustic wave anti-wax technology has reached the international advanced level. J Univ Petrol (06):79 (2000)
Tung N (2001) Studying the mechanism of magnetic field influence on paraffin crude oilviscosity and wax deposition reduction. Jakarta: SPE AsiaPacific Oi1 and Gas Conferencc and Exhihition, SPE 68789
Visintin RFG (2005) Rheological behavior and structural interpretation of waxy crude oil gels. Langmuir 21(14):6240–6249

Wang D (2011) Studies on the relationship between viscoelasticity and wax crystal structure of waxy crude. Qingdao: China University of Petroleum
Wei H (2018) A review of test methods for wax precipitation point of waxy crude oil. Contemp Chem Indus 47(07):1441–1444
Wenchao L (2019) Viscosity reduction test of waxy crude oil by static magnetic treatment[J]. Oil Gas Storage Transp 38(08):899–903
Xiubo M (2005) The mechanism of magnetic treatment of crude oil for wax prevention and viscosity reduction. J Xi'an Shiyou Univ (04):50–52
Xuanfeng Z, Cheng W (2019) Wax deposition characteristics of mixed transportation of waxy crude oil in Nanyang. Petrochemical Indus. 48(01):65–70
Yang L (2012) Research on optimization of low-volume safe operation scheme of waxy crude oil pipeline. Pipeline Technol Equipment 20(05):1–3
Ye X (2016) Oil well wax cleaning and wax removal technology prospects. Cleaning the World 30(09):19–22
Ying Z (2013) Research on the status quo of oil well cleaning and wax prevention technology. China Petrol Chem Stan Qual 33(15):67
Zhang WW (2013) The effect of magneticfield on the deposition of paraffin wax on the oil pipe. Adv Mater Res 788:719–722

Chapter 7
Impact of Abandoned Oil Well on Ecological Environment and Analysis of Geothermal Exploitation

Lirong Yao, Yi Zhao, Deyin Zhao, Rongqiang Zhong, and Jinbao Li

Abstract With the oilfield entering into the late stage of development and production, the difficulty of exploitation is increasing. The passage between the abandoned oil and gas wells and the formation is often caused by the influence of exploitation. There is the possibility of oil and gas leakage, polluting the underground water, and then causing serious environmental pollution accidents. If waste oil wells can be utilized to exploit geothermal energy, safety hazards or leakage problems caused by improper plugging can be solved, and high drilling costs can also be saved. Therefore, built on the current research status. This paper analyzes the feasibility of geothermal energy exploitation of abandoned oil Wells, discusses the retrofit technology of abandoned oil Wells and the related applications of geothermal energy, and gives reasonable suggestions for development.

Keywords Abandoned oil wells · soil environmental pollution · Geothermal energy · Research status of technology

7.1 Introduction

With the development of the oil industry in the late stage, a large number of abandoned oil wells are produced in the world. Abandoned oil wells are production wells that, after exploration and drilling, have been tested and identified as oil-free, depleted or unusable after years of exploitation. These abandoned oil wells have caused a series of serious environmental pollution and safety problems. In response to environmental degradation and fossil energy depletion, the world has in recent years been focusing on the development of new renewable energy sources in order to transform a more rational energy supply architecture. Geothermal Energy, as a

L. Yao · Y. Zhao · D. Zhao · R. Zhong
Sinopec Northwest Oil Field Company, Wulumuqi city, China

J. Li (✉)
School of Civil and Engineering, Northeast Petroleum University, Daqing 163318, China
e-mail: 747172486@qq.com

H.-Y. Jeon (ed.), *Sustainable Development of Water and Environment*,
Environmental Science and Engineering,
https://doi.org/10.1007/978-3-030-75278-1_7

new clean energy, has become the world's most potential renewable energy after hydraulic and biomass energy due to its advantages such as reproducibility, wide distribution and not restricted by spatial distribution. However, high drilling costs make it difficult to develop geothermal energy on a large scale (Bu et al. 2012). Therefore, reducing the cost of geothermal drilling is an important measure to promote the large scale utilization of geothermal energy, and exploiting geothermal resources by using abandoned wells is expected to be an effective way to solve the problem of geothermal well development cost.

7.2 Ecological and Environmental Problems in Abandoned Oil Well Area

7.2.1 Effects of Abandoned Wells on Surrounding Ecological Environment and Plants

First of all, the abandoned oil well area has not been timely ecological restoration, long-term bare ground soil becomes soft, in windy weather, it is very easy to cause sandstorm weather. Secondly, when the mine is abandoned and the hole is not tightly sealed, methane, sulfur dioxide, petroleum hydrocarbons, nitrogen oxides, hydrogen sulfide and other gases will enter the atmosphere, which will do great harm to the surrounding plants and harm human health after being inhaled. When petroleum pollutants around abandoned oil Wells enter plant leaf cells, their ability to detoxify will weaken or lose the photosynthetic capacity of leaves, resulting in injury or even death of plants. For example, in the case of acute damage to apple, the leaf tissues show speckled necrosis within a short period of time; in the case of severe damage, the leaves wither, fall off or even die; in the case of chronic damage, the lesions are invisible to the naked eye in the appearance of the fruit trees, and the physiological functions are damaged, leading to a decline in yield. When the concentration of mineral oil in soil is low, it can stimulate the growth and inhibit the growth. The harmful substances of mineral oil are absorbed and accumulated by plants, which eventually lead to the death of plants.

7.2.2 Surface Water Pollution and Soil Pollution Occurred in the Abandoned Oil Well Area

Abandoned oil Wells in the region of oil pollution mainly includes the following several ways: first is the exploitation of the untreated ground crude oil, the second is abandoned mine did not cause oil spills to block or block is lax, the third is when the oil well drilling in oil tank or oil storage box residual oil hydrocarbons, the fourth is to build in the process of mining of small oil tank contains petroleum

hydrocarbons. When these pollution sources encounter precipitation, some of them enter the soil and pollute the soil; some enter the river and pollute the water body along with surface water runoff; and some migrate to the underground and pollute the groundwater, causing damage to the surrounding water environment and soil environment and other ecosystems. Soil pollution caused by crude oil is usually caused by scattering during well testing, well flushing and underground operation. Drilling wastes entering the soil will aggravate soil salinization. The waste drilling mud contains a certain amount of oil, which is eroded by precipitation and causes local soil pollution.

Therefore, it is imperative to solve the problems of abandoned oil Wells, such as potential safety hazards and leakage pollution of soil environment. Some scholars around the world have proposed to use waste oil Wells to exploit geothermal energy and turn them into geothermal Wells through technological transformation, which can not only eliminate environmental pollution and turn waste into treasure, but also create new ways to exploit geothermal energy.

7.3 Feasibility Analysis of Geothermal Energy Development in Abandoned Oil Wells

Generally, the geothermal resources of the oil-bearing basin where the abandoned Oil wells is located are abundant, and the geothermal gradients and terrestrial heat flow values are relatively high. Take Shengli Oilfield for example, most of its oil wells have a depth of 1000–3000 m, and the temperature of the produced liquid can reach 60–100 °C, and some of them are even higher (Liu 2001), which can be used for the transformation from abandoned wells to geothermal wells.

In addition, geothermal well reconstruction using abandoned wells has many advantages (Davis 2009; Wang et al. 2016): (i) Existing well-born can be used for reconstruction, so as to significantly reduce drilling costs; (ii) It can reduce the cost of well sealing and the expenditure of equipment inspection and maintenance in the later stage; (iii) The existing production data (mainly reservoir thermal and physical property data) can be used to formulate a scientific and reasonable geothermal development plan; (iv) Can provide energy for oil field production and create income; (v) It is conducive to the popularization and utilization of geothermal energy in China; (vi) It is conducive to the scientific and efficient development of resources.

In order to better obtain geothermal resources from abandoned wells, scholars at home and abroad have conducted a large number of numerical simulation studies and field test studies. A relatively complete theoretical system of development and utilization has been formed, and rich experience in field reconstruction has been accumulated, which proves that geothermal development of abandoned wells has a good feasibility.

Kujawa et al. (2005, 2006), Nian and Cheng (2018) first used water as the circulating working fluid to obtain geothermal energy in the formation by using abandoned

wells, and established the heat transfer model between the concentric tube heat exchanger and the formation. Davis and Michaelides (2009) used an abandoned well with a depth of 3,000 m for power generation, studied the ability of using isobutane as working medium to obtain geothermal energy from the abandoned well, and believed that the maximum power depends largely on bottom hole temperature and injection pressure. Cheng et al. (2013, 2014) studied the influence of seven different organic working substances on the heat extraction effect, established a single well bore heat transfer model of an abandoned oil well with a depth of 6,000 m, and studied the influence of factors such as insulation pipe thickness on outlet temperature. Bu et al. (2012) proposed a transient model considering the heat transfer of surrounding rocks of abandoned wells, and simulated the rock temperature distribution in the process of power generation, and concluded that the performance of coaxial heat exchangers depends on the working medium flow rate and geothermal gradient. Noorollahi et al. (2015) used three-dimensional technology to simulate the heat transfer between the fluid injected into the well and the surrounding hot rock in two oil wells in southern Iran, with bottom hole temperatures of 138.7 °C and 159.8 °C respectively. The results demonstrate that in addition to the thermal gradient and the input mass flow rate, the geometry of the casing and the size of the injection and extraction pipes are essential for the output heat extraction rate. The small inner diameter of the well and the design of the injection and extraction pipes are limited, resulting in lower mass flow and higher power consumption of the injection pump. Caulk and Tomac (2017) studied the applicability of transforming abandoned wells in California into BHE and EGS. The research shows that when the temperature gradient is 7 °C/100 m in 1000 m deep wells, the liquid outlet temperature can be higher than 40 °C. Although the production temperature is higher at the low flow rate, the COP is higher at depth (5000 m) and medium flow rate (4.4 L/S). At present, the flow rate of 0.8–6.0 L/S is used in deep BHE for district heating of various buildings in Europe. Liang et al. (2017) studied and concluded that the most important factors affecting outlet temperature of working medium were inlet temperature, geothermal gradient and mass flow rate, taking abandoned oil wells as injection and production wells and high-temperature dissolved cavity as the main heat storage. They believed that the above factors should be considered in the actual mining process.

In addition to numerical simulation, field tests of geothermal wells with abandoned wells have also been carried out. Kohl et al. (2002) studied the waste well heat exchanger system that had been operating in Switzerland for several years, and concluded that its production temperature could still reach 40 °C. Westphal and Weijermars (2018) carried out field tests, using the abandoned oil well with a bottom temperature close to 70 °C to extract underground heat to drive the air conditioning system, and achieved success. Domestic oil well heating test has also been performed. Hua and Zhonghao (2007), based on the analysis of the geological characteristics of Dagang oilfield, proposed three methods of transforming the abandoned oil wells into geothermal wells with low cost and short time limit, namely, sunroof sideway drilling method, direct perforation method and pump room perforation method, and the feasibility of the transformation method was verified by application examples.

Wei et al. (2009) carried out geothermal resource evaluation, geothermal development drainage and injection research, geothermal field development and utilization research, and geothermal field development economic evaluation research to optimize the exploitation method and drainage and production equipment of old oil wells to geothermal wells. Field tests of 5 wells prove that it is of great significance to developing new energy construction industry and enhance the comprehensive strength of enterprise development.

7.4 Technology of Wasting Well Reconstruction and Application of Geothermal Energy

7.4.1 Selection of Abandoned Wells

There are many abandoned Oil and Gas wells, not all of them are suitable for reconstruction and reuse. abandoned wells in the process of transformation, the target well selection should follow the following principles: (i) there are geothermal development value of the abandoned wells, have higher porosity and permeability reservoir temperature, the better (using open system), the physical parameters need to be according to the analysis of the existing historical data, and to evaluate the economic value of the target well; (ii) The generated heat should be easy to use. Geothermal power stations (for power generation) and residential areas (for refrigeration and heating and bathing) should be located around the abandoned wells. Excessive heat loss caused by a long heating path should be avoided as far as possible; (iii) abandoned wells with casing completion should be selected as far as possible to facilitate later reconstruction; (iv) With a reasonable spacing between injection and production wells, the distance between two wells should be no less than 40 m, so as to avoid inter-well interaction and cause premature thermal breakthrough. In conclusion, numerous factors should be taken into consideration in the selection of abandoned wells, and the comprehensive evaluation of their screening indicators will be the focus of future research.

7.4.2 Retrofit of Abandoned Well and Way of Heating Extraction

At present, heat extraction from EGS or BHE is the focus of the study on the reconstruction of abandoned wells. EGS is mainly composed of Injection wells, Production wells, heat storage and surface facilities, etc. This method was previously mainly used for dry and hot rock advance. The working mode is as follows: firstly, artificial hydraulic fracturing is performed on the target thermal reservoir section; then, the working medium with good thermal conductivity is pumped into the formation

through the injection well; after full contact with the fracture network of high temperature rock mass, the working medium entering the thermal reservoir is produced from the production well in the form of high temperature steam and converted into electric energy by the ground power generation unit (Dengwei et al. 2006). After that, the working medium is pumped into the formation again for circulating heat extraction. Different from EGS, the heat extraction efficiency of BHE depends on the heat exchanger configuration and thermal properties of the heat storage rock, rather than hydraulic properties such as porosity and permeability, mainly because the circulating working medium does not have direct contact with the heat storage during the heat extraction process.

7.4.3 Application of Thermal Energy from Abandoned Wells

Normally, geothermal heat sources can be divided into three types: high temperature (> 150 °C), medium temperature (90–150 °C) and low temperature (< 90 °C). The waste well heat source generally belongs to the medium–low temperature geothermal resources, low temperature can be used for bathing, heating and refrigeration, and medium–high temperature can be combined with advanced energy conversion devices for industrial power generation (Davis 2009). Electricity generation in the Organic Rankine Cycle (ORC) requires an outlet temperature of at least 74 °C (GeoHeat Center 2006), and the fluid temperature generated by many oil and gas wells in the world is 65–150 °C. Therefore, theoretically, this system can be utilized to electricity generation (Liu et al. 2018). Moreover, treating water produced by oil of wells is also an important way to utilize the heat produced by the abandoned wells. During the oil and gas produced water always exists and is gradually increasing proportion, produced water contain a higher total soluble solid, total dissolved solids, TDS), the need for desalination processing, and isolated oil composition, formation of minerals, chemicals, and dissolved gas (Torres et al. 2016). Depending on statistics, nearly 2.5 $\times 10^{12}$ L of produced water can be obtained every year for the extraction and utilization of a large number of by-products (Gregory et al. 2011). Relevant studies have shown that 4,000 m deep wells with a geothermal gradient of 0.05 °C/m can provide nearly 600,000 L of clean water per day (Kiaghadi et al. 2017). In the process of treatment of produced water, the cost of power can account for 60% of the total treatment cost (Kiss et al. 2012). The development and promotion of membrane distillation (Duong et al. 2016) technologies mean that it is possible to use the low-temperature heat source provided by the abandoned wells to treat the high-TDS produced water. In terms of power supply for the desalination plant, geothermal energy is more stable than the most common solar energy at present, which also indicates that the heat produced by the abandoned wells will be more commonly used in oil fields.

7.5 Conclusions

There are a large number of abandoned oil Wells in the world. If these abandoned Wells cannot be plugged in time, they will cause serious environmental pollution. However, formation temperature gradients in the areas where these abandoned Wells are located are generally higher. Exploiting these geothermal resources through abandoned wells is an essential way to reuse the abandoned wells. The thermal energy from abandoned wells has a good application prospect in the fields of power generation, heating and refrigeration, treatment of oil well water production, development of oil well heat tracing, drying of agricultural products, ore recovery and aquaculture. In the process of waste well reconstruction, it is very important to collect geothermal and hydrogeological data in the early stage, so it is necessary to demonstrate and evaluate water quantity, water temperature, recharge rate, feasibility of reconstruction plan and construction cost. The development of geothermal resources is mainly about how to use different technological methods to drill geothermal Wells at different depths and bring geothermal energy to the ground to make full use of it. However, due to the high cost of specialized development and high geological risk, the abandoned Oil Wells in the exploration and development process can be developed into valuable geothermal Wells combined with technical transformation. Field tests and numerical simulation have proved that it is completely feasible technically, with low cost, high application value and broad market prospect. It should be pointed out that the research and development of thermal energy from abandoned wells are of great significance to the scientific utilization of renewable resources, the alleviation of energy pressure, the optimization of energy structure and the realization of green and low-carbon development in China.

References

Bu X, Ma W, Li H (2012) Geothermal energy production utilizing abandoned oil and gas wells. Renewable Energy 41:80–85

Caulk R, Tomac I (2017) Reuse of abandoned oil and gas wells for geothermal energy production. Renewable Energy 112:388–397

Cheng W, Li T, Nian Y et al (2013) Studies on geothermal power generation using abandoned oil wells. Energy 59:248–254

Cheng W, Li T, Nian Y et al (2014) Evaluation of working fluids for geothermal power generation from abandoned oil wells. Appl Energy 118:238–245

Davis AP (2009) Geothermal power production from abandoned oil wells. The University of Texas at San Antonio, San Antonio

Davis AP, Michaelides EE (2009) Geothermal power production from abandoned oil wells. Energy 34(7):866–872

Dengwei L, Liehui Z, Liaoping G et al (2006) Alternative and renewable energies of China in the 21st century. Nat Gas Ind 26(5):1–4

Duong HC, Cooper P, Nelemans B et al (2016) Evaluating energy consumption of air gap membrane distillation for seawater desalination at pilot scale level. Sep Purif Technol 166:55–62

Geo-Heat Center (2006) Oregon Institute of Technology. Hot springs power & ice. Geo-Heat Center Quarterly Bulletin 27(3):1–18
Gregory KB, Vidic RD, Dzombak DA (2011) Water management challenges associated with the production of shale gas by hydraulic fracturing. Elements 7(3):181–186
Hua Z, Zhonghao M (2007) Methods for transforming abandoned oil well into geothermal well. Gas Heat 27(1):47–50
Kiaghadi A, Sobel RS, Rifai HS (2017) Modeling geothermal energy efficiency from abandoned oil and gas wells to desalinate produced water. Desalination 414:51–62
Kiss AA, Flores LSJ, Infante FCA (2012) Towards energy efficient distillation technologies—making the right choice. Energy 47(1):531–542
Kohl T, Brenni R, Eugster W (2002) System performance of a deep borehole heat exchanger. Geothermics 31:687–708
Kujawa T, Nowak W, Stachel AA (2005) Analysis of the exploitation of existing deep production wells for acquiring geothermal energy. J Eng Phys Thermophys 78:127–135
Kujawa T, Nowak W, Stachel AA (2006) Utilization of existing deep geological wells for acquisitions of geothermal energy. Energy 31(5):650–664
Liang C, Chen K, Zheng H (2017) Numerical simulation of exploiting geothermal energy using abandoned oil well and hot cavity. Acta Energiae Solaris Sinica 38(2):386–392
Liu Y (2001) Research on Dongying geothermal resources. Geoth Energy 2001(4):8–12
Liu X, Falcone G, Alimonti C (2018) A systematic study of harnessing low-temperature geothermal energy from oil and gas reservoirs. Energy 142:346–355
Nian Y, Cheng W (2018) Insights into geothermal utilization of abandoned oil and gas wells
Noorollahi Y, Pourarshad M, Jalilinasrabady S et al (2015) Numerical simulation of power production from abandoned oil wells in Ahwaz oil field in southern Iran. Geothermics 55:16–23
The research of acoustic wave anti-wax technology has reached the international advanced level. J University Petroleum (06):79(2000)
Torres L, Yadav OP, Khan E (2016) A review on risk assessment techniques for hydraulic fracturing water and produced water management implemented in onshore unconventional oil and gas production. Sci Total Environ 539:478–493
Wang S, Yan J, Li F et al (2016) Exploitation and utilization of oilfield geothermal resources in China. Energies 9(10):798–811
Wei Y, Wang F, Ren B (2009) Drainage and production by using geothermal in Huabei oil region. Oil Drilling Prod Technol 31(supplement 1):93–95,100
Westphal D, Weijermars R (2018) Economic appraisal and scoping of geothermal energy extraction projects using depleted hydrocarbon wells. Energ Strat Rev 22:348–364

Chapter 8
Numerical Evaluation of the Temperature Distribution in a Tree Trunk in a Forest Fire Environment

Eusébio Conceição, João Gomes, Maria Manuela Lúcio, Jorge Raposo, Domingos Xavier, and Maria Teresa Viegas

Abstract The numerical simulation presented in this paper is focused on the development of a numerical model used to calculate the evolution of the temperature distribution in a tree trunk when it is affected by the passing of a fire front. The purpose is to assess which points on the tree trunk exceed the tree lethal threshold. Heat conduction inside the trunk tree, heat convection between the tree trunk surface and the air environment and heat exchange by radiation between the trunk surface and the surrounding body surfaces are thermal phenomena considered in the numerical model. The case considered in the numerical simulation is characterized by the propagation of a fire front at a constant fire spread rate from a distance of 5 m upstream of the tree trunk to a distance of 25 m downstream of the tree trunk. The tree trunk has a height of 2 m and a diameter of 0.3 m. The fire front has a flame temperature of 1000 °C, a fire spread rate of 0.01 m/s, a tilt angle of 45°, 10 m wide and 1.2 m high. The results obtained demonstrate that the tissues of the tree trunk located on its surface and in the first layers below its surface will die due to the temperatures calculated there being above the tree lethal threshold.

Keywords Front fire · Grid generation · Lethal threshold · Numerical simulation · Trunk tree

E. Conceição (✉) · M. M. Lúcio
FCT-Universidade do Algarve, Campus de Gambelas, 8005-139 Faro, Portugal
e-mail: econcei@ualg.pt

E. Conceição · J. Gomes
CINTAL, Campus de Gambelas, 8005-139 Faro, Portugal

J. Raposo · D. Xavier · M. T. Viegas
FCT-Universidade de Coimbra, Pinhal de Marrocos, Pólo II, 3030-290 Coimbra, Portugal

E. Conceição · J. Raposo · D. Xavier · M. T. Viegas
ADAI, Pedro Hispano 12, 3030-289 Coimbra, Portugal

H.-Y. Jeon (ed.), *Sustainable Development of Water and Environment*,
Environmental Science and Engineering,
https://doi.org/10.1007/978-3-030-75278-1_8

8.1 Introduction

In Portugal, forests occupy about 39% of its mainland, with maritime pine ("pinus pinaster") being the predominant species (ICNF 2020). Portugal also has the highest incidence of forest fires in Europe (Botequim et al. 2017; Carvalho et al. 2010), with more than 20,000 occurrences of annual fires usually reported in previous years (Radovanovic et al. 2019). These forest fires cause negative impacts on "carbon storage, biodiversity conservation, hydrologic processes, and economic and social services" (Bowman 2009). It is therefore important to understand the behavior of fire and how it harms and kills trees. The mechanism of direct tree death from fire is the cambium necrosis via heat transfer by convection, conduction, and radiation to the crown, stem and root tissue (Sharon et al. 2018). All three processes can cause tree injury and mortality. The lethal threshold for trees is obtain for temperatures above or equal to 60 °C, although longer exposure at lower temperatures can also cause tissue death (Kelsey and Westlind 2017).

This article describes a preliminary study focused on the development of a model that calculates the evolution of the temperature inside the tree and thereby evaluating the points of the tree that equal or exceed the lethal threshold in the presence of a forest fire. The numerical model developed in this work is based on the geometry of the human body, applied on the model that simulates the thermal response of the human body. The application of this model can be seen in the studies by Conceição (Conceição 1999, 2000), Conceição and Lúcio (Conceição and Lúcio 2001, 2016), and Conceição et al. (Conceição et al. 2007, 2010a, 2013).

The numerical model analyzes the thermal behavior inside the tree using differential energy equations and the generalized mesh. At the boundary between the tree and the outside, the model considers energy balance equations: by conduction, with the interior of the tree; by natural, forced and mixed convection, between the surface of the tree and the outside environment; by radiation, between the surface of the tree and the surrounding environment and between the surface of the tree and the fire front.

In the calculation of radiative exchanges, a procedure similar to heat exchanges between surfaces inside building compartments is used. This procedure is implemented in the thermal response model of buildings with complex topology. Its application can be seen in the following works by Conceição et al. (Conceição et al. 2000, 2008, 2009, 2010b, 2018) and Conceição and Lúcio (Conceição and Lúcio 2009, 2010). In calculating the temperature distribution inside the tree an implicit model of finite differences is used.

The aim of this work is to apply a numerical model that uses adaptive mesh generation to determine the temperature field inside a trunk of a tree in transient conditions. The knowledge of this temperature distribution, caused by the presence of a forest fire front, will allow to identify the location of dead tissues inside the trunk due to the value of its lethal threshold having been reached.

8.2 Numerical Model

In the tree trunk, the following thermal phenomena are considered: heat conduction inside the tree, heat convection between the tree surface and the air environment and heat exchange by radiation between the trunk surface and the surrounding body surfaces, namely, the fire front, the fuel bed and the sky.

The hypothesis used to write the energy balance equations are the following:

- The heat flux is treated as two dimensional;
- The air temperature around the trunk, that is uniform and equal to the environment temperature, increases when the fire front approaches the tree;
- Use of heat transfer coefficients by convection developed for isothermal surfaces;
- The trunk is composed by bark and cambium;
- The fire effects around the trunk are not considered.

The type of grid used in the numerical simulation influences the results. In this study a numerical grid generation where the mesh is adapted to the body surface contours was developed using the finite difference method approach. In this adaptive grid generation, a physical space and a computational space were considered. The idea of this method consists of transforming the physical domain into the computational plan. This grid transformation is done by two elliptic partial differential equations, of Poisson's type. The adaptive grid generation used in this work can be seen in Fig. 8.1. The data input of this model are the wind speed, the fire front conditions (dimensions, inclination, flame temperature, fire rate spread), the tree dimensions, initial distance of the fire front from the tree and other initial conditions.

8.3 Numerical Methodology

The scheme of the forest fire scenery used in the numerical simulation is presented in the Fig. 8.2. This scheme is constituted by an inclined fire front, tree trunk and a fuel bed. Figure 8.2 also shows the symbology used in the representation of the wind speed (v_{air}), the fire spread rate (R), the dimensions of the fire front and the tree trunk. The fuel bed is considered to have finite dimensions $a \times b$.

The simulation analyzes the situation in which the fire front moves at a constant fire spread rate from a distance of 5 m upstream of the tree trunk to a distance of 25 m downstream of the tree trunk. The input data of the simulation are present in Table 8.1. The output data of the simulation are the temperature distribution obtained in a plane that cuts the tree at a height of 2 m at 30 points (P) equidistant distributed along the bark of the tree trunk, Fig. 8.3, and at 20 points (Q) distributed along the radius of the tree trunk, Fig. 8.4. In Fig. 8.4, the line of points chosen is in a plane perpendicular to the direction of propagation of the fire front.

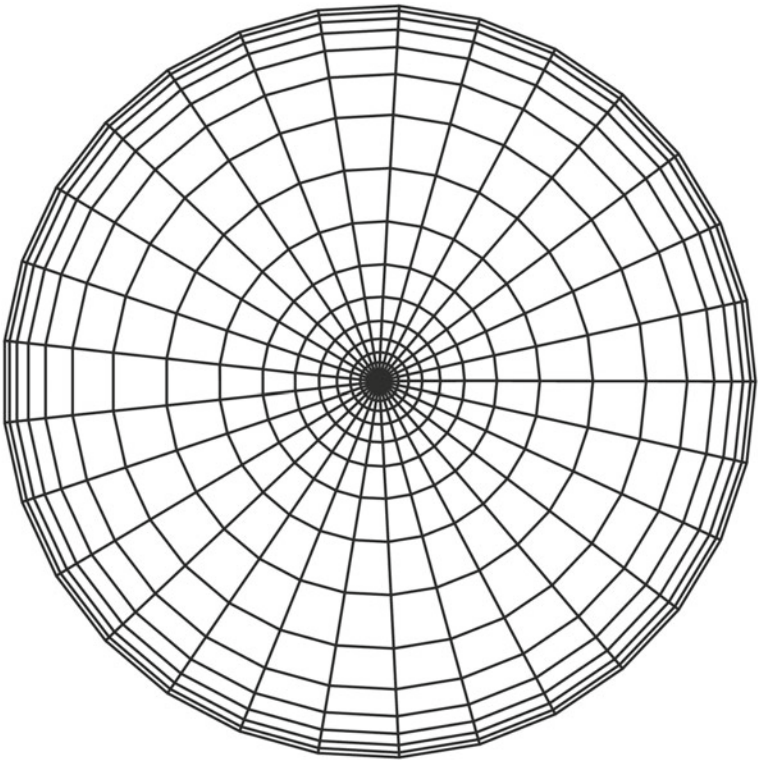

Fig. 8.1 Adaptive grid generation used in the tree trunk (30 × 20 grid points)

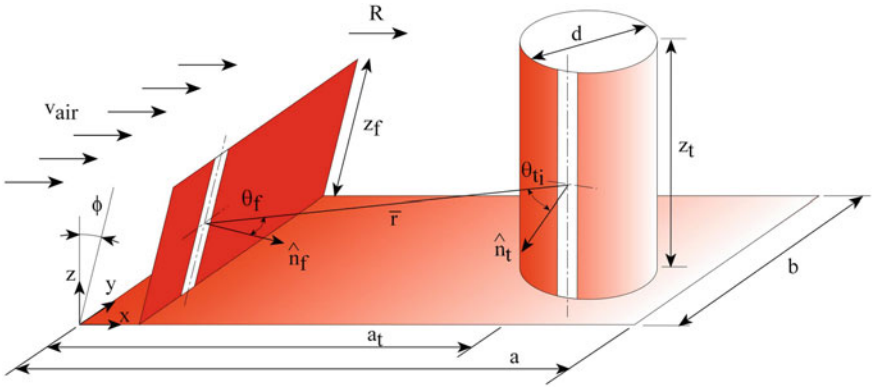

Fig. 8.2 Scheme of the forest fire scenery used in the numerical simulation

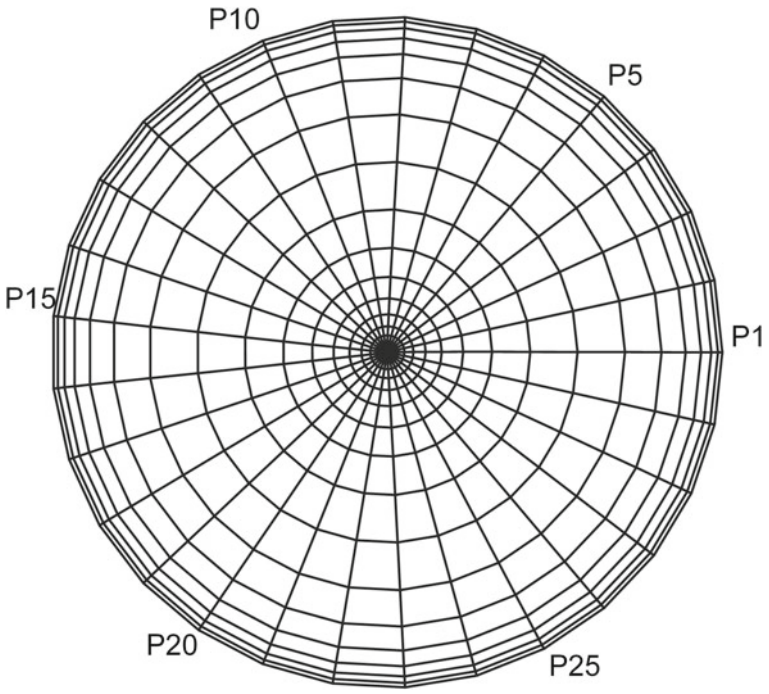

Fig. 8.3 Location of the 30 points distributed along the bark of the tree trunk where the temperature is numerically calculated

8.4 Results and Discussion

The evolution of the temperature values obtained at points P1–P15 (see Fig. 8.3), located on the bark of the tree trunk facing upstream of the fire front, can be seen in Fig. 8.5. The evolution of the temperature values obtained at points P16–P30 (see Fig. 8.3), located on the bark of the tree trunk of the beam downstream of the fire front, can be seen in Fig. 8.6. The evolution of the temperature values obtained at points Q1–Q20 (see Fig. 8.4), located on the line of the tree trunk radius, can be seen in Fig. 8.7. In Figs. 8.5, 8.6 and 8.7, the dashed line represents the tree trunk lethal threshold ($T_{trunk} \geq 60$ °C).

The temperature values in the tree trunk bark on the upstream side of the fire front are much higher when approaching than after the passage of the fire front. On the other hand, the temperature values in the tree trunk bark on the downstream side of the fire front are much higher after passing than when approaching the fire front. The temperatures reached are higher on the upstream side than on the downstream side of the fire front. The highest temperatures obtained in the tree trunk bark on the upstream and downstream side were, respectively, 515 °C and 276 °C. The lethal threshold of the tree trunk bark was reached more quickly on the upstream side than on the downstream side. All points on the upstream side reached the lethal threshold

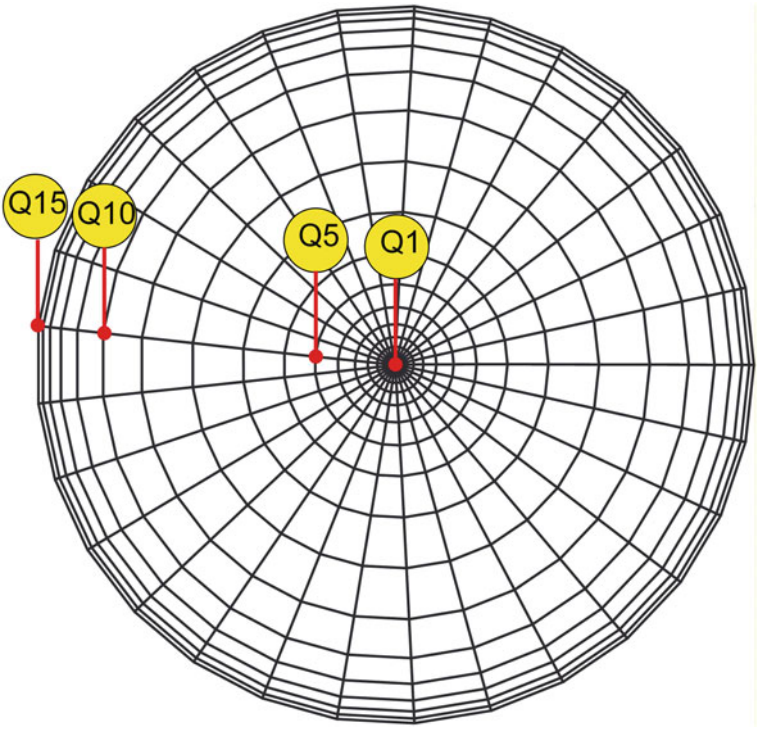

Fig. 8.4 Location of the 20 points distributed along the radius of the tree trunk where the temperature is numerically calculated

Table 8.1 Input data of the numerical simulation

Fire front	
Flame temperature (T_f)	1000 °C
Height (z_f)	1.2 m
Width (b)	10 m
Tilt angle (ϕ)	45°
Fire spread rate (R)	0.01 m/s
Tree Trunk	
Height (z_t)	2 m
Diameter (d)	0.3 m
Others	
Wind speed (v_{air})	0.1 m/s
Environmental air temperature (T_{air})	20 °C
Fuel bed length (a)	30 m

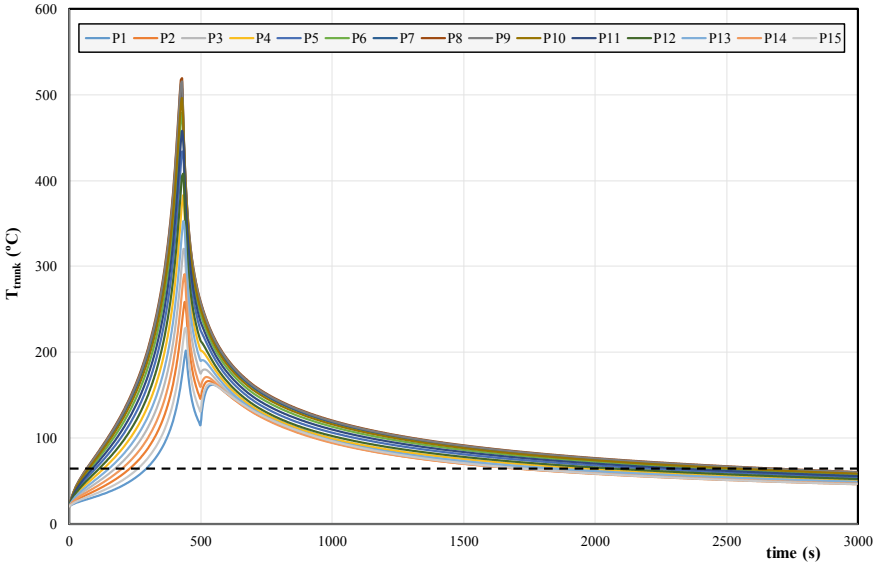

Fig. 8.5 Evolution of the temperature values obtained at points P1–P15, located on the bark of the tree trunk facing upstream of the fire front. The dashed line represents the tree trunk lethal threshold ($T_{trunk} \geq 60$ °C)

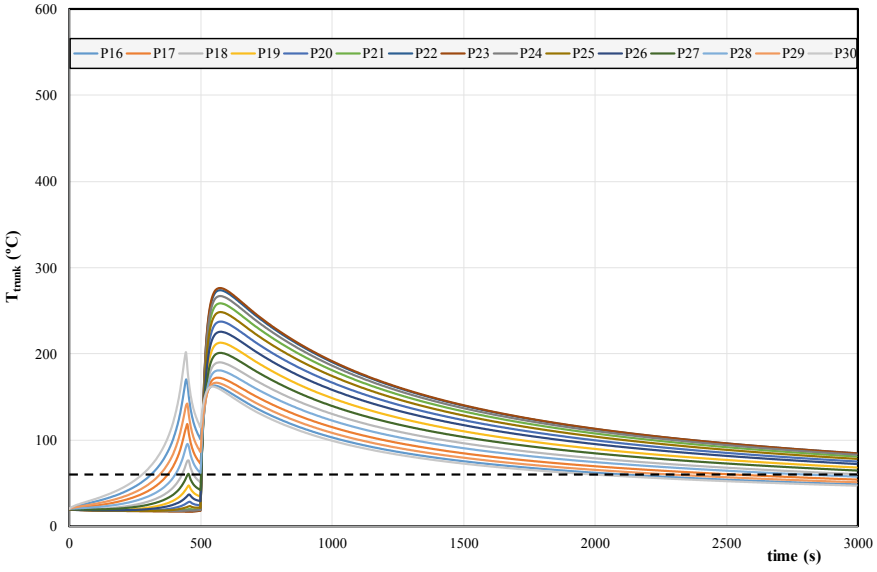

Fig. 8.6 Evolution of the temperature values obtained at points P16–P30, located on the bark of the tree trunk facing downstream of the fire front. The dashed line represents the tree trunk lethal threshold ($T_{trunk} \geq 60$ °C)

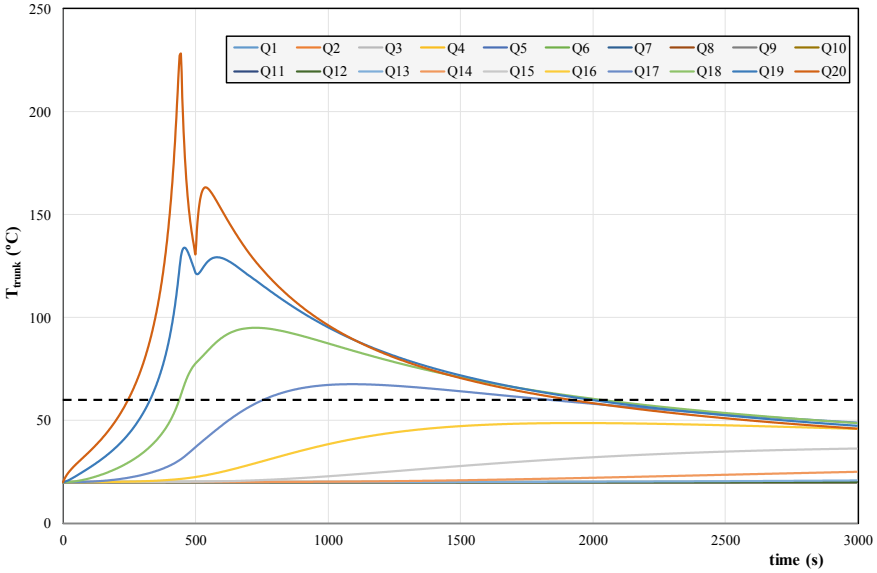

Fig. 8.7 Evolution of the temperature values obtained at points Q1–Q20, located on the line of the tree trunk radius. The dashed line represents the tree trunk lethal threshold ($T_{trunk} \geq 60$ °C)

before 280 s, while on the downstream side the lethal threshold was only reached on all points at 500 s of simulation time. The temperature at all points on the tree trunk bark upstream side drops below the lethal threshold after approximately 2500 s of simulation time. On the tree trunk bark downstream side, in general, after the passage of the fire front through the tree trunk, the temperature in almost all points remains above the lethal threshold during the simulation time.

The temperatures obtained in the core of the tree trunk are lower than those obtained in the tree trunk bark. The temperatures obtained in the outer rings of the tree trunk are higher than those obtained in the rings closer to the center of the tree trunk. The highest temperature (228 °C) was reached in the outermost ring of the tree trunk. The results of the temperature evolution obtained in points Q17–Q20 show that the lethal threshold is only reached in the 4 outer rings. The lethal threshold is reached in different simulation times; in the outermost ring of the trunk tree it is reached after about 60 s. The innermost rings of the trunk tree are little affected by the fire front, showing a temperature evolution around 20 °C.

The tree trunk before the progression of a fire front, with a flame temperature of 1000 °C, suffers different consequences and at different times: all the tissues of the bark die, while only the outermost tissues of the trunk die; the tissues of its bark die faster than those of its core; and the tissues of its bark upstream die faster than those of its bark downstream of the fire front.

8.5 Conclusion

This paper presents a preliminary study about the development of a numerical model used to calculate the evolution of the temperature distribution in a tree trunk in the presence of a fire front. Knowing this temperature distribution, it will be possible to identify the points on the tree that will reach the tree's lethal threshold and thus know the tree tissues that were damaged and those that died.

The main results obtained show that, in general, the temperatures in the tree trunk bark on the upstream side of the fire front are higher than that on the downstream side. The temperatures in the core of the tree trunk are lower than the temperatures in the tree trunk bark. The lethal threshold of the tree trunk is reached most quickly in its bark on the upstream side of the fire front. Only the points analyzed in the four outer rings of the tree trunk reach the lethal threshold.

Thus, it is confirmed that the area most damaged by the fire front is located on the surface of the tree trunk and in the first layers below its surface. In these areas the tree's tissues die. However, as only the most superficial layers of the tree trunk are severely affected, a good cleaning of the combustible material around the tree trunk and an efficient pruning of the tree trunk to a height of 2 m will allow the tree to recover from the damages suffered by forest fire.

In future works, the influence of the flame temperature, the fire spread rate, the wind speed, and others variables, on the temperature distribution in the tree will be analyzed.

Acknowledgements The authors would like to acknowledge the support of the project reference PCIF/MPG/0108/2017, funded by the Portuguese Foundation of Science and Technology (FCT).

References

Botequim B, Arias-Rodil M, Garcia-Gonzalo J, Silva A, Marques S, Borges J, Oliveira M, Tomé M (2017) Modeling post-fire mortality in pure and mixed forest stands in Portugal—a forest planning-oriented model. Sustainability 9:390

Bowman D et al (2009) Fire in the Earth system. Science 324:481–484

Carvalho A, Flannigan M, Logan K, Johnston L, Miranda A, Borrego C (2010) The impact of spatial resolution on area burned and fire occurrence projections in Portugal under climate change. Clim Change 98:177–197

Conceição E (1999) Avaliação de condições de conforto térmico: simulação numérica do sistema térmico do corpo humano e do vestuário. V Iberia and Inter-American Air Conditioning and Refrigeration Congress, CIAR'99, Lisbon, Portugal

Conceição E (2000) Evaluation of thermal comfort and local discomfort conditions using the numerical modelling of the human and clothing thermal system. In: Proceedings of the 7th International Conference on Air Distribution in Rooms, RoomVent 2000, Reading, UK

Conceição E, Lúcio M (2001) Numerical and subjective responses of human thermal sensation. In: Proceedings of the 6th Portuguese Conference on Biomedical Engineering, Faro, Portugal

Conceição E, Lúcio M (2009) Numerical study of the thermal efficiency of a school building with complex topology for different orientations. Indoor Built Environ 18(1):41–51

Conceição E, Lúcio M (2010) Numerical simulation of passive and active solar strategies in building with complex topology. Build Simul 3:245–261
Conceição E, Lúcio M (2016) Numerical simulation of the application of solar radiant systems, internal airflow and occupants' presence in the improvement of comfort in winter conditions. Buildings 6(3):38
Conceição E, Silva M, André J, Viegas D (2000) Thermal behaviour simulation of the passenger compartment of vehicles. Int J Veh Des 24(4):372–387
Conceição E, Lúcio M, Farinho J (2007) Experimental and numerical study of personalized of ventilation in classrooms desks. In: Proceedings of the 10th International Conference on Air Distribution in Rooms, Helsinki, Finland
Conceição E, Lúcio M, Lopes M (2008) Application of an indoor greenhouse in the energy and thermal comfort performance in a kindergarten school building in the south of Portugal in winter conditions. WSEAS Trans Environ Dev 4:644–654
Conceição E, Lúcio M, Ruano A, Crispim E (2009) Development of a temperature control model used in HVAC systems in school spaces in Mediterranean climate. Build Environ 44(5):871–877
Conceição E, Rosa S, Custódio A, Andrade R, Meira M, Lúcio M (2010a) Study of airflow around occupants seated in desks equipped with upper and lower air terminal devices for slightly warm environments. HVAC&R Research 16(4):401–412
Conceição E, Nunes A, Gomes J, Lúcio M (2010b) Application of a school building thermal response numerical model in the evolution of the adaptive thermal comfort level in the Mediterranean environment. Int J Vent 9(3):287–304
Conceição E, Lúcio M, Awbi H (2013) Comfort and airflow evaluation in spaces equipped with mixing ventilation and cold radiant floor. Build Simul 6:51–67
Conceição E, Gomes J, Ruano A (2018) Application of HVAC systems with control based on PMV index in university buildings with complex topology. IFAC PapersOnLine 51(10):20–25
ICNF – Instituto de Conservação da Natureza e das Florestas. 6° Inventário Florestal Nacional (IFN6), http://www2.icnf.pt/portal/florestas/ifn/ifn6. Accessed 13 Dec 2020
Kelsey R, Westlind D (2017) Physiological stress and ethanol accumulation in tree stems and woody tissues at sublethal temperatures from fire. Bioscience 67:443–451
Radovanovic M, Vyklyuk Y, Stevancevic M, Milenkovic M, Jakovljevic D, Petrovic M, Milicevic S, Vukovic N, Vujko A, Yamashkin A, Sydor P, Vukovic D, Skoda M (2019) Forest fires in Portugal—case study. Therm Sci 23(1):7–86
Sharon M, Varner J, van Mantgem P, Cansler C (2018) Fire and tree death: understanding and improving modeling of fire-induced tree mortality. Environ Res Lett 13, 113004

Chapter 9
Analysis of Soluble Organic Polar Fractions from Sea Salt by GC–MS

Guo-hua Chang, Kang-ping Zhao, Bin Yue, Zhuo-xin Yin, Xiao-ke Li, and Hai-li Sun

Abstract In order to investigate the organic compounds from sea salt, soluble organic polar fractions as a result of chloroform extraction followed by being esterified with BF_3 in methanol were determined using gas chromatography-mass spectrometry (GC–MS). There were greater than 20 soluble organic polar fractions presented in sea salt, and the major components were C_{15}–C_{28} fatty acid compounds series, plasticizers and sulfur. The total amount of fatty acids accounted for more than 50%, and C_{16} was the main peak. The relative abundance of *n*-hexadecanoic acid was the highest (41.19%) among the soluble organic polar fractions from the analyzed sample. At the same time, a certain amount of phthalate acid esters (PAEs) such as dibutyl phthalate (DBP), diisobutyl phthalate (DIBP) and bis(2-ethylhexyl) phathalate (DEHP) and sulfur (S6, S7 and S8) were detected, and the contents of the two component types were relatively close. Among the three PAEs, the relative abundance of DIBP (17.678%) was the highest. Further, their effects on marine organisms and ecosystem should be concerned based on the potential risks of PAEs.

Keywords Salt · Polar components · GC–MS · Fatty acid · Plasticizer

9.1 Introduction

Salt is one of the necessities of people's production and life, and it is widely used in food, leather, ceramics, glass, soap and dye industries. Inorganic elements from salt such as sodium chloride, iodine and heavy metal elements were mainly focused on (Huang et al. 2020), while the studies for organic compounds from salt were few. Fang et al. determined volatile organic acids from edible salt samples, and the results showed that butyric acid and isovaleric acid were presented in some salt samples

G. Chang · B. Yue · Z. Yin · X. Li · H. Sun
College of Geography and Environmental Engineering, Lanzhou City University, Lanzhou City, Gansu 730000, China

K. Zhao (✉)
Gansu Guoxin Runda Analyses and Testing Center, Lanzhou City, Gansu 730000, China
e-mail: skyzkp@126.com

H.-Y. Jeon (ed.), *Sustainable Development of Water and Environment*,
Environmental Science and Engineering,
https://doi.org/10.1007/978-3-030-75278-1_9

(Fang et al. 2019). The determination and analysis of the organic compounds from salt is helpful for people to fully understand the composition of salt. The analysis and identification soluble organic polar fractions of salt from inland natural lake water were performed by GC–MS in our previous studies, and soluble polar fractions extracted by chloroform from the samples could be divided into three types (fatty acids, PAEs, and sulfur ring) (Chang et al. 2020a). The effect of PAEs on organisms have gradually recognized and concerned by people. In the study, the organic polar (non-hydrocarbon) fractions from sea salt were analyzed by GC–MS, which could help us to further understand the composition characteristics of organic compounds from salt.

9.2 Samples and Methods

Sea salt samples were purchased from supermarkets. The detailed pretreatment process and analysis of the sample were given in the literature (Chang et al. 2020a). Briefly, samples of sea salt (120.0000 g) were weighed accurately and placed in a beaker. An appropriate amount of refined chloroform just submerged the sample were added into the sample to extract organic compounds. The extracts were subsequently mixed after 3 separate ultrasonic treatments (30 min each), and the organic compounds extracted three times were combined and put it into a 500 mL beaker. Then, methyl esterification of the extracts in a water bath was carried out at 60 °C for 10 h after chloroform in the extracts volatilized completely (Chang et al. 2020a; Pancost et al. 2000; Duan et al. 2014). Finally, the composition of polar fractions was performed using an Agilent GC6890N/MSD5973N system. Agilent J&W HP-5 column (30 m × 0.32 mm i.d. × 0.25 μm film) was used as capillary column, and high purity helium (He) (99.999%) were applied in the GC–MS detection system as the carrier gas. The sample injection was 1 μL, and the flow rate of carrier gas was 1.0 mL/min with 40 cm/sec of linear velocity. The organic substances from the sea salt samples were identified using NIST05 L (U.S.A.), and the peak area was normalized to calculate the content of each component.

9.3 Results and Discussion

The soluble organic polar fractions profile from the sea salt sample was obtained by GC analysis (Fig. 9.1), and the results of their compounds identification were shown in Table 9.1. The fatty acid compounds with the carbon number distribution range between 12 and 22 were detected in the samples, and their total relative abundance was more than 50%; *n*-C_{16} fatty acid represented the main peak in sea salts with retention times 17.265 min. The other components consisted of phthalate acid esters and sulfur, and the abundances of the two types were less than 20%, respectively. Among the soluble organic polar components detected, *n*-hexadecanoic acid

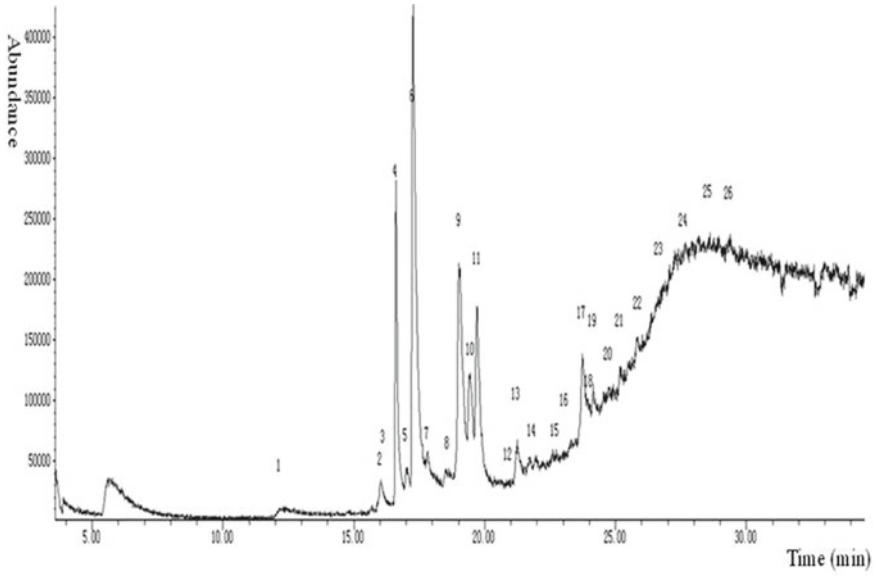

Fig. 9.1 GC profile of soluble organic polar components (methyl esters) from sea salt obtained by chloroform extraction

(41.19%) was the most abundant fatty acid, accounting for almost half of the soluble organic components; followed by *n*-octadecatrienoic acid accounted for one tenth of the total organic matter, and the relative abundances of the other fatty acids in the samples were minor, which were all less than 6%. Among the observed the fatty acids from the sea salt sample, the total abundances of saturated fatty acids was almost five times greater than that of unsaturated fatty acids. The ratio of total amount of odd carbon *n*-fatty acids to that of even carbon *n*-fatty acids was defined as carbon preference index (CPI_{total}) of *n*-fatty acids (Chang et al. 2020b), and the CPI_{total} index could be used to analyze the characteristics of *n*-fatty acids from various samples. The CPI_{total} in the sea salt samples was 0.005, which suggested that the total amount of the former was lower than that of the latter obviously. Furthermore, the content characteristic of the saturated fatty acids that were showed in the study were in accordance with the previously observed characteristic of even carbon content being higher than odd carbon content (Petrovic and Arsic 2016).

The unsaturated fatty acid composition in the sea salt sample were 9-hexadecenoic acid ($C_{16}H_{30}O_2$) (0.122%), 9-Octadecenoic acid ($C_{18}H_{34}O_2$) (5.798%), and erucic acid (4.658%).

Sulfur (S6, S7 and S8) was founded in the sea salt, and the relative abundance of them was as follows: S8 (19.39%) > S6 (0.006%) > S7 (0.003%), respectively. In addition to the above substances observed, phthalate acid esters (PAEs) were detected from the sea salt, and the relative abundance of PAEs was close to that of sulfur rings (Fig. 9.2).

Table 9.1 Soluble organic polar components (methyl esters) identification from sea salt detected by GC–MS

Peak number	Chemical formula	Molecular mass	Compound name	Percentage (%)
1	S_6	192	S_6	0.006
2	S_7	224	S_7	0.003
3	$C_{16}H_{32}O_2$	256	Pentadecanoic acid, methyl ester	0.025
4	$C_{16}H_{22}O_4$	278	Diisobutyl phthalate (DIBP)	17.678
5	$C_{17}H_{32}O_2$	268	9-Hexadecenoic acid, methyl ester	0.122
6	$C_{17}H_{34}O_2$	270	Hexadecanoic acid, methyl ester	41.19
7	$C_{16}H_{22}O_4$	278	Dibutyl phthalate (DBP)	0.03
8	$C_{18}H_{36}O_2$	284	Heptadecanoic acid, methyl ester	0.024
9	S_8	256	Cyclic octaatomic sulfur	19.39
10	$C_{19}H_{36}O_2$	296	9-Octadecenoic acid, methyl ester	5.798
11	$C_{19}H_{38}O_2$	298	Octadecanoic acid, methyl ester	10.087
12	$C_{20}H_{40}O_2$	312	Nonadecanoic acid, methyl ester	0.007
13	$C_{21}H_{42}O_4$	358	8, 10-Dimethexy-octadecanoic acid, methyl ester	0.137
14	$C_{21}H_{42}O_2$	326	Eicosanoic acid, methyl ester	0.024
15	$C_{22}H_{44}O_2$	340	Heneicosanoic acid, methyl ester	0.046
16	$C_{23}H_{46}O_4$	386	10, 12-Dimethexy-octadecanoic acid, methyl ester	0.105
17	$C_{23}H_{44}O_2$	352	Erucic acid, methyl ester	4.658
18	$C_{23}H_{46}O_2$	354	Docosenoic acid, methyl ester	0.018
19	$C_{24}H_{38}O_4$	390	Bis(2-ethylhexyl) phathalate (DEHP)	0.052
20	$C_{24}H_{48}O_2$	368	Tricosanoic acid, methyl ester	0.04
21	$C_{25}H_{50}O_4$	414	12, 14-Dimethexy-octadecanoic acid, methyl ester	0.058
22	$C_{25}H_{50}O_2$	382	Tetracosanoic acid, methyl ester	0.034
23	$C_{26}H_{52}O_2$	396	Pentacosanoic acid, methyl ester	0.071

(continued)

Table 9.1 (continued)

Peak number	Chemical formula	Molecular mass	Compound name	Percentage (%)
24	$C_{27}H_{54}O_2$	410	Hexacosanoic acid, methyl ester	0.26
25	$C_{28}H_{56}O_2$	424	Heptacosanoic acid, methyl ester	0.056
26	$C_{29}H_{58}O_2$	438	Octacosanoic acid, methyl ester	0.081

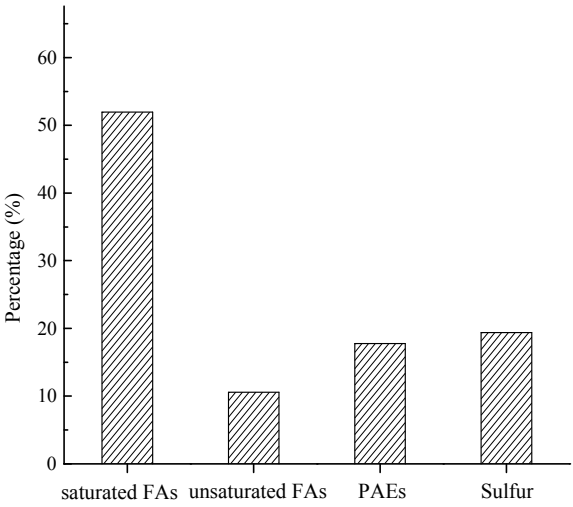

Fig. 9.2 Relative content of different types from soluble organic polar fractions in sea salt

Fatty acids (FAs) as the main components of lipids within the body play a key role in cellular structures and functions, such as the regulation of apoptosis, the main energy pool in adipose tissue and the activity of hypothalamic neurons (Rudolph et al. 2001; Michael and Watt 2020). In our study about soluble organic polar substances from *Hydrilla verticillata* (an aquatic plant) which is widely found in freshwater, the carbon number distribution range from C_{12} to C_{24} was observed in the plant. In the plant, *n*-hexadecanoic acid with relative abundance of 47.06% representing the main fatty acid peak was observed and the total relative abundance of saturated FA was almost twice that of unsaturated FA (Chang et al. 2020b). Moussa and Almaghrabi (Moussa and Almaghrabi 2016) reported that hexadecanoic acid with relative abundance 48.13% was the highest abundant fatty acid among the saturated fatty acid compositions from *Peganum harmala* plant. Hexadecanoic acid was detected also as the main component in some essential oils involving in those from *Oryzasativa* L. (74.57%) (Sayaka and Mitsuo 2006), *Ardisia brevicaulis* Diels leaves (43.32%) (Pu et al. 2009) and from *Allium roseum* var. *randiflorum* subvar. *typicum* Regel leaves (75.9%) (Rouis-Soussi et al. 2014). C_{15}–C_{28} fatty acid compounds constituted the main polar component of sea salt samples, in which the highest abundant

of *n*-hexadecanoic acid was analyzed, which was almost half of the total amount of the soluble organic components.

In previous research on the soluble organic polar substances in salt from inland natural lake water, the fatty acids with the carbon number distribution range from C_{14} to C_{24} were observed, and among them erucic acid was the highest relative abundance (50.610%), accounting for half of the total amount of soluble organic polar substances, the followed by *n*-hexadecanic acid with relative abundance of 13.637% and then 9-octadecenoic acid (8.747%) (Chang et al. 2020a).

In addition, these results showed that the distribution characteristic of fatty acids in salt from different areas could be closely associated with the biological characteristics of water source of the salt.

Although the content of sulfur in the sea salt sample is significantly higher than that in salt from natural lake (Chang et al. 2020a), the existence forms of sulfur element, that is S6, S7 and S8 in the two salts is the same. Phthalate acid esters, as one group of endocrine dispersing chemicals have been found in water, soil, atmosphere, plants and animals based on their wide application in production, and the environmental impact and the harm to organisms caused by phthalate acid esters also attracted the attention of scholars (Cai et al. 2017; Kong et al. 2019; Paluselli et al. 2018; Takeuchi et al. 2018; Vered et al. 2019; Gao et al. 2018; Li et al. 2020). Vered et al. reported that high contents of PAEs (DBP and DEHP) were found in *Herdmania momus* and *Microcosmus exasperatus* which were obtained from the Israel Mediterranean and Red Sea coasts (Vered et al. 2019). The effect of phthalate acid esters on organisms has also attracted the attention of many researchers. Lu et al. reported that three PAEs exposures, including DBP, mono-(2-ethylhexyl) phthalate, and DEHP, could result in developmental abnormalities in zebrafish larvae and induced cytotoxicity in HEK293T cells (Lu et al. 2021). Phthalate acid esters involving in DIBP, DBP and DEHP were detected in the sea salt, which were also founded in edible salt sampls from inland natural lake water (Chang et al. 2020a). The phenomenon indicates that PAEs are common in water, which should be taken seriously. In addition, the proportion of plasticizer content in the sea salt is relatively high, accounting for more than one tenth of the total soluble organic polar substances, which also suggested that the plasticizer content in sea water should not be ignored. In view of the universality of plasticizers, their biological effects should be further studied. It should be paid more attention to the study of the types and concentrations of plasticizers in seawater, their migration characteristics from water to soil or organisms, their effects on marine organisms and marine ecology and their enrichment and degradation characteristics in organisms.

9.4 Conclusions

The analysis results by using GC–MS showed there were greater than 20 soluble organic substances existed in sea salt. These compounds were mainly devided into three types: fatty acids, PAEs, and sulfur. The characteristics of soluble organic polar

fractions in salt and the carbon number distribution range of fatty acids have close association with the water quality characteristics of their sources. The total amount of the even carbon *n*-fatty acids was higher obviously than that of odd carbon *n*-fatty acids from the sea salt. The content order of the above three components was fatty acids > sulphur ~ PAEs. The relative abundance of phthalate acid esters (17.76%) in soluble organic polar components extracted by chloroform from sea salt was not low, which should be paid more attention.

Acknowledgements The financial assistance of the work is supported by Research Project of Universities from Gansu (2019B-169 and 2018B-062) and Natural Science Foundation of Gansu Province, China (20JR5RA210).

References

Cai QY, Xiao PY, Zhao HM, Lu H, Zeng QY, Li YW, Li H, Xiang L, Mo CH (2017) Variation in accumulation and translocation of di-*n*-butyl phthalate (DBP) among rice (*Oryza sativa* L.) genotypes and selection of cultivars for low DBP exposure. Environ Sci Pollut Res 24:7298–7309

Chang GH, Yue B, Li J, Yin ZX, Gao TP, Li XK, Cheng YX (2020) Analysis of polar components in salt by GC-MS. In: 2nd Global Conference on Ecological Environment and Civil Engineering, vol 568, IOP Publishing Ltd., pp 012037

Chang GH, Yue B, Gao TP, Yan WD, Pan G (2020) Phytoremediation of phenol by *Hydrilla verticillata* (L.f.) Royle and associated effects on physiological parameters. J Hazard Mater 388:121569

Duan Y, Wu YZ, Cao XX, Zhao Y, Ma LH (2014) Hydrogen isotope ratios of individual *n*-alkanes in plants from Gannan Gahai Lake (China) and surrounding area. Org Geochem 77:96–105

Fang PP, Guo TY, Yong W, Dong YY, Zhang F (2019) Rapid determination of volatile organic acids in edible salt and high-salinity food by direct analysis in real time mass spectrometry. Int J Mass Spectrom 444:11616

Gao D, Li Z, Wang H, Liang H (2018) An overview of phthalate acid ester pollution in China over the last decade: environmental occurrence and human exposure. Sci Total Environ 645:1400–1409

Huang ZB, Su ZJ, Fan JB, Hu SG, Chen M, Cai WH (2020) Study on simultaneous determination of multiple indexes of table salt by inductively coupled plasma mass spectrometry. China Food Addit 31(9):104–111

Kong X, Jin D, Wang XX, Zhang FS, Duan GL, Liu HJ, Jia MH, Deng Y (2019) Dibutyl phthalate contamination remolded the fungal community in agro-environmental system. Chemosphere 215:189–198

Li Y, Wang J, Yang S, Zhang S (2020) Occurrence, health risks and soil-air exchange of phthalate acid esters: a case study in plastic film greenhouses of Chongqing, China. Chemosphere 128821

Lu C, Luo J, Liu Y, Yang X (2021) The oxidative stress responses caused by phthalate acid esters increases mRNA abundance of base excision repair (BER) genes in vivo and in vitro. Ecotoxicol Environ Saf 208:111525

Michael NJ, Watt MJ (2020) Long chain fatty acids differentially regulate sub-populations of arcuate pomc and npy neurons long chain fatty acids differentially regulate sub-populations of arcuate POMC and NPY neurons. Neuroscience 451:164–173

Moussa TAA, Almaghrabi OA (2016) Fatty acid constituents of *Peganum harmala* plant using gas chromatography–mass spectroscopy. Saudi J Biol Sci 23:397–403

Paluselli A, Aminot Y, Galgani F, Net S, Sempéré R (2018) Occurrence of phthalate acid esters (PAEs) in the northwestern Mediterranean Sea and the Rhone River. Prog Oceanogr 163:221–231

Pancost RD, Sinninghe Damsté JS, de Lint S, van der Maarel MJEC, Gottschal JC (2000) Biomarker evidence for widespread anaerobic methane oxidation in Mediterranean sediment by a consortium of methanogenic archaea and bacteria. Appl Environ Microbiol 66(3):1126–1132

Petrovic S, Arsic A (2016) Drying: fatty acids. Encycl Food Health 623–631

Pu LX, Yuan XH, Tang TJ (2009) Analysis of volatile oil from *Ardisia brevicaulis*. J Chin Med Mater 32:1694–1697

Rouis-Soussi LS, Boughelleb-M'Hamdi N, El Ayeb-Zakhama A, Flamini G, Ben Jannet H, Harzallah-Skhiri F (2014) Phytochemicals, antioxidant and antifungal activities of *Allium roseum* var. *grandiflorum* subvar. *typicum* Regel. S AFR J BOT 91:63–70

Rudolph IL, Kelley DS, Klasing KC, Erickson KL (2001) Regulation of cellular differentiation and apoptosis by fatty acids and their metabolites. Nutr Res 21:381–393

Sayaka N, Mitsuo M (2006) Characteristic flavor and components of essential oil from *Oryza sativa* L. *Koryo*. Terupen Oyobi Seiyu Kagaku Ni Kansuru Toronkai Koen Yoshishu 50:88–90

Takeuchi S, Tanaka-Kagawa T, Saito I, Kojima H, Jin K, Satoh M, Kobayashi S, Jinno H (2018) Differential determination of plasticizers and organophosphorus flame retardants in residential indoor air in Japan. Environ Sci Pollut Res 25:7113–7120

Vered G, Kaplan A, Avisar D, Shenkar N (2019) Using solitary ascidians to assess microplastic and phthalate plasticizers pollution among marine biota: a case study of the Eastern Mediterranean. Mar Pollut Bull 138:618–625

Chapter 10
Microplastics in Industrial Wastewater Treatment Plants: Dynamic Distribution, Seasonal Variation, and Removal Efficiencies

Sujarat Saiwaree and Vorapot Kanokkantapong

Abstract Wastewater treatment plants (WWTPs) are one of the significant pathways of microplastics (MPs) entering the environment. Thus, information regarding this issue is still requisite in Thailand. In this study, wastewater and sludge samples were collected from an activated sludge operation of an industrial WWTP in different seasons, that is, dry season and wet season. The MP particles were identified by size, shape, and polymer types under stereomicroscope and μFT-IR. From the wastewater, MPs were detected in the highest amounts after the aeration unit (134.35 ± 20.79 particles/L) during dry season and from influent (103.13 ± 59.48 particles/L) during wet season. In addition, sludge contained relatively low MP concentrations (2.27 ± 0.08 in the dry and 1.86 ± 0.28 particles/g dw. in the wet seasons). The size fraction in wastewater varied, but in sludge was > 300 μm commonly in both seasons. Fragments and pellets were identified as the most common shape of wastewater and sludge in both seasons. The treatment units and seasonal variation had a significant effect on MP abundance. The suspected particle was confirmed to be 71.13% plastic polymer, mainly polypropylene (PP) and polyethylene (PE). The overall removal efficiency was 93.86%, indicating that there are many MPs still discharged to the river due to effluent MPs, which was approx. 1.8×10^8 particles per day. Consequently, this study suggests that, to define the effect of a season, prolonged monitoring is required. Moreover, the attention must be on WWTPs in Thailand, as they act as the greatest source of MP contamination in the environment.

Keywords Activated sludge · Pollution · Treatment unit · Wastewater

S. Saiwaree · V. Kanokkantapong (✉)
Department of Environmental Science, Chulalongkorn University, Bangkok, Thailand
e-mail: vorapot.ka@chula.ac.th

V. Kanokkantapong
Special Task Force for Activating Research (STAR) of Waste Utilization and Ecological Risk Assessment, Chulalongkorn University, Bangkok 10330, Thailand

H.-Y. Jeon (ed.), *Sustainable Development of Water and Environment*,
Environmental Science and Engineering,
https://doi.org/10.1007/978-3-030-75278-1_10

10.1 Introduction

Worldwide plastic production has increased continuously from year to year, leading to plastic pollution in environment. These plastics, typically with a diameter less than 5 mm, are defined as microplastics (MPs) (Hidalgo-Ruz 2012; Thompson et al. 2009). There are several adverse effects of MPs, not only in naturally persistent and enormous abundance in the environment but also chemically and physically. It was found that MPs can adsorb heavy metals such as lead, manganese, etc. (Gao 2019), which might harm aquatic ecosystems.

MPs have been detected in numerous environments, including oceans (Mason 2016; Eriksen et al. 2013), freshwater (Shruti 2019; Rodrigues 2018), soil sediments (Borges Ramirez et al. 2019), and aquatic life forms (Desforges et al. 2015; Peters 2018). MPs enter by several pathways, such as direct dumping, drainage water, and a wastewater treatment plant (WWTP). WWTPs are not only the endpoint of the anthropogenic water cycle but also receive many MPs through multiple ways, such as textiles from washing, cosmetics and personal care products, abrasion of plastic composite products, and pipes and landfill leachates (Kole 2017). The high removal efficiency of MPs in almost all WWTPs can still be found, at higher than 95% (Sun 2019). However, its contribution to the environment is still worrisome due to the great volume of treated water coming from each WWTP, which could lead to the transfer of large amounts of MPs into aquatic environments. Some research revealed that a WWTP with daily treated 10,000 m^3 of WWTP could release approximately 10,000,000–460,000,000 particles per day (Lares 2018). Indeed, several countries' have been studied, except in Thailand. Hence, this work aims to verify the performance and effectiveness of MP removal by each treatment unit of an industrial WWTP in Thailand. The identification of MP type, its polymer types, and the effect of seasonal variation were recognized.

10.2 Materials and Methods

10.2.1 Study Area and Sample Collection

Wastewater and sludge samples were collected from an Industrial Estate Wastewater Treatment Plant in Thailand, the activated sludge WWTP. The average influent flow rate is about 8,000 m^3/day. The samples were collected in February and July 2020, which represented the winter and rainy seasons. As shown in Fig. 10.1, the sampling points are at influent, after the grit chamber, aeration, sedimentation, effluent, and sludge. Moreover, 2–5 L of water and 60 g of sludge were collected by bulk sampling with three replications. The wastewater samples were sieved through an 8-inch-diameter steel sieve of four size fractions (300 μm, 212 μm, 100 μm, 20 μm) in the field.

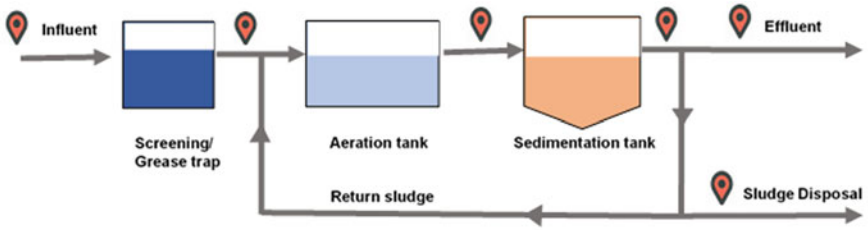

Fig. 10.1 Wastewater treatment plant and sampling point

10.2.2 Sample Processing

Processes were based on the NOAA Marine Debris Program method (Masura et al. 2015). Samples were transferred into beakers and dried in a 60 °C oven for 24 h. Moreover, 20 mL of 0.05 M Fe (II) solution and 20 mL of 30% hydrogen peroxide were added to the samples and heated to 65 °C in a hot plate for dissolved organic removal. Subsequently, 20 mL of NaCl (density of 1.2 g/cm^3) were mixed with samples and settled for 24 h. in a separatory funnel. Settled solids were discarded, the funnel was rinsed with NaCl to wash out remaining particles that attached to the glass, and then was left to settle down for 2–3 h. These steps were repeated 2–3 times. Next, the sample was transferred from the glass funnel directly to vacuum filtration through a cellulose nitrate microfiber filter with 0.45 μm pore size.

Background blanks for estimating the potential for airborne contamination were taken whenever samples were processed by examining a membrane filter placed in a petri dish without a cover in the area site for an eight-hour period (Gies 2018). Field blank, in which samples were treated exactly the same way as other samples, used distilled water instead of wastewater and sludge (Lares 2018). To avoid external plastic contamination, most of the vessels used during the experiment were glassware or stainless steel.

10.2.3 Sample Characterization

The physical shape of MP particles was characterized using a stereo microscope (NSZ-405J3 Olympus) as fiber, film, pellet, and fragment. Polymer composite was examined by micro-Fourier Transform infrared spectroscopy (μFTIR PerkinElmer Spectrum IR 10.6.2) with 24 scans to incur a wavelength region of 450 –4,000 cm-1. Spectra were compared to the libraries provided by PerkinElmer.

10.2.4 Statistical Analysis

The average numbers and standard deviations of three replicates were calculated and presented as mean ± standard deviation (Lusher 2015). To evaluate the influence of season variational (dry and wet season) and treatment units (influent, after-grit chamber, after aeration, after sedimentation, effluent, and sludge) on MP abundances, a two-way ANOVA was performed. Regarding the differences in MP content in each unit and season, a paired t-test was conducted. The statistically significant value was $P < 0.05$.

10.3 Results and Discussion

10.3.1 Method Validation and Efficiency

According to the field blank test, 20 particles were found. While in background blank was undetected. These amounts were lower than 10% of the MPs' average found, considered good contamination control, as suggested by Lusher (2015). The method's efficiency was discerned using 30 green column-shaped Polypropylenes and 10 red column-shaped Polyethylene Terephthalates spiked into the sample. Thirty-six particles were detected, accounting for 90% of spike microplastics, indicating that most MPs were recovered.

10.3.2 Microplastic Abundance

The shape of MPs observed from a stereo microscope can be categorized as fiber, film, pellet, and fragment as shown in Fig. 10.2. The number of MPs presented in each wastewater treatment unit differed, as shown in Fig. 10.3. The MPs detected in influent from this work were 103.13 ± 59.48 particles/L.

The influent sample was presented only in the wet season due to inconvenience in the dry season. The highest number of MPs was found in the aeration unit, where the wet and dry seasons were 134.35 ± 20.79 and 31.38 ± 10.36 particles/L, respectively. This result was like WWTPs in eastern China (Lv 2019) that also reported the highest value of MPs was presented in the aeration unit, as an air generator might cause broken MP particles to be distributed thoroughly in the following treatment units.

The lowest MP numbers were found in the sedimentation unit of the dry season (13.98 ± 4.50 particles/L) and in the effluent of the wet season (6.33 ± 1.36 particles/L). The sediment unit was designed to remove organic matter, and MPs were affected by this process through adsorption and fouling by bacteria. Other physical processes could cause sinking (Magni 2019), according to the wet season sample. However, the dry season sample acted in a dissimilar way; the effluent MPs were

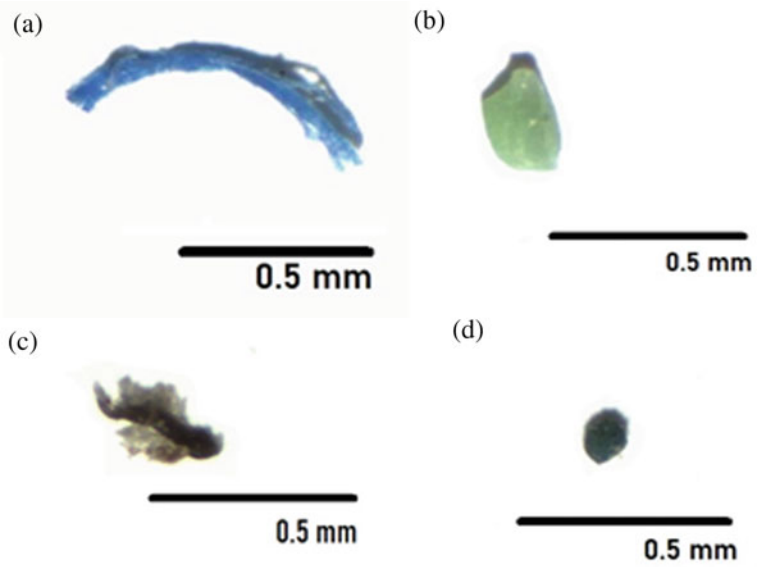

Fig. 10.2 Microplastic particles from a stereomicroscope (**a**) fiber, (**b**) fragment, (**c**) film, and (**d**) pellet

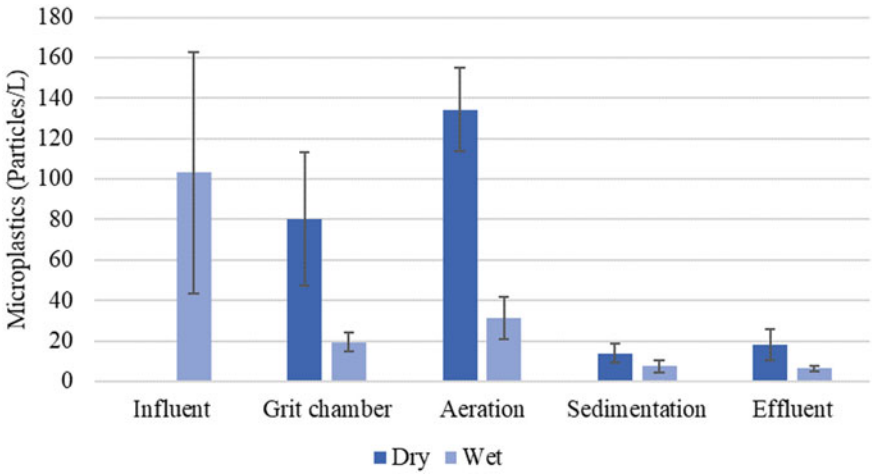

Fig. 10.3 Microplastic abundance in wastewater treatment units in dry and wet seasons

higher than in sedimentation because the increased contact time of sludge in the treatment system may lead to higher MPs found in the effluent (Carr et al. 2016). Hence, there is no significant distinction between sedimentation MPs and effluent in both the dry and wet seasons ($P = 0.426$, $P = 0.695$). Previous same-size limitation studies (20–25 μm) reported effluent MP abundance as 0.005–13.5 particles/L

(Ziajahromi 2017; Mintenig 2017; Talvitie 2017, 2015; Michielssen 2016), which was quite similar to this study. The MPs in sludge abundance were 2.27 ± 0.08 and 1.86 ± 0.28 particles/g dw in the dry and wet seasons. It was a higher number than WWTP from the Netherlands (0.37–0.95 particles/g dw (Brandsma et al. 2013)) and Sweden (1.7 ± 1.96 particles/g dw (Magnusson and Norén 2014)).

In contrast, compared to a study from Spain (165 ± 37 particles/g (Edo 2020) and Finland (170.9 ± 28.7 particles/g dw (Lares 2018)), their number was much higher than this study. Some studies have shown that microplastics are effectively removed from wastewater, and most particles end up in sludge (Talvitie 2017, 2015; Michielssen 2016). It is also possibly dependent on the effectiveness of sedimentation units or MP particle properties.

According to the wet season sample, the most effective MP removal unit was from the grit chamber (81.27%). Liu (2019) reported the highest reduction rate of MPs at 40.7%, which originated from the grit chamber and primary settling tank. The high reduction in this stage possibly caused many MP particles to be adsorbed by suspended solids in wastewater (Lares 2018; Carr et al. 2016). The final removal efficiency of this treatment plant was 93.86%, which was relatively high compared to the nearby site study as the studies in Asia reported 53.7–83.60% efficiency (Lv 2019; Liu 2019; Jiang 2020; Hongprasith et al. 2020). However, in Europe, researchers reported higher efficiency ranging from 75–9% (Gies 2018; Ziajahromi 2017; Murphy 2016; Leslie 2017; Jambeck et al. 2015). This is possibly attributed to lower population densities and better waste management systems in highly developed countries (Jambeck et al. 2015).

10.3.3 Microplastic Characteristic Distribution

The largest scale of MPs in the influent was >300 μm. When the water passed through the grit chamber, the large-scale MPs were removed (Fig. 4b). Grit chambers could effectively prevent large debris and cause the significant reduction of MPs in wastewater (Liu 2019). In the aeration unit, there was a differentiation between dry and wet seasons; the dominant size in the dry season was 100–20 μm and in the wet season was 212–100 μm. The large MPs (>300 μm) were significantly removed during the processes ($P = 0.006$). Hence, the number of smaller MPs increased, and larger MPs decreased from influent wastewater, just as Liu et al. (2019) found that the smaller-sized fraction (300–20 μm) becomes higher throughout treatment units. Some MP particles were broken by mechanical contact in the grit chamber and aeration unit. In the sedimentation unit, the size fraction was like the aeration unit and effluent, where most of the larger-scale MPs were removed significantly from the influent wastewater.

The most common size of MPs in sludge in both the dry and wet seasons was >300 μm. The larger particles showed heavier weight, leading to settling in the sludge. Likewise, Murphy et al. (2016) concluded the size of MPs in the sludge was higher than in the wastewater because the smaller particles might still remain

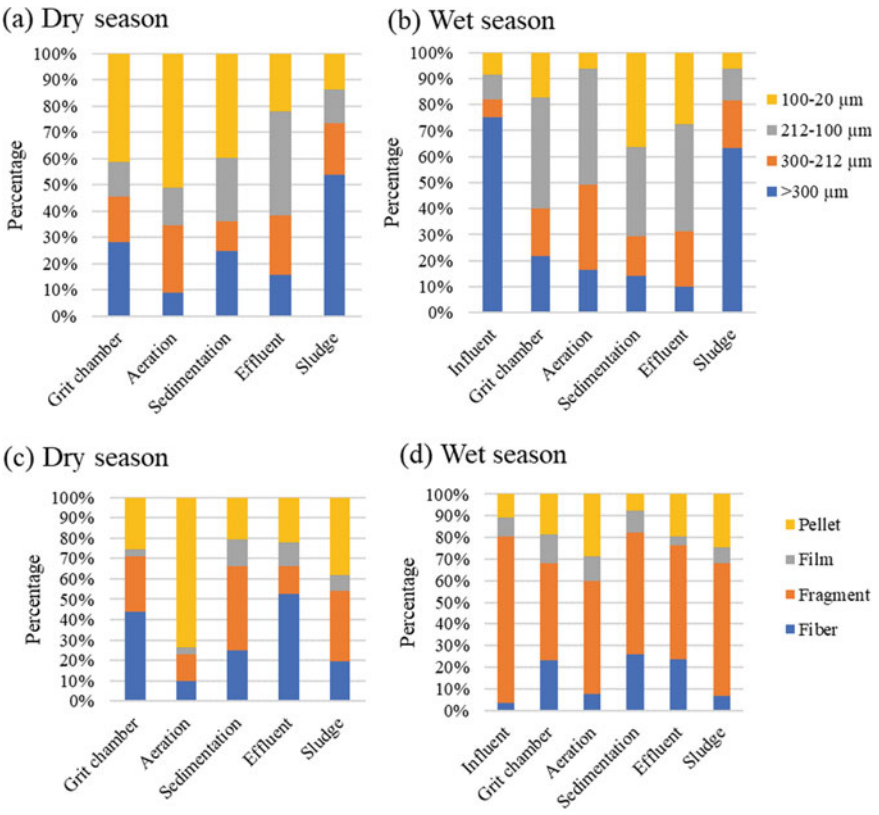

Fig. 10.4 Microplastic percentage (**a**) size fraction in dry season, (**b**) size fraction in wet season, (**c**) shape fraction in dry season, and (**d**) shape fraction in wet season

in the water mass. According to the results shown in Fig. 4c, the dominant shape of MPs in wastewater in the dry season was pellet (51%), while in the wet season (see Fig. 4d), it was fragment (67%). Similarly, the dominant shape of sludge MPs in the dry season was pellet (38%) and fragment (34%), while in the wet season, it was fragment (61%). Murphy et al. (2016) also reported that mainly fragments (67.3%) were found in wastewater. Suspected MP particles in sludge were dominated by fragments (Gies 2018) due to an opportunity in which larger MPs can crack down throughout the treatment processes.

In this study, 97 MP particles were randomly selected from dry season ($n = 44$) and wet season samples ($n = 53$) to verify the polymer type. Moreover, 69 MP particles were confirmed as plastic polymers (71.13%). As shown in Fig. 10.5, polypropylene (PP) was the majority polymer type in the wet season sample (35%), and polyethylene (PE) was common in the dry season sample (25%). Edo et al. (2020) reported PE followed by PP as a majority polymer in wastewater and sludge. In Valencia, Spain, MP fragments were characterized as PE and PP as the main

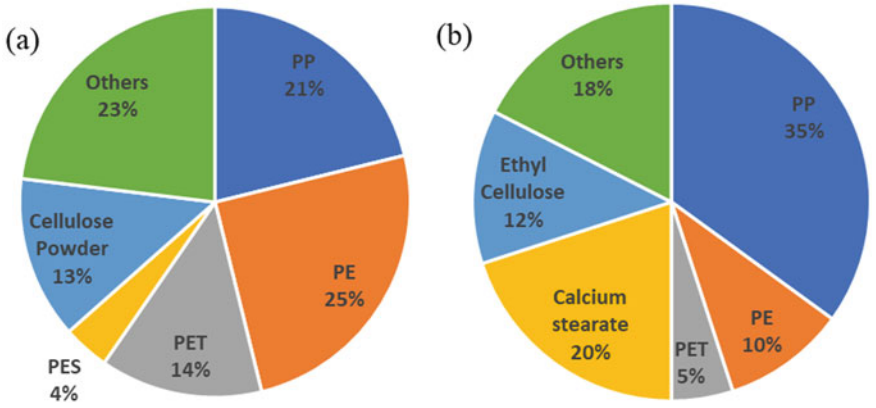

Fig. 10.5 Polymer percentage: (**a**) dry season sample and (**b**) wet season sample

polymer (63% and 25%, respectively (Alvim et al. 2020). Polyethylene accounted for most plastics used in flexible packaging, plastic bags, film, and plastic bottles. Polypropylene also is popular for film usage. Both polymers generally originated from everyday products.

According to the micro FTIR results, the transparent fiber found in the dry season sample was related to PE (0.92–0.97 g/cm^3) and cellulose fiber. Fragments and film were characterized as PP (0.85 to 0.94 g/cm^3) and PE. The pellet MPs, which had the highest abundance in the dry season sample, were verified as polymethacrylate (PMMA- 1.17–1.20 g/cm^3). In the wet season sample, fragments were considered PP and PE, but some fibers were PET, PP, and calcium stearate. Cellulose was found to be a mainly natural polymer from the results. Some particles taken from the same sample physically look alike under a stereomicroscope, showing different types of polymers due to the adhesive interfering with the scanner, leading to the misinterpretation of results.

10.3.4 Effect of Seasonal Variation on MP Abundance and Characterization

This study found that seasonal variation influenced MP abundance ($p = 1.18E\text{-}06$), size fraction ($p = 7.66E\text{-}08$), and shape ($P = 5.65E\text{-}08$). The difference between seasons was found on the aeration unit ($p = 0.029085$), 100–20 μm size fraction ($p = 0.013449$), and pellet shape ($p = 0.011918$). The others found no significant distinction. As the run-off water system was separated from the wastewater treatment system, only small effects were observed. Rainfall and storm events are regarded as major periods of contaminant input to recipient water (Andrady 2011; Hitchcock 2020). Mason et al. (2016) reported that a WWTP with a combined sewer system

(i.e., including stormwater runoff), after a storm event, could increase fragmented particles in effluent. However, the researchers who paid attention to the effect of weather on MP abundance mostly focused on the environment sample base, that is, the coast of Hong Kong (Cheung et al. 2016), Cook River Estuary, Australia (Hitchcock 2020), and the coast of California, USA (Moore 2002). By the way, this study did not focus on storm events, rainy days, or prolonged sampling periods. Thus, this is an important factor in evaluating the effect of seasonal variation.

10.4 Conclusion

The MP abundance from an industrial wastewater treatment plant in Thailand during dry and wet seasons varied. Most MPs detected on the aeration unit in the dry season sample were 134.35 ± 20.79 particles/L with a pellet shape (51%) and in influent was 103.13 ± 59.48 particles/L with a fragment shape (67%) in the wet season sample. The most common size fraction in the dry sample of the sludge sample contained 2.27 ± 0.08 and 1.86 ± 0.28 particles/g dw, which was relatively low. The most common size fraction in sludge was >300 μm in the shape of fragments (34% in dry, 61% in wet season) and pellets (38% in dry, 25% in wet season), due to the settling down of larger sizes and wrecking by mechanical processes that cause fragmentation. In addition, the 93.86% removal efficiency of this study was discovered, which was quite a high percentage, even though there are still some MPs discharging into the environment, accounting for 1.2×10^8 particles/day.

According to FTIR results, 71.13% was confirmed as a plastic polymer. Polypropylene (PP) was the majority polymer type in the wet season sample (35%), and polyethylene (PE) was common in the dry season sample (25%). Seasonal variations also influence MP abundance. Therefore, the result needs to be confirmed by prolonged sampling and atmospheric data for a better understanding of MPs during different seasons. Moreover, microplastics from WWTPs in Thailand must be considered, as they can be a major source of MP contamination in the environment.

Acknowledgements This work was supported by Microplastic and plastic waste cluster and Graduate School, Chulalongkorn University.

References

Alvim CB, Mendoza-Roca J, Bes-Piá A (2020) Wastewater treatment plant as microplastics release source–quantification and identification techniques. 255:109739

Andrady AL (2011) Microplastics in the marine environment. Mar Pollut Bull 62(8):1596–1605

Borges Ramirez MM, Dzul Caamal R, Rendon von Osten J (2019) Occurrence and seasonal distribution of microplastics and phthalates in sediments from the urban channel of the Ria and coast of Campeche, Mexico. Sci Total Environ 672:97–105

Brandsma S et al (2013) Microplastics in river suspended particulate matter and sewage treatment plants
Carr SA, Liu J, Tesoro AG (2016) Transport and fate of microplastic particles in wastewater treatment plants. Water Res 91:174–182
Cheung PK, Cheung LTO, Fok L (2016) Seasonal variation in the abundance of marine plastic debris in the estuary of a subtropical macro-scale drainage basin in South China. 562:658–665
Desforges JP, Galbraith M, Ross PS (2015) Ingestion of Microplastics by Zooplankton in the Northeast Pacific Ocean. Arch Environ Contam Toxicol 69(3):320–330
Edo C et al (2020) Fate of microplastics in wastewater treatment plants and their environmental dispersion with effluent and sludge. 259:113837
Eriksen M, Mason S, Wilson S (2013) Mar Pollut Bull 77(null):177
Gao F et al (2019) Study on the capability and characteristics of heavy metals enriched on microplastics in marine environment. Mar Pollut Bull 144:61–67
Gies EA et al (2018) Retention of microplastics in a major secondary wastewater treatment plant in Vancouver, Canada. Mar Pollut Bull 133:553–561
Hidalgo-Ruz V et al (2012) Microplastics in the marine environment: a review of the methods used for identification and quantification. Environ Sci Technol 46(6):3060–3075
Hitchcock JN (2020) Storm events as key moments of microplastic contamination in aquatic ecosystems. Sci Total Environ 734
Hongprasith N et al (2020) IR microspectroscopic identification of microplastics in municipal wastewater treatment plants. 1–8
Jambeck JR et al (2015) Marine pollution. Plastic waste inputs from land into the ocean. Science 347(6223):768–71
Jiang J et al (2020) Investigation and fate of microplastics in wastewater and sludge filter cake from a wastewater treatment plant in China. Sci Total Environ 746:141378
Kole PJ et al (2017) Wear and Tear of Tyres: A Stealthy Source of Microplastics in the Environment. Int J Environ Res Public Health 14(10)
Lares M et al (2018) Occurrence, identification and removal of microplastic particles and fibers in conventional activated sludge process and advanced MBR technology. Water Res 133:236–246
Leslie HA et al (2017) Microplastics en route: field measurements in the Dutch river delta and Amsterdam canals, wastewater treatment plants, North Sea sediments and biota. Environ Int 101:133–142
Liu X et al (2019) Transfer and fate of microplastics during the conventional activated sludge process in one wastewater treatment plant of China. 362:176–182
Lusher A (2015) Microplastics in the Marine Environment: distribution, interactions and effects. pp 245–307
Lv X et al (2019) Microplastics in a municipal wastewater treatment plant: fate, dynamic distribution, removal efficiencies, and control strategies. J Clean Prod 225:579–586
Magni S et al (2019) The fate of microplastics in an Italian wastewater treatment plant. Sci Total Environ 652:602–610
Magnusson K, Norén F (2014) Screening of microplastic particles in and down-stream a wastewater treatment plant
Mason SA et al (2016) Microplastic Pollution Is Widely Detected in US Municipal Wastewater Treatment Plant Effluent. 218:1045–1054
Masura J et al (2015) Laboratory methods for the analysis of microplastics in the marine environment: recommendations for quantifying synthetic particles in waters and sediments
Michielssen MR et al (2016) Fate of microplastics and other small anthropogenic litter (SAL) in wastewater treatment plants depends on unit processes employed. Environ Science-Water Res Technol 2(6):1064–1073
Mintenig SM et al (2017) Identification of microplastic in effluents of waste water treatment plants using focal plane array-based micro-Fourier-transform infrared imaging. Water Res 108:365–372
Moore CJ et al (2002) A comparison of neustonic plastic and zooplankton abundance in southern California's coastal waters. Mar Pollut Bull 44(10):1035–1038

Murphy F et al (2016) Wastewater treatment works (WwTW) as a source of microplastics in the aquatic environment. Environ Sci Technol 50(11):5800–5808
Peters CA et al (2018) Pyr-GC/MS analysis of microplastics extracted from the stomach content of benthivore fish from the Texas Gulf Coast. Mar Pollut Bull 137:91–95
Rodrigues MO et al (2018) Spatial and temporal distribution of microplastics in water and sediments of a freshwater system (Antua River, Portugal). Sci Total Environ 633:1549–1559
Shruti VC et al (2019) Microplastics in freshwater sediments of Atoyac River basin, Puebla City, Mexico. Sci Total Environ 654:154–163
Sun J et al (2019) Microplastics in wastewater treatment plants: Detection, occurrence and removal. Water Res 152:21–37
Talvitie J et al (2015) Do wastewater treatment plants act as a potential point source of microplastics? Preliminary study in the coastal Gulf of Finland. Baltic Sea. Water Sci Technol 72(9):1495–1504
Talvitie J et al (2017) Solutions to microplastic pollution—removal of microplastics from wastewater effluent with advanced wastewater treatment technologies. Water Res 123:401–407
Thompson RC, Swan SH, Moore CJ (2009) Philos Trans R Soc B Biol Sci 364(null):1973
Ziajahromi S et al (2017) Wastewater treatment plants as a pathway for microplastics: development of a new approach to sample wastewater-based microplastics. Water Res 112:93–99

Chapter 11
Spatial–Temporal Variation Analysis on Ecosystem Service Values in a Typical Inland River Basin, Northwest China

Mingtao Li, Lingfen Kang, and Chuancheng Zhao

Abstract Ecosystem services value (ESV) is a direct manifestation of the change of ecosystem service function and benefits. In this study, we evaluated the value of 11 primary ecosystem services in the upper and middle region of Heihe River Basin (UMHRB) from 2000 to 2018. The spatial–temporal heterogeneity was explored at the grid-scale by using ecosystem service value model, and hot spot analysis. The results showed that: (1) The structure of land use in UMHRB was dominated by unused land, followed by grassland, farmland, forestland, water area and built-up land. The change trend of land use was the decrease of unused land and grassland, and the increase of built-up land, water area, farmland and forest land. (2) The temporal evolution of total ESV in UMHRB had shown a steady upward trend from 2000 to 2018. Among the ecosystem types, grassland and water area contributed the most to ESV. The trend of ESV changes showed that the ESV of unused land, grassland and forestland decreased, while the ESV of built-up land, farmland and water increased. For each individual ESV, hydrological regulation and climate regulation had the largest ESV contribution. Only the ESVs of climate regulation have slightly decreased, while other ecosystem services have increased. (3) The spatial distribution of ESV in UMHRB showed a spatially clustered distribution pattern and the degree of clustering was slightly weakened. From 2000 to 2018, the hot spots were mainly distributed in the southern Qilian Mountains, and sporadically scattered near reservoirs and rivers in the northern region. The cold spots were concentrated in the northern part near the desert area.

Keywords Ecosystem service values · Spatial–temporal variation · Heihe River Basin

M. Li (✉) · L. Kang · C. Zhao
College of Geography and Environmental Engineering, Lanzhou City University, Lanzhou 730000, People's Republic of China
e-mail: lzculimt@163.com

H.-Y. Jeon (ed.), *Sustainable Development of Water and Environment*,
Environmental Science and Engineering,
https://doi.org/10.1007/978-3-030-75278-1_11

11.1 Introduction

Ecosystem service refers to the goods and services obtained directly or indirectly through the structure, process and function of ecosystem (Wei et al. 2016). It has a key role in maintaining human well-being and sustainable regional development, and has become a hot area of interest in ecology and geography (Duan et al. 2012). Ecosystem services value (ESV) is both a core indicator of ecosystem services and an important tool for assessing the effectiveness of ecological conservation (Guan et al. 2018; Huang et al. 2018). Daily (1997), Costanza et al. (1997) proposed the connotation and value evaluation method of ecosystem services, which laid the theoretical foundation for the valuation of ecosystem services. Ouyang et al. (1999) and Xie et al. (2015) proposed a methodology for valuing ecosystem services in China based on the results of Costanza's study. Based on this, many scholars have done a lot of research on the quantitative measurement of the value of terrestrial ecosystem services in China at different regions, different land types and different spatial scales, including correction of equivalent factors, sensitivity analysis, spatiotemporal distribution pattern and influencing factor analysis (Ding et al. 2020; Geng et al. 2020; Qiao et al. 2020; Wang and Ma 2020).

The Heihe River Basin is located in the inland area of northwest China, with a very fragile ecological environment. This paper reveals the main characteristics of regional land use changes from 2000 to 2018, based on land use data from 2000, 2015 and 2018, in the middle and upper reaches of the Heihe River basin. The spatial–temporal heterogeneity and spatial autocorrelation patterns of ESV were explored at the grid-scale and county-scale by using the modified ESV equivalent, ESV assessment models, and hot spot analysis. The results of the study will provide a theoretical basis for the construction of the ecological barrier zone and the sustainable development of the ecological environment in the Hexi Corridor, China.

11.2 Materials and Methods

11.2.1 Study Area

The middle and upper reaches of the Heihe River Basin (UMHRB), covering an area of 98,900 km^2, is located in Gansu and Qinhai Province, China (96°08′—101°37′E, 37°41′—42°45′N) (see Fig. 11.1). The topography of the basin is complex, with the terrain sloping from southeast to northwest. The upstream region is located in the Qilian Mountains, with high and steep mountains. The midstream region has a lower topography and consists of basins and corridor plains. The climate of Heihe River Basin has obvious zonal and regional characteristics. The upstream area has an annual average temperature of less than 2 °C and an annual precipitation of 350 mm, while the midstream area has an annual average temperature of 6~8 °C and an annual precipitation of 140 mm. The major land use types of UMHRB are

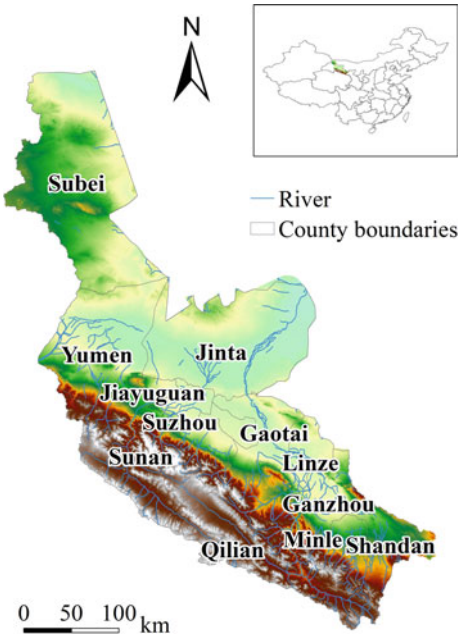

Fig. 11.1 Location of the UMHRB region

farmland, forestland, grassland, built-up land, water, and unused land. The upstream area of Heihe River Basin is dominated by grassland and forestland, which is the runoff formation area of Heihe River, while the midstream area is dominated by oasis, which is an important irrigated agricultural area. Due to the rapid transformation of regional land use, ecosystem structure and function have been greatly affected, resulting in changes in the spatial and temporal distribution of ESVs.

11.2.2 Data Sources

Land use data with a spatial resolution of 30 m in 2000, 2010 and 2018 were acquired from the Resource and Environmental Science Data Center of the Chinese Academy of Sciences (http://www.resdc.cn). Six primary classes of land use types (farmland, forestland, grassland, built-up land, water, and unused land) are classified according to the actual land use characteristics of the study area. Agricultural products were obtained from Gansu and Qinhai Statistical Yearbook.

11.2.3 Ecosystem Service Assessment Model

The ESV equivalent per unit area in the study area was corrected using crop yields and food prices with reference to the research results of Xie et al. (2015) (see Table 11.1). In order to study the spatial characteristics of ESV, the study area was divided into 1 × 1 km grid scale. The calculation formula is as follows:

$$\mathrm{ESV} = \sum_{i=1}^{n} (U_i \cdot VC_i) \tag{11.1}$$

where ESV represents the total ecosystem services value in the study area (yuan). VC_i is the ESV of 1 standard unit equivalent factor (yuan/hm^2). U_i is the i type land area in the study area.

Table 11.1 Ecosystem service value equivalent per unit area of different land use in UMHRB

Type of service		Ecological service value					
		Farmland	Forestland	Grassland	Water	Built-up land	Unused land
Provisioning service	Food production	1809.16	404.40	808.80	1702.74	0.00	42.57
	Raw material	830.08	915.22	1191.92	48,953.66	0.00	63.85
	Water supply	42.57	468.25	659.81	17,644.60	0.00	42.57
Regulating service	Gas regulation	1426.04	3001.07	4192.99	1638.88	0.00	234.13
	Climate regulation	766.23	9003.22	11,089.07	4874.08	0.00	212.84
	Waste treatment	212.84	2724.38	3660.88	11,812.73	0.00	659.81
	Hydrological regulation	574.67	7130.21	8130.56	217,609.66	0.00	446.97
Supporting service	Soil conservation	2192.27	3660.88	5108.21	1979.43	0.00	276.69
	Nutrient cycling	255.41	276.69	383.12	148.99	0.00	21.28
	Biodiversity protection	276.69	3341.62	4639.96	5427.47	0.00	255.41
Cultural service	Recreation and culture	127.71	1468.61	2043.28	4022.71	80.57	106.42

11.2.4 Hot Spot Analysis

Hotspot analysis Gi* index was used to identify spatial clusters with statistically significant high values (hot spots) and low values (cold spots), which can effectively reveal the spatial heterogeneity of ESVs. The calculation formula is as follows:

$$G_i^* = \frac{\sum_{j=1}^{n} w_{ij}x_{ij} - \bar{x}\sum_{j=1}^{n} w_{ij}}{s\sqrt{[n\sum_{j=1}^{n} w_{ij}^2 - (\sum_{j=1}^{n} wij)^2]/(n-1)}} \tag{11.2}$$

where w_{ij} is the spatial weight, x_{ij} is the observed values of the ESV evaluation unit, n is the total number of ESV evaluation units at a given scale in the study area. The higher the Z score of G_i^* index, the more obvious the clustering of hot spot areas, while the lower the score, the more obvious the clustering of cold spots.

11.3 Results

11.3.1 Land Use Change from 2000 to 2018 in UMHRB

From 2000 to 2018, unused land and grassland were the two primary land use types in UMHRB, accounting for more than 86% of the total area, while other land use types accounted for only a small proportion (see Fig. 11.2). The change trend of different land use types in the study area is as follows: the area of unused land and grassland gradually decreased, the area of built-up land, water area, forest land and farmland gradually increased.

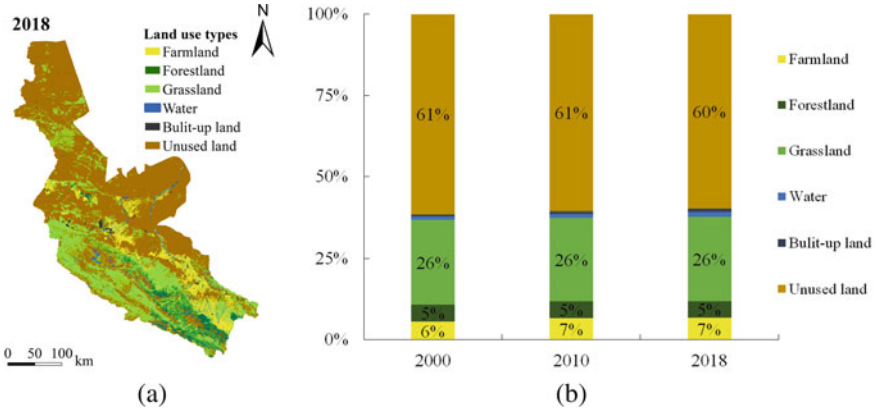

Fig. 11.2 Land use types of UMHRB in 2018 (**a**) and proportions from 2000 to 2018 (**b**)

11.3.2 Spatial–Temporal Variation of ESV in UMHRB

Characteristics of temporal development

As can be seen from Table 11.2, the ESV of UMHRB presented an upward trend from 2000 to 2018, from 1808.22×10^8 yuan to 1889.66×10^8 yuan, with an increase of 4.50% and an average annual increasing rate of 0.25%. The increase from 2000 to 2010 was slow, increasing by only 1.23%, while the increase from 2010 to 2018 was larger, increasing by 3.24%. It indicates that there was a trend of ecosystem improvement in the middle and upper reaches of the Heihe River Basin.

Among the ecosystem types, grassland and water contributed the most with 57.29% and 23.43%, respectively, while built-up land contributed the least with 0.004%. Although water area account for a small proportion of the total study area, it contributed more to the ecosystem services of the basin. As a typical inland river basin in the arid zone, increasing the watershed area has an important positive effect on improving the regional ecological environment and ecosystem services.

The change trend of ESV of different land use types is as follows: the ESV of unused land, grassland and forestland declined, and the ESV of built-up land, farmland, and water increased. The ESV of built-up land was increasing at the fastest rate, with an increment rate of 59.15% and an average annual increasing rate of 4.17%. The conversion of desert and grassland to farmland and built-up land due to urbanization and irrigated agriculture is the primary reason for the change in ESV of different land types.

The most dominant ecological service in the UMHRB is the regulating service, accounting for 66.41%, followed by the supporting service, provisioning service, and cultural service. In the regulating services, the ESV of hydrological regulation were the largest, accounting for 30.81% of the total ESV. Followed by climate regulation, which accounting for 18.91%. There are two national nature reserves in the study area, Qilian Mountain and Heihe River, with abundant forest resources and water systems, which enhance the functions of hydrological regulation and climate regulation.

Table 11.2 Change of ESV in UMHRB from 2000 to 2018

Land use types	ESV/(10^8 Yuan·a^{-1})			Change rate of ESV (%)	Average annual increasing rate (%)
	2000	2010	2018		
Farmland	47.25	56.30	57.14	20.93	1.16
Forestland	166.42	165.92	166.38	−0.03	0.00
Grassland	1090.31	1072.04	1082.64	−0.70	−0.04
Water	359.68	393.56	442.72	23.08	1.28
Built-up land	0.04	0.05	0.07	59.15	4.17
Unused land	144.52	142.52	140.72	−2.63	−0.15
Total	1808.22	1830.40	1889.66	4.50	0.25

From 2000 to 2018, only the ESVs of climate regulation have slightly decreased, while other ecosystem services have increased. The ESV of raw material production, water supply and hydrological regulation increased faster, by 13.52%, 10.58% and 10.57% respectively. The construction of ecological projects such as natural forest protection and return of cultivated land to forest has increased the area of forest land in the study area. The water connotation function of forest land is the main reason for the increase of the ESV of these three ecosystem services (Table 11.3).

Characteristics of spatial variation

The spatial distribution of ESVs at the 1-km grid scale from 2000 to 2018 was shown as Fig. 11.3. The spatial variation of ESVs in UMHRB showed a decreasing spatial pattern from the Qilian Mountains to the corridor plains. From 2000 to 2018, the high-value area was stably distributed in the Qilian Mountains, whose vegetation cover was dominated by woodlands and grasslands, with a good ecological environment. Meanwhile, a medium–high value aggregation zone was formed along the main stream of the Heihe River, under the influence of the distribution of water in the region. The low-value areas were mainly located in the midstream plains and desert areas, which were more disturbed by human activities and dominated by farmland, built-up land and unused land, with relatively poor ecological environment.

Table 11.3 The individual ESVs in UMHRB from 2000 to 2018

Ecosystem service	ESV/(10^8 Yuan·a^{-1})			Change rate of ESV (%)	Average annual increasing rate (%)
	2000	2010	2018		
Food production	37.70	39.42	40.03	6.19	0.34
Raw material	99.98	105.52	113.49	13.52	0.75
Water supply	42.51	44.11	47.01	10.58	0.59
Gas regulation	148.61	148.23	149.55	0.63	0.04
Climate regulation	357.57	353.76	357.36	−0.06	0.00
Waste treatment	164.23	163.53	165.85	0.99	0.05
Hydrological regulation	526.53	546.45	582.19	10.57	0.59
Soil conservation	183.05	183.08	184.73	0.92	0.05
Nutrient cycling	14.28	14.38	14.51	1.62	0.09
Biodiversity protection	161.22	159.81	161.71	0.30	0.02
Recreation and culture	72.55	72.12	73.23	0.94	0.05

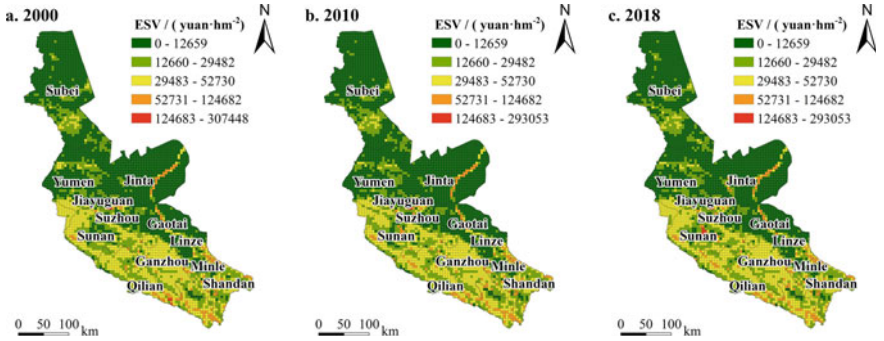

Fig. 11.3 Spatial distribution of ESV in the UMHRB from 2000 to 2018

In 2000, the high-value areas of unit area ESV mainly distributed in Qilian and Minle, and low-value areas primarily distributed in Subei, Yumen, and Jinta. Compared with 2000, there was no significant change in the high value area and the low value area in 2010. In 2018, the high-value areas decreased and were mainly concentrated in Qilian County. The development of urbanization in the region had led to the encroachment of built-up land on farmland and grassland.

Hotspot analysis showed that the spatial distribution pattern of hot and cold spots of ESV in UMHRB remained basically stable from 2000 to 2018 (see Fig. 11.4). The hot spots were mainly distributed in the southern Qilian Mountains, and sporadically scattered near reservoirs and rivers in the northern region. The cold spots were concentrated in the northern part near the desert area, while the rest of the area had no obvious spatial clustering characteristics. In 2000, the spatial concentration of ESV was most pronounced. Compared with 2000, the changes of cold spots and hot spots were not obvious in 2010, and some hot spots in southern area of Subei became insignificant, while hot spots in western area of Sunan increased. In 2018, the hot spots and cold spots showed a shrinking trend compared with the previous stage. The

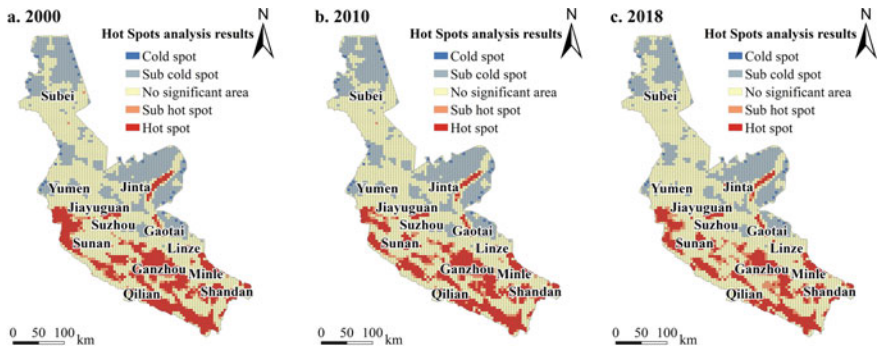

Fig. 11.4 Spatial clustering of ESV in UMHRB from 2000 to 2018

hot spots in Sunan were greatly reduced, while the secondary cold spots in Yumen gradually disappeared and became non-significant areas.

11.4 Conclusions

The structure of land use in UMHRB was dominated by unused land, followed by grassland, farmland, forestland, water area and built-up land. The change trend of land use was the decrease of unused land and grassland, and the increase of built-up land, water area, farmland and forest land.

The temporal evolution of total ESV in UMHRB had shown a steady upward trend from 2000 to 2018. Among the ecosystem types, grassland and water area contributed the most to ESV. The trend of ESV changes showed that the ESV of unused land, grassland and forestland decreased, while the ESV of built-up land, farmland and water increased. For each individual ESV, hydrological regulation and climate regulation had the largest ESV contribution. Only the ESVs of climate regulation have slightly decreased, while other ecosystem services have increased.

The spatial distribution of ESV in UMHRB showed a spatially clustered distribution pattern and the degree of clustering was slightly weakened. From 2000 to 2018, the hot spots were mainly distributed in the southern Qilian Mountains, and sporadically scattered near reservoirs and rivers in the northern region. The cold spots were concentrated in the northern part near the desert area.

Acknowledgements This work was supported by Doctoral Research Fund of Lanzhou City University (LZCU-BS2018-16), and Humanities and Social Sciences Research Project of Gansu province, China(20ZZ06).

References

Costanza R, Groot RD, Stephen F et al (1997) The values of the world's ecosystem services and natural capital. Nature 387(15):253–260

Daily GC (1997) Nature's services: societal dependence on natural ecosystems. Island Press, Washington

Ding MT, Pei FS, Hu YC et al (2020) Spatial and temporal changes of ecosystem service value in Jiangsu Province based on LUCC. Acta Ecol Sin 40(19):6801–6811 (in Chinese)

Duan J, Kang MY, Jiang Y (2012) Dynamic valuation on ecosystem services of Dongjiang River Basin. J Nat Resour 27(1):90–103 (in Chinese)

Geng TW, Chen H, Zhang X et al (2020) Spatiotemporal evolution of land ecosystem service value and its influencing factors in Shaanxi province based on GWR. J Nat Resour 35(7):1714–1727 (in Chinese)

Guan QC, Hao JM, Shi XJ et al (2018) Study on the changes of ecological land and ecosystem service value in China. J Nat Resour 33(2):195–207 (in Chinese)

Huang L, Cao W, Xu XL et al (2018) Linking the benefits of ecosystem services to sustainable spatial planning of ecological conservation strategies. J Environ Manage 222:385–395

Ouyang ZY, Wang XK, Miao H (1999) A primary study on Chinese terrestrial ecosystem services and their ecological-economic values. Acta Ecol Sin 19(5):607–613 (in Chinese)
Qiao B, Zhu CX, Cao XY et al (2020) Spatial autocorrelation analysis of land use and ecosystem service value in Maduo County, Qinghai Province, China at the grid scale. Chin J Appl Ecol 31(5):1660–1672 (in Chinese)
Wang YQ, Ma JM (2020) Effects of land use change on ecosystem services value in Guangxi section of the Pearl River-West River Economic Belt at the county scale. Acta Ecol Sin 40(21):7826–7839 (in Chinese)
Wei H, Zhao WW, Zhang X et al (2016) Regional ecosystem service value evaluation based on land use changes: a case study in Dezhou, Shandong Province, China. Acta Ecol Sin 37(11):3830–3839 (in Chinese)
Xie GD, Zhang CX, Zhang LM et al (2015) Improvement of the evaluation method for ecosystem services based on per unit area. J Nat Resour 30(8):1243–1254 (in Chinese)

Chapter 12
Transportation of Chromium(VI) from Hydrochloric Acid Medium via a Dispersion Supported Liquid Membrane Using N235

Yingxue Li, Yijian Zhong, Jiaheng Wu, Qingsong Shao, Xiaoyan Chen, and Yan Zhu

Abstract The permeation of Cr(VI) from acidic media, through a dispersion supported liquid membrane (DSLM), impregnated with tri-n-octylamine (N235) in diluent has been investigated in flat-sheet operational mode. Effects of operational factors including stirring speed, initial Cr(VI) concentration, N235 concentration, NaOH concentration, and the volume ratio of liquid membrane and strip liquor in dispersion phase on Cr(VI) transport have been studied. The evaluation of Cr(VI) separation from hydrochloric acidic media was carried out. Under the optimal condition, the migration rate of 0.01 g/L Cr(VI) was observed as 94%.

Keywords Separation · Dispersion supported liquid membrane · N235 · Cr(VI)

12.1 Introduction

As an important raw material, Cr(VI) is widely used in various fields of industrial and agricultural production. With the development of industries such as tanning, electroplating and non-ferrous metal smelting, Cr(VI) containing wastewater is discharged into aqueous ecosystem. Due to its non-biodegradability, Cr(VI) thus accumulate in human body via the amplification effect of food chain, leading to the public

Y. Li · J. Wu · Q. Shao · X. Chen · Y. Zhu
School of Inspection and Testing Certification, Changzhou Vocational Institute of Engineering, Changzhou 203164, Jiangsu, China

Y. Zhong (✉)
College of Environmental Science and Engineering, Guilin University of Technology, Guilin 541006, China
e-mail: zhongyijian@glut.edu.cn

Guangxi Key Laboratory of Theory and Technology for Environmental Pollution Control, Guilin University of Technology, Guilin 541006, China

Collaborative Innovation Center for Water Pollution Control and Water Safety in Karst Area, Guilin University of Technology, Guilin 541006, China

H.-Y. Jeon (ed.), *Sustainable Development of Water and Environment*,
Environmental Science and Engineering,
https://doi.org/10.1007/978-3-030-75278-1_12

concern. The conventional methods for treating Cr(VI) containing wastewater are mainly chemical precipitation, adsorption, membrane separation. Owning to the low cost, high treatment capacity, operational simplicity, the methods above have been applied in practical cases widely. Yet, the conventional methods cannot recover the non-renewable Cr(VI), resulting in potential secondary pollution. Thus, it is urgent to develop a Cr(VI) containing wastewater treatment technology with low energy consumption, low cost and high recovery rate. As a novel separation technology, liquid membrane with fast mass transfer rate, high selectivity and non-secondary pollution has been attracted much research attention in recent years (Zhao et al. 2017; Yang et al. 2017; Rajewski and Rajewska 2017; Nawaz et al. 2017; Mohebali et al. 2017; Duan et al. 2017).

Briefly, in a supported liquid membrane (SLM) process, an liquid membrane is immobilized in the pores of a microporous polymer or an inorganic support by capillary forces. Liquid membrane technology is derived from extraction. A liquid–liquid extraction combined with a stripping process occurs with the concentration difference as the driving force. The liquid membrane adsorbed on the hydrophobic microporous membrane support, then the pollutant will transport from aqueous solution to stripping solution via interface coordination chemical reaction on both sides of liquid membrane and promoted transmission inside liquid membrane. In general, carrier related mass transfer process plays a key role in SLM process.

Although low stability during long-term operation, liquid membrane technologies are increasingly applied to separate heavy and toxic metals from diluted solutions. However, owing to the stirring process and physical reactions, the leakage of liquid membrane from microporous support could lower the mass flux and the stability of SLM. To improve the stability of SLM, the emerging techniques for strip/organic dispersion methodologies, including dispersion supporting liquid membrane (DSLM) have been paid more attention(Yen et al. 2016; Lu and Pei 2016; Li et al. 2015; Hao et al. 2014a,b). The liquid membrane solution is organic solution in a certain proportion to produce the dispersion solution. Under the action of external stirring, the liquid membrane in the support can be renewed in time during the migration, providing guarantee for simultaneous extraction and stripping process. The utility model can overcome the defect that the carrier leaks from the microporous membrane support and prolong the service life of the membrane.

In this paper, polyvinylidene fluoride (PVDF) was used as microporous support, DSLM was applied to separate Cr(VI). The operational parameters were optimized.

12.2 Experimental

12.2.1 Reagents

Tri-n-octylamine (N235, CP, wt% $\geq$ 98%, Shaoyang Chemical Research Institute, Hunan, China). Hydrogen chloride (HCl), phosphoric acid (H_3PO_4), sulfuric acid

(H_2SO_4), sodium hydroxide (NaOH), n-heptane, diphenylcarbazide are all analytical reagents and purchased from Sinopharm Chemical Reagent Co., Ltd. Deionized water was applied in all the experiments. Cr(VI) hydrochloric acid solution was produced by dissolving appropriate amount of $K_2Cr_2O_7 \cdot xH_2O$ in hydrochloric.

12.2.2 Instruments

HD2004W motor stirrer was purchased from Shanghai Si Le Instrument Co., LTD. PHS-3C pH meter was commercially accessible from Shanghai Precision Scientific Instrument Co., LTD. ATY224 electronic balance was purchased from Shimadzu. 722 uv–visible spectrophotometer was purchased from Shanghai Spectral Instrument Co., LTD. Cr(VI) species analysis was conducted spectrophotometrically using diphenylcarbazid as chromogenic regent.

12.2.3 Experimental Procedure

DSLM studies were conducted with pyrex glass cell consisting of two compartments (each volume = 200 mL) with the feed and stripping solutions being stirred (200 rpm). N235 was dissolved in n-heptane to produce a liquid membrane solution. A certain concentration of organic solution was prepared as the liquid membrane solution. PVDF membrane support were kept in N235/n-heptane solution (liquid membrane solution) for 12 h prior to use. Forced by capillary action, the liquid membrane solution filled the pores of PVDF membrane support. Afterwards, the submerged membrane was removed from the solution and wiped carefully with a tissue paper to remove the excess liquid membrane. A certain concentration of aqueous solution and a certain volume of dispersion solution were added to the migration tank on both sides of the microporous membrane, and stirred simultaneously on both sides. After a certain time, the concentration of Cr(VI) was determined by diphenylcarbazide spectrophotometer. Determination of Cr(VI) in the aqueous solution was conducted at different time intervals to calculate the permeability coefficients. The extraction studies were carried out at ambient temperatures (24–26°C). DSLM reactor is composed of a unique membrane support for separating and recycling of Cr(VI). The waste liquid containing the target species, and the mechanical agitation was introduced to homogenize the solution. The stripping agent (NaOH) was dispersed in the liquid membrane organic solution in a tank with an impeller stirrer to form the dispersion solution. PVDF hydrophobic microporous polymeric membranes (flat-sheet type) were applied. The support is hydrophobic PVDF membrane (pore diameter = 0.22 μm, thickness = 0.13 mm, porosity = 65%, effective area = 11.93 cm^2). The volume of aqueous phase tank and stripping dispersion tank are 200 mL. The PVDF support was set between the aqueous phase tank and stripping dispersion tank. The porosity of membrane (pore size = 0.22 μm) was determined as 65% with

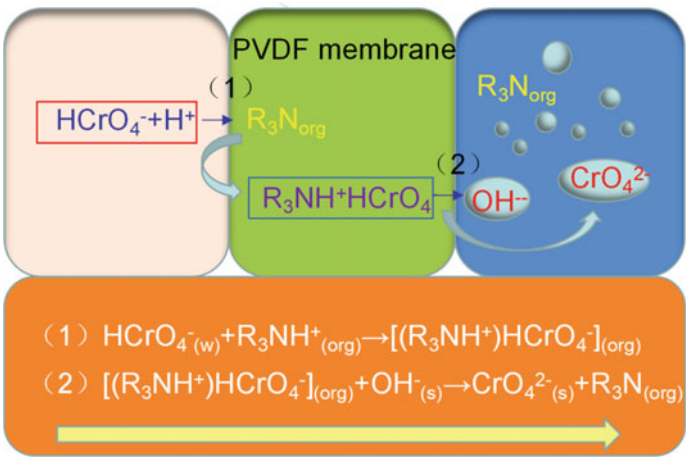

Fig. 12.1 Schematic illustration presenting the formation mechanism of $Na_2Cr_2O_4$ using the DSLM

an effective area (calculated from the geometrical area and membrane porosity) of 11.93 cm^2.

The liquid membrane solution is permeated by capillary forces (surface tension) and filled with porous channels of inert PVDF supported membrane. The complex formed by the reaction of Cr(VI) ion with the N235 in the liquid membrane loaded on the hydrophobic micropore at the aqueous-membrane interface, and then the decomplexation reaction occurred at the interface between the liquid membrane solution and the dispersion solution and recovered the metal ions. The principle of the experiment is shown in Fig. 12.1. The main reaction principle of separation of Cr(VI) from hydrochloric acid solution by N235 is described in Ref. (Alguacil et al. 2008).

12.2.4 Transport Equations

Transport process in DSLM involves three steps: (1) extraction reaction at the feed-membrane interface, (2) diffusion inside the membrane and (3) stripping at the membrane-receiver interface.

Extraction rate of Cr(VI):

$$E = \left(1 - \frac{C_t}{C_0}\right) \times 100\%$$

where C_0 and C_t are the metal Cr(VI) ion concentration (mol/L) at the feed side at the initial time and t time respectively.

According to literature (Alguacil et al. 2008):

$$\ln \frac{C_t}{C_0} = -\frac{A}{V_w} Pt$$

where A is the exposure area of the membrane (m^2); P is the permeability coefficient of metal ions at the feed-membrane interface(m/s); V_w is the aqueous solution volume (m^3); t is the reaction time (s).

12.3 Results and Discussion

12.3.1 Effect of PVDF Membrane Before and After Loading on Cr(VI) Permeation

Before liquid membrane extraction, it is necessary to load the liquid membrane on the support of PVDF for 12 h. Figure 12.2 shows the migration of Cr(VI) in the liquid membrane before and after PVDF loading. The relationship between-ln (C_t/C_0) and time t is linear. After loading PVDF membrane with liquid membrane for 12 h, the mobility of Cr(VI) is stronger than that of DSLM without liquid membrane loading. Therefore, before the reaction, it is necessary to load a certain concentration of liquid membrane solution on PVDF membrane. The reason is that when the ions are separated by the unloaded DSLM, the liquid membrane in the dispersion solution needs to be loaded on PVDF membrane before it reacts with Cr(VI) ion in the boundary layer of the aqueous membrane, therefore, the liquid membrane solution

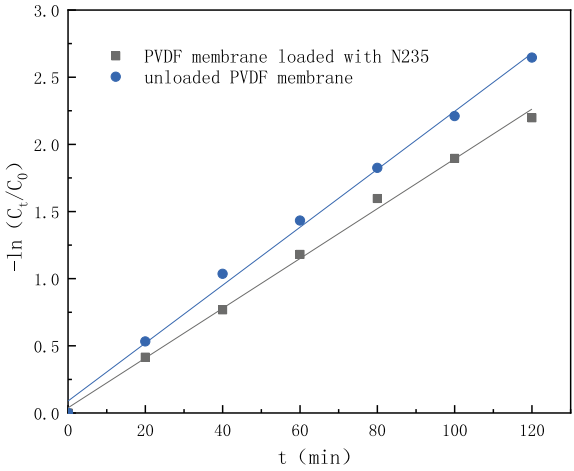

Fig. 12.2 Effect of PVDF membrane status on Cr(VI) permeation

in the dispersion solution will have some resistance when it migrates to the PVDF support.

12.3.2 *Effect of Stirring Rate on Cr(VI) Permeation*

A linear relationship between $-\ln(C_t/C_0)$ and t was observed (Fig. 12.3). The slope of the straight line increases with increasing stirring rate, and the extraction rate increases with increasing stirring time and stirring rate. Because with the increase of the stirring rate of the aqueous solution and the dispersion solution, the contact chance between Cr(VI) and the extractant N235 increases, which is beneficial to the mass transfer of the complex through the liquid membrane, In addition, the increasing of stirring rate can also promote the decomplexation reaction. When the stirring rate was higher than 400 r/min, the extraction rate was not increased. For the strip dispersion solution, although the Cr(VI) permeation also increases with the stirring rate increasing, but when the stirring rate is more than 200 r/min, the liquid volatilization loss in the strip dispersion solution is serious, and when the stirring rate is 200 r/min, there is little loss of liquid in the strip dispersion solution. Therefore, the stirring rate of aqueous solution 400 r/min and the stirring rate of strip dispersion solution 200 r/min is considered as the optimal stirring condition. And 94% extraction rate of Cr(VI) was observed under the optimal stirring condition.

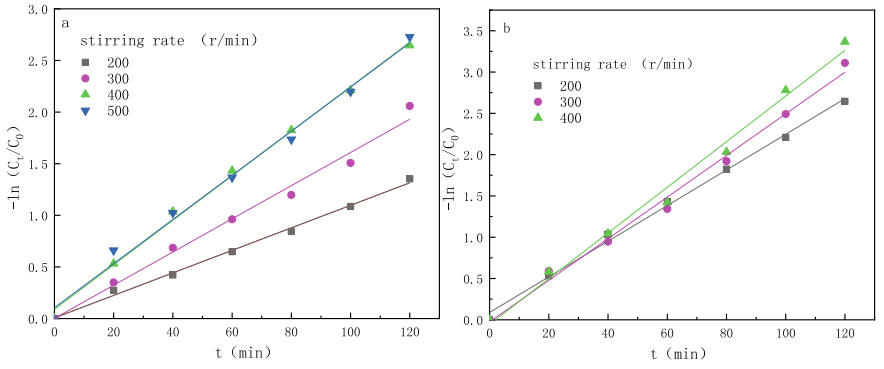

Fig. 12.3 Effect of stirring rate on Cr(VI) permeation (**a**:The stirring rate of aqueous solution **b**:The stirring rate of dispersion solution)

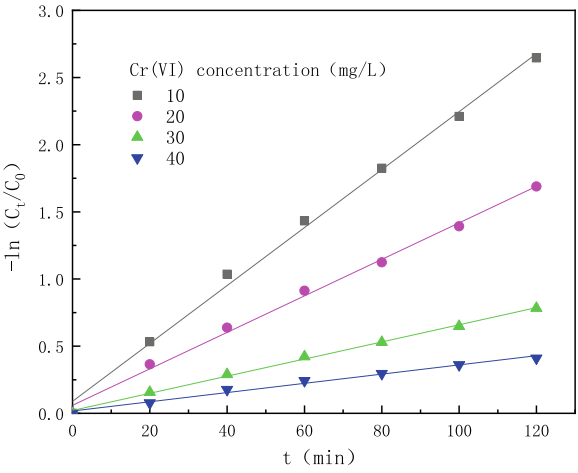

Fig. 12.4 Effect of Cr(VI) initial concentration on Cr(VI) migration

12.3.3 Effect of Initial Concentration of Metal Ions on Cr(VI) Permeation

Diffusion resistance plays a dominant role in the passage of Cr(VI) through the migration interface. As can be seen from Fig. 12.4, the slope of the straight line between $-\ln (C_t/C_0)$ and t decreases with the increase of Cr(VI) concentration, so the migration of Cr(VI) decreases with the increase of Cr(VI) concentration. This is attributed to the reason that extraction capacity is limited when the composition of dispersion solution and structure of the transfer device are fixed.

12.3.4 Effect of N235 Concentration on Cr(VI) Permeation

In the DSLM, the amount of extractant N235 not only affects the mass transfer rate of Cr(VI), but also changes the physical chemistry properties (viscosity and surface tension) of the membrane solution, thus affecting the mass transfer of Cr(VI) through the liquid membrane. As can be seen from Fig. 12.5, when the concentration of N235 was increased from 0.004 mol/L to 0.020 mol/L, the permeation of Cr(VI) increased gradually, and then decreased with the increase of N235 concentration. This is because the separation process of Cr(VI) in DSLM is cooperatively controlled by the chemical reaction between Cr(VI) anions and the N235 and the diffusion process after their combination. when the N235 concentration is less than 0.020 mol/L, the migration process is controlled by the complexation reaction. According to the chemical reaction equilibrium principle, the higher the concentration of the N235 is, the more complete the reaction is. However, when the concentration of N235 reached 0.028 mol/L, the diffusion mass transfer process of complex was dominant,

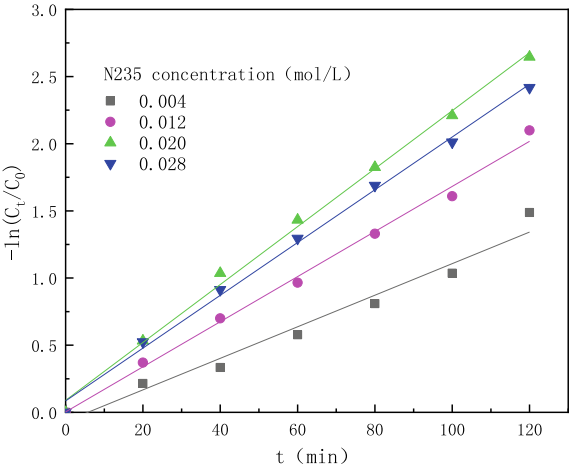

Fig. 12.5 Effect of N235 concentration on Cr(VI) permeation

and the viscosity of the liquid membrane was increased, the mass transfer resistance of Cr(VI) in liquid membrane is increased and the permeation of Cr(VI) is decreased.

12.3.5 Effect of NaOH Concentration on Cr(VI) Permeation

After Cr(VI) anions reacted with N235 at the interface of aqueous membrane, the products transferred to the interface between the liquid membrane and the dispersion solution and formed Na_2CrO_4 in the presence of NaOH in dispersion solution, leading to the recovery of Cr(VI). Therefore, the concentration of NaOH has a direct effect on the transport of Cr(VI) ions. When the pH of aqueous solution is 1.0, the volume ratio of liquid membrane organic solution to NaOH solution is 1:1, the initial concentration of Cr(VI) is 0.01 g/L, the concentration of N235 is 0.02 mol/L, the relationship between $\ln(C_t/C_0)$ and time t under different concentration of NaOH is shown in Fig. 12.6. A linear relationship between $-\ln(C_t/C_0)$ and t was observed. With the increase of NaOH concentration, $-\ln(C_t/C_0)$ increases. When OH^- concentration is Less than 1.0 mol/L, the driving force for the production of Na_2CrO_4 is small at the interface of membrane and stripping solution, resulting in the decreasing of extraction rate of Cr(VI). With the increase of the concentration of the extractant, the amount of the extractant molecules in the dispersion solution also increases, which accelerate the reaction rate of the whole reaction process, increases the mass transfer of Cr(VI) in the transport process, and increases the extraction rate. With the increase of NaOH concentration, the transfer rate of Cr(VI) increases gradually. When the concentration of NaOH is 1.0 mol/L, the optimal separation rate of Cr(VI) can be realized. As the concentration of NaOH continues to increase, the transfer rate decreases. With the increase of NaOH concentration in the stripping solution, the dispersion liquid become unstable and is easy to be emulsified, hindering the

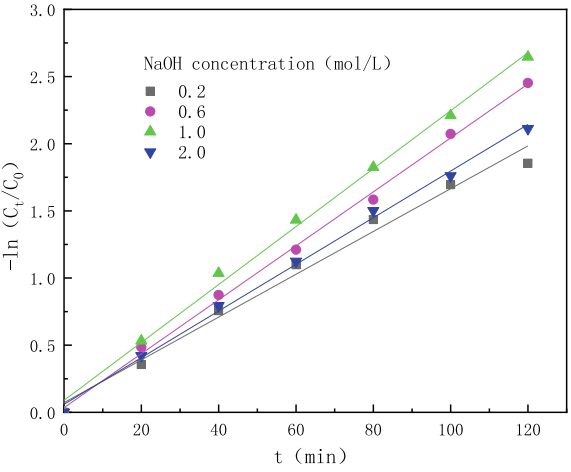

Fig. 12.6 Effect of NaOH concentration on Cr(VI) permeation

transmission of Cr(VI). The optimal concentration of the stripping agent is 1.0 mol/L, considering the process cost.

12.3.6 The Effect of the Volume Ratio of Liquid Membrane Solution to NaOH on Cr(VI) Permeation

When the pH of the aqueous solution is 1.0, the initial concentration of Cr(VI) is 0.01 g/L, the concentration of NaOH is 1.0 mol/L, and the concentration of N235 is 0.02 mol/L, the permeation of Cr(VI) in the dispersion solution is shown in Fig. 12.6. As can be seen from the Fig. 12.7, $-\ln(C_t/C_0)$ has a linear relationship with t, and the slope of its straight line varies with the volume ratio. In DSLM, the dispersion solution is formed by the uniform mixing of the stripping solution and the liquid membrane solution. Such a combination can effectively compensate for the loss of the liquid membrane solution in the supported PVDF membrane during migration, therefore, the composition of the dispersion solution plays an important role in supporting the migration of Cr(VI). As the dispersion solution is formed by the homogeneous dispersion of NaOH in the liquid membrane solution, the larger the proportion of NaOH in the dispersion solution, the larger the alkalinity of the dispersion solution, and the more unstable the emulsion formed, so when W/O is larger than 1:1, the transmission of Cr(VI) is disadvantageous. With the decrease of W/O, the concentration of liquid membrane solution in the dispersion solution increases. The membrane solution in the dispersion solution can provide more extraction interface and renew the liquid membrane in PVDF supported membrane in time, therefore, the ion extraction rate and the service life of the supported liquid membrane can be increased to a certain extent. However, the smaller the proportion of NaOH leads to the smaller extraction area, resulting in the low separation ration of Cr(VI).

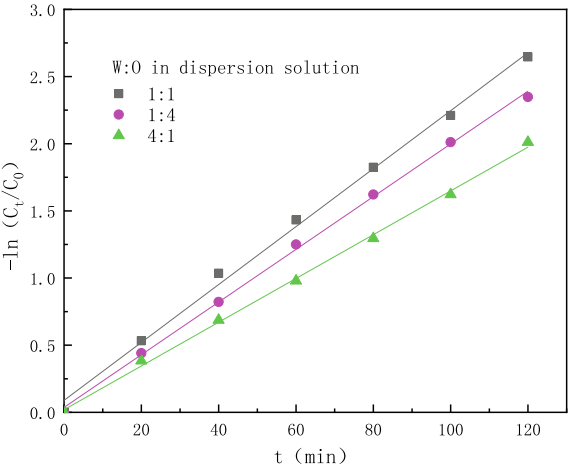

Fig. 12.7 The effect of the W/O in dispersion solution on Cr(VI) permeation

12.4 Conclusion

The DSLM technique was applied to separate Cr(VI) with N235. The optimal separation conditions of Cr(VI) were 1.0 mol/L NaOH concentration of the dispersion solution, 1:1 ratio of liquid membrane solution to stripping solution, 1.0 pH of the aqueous solution and 0.02 mol/L N235 concentration of the extractant. When the concentration of Cr(VI) in acid solution is 0.01 g/L, the separation rate of Cr(VI) can reach 94% under the optimal conditions in 2 h.

Acknowledgements Foundation item: Natural Science Foundation of the Jiangsu Higher Education Institutions of China (No. 18KJD610001); Guangxi innovation research team project (No. 2018GXNSFGA281001); Doctor of Philosophy (PhD) Start-up Foundation of Changzhou Vocational Institute of Engineering (No.11130900117002); Students' Platform for Innovation and Entrepreneurship Training Program, China (No. 201813102026H); Guangxi Mid-Youth Capability Project (No. 2018KY0249); Jiangsu Research funds of Guangxi Key Laboratory of Environmental Pollution Control Theory and Technology (No. 001102216078)

References

Alguacil FJ, Alonso M, Lopez F, Lopez-Delgado A (2008) Uphill permeation of Cr(VI) using Hostarex A327 as ionophore by membrane-solvent extraction processing. Chemosphere 72:684–689

Duan HP, Yuan XH, Zhang Q, Wang ZY, Huang ZJ, Guo H, Yang XJ (2017) Separation of Ni^{2+} from ammonia solution through a supported liquid membrane impregnated with Acorga M5640. Chem Pap 71(3):597–606

Hao ZS, Wang ZH, Zhang WD, Ho WSW (2014a) Supported liquid membranes with organic dispersion for recovery of Cephalexin. J Membr Sci 468:90–97

Hao ZS, Vilt ME, Wang ZH, Zhang WD, Ho WSW (2014b) Supported liquid membranes with feed dispersion for recovery of Cephalexin. J Membr Sci 468:423–431

Li GP, Xue JQ, Yu LH, Liu NN (2015) Study of cyanide wastewater treatment by dispersion supported liquid membrane using trioctylamine and kerosene as liquid membrane. Water Sci Technol 72(4):643–650

Lu SB, Pei L (2016) A study of zinc borne waste water treatment with dispersion supported liquid membrane. Int J Hydrog Energy 41(35):15717–15723

Mohebali S, Nazari M, Rahbar-Kelishami A, Davoodi-Nasab P (2017) Performance of sunflower oil as green solvent for Cr(VI) extraction using supported liquid membrane. Desalin Water Treat 64:173–178

Nawaz R, Ali K, Ullah R (2017) Facilitated transport of Cd(II) through supported liquid membrane with tridodecylamine as carrier. Environ Eng Sci 34(8):585–598

Rajewski J, Rajewsk P (2017) Possibilities of chromium (III) separation from acid solution using the double-carrier supported liquid membrane (DCSLM). Water Sci Technol 75(10): 2358–2368

Yang XJ, Zhang Q, Wang ZY, Li SJ, Xie QY, Huang ZJ, Wang SX (2017) Synergistic extraction of gold(I) from aurocyanide solution with the mixture of primary amine N1923 and bis(2-ethylhexyl) sulfoxide in supported liquid membrane. J Membr Sci 540:174–182

Yen FC, Chang TC, Laohaprapanon S, Chen YL, You SJ (2016) Recovery of indium from LCD waste by solvent extraction and the supported liquid membrane with strip dispersion using D(2)EHPA as the extractant. Solvent Extr Res Dev Jpn 23: 63–73

Zhao PP, Yang F, Zhao ZG, Liao QX, Zhang Y, Chen P, Guo WH, Bai RX (2017) A simple preparation method for rare-earth phosphate nano materials using an ionic liquid-driven supported liquid membrane system. J Ind Eng Chem 54:369–376

Chapter 13
Effects of Important Factors on Determination of Metals in Soil Samples Using Hand-Held X-ray Fluorescence

Zhuoxin Yin, Yijun Wen, Weidong Chen, Fanxiang Han, Guohua Chang, and Caiping Yao

Abstract The influence of the releasion, migration and transformation of heavy metals in the process of mineral mining on the content of soil components near the mine needs to be studied, and some reliable element determination methods need to be adopted in the research process. Soil samples in 20 mesh (0.850 mm), 40 mesh (0.425 mm), 80 mesh (0.180 mm) and 100 mesh (0.150 mm) from farmland and mining areas of Longnan City in Gansu Province were determined by S1 Titan hand-held X-ray Fluorescence (XRF) spectrometer for understanding factors affecting composition contents determination. Results showed that mesh of samples sieved had a definite impact on determination of heavy metals. Repeatability was greatly affected when samples were in 20 mesh and 100 mesh. Contents of As and Al_2O_3 in samples were easily affected by mesh of sample. It should be concerned that As contents of some soil samples from farmland in Longnan City of Gansu Province were more than 30 mg/kg, contents of metals, sucn as Pb, Zn and As from mining area in Longnan City of Gansu Province were more than 1000 mg/kg. The phenomenon revealed by these measurement data required attention.

Keywords Soil · XRF · Metal

Z. Yin · F. Han · G. Chang (✉) · C. Yao
College of Geography and Environmental Engineering, Lanzhou City University, Lanzhou City, Gansu 730070, China
e-mail: cgh@lzcu.edu.cn

Y. Wen
Jinchang Pollution Source Control Center, Jinchang City, Gansu 737100, China

W. Chen
Gansu Xinjia Environmental Protection Engineering Co., Ltd, Lanzhou City, Gansu 730030, China

H.-Y. Jeon (ed.), *Sustainable Development of Water and Environment*,
Environmental Science and Engineering,
https://doi.org/10.1007/978-3-030-75278-1_13

13.1 Introduction

The main sources for soil, water and air environmental resources pollution near the mining area, was the releasion, migration and transformation of heavy metals in the process of metal mining. Heavy metal pollution of soil is an important factor restricting the sustainable and stable development of agriculture in China. Heavy metals in the soil can enter the human body through the food chain after being enriched by crops, which posed potential risks to human health (Shah and Daverey 2020; Haller and Jonsson 2020).

At present, there are many detection methods of metal elements in soil (Zhou et al. 2019; Lu et al. 2018; Soodan et al. 2014), including Atomic Absorption Spectrometry (AAS), Inductively Coupled Plasma Mass Spectrometry (ICP-MS) and voltammetry. In the application of these methods, the samples need to be pretreated for a long time, and consumes reagents and energy. Therefore, it is very important to detect the content of metal elements in soil quickly and accurately.

The hand-held XRF spectrometer is a portable on-site analyzer, which uses X-ray to irradiate the sample to produce fluorescence. The instrument records the energy and frequency of the secondary characteristics of the X-ray, and finally carries out quantitative or qualitative analysis. It can simultaneously determine a variety of metal elements. The pretreatment method is simple, fast and non-destructive (Peralta et al. 2020; Brent et al. 2017; Peng et al. 2018).

One of the main influencing factors for the repeatability and accuracy of sample determination was the sample mesh in the analysis process with the hand-held XRF spectrometer. Our staff collected soil samples from farmland and mining area, and applied hand-held XRF spectrometer to samples of different meshes for assay determination for the sake of understanding the impact of sample mesh on analysis. The results could provide important reference to rapid determination and improved accuracy for usinig this instrument in the future.

13.2 Method and Material

Soil samples used in the experiments came from Longnan City in the south of Gansu Province. Longnan City is located from east longitude 104°01′19″ to 106°35′20″, northern latitude from 32°35′45″ to 34°32′00″, the land area of Longnan City is medium, and the texture soil is heterogene. Checkerboard sampling method was selected according to Technical Specification for Soil Environmental Monitoring (State Environmental Protection Agency of China 2004a). Sampling points were mainly within local farmland and the mining area of Zhongbao Mining in Xihe County (E 105°27′9″, N 33°48′32″, E 105°19′25″, N 33°53′30″). Thirteen soil sample, including eleven farmland samples (S1–S11) and two mining samples (S12, S13) were analyzed for determination. Soil samples were spread into a thin layer of 1–2 cm thick on plastic cloth indoors, and the impurities of gravel, crushed

stone and plant debris were picked out. Soil sample of 500 g was grinded in a large mortar, and after sampling by quartering, and passed through a 20 mesh (0.850 mm) sieve. Remaining sample was sieved separately by quarter method through 40 mesh (0.425 mm), 80 mesh (0.180 mm) and 100 mesh (0.150 mm). Hand-held XRF spectrometer was used for determination by pointing the instrument probe at the sample and measuring for 60 s according to Instrument Usage Specifications of S1 TITAN hand-held XRF spectrometer, and then we took notes of the type and content of the metal in samples. Every sample was parallel measured three times; determination results were demonstrated as Average Value ±SD.

13.3 Results and Discussion

13.3.1 Effect of Different Mesh on Determination of Metal Content

Analytical results from soil samples from farmland (S1–S11) and mining area (S12, S13) of different meshes were shown in all figures from Figs. 13.1, 13.2, 13.3, 13.4 to 13.5. Figures 13.1, 13.2, 13.3, and 13.4 showed the analytical results of different soil samples from farmland areas (S1–S4, S5–S8, S9–S11) and mining areas (S12,

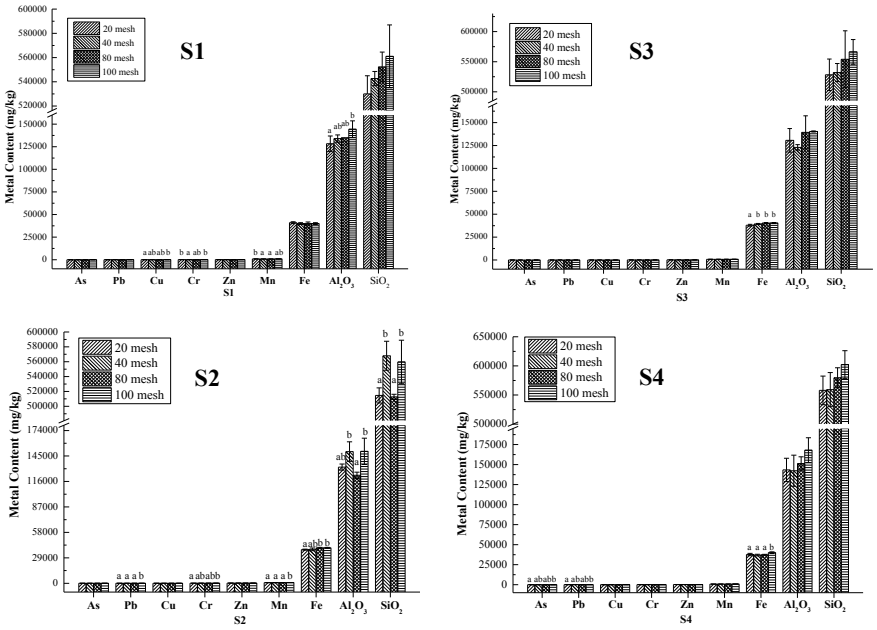

Fig. 13.1 Analytical results of different soil samples from farmland area (S1–S4)

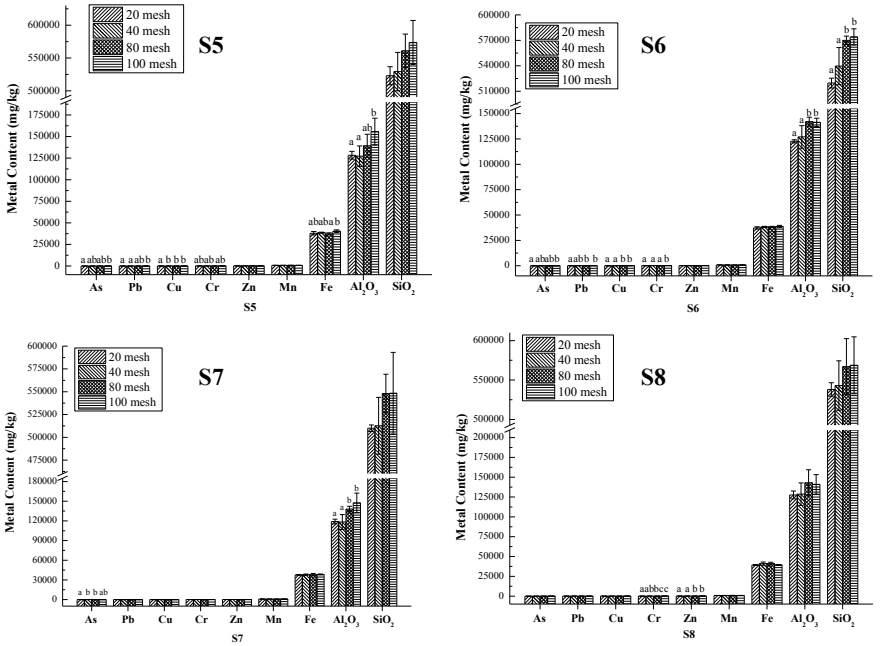

Fig. 13.2 Analytical results of different soil samples from farmland area (S5–S8)

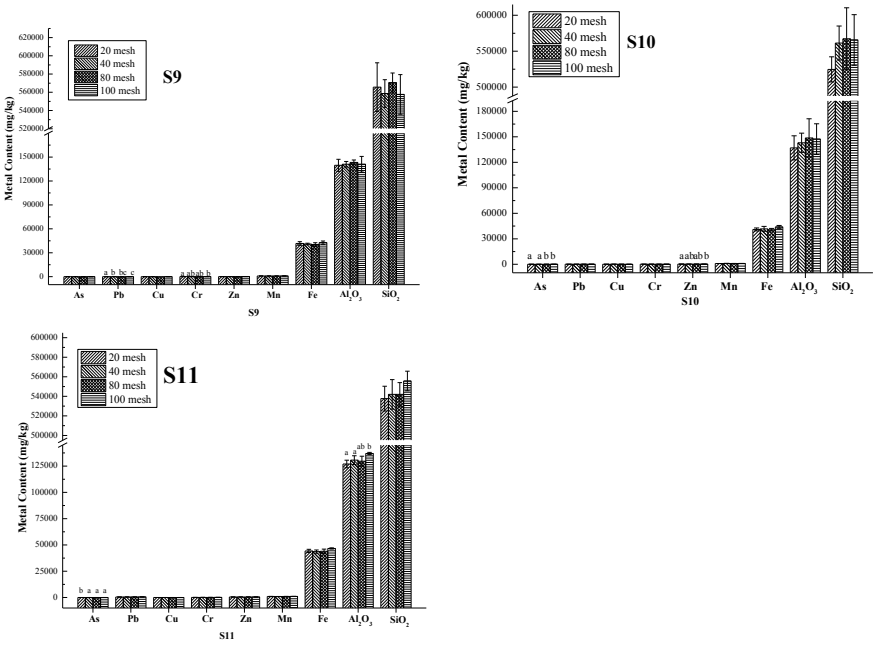

Fig. 13.3 Analytical results of different soil samples from farmland area (S9–S11)

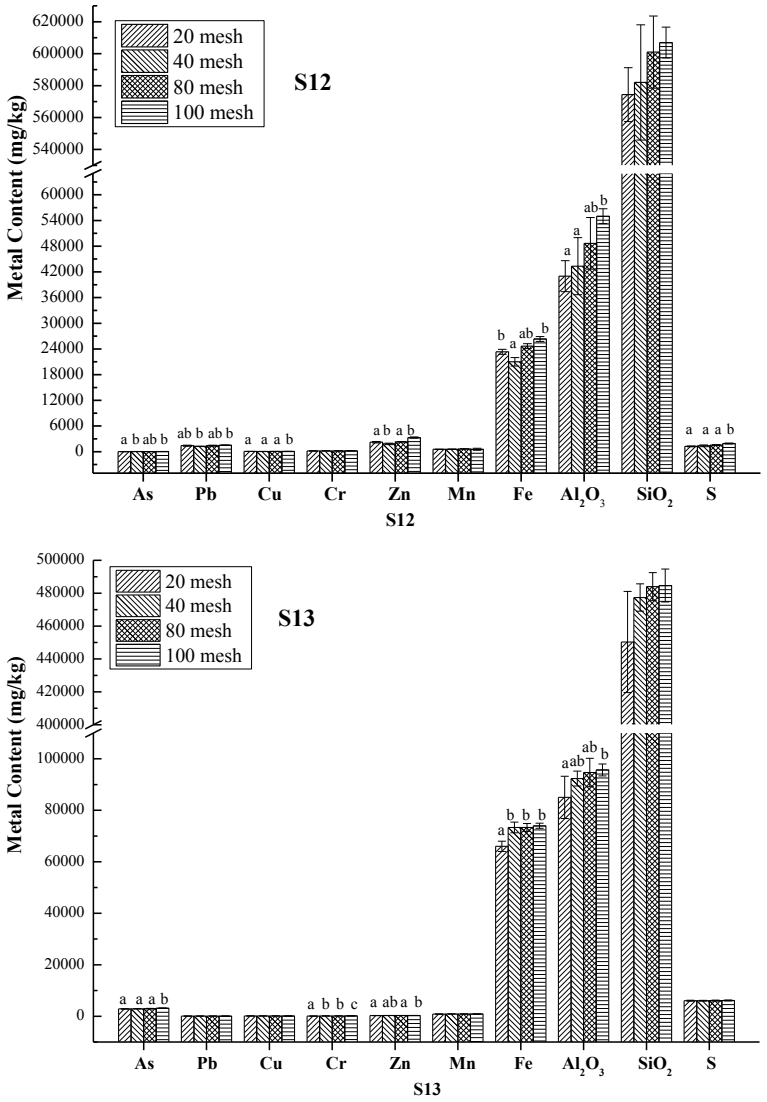

Fig. 13.4 Analytical results of different soil samples from mining area (S12, S13)

S13), and ten kinds of chemical constituents were analyzed in soil samples including arsenic, lead, copper, chromium, znic, manganese, iron, aluminium oxide, silicon oxide and sulfur. The content of each constituent in the sample was expressed in form of mass content, as milligrams per kilogram (mg/kg). As the content of sulfur in soil samples from farmland is below the detection limit of hand-held XRF spectrometer used for detection, the Sulfur content in samples cannot be detected by XRF. Thus sulfur content of sample was not demonstrated in Figs. 13.1, 13.2, 13.3 and 13.5,

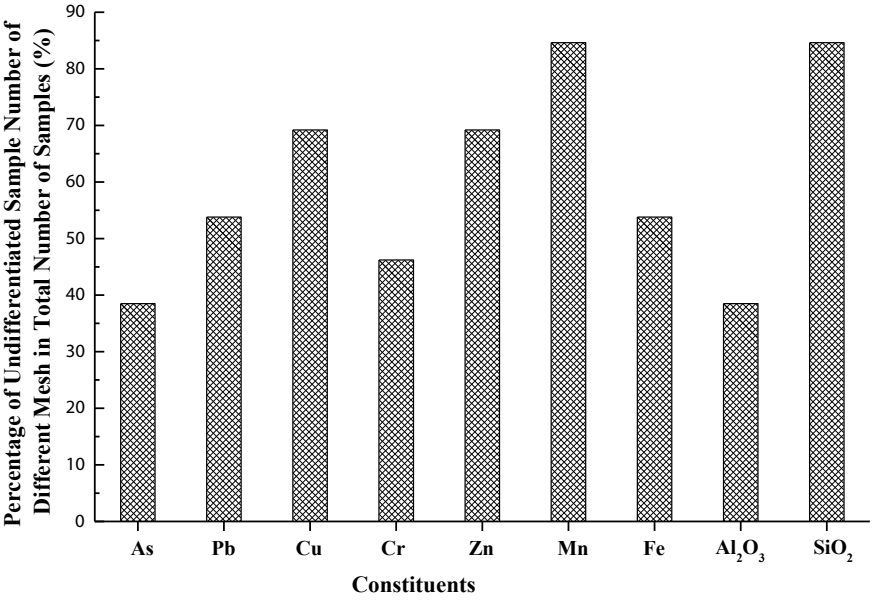

Fig. 13.5 Indifference analysis of compounds with samples of different meshes

it was shown in Fig. 13.4 of analytical results for soil samples from mining areas. Figure 13.5 showed the results of indifference analysis of compounds with samples of different meshes, that is percentage of undifferentiated sample number of different mesh in total number of samples for nine kinds of components, except sulfur.

The analytical results of samples demonstrated that the determination results from samples of different meshes of As concent showed complete indifference in 38.5% of all samples. The proportion with significant difference of determinated As concents is 46.2% when the analysis sample was at 20 mesh or 100 mesh. While there was little significant difference between groups when the analysis sample at 40 mesh or 80 mesh. It meant that there was great impact on repeatability of As content analysis in samples of 20 mesh and 100 mesh. The measurement results of elements Cu, Zn, Mn and compound SiO_2 showed Samples of different meshes with no difference in measurement results respectively in 69.2%, 69.2%, 84.6% and 84.6% of the total number of samples.

While the measurement results from concents of Pb, Cr, Fe and Al_2O_3 demonstrated that samples of different meshes with no difference in measurement results respectively account for 53.8%, 46.2%, 53.8% and 38.5% of the total number of samples. A considerable proportion of the samples showed higher measured metal content of 100 mesh sample compared with that of 20 mesh sample. So, the mesh size of the sample affects the reproducibility of the measurement to a certain extent. Furthermore, the characteristics of metallic elements themselves should be taken into consideration. Measurement results showed that the determination concents of

Zn and Mn were less affected by different sample mesh, while the determination concents of As and Al_2O_3 were easy to be affected by changes in sample mesh.

13.3.2 Analysis of Metal Concents in Soil Samples

Determination results of heavy metal contents from soil samples of farmland (S1–S11, 100-mesh) in the previous were compared with data according to Environmental Quality Standard for Soils (Level III) (State Environmental Protection Agency of China 2004b). It was clear that the concents of As were all higher than 30 mg/kg in soil samples of S1, S8, S9 and S10 which was more than Environmental Quality Standard for Soils (Level III) (State Environmental Protection Agency of China 2004b), while the concents of other heavy metal, Pb, Cu, Cr and Zn were all within the National Level-Three Standard. Howerever, concents of Pb and Zn were respectively 511.3 mg/kg and 500.7 mg/kg in soil sample S11, which was exceeded Environmental Quality Standard for Soils (Level III). Concents of sulphur in sample S12 and S13 were more than 1000 mg/kg in soil samples from mining area, and the concents of Pb and Zn were separately 1518 mg/kg and 3302.7 mg/kg from S12, while the concent of As from S13 was 3152 mg/kg.

13.4 Conclusions

The distinction in mesh of soil samples would have a certain impact on the measurement results when the hand-held XRF spectrometer was used for determining soil samples. The favorable suggesstion was passing the soil sample through 100 mesh sieve as much as it could be before determination. The soil samples of farmland tested this time came from Longnan Region in Gansu Province, the content of As in the sample has exceeded Environmental Quality Standard for Soils (Level III). As soil samples from mining area nearby with high contents of Pb, Zn and As, local government departments should pay attention to this situation.

Acknowledgements This research was funded by Research Project of Universities in Gansu (2019B-169) and Doctoral Research Fund of Lanzhou City University (LZCU-BS2019-26).

References

Brent R, Wines H, Luther J et al (2017) Validation of hand-held X-ray fluorescence for in situ measurement of mercury in soils. J Environ Chem Eng 5(1):768–776

Haller H, Jonsson A (2020) Growing food in polluted soils: a review of risks and opportunities associated with combined phytoremediation and food production (CPFP). Chemosphere 254(1): 126826

Lu Y, Liang X, Niyungeko C et al (2018) A review of the identification and detection of heavy metal ions in the environment by voltammetry. Talanta 178(1):324–338

Peng H, Yang Z, Zhao J et al (2018) Use of high-precision portable X-ray fluorescence spectrometer on the heavy metal rapid determination for contaminated agricultural soils. J Agro Environ Sci 37(1):1386–1395

Peralta E, Pérez G, Ojeda G, et al (2020) Heavy metal availability assessment using portable X-ray fluorescence and single extraction procedures on former vineyard polluted soils. Sci Total Environ 726(1): 138670

Shah V, Daverey A (2020) Phytoremediation: a multidisciplinary approach to clean up heavy metal contaminated soil. Environ Technol Innov 18(1):1–16

State Environmental Protection Agency of China (2004b) Environmental quality standard for soils (GB 15618-1995). Standards Press of China, Beijing

State Environmental Protection Agency of China: State Environmental Protection Administration of China (2004a) Technical specification for soil environmental monitoring (HJ/T166–2004). China Environmental Science Press, Beijing, China

Soodan R, Pakade Y, Nagpal A et al (2014) Analytical techniques for estimation of heavy metals in soil ecosystem: a tabulated review. Talanta 125(1):405–410

Zhou X, Zheng N, Su C, et al (2019) Relationships between Pb, As, Cr, and Cd in individual cows' milk and milk composition and heavy metal contents in water, silage, and soil. Environ Pollut 255(1): 113322

Chapter 14
Collaboration Mapping in Sustainable Development: A Case Study from Haze in Chiang Mai

Pongtip Thiengburanathum

Abstract A sustainable city does not come from only high technological development in many cases; an area based sustainable development was found in the city with good collaboration between stakeholder within the city. Taken from a case study of haze pollution in Chiang Mai, the government has been dealing with haze in a temporary and short-term manner for over a decade, rather than implementing sustainable solutions. The reoccurrence of haze has caused conflict between the local government and its citizen. The new socially organized group "Breath Council" has sparked a new light and shifted the power to solve haze in Chiang Mai. This is a new space for collaboration and participation between previously conflicted actors. This paper depicts implementing a social collaboration strategy in the institution/relationship arrangement toward sustainable development.

Keywords Haze pollution · Sustainable city · Stakeholder analysis · Chiang Mai

14.1 Introduction

A sustainable city does not come from only high technological development in many cases; an area-based sustainable development was found in the city with good collaboration between stakeholders within the city (Leeb et al. 2014). Chiang Mai has been the second most important city in Thailand, not in terms of population but in politics, social, economic, and geographical location as the center for trade in the north of Thailand. The changes occurred in the city as its population increases through growth and migration. New buildings and housings are required to provide living spaces for the people. Influence from international tourists and globalization also changes the businesses, and interaction between people has changed over time. The urban area in Chiang Mai has grown from 10 square kilometers in 1952 to 137 square kilometers in 2009 (Sangawongse 2009). Foreigners have been flooding to Chiang Mai city for visiting, long term stay, expatriate workers, missionary and NGO workers. In 2014

P. Thiengburanathum (✉)
Chiang Mai University, Chiang Mai 50200, Thailand

H.-Y. Jeon (ed.), *Sustainable Development of Water and Environment*,
Environmental Science and Engineering,
https://doi.org/10.1007/978-3-030-75278-1_14

there were more than 30,000 foreign retirees who live in Chiang Mai (Nation TV 2018).

Chiangmai city has been confronting a major challenge toward city sustainability, the haze pollution issue during the dry season from February-April before the monsoon season starts, and the rain washed down the dust and smoke particles. Haze has been recognized as a seasonal phenomenon for more than 200 years since its first record was 1891 (McCarthy 1900). The fire was commonly used in agricultural practice in the highland due to its efficiency and lack of machinery. A rotational farming practice that requires burning is common in highland agriculture since the first settlement in the highland (Kunstadter et al. 1978). Air pollution itself is progressing based on human activity or development, i.e., globalization (modern trade), urbanization, and climate change, and the perception of city citizens themself due to the better information technology (Pardthaisong et al. 2018).

The combination of air pollution sources, geographical terrain, and weather conditions in Northern Thailand resulted in the haze. During the dry season, dust and smoke particles accumulate over the ground when the cooler air suppresses dust and smoke particles' dispersion over the ground, reducing visibility and causing health impact. Such a phenomenon is commonly known as "Haze."

Haze had been recognized as air pollution at the national level in 1997 from Indonesia's trans-boundary haze impact. Chiang Mai has been recognized as a disaster zone from the high concentration level of PM10 above the legal limit at 120 μg per cubic meter from 21 March to 11 April 2006 (Simachaya 2007). In 2008 the cabinet authorized Provincial Haze Command Center to mitigate haze's impact at the provincial level (The Secretariat of the Cabinet 2008). The reoccurrence of haze has initiated a negative dilemma in the city of Chiang Mai, what if the situation does not improve, urban decay will happen, e.g., no tourists, investors move out, ex-pats move out, property value reduces, degradation of the environment and health of the people, etc.

The haze issue has been classified as a complex problem involving multi stakeholders at multilevel (Blake et al. 2019). The main source of haze in Northern Thailand is human activities, whether it is a forest fire, rotational farming, or cash crops. To strategically resolve this problem, one key strategic goal is to "improve social collaboration." This paper depicts implementing a social collaboration strategy-institution/relationship arrangement, toward sustainable development.

14.2 Material and Methodology

The study reviewed secondary data on policy, plans, and decisions made by government authorities. This study used primary data and secondary data collected from books, news articles, government decisions, official announcements, papers, journals, and websites. Primary data were collected from an interview with representatives from government officials, rural populations, urban populations, private sectors, and non-government organizations.

The methodology adopted for this study Stakeholder Analysis and mapping to understand (1) social collaboration, (2) balance of power, (3) deliberative dialogues, and (4) complex arrangement in complex society and issue.

14.3 Stakeholders Analysis

14.3.1 Stakeholder Identification

In the stakeholder mapping process, haze in Chiang Mai Province is viewed as a system, and the stakeholders are people who matter to a system (Mayers 2005). The process focused on the haze pollution supply chain and not on the related supply chain; hence, it does not capture other supply-chains related to haze, such as forest fire and forest land clearing for food scavenging. The purpose of this exercise is to illustrate and describe the interest, characteristics, and circumstances of each stakeholder, their power, and roles involved in policy formulation and decision-making related to haze pollution in Chiang Mai Province. A simplified illustration of haze sources, impact, and government measures is shown in Fig. 14.1. The government has been focusing on reducing forest fire burning rather than the long-term program to improve the economy in rural and highland communities (The Secretariat of the Cabinet 2008; Kamton et al. 2019).

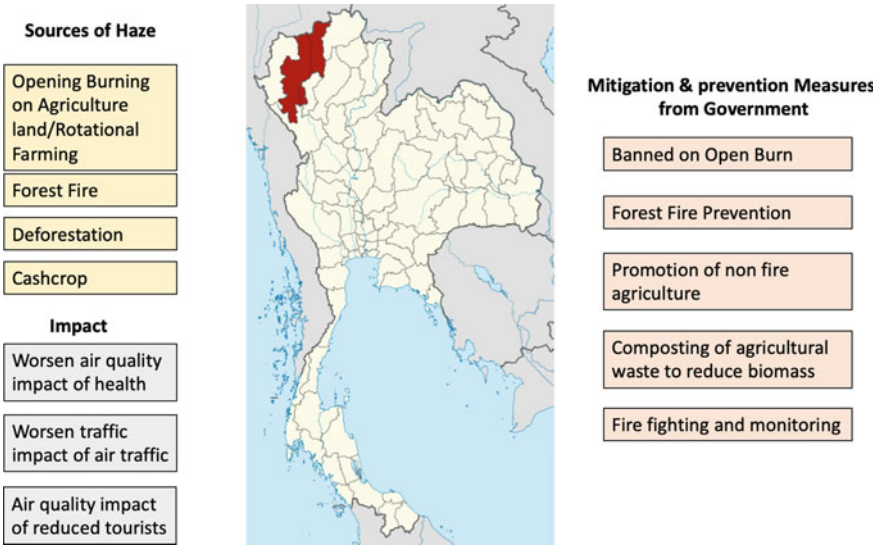

Fig. 14.1 Sources, impact and mitigation & prevention measure from government related to haze. Source: Map of Chiang Mai from NordNordWest

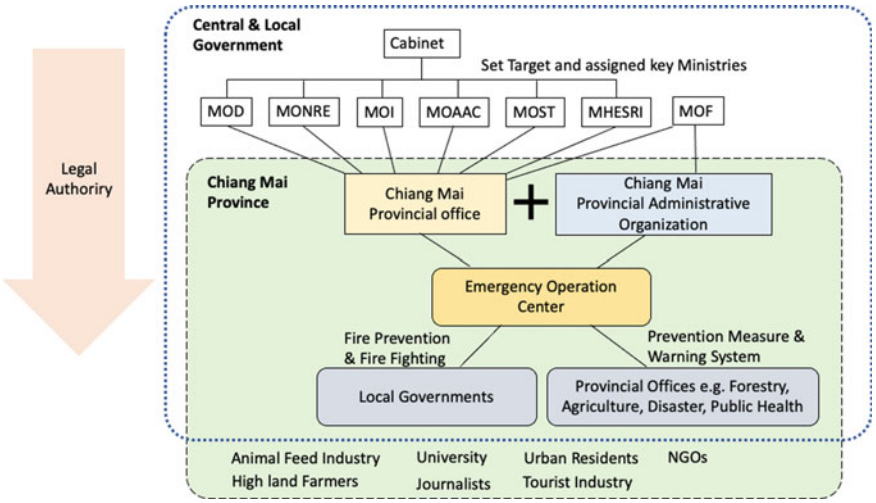

Fig. 14.2 Stakeholder relations between government authorities and Chiang Mai Province in the event of haze

The relationship between stakeholders is shown in Fig. 14.2. The provincial office has a temporary authority during haze (January–May) to manage all parties involved in haze pollution from fire management to health impact mitigation of the National Disaster Prevention and Mitigation Act (MOI 2007).

Despite a clear government policy and plan to reduce haze's impact in northern Thailand since 2008, the problem persists through to 2020, when it has reached its highest PM2.5 concentration level recorded (Prachachart 2020). Many sectors are involved with the haze government sector, private sector, academic sector, general public, non-governmental organization, and media sector. The challenge remains in an opportunity for the community/village level to participate with a higher level in the decision-making process related to haze (Pardthaisong et al. 2018). The worsening situation of haze has the highest impact on tourism and related industries in Chiang Mai, with a sharp drop of tourists visiting Chiang Mai in the dry season. The people of Chiang Mai had been come together through "Chiang Mai Breath Council" or "Sapa Lom Hai Jai" to engage with the Provincial Government and assist them (Breath Council 2021). This paper aims to study stakeholder interaction through stakeholder mapping and stakeholder analysis between different haze pollution groups. The outcome of people engagement in the process to tackle haze, reducing conflict between the Provincial Government and the citizen of Chiang Mai.

The supply chain of haze in Chiang Mai Province is related to 11 key stakeholder groups. The stakeholder is divided into 3 groups, primary direct interest (Central Government, Local Government, Animal Feed Industry, Forest Fire Management agencies, and High Land Farmers), primary indirect interest (Parliament, University, NGOs, Urban Residents, Journalists, and Tourist Industry), and secondary interest (Global Community). The groups with primary interest are those with decision

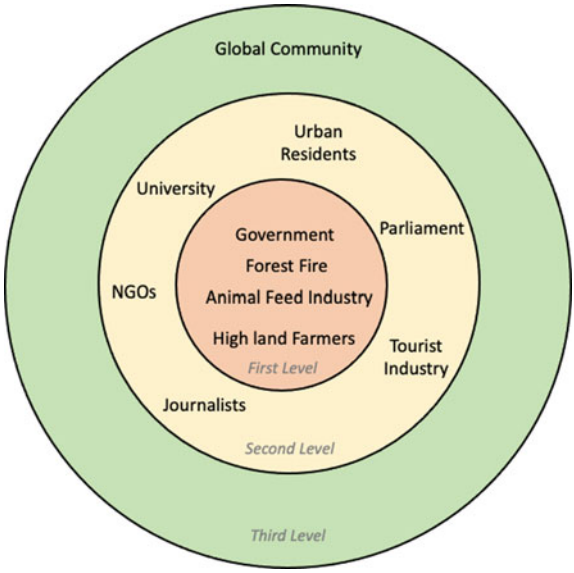

Fig. 14.3 Stakeholder map illustrating different level of involvement in haze pollution

making authorities in contributing to the source of haze or prevention and mitigation of haze. They would have high interest, high importance, and a high level of influence in the haze decision-making process. This group would also be identified as the core group in Fig. 14.3. The group with primary indirect interest is the group with high interest, medium importance, and high-medium influence. They are not identified as the key actor, but they are the people who experience the impact of haze.

The second group is the group with primary indirect, where they neither contribute to the sources or directly involved with prevention or mitigation of haze, but they are suffering from the impact of haze. Their interest is high, with high-medium importance but a low level of influence. They are identified as having second level of influence on haze in Fig. 14.3.

The third group is the second group with a low level of interest, low level of importance, and low influence level. They neither contribute directly not experience haze first handed. They are identified in the third level of influence. They may pressure the government in the decision-making process, but their influence is still on a low level.

The main decision-maker for haze policy in Thailand is the Cabinet, where it approved policy guidelines and a national plan to mitigate haze pollution. In comparison, the parliament allocates budget involved in preventing and mitigating haze pollution. An average of ten million tourists visits Chiang Mai from 2016 to 2019, except 2020, with an outbreak of COVID-19 (MOTS 2021). The tourism-related sector largely drives the city economy; the onset of haze pollution during the summer months greatly affects the tourist industry; a loss of 4000 million Thai Baht was estimated (BOT 2020). The tourism sector was identified separately from other private sectors that may not suffer directly.

14.3.2 Stakeholder Power Analysis

To further analyse the influence of each stakeholde and salience based on the stakeholder posessing one of these three attributes: power, legitimacy and urgency (Mitchell et al. 1997). In the case of haze pollution the attributes are define differently from business manamgent perspective. Power is the an attribute related to being able to make decision and changes on their own and highly influence the ourcome of their decision. Legitimacy is an attribute that allow its owner the right to make decision on legal basis. And urgency is an attribute that related to those needed the change urgently. The recurrence of haze pollution in Chiang Mai in the past 14 years has shown that the key decision maker has both power and legitimacy but lacking urgency to prevent and mitigate haze in a sustainable manners. The policy has been based on short term management during the dry season.

Another key agency is the animal feed industry that has been promoting and financing animal feed corn in the highland that caused deforetation, and fire was use to clear the land as well as burn the agricultural waste (Blake et al. 2019). The majoritry of animal feed corn produced in Thailand in 2015 was from Northern Thailand or 3.29 million tons of the total 4.7 million tons produced. In case of Mae Cham 65% of all household are inolved in animal feed corn supply chin one way or antoher (Watcharasakonpong et al. 2016). Therefore, animal feed corn supply chain is one of the key actor that contributed to haze in northern Thailand from it fired based naturn of cultivating animal feed corn in the highland. The industry is strong supply chain with repesenative from community/village level to policy makers. The changes in animal feed industry will have strong influence on cash crop plantation in the highland land, where it is mostly fired based. Univerity or academic sector has knowledge legitimary and urgency to prevent and mitigate haze, but it holds no power.

Tourist industry has a limited power to request changes from the govenrment as it has a high contribution to the economy of the province, but it holds no legitimacy to make decision. Other stakeholders; including urban resident, highland farmers, journalists, and NGOs; suffer from haze are classified as having urgency by no power nor legitimacy to make decision that influence haze as shown in Fig. 14.4.

14.3.3 Stakeholder Deliberative Dialogue

In the stakeholder map (Fig. 14.5), those in the dominant section (high interest and high power) will be able to make decisions that are critical to haze in Chiang Mai. Nevertheless, in the case of haze in Chiang Mai, there is no dominant agency. The government has taken haze as a seasonal issue rather than a top priority with high interest. The policy issued only applies to short-term solutions such as a ban on open burning and limited prosecuted cases. Therefore, the government, both central and local, animal feed industry and parliament are placed in the section with high power

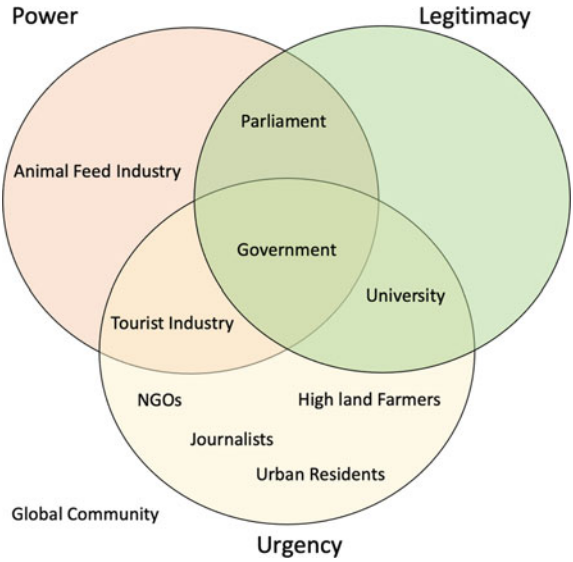

Fig. 14.4 A salience diagram of stakeholder involved in haze pollution in Chiang Mai

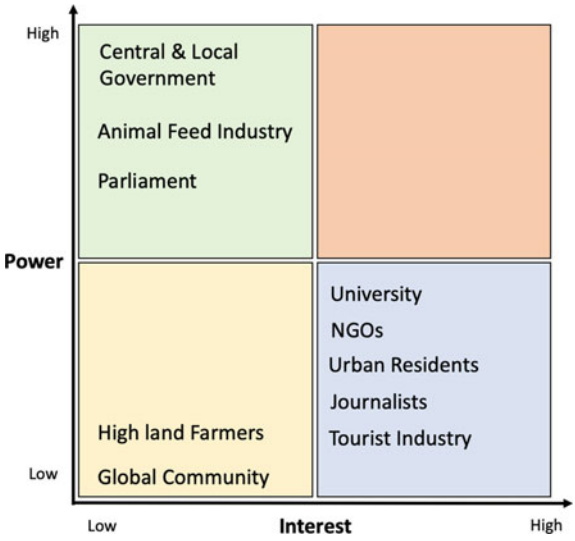

Fig. 14.5 Stakeholder map for haze in Chiang Mai prior to 2020

but low interest to sustainably reduce the occurrence and severity of haze in Chiang Mai. Other groups; university, NGOs, urban residents, journalists, tourist industry and are those with high interest to reduce haze pollution. However, the highland farmers are with low interest in haze and low power to reduce haze due to their limited production resources. The global community is also classified in the same quadrat as neither power nor interest to reduce haze.

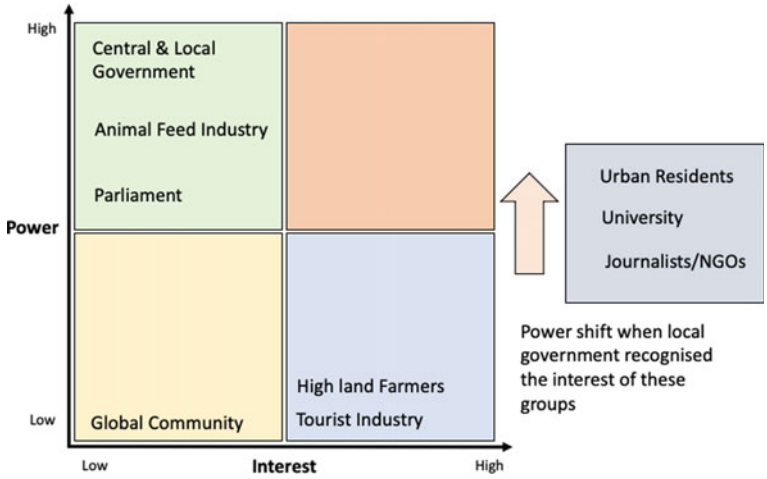

Fig. 14.6 Stakeholder map for haze in Chiang Mai after 2020

In 2019, a group of non-governmental organizations (NGOs), urban citizens, private sectors, and the academic sector came together to form "Breath Council" or "Sapa Lom Hai Jai" in Chiang Mai to tackle haze from the citizen perspective. The Breath Council's objective is to sustainably reduce air pollution in Chiang Mai for better air quality (Breath Council 2021). The Breath Council was appointed to become a Committee member to prevent and solve haze problem integrated and participatory (Chiang Mai News 2020). The Committee allows participation from civil society, also appoint several working groups to work towards a long-term goal, such as the rural working group, the urban working group, and the academic support group (Chiang Mai Province 2020).

The dialogues between civil society groups represented through the Breath Council adjusted the stakeholder's power level from Fig. 14.5 to Fig. 14.6 for urban residents, universities, and Journalists/NGOs. The participation of civil society groups in the "Committee to prevent and solve haze problem integrated and participatory" has reduced the conflict between local government and urban citizens that has been an on-going issue for several years (BOT 2020).

14.4 Discussion

14.4.1 Sustainable City is the Space for Interaction and Collaboration

In Chiang Mai's case, the main actors and institutions that influence changes are the central government, local government, private sectors, and local people. The central

government played a key role in large-scale projects in the city that enables economic growth, while the private hold a key role in capital accumulation in Chiang Mai. In terms of haze pollution, another key sector is the academic sector (Pardthaisong et al. 2018). Academic research and experts had been assisting the government in shaping policy and the city expands to accommodate the population increase as well as others who move to Chiang Mai for employment and business opportunities. The local residents of Chiang Mai also play a role in shaping the city's space through their social movements. The urbanization process of the city has resulted in not only changes in land use, economic growth, but also social urbanization. There were some projects that were opposed by the local residents due to environmental degradation, and some projects were against local traditions or "Kud" (Charoenmuang 2007). Especially projects that have been designing with insufficient public participation and caused environmental degradation. Therefore, the local residents have organized themselves into groups to contest with the central government in shaping the growth of Chiang Mai, especially during 1997–2008 (Prakasvuthisarn 2019). Similar to the case haze, when civil society organized themselves and represented through "Breath Council" as a means to the conflict resolution between civil society and government. Social collaboration created a new space for the city to work together for a livable and sustainable city.

The Breath Council was a newly constructed civil society group in 2019. The strategy of the Breath Council is different from convention NGOs. It uses knowledge and facts to negotiate with the government instead of complaining about the situation that eventually leads to conflicts. It offers to work with the government constructively rather than criticizing the government. The Breath Council also provides much-needed assistance to the government through funding from civil society donations (Breath Council 2021). The Breath Council has been the spokesman for the people. The Breath Council is financially independent, which allows the council to represent the people's opinion and persuade the government to tackle haze differently. Hence, the factors critical to social collaboration towards sustainable development in Chiang Mai are (1) positive engagement with the government (2) using knowledge and facts to assist the government, and (3) Financially independent and do not rely on the government budget.

14.5 Conclusion

The Thai government has recognized that public opinion and participation are importing the planning and policy decision-making. Limited public involvement in policy decision-making, while haze has been reoccurring annual for the past 15 years, which leads to conflict been residents and the government. The social organization of a new public group that uses Knowledge to negotiate and assist the government in dealing with haze has been a successful strategy for participation. Engagement based on Knowledge is much more powerful than the public's complaints and requests, leading to conflict. The power of negotiation and contestation requires Knowledge

for successful engagement. Hence, Sustainable cities need active participation with good Knowledge to engage in the city's activity.

Acknowledgements This study was funded by the Haze Free Thailand Project, National Research Council of Thailand (NRCT).

References

Blake DJH, Thiengburanathum P, Thiengburanathum P, Friend RM, Doherty B, Thankappan S (2019) Chapter Two - Looking at complex agri-food systems from an actor perspective: the case of Northern Thailand (Barling D, J B. T.-A. in F. S. and S. Fanzo (eds), vol. 4, pp 33–65). Elsevier

BOT (2020) Haze problem in northern region, and Sandbox CMU Model. BOT Magazine. https://www.bot.or.th/Thai/BOTMagazine/Pages/256303LocalEconomy.aspx

BOT (2020) สรุปมาตรการเพื่อเยียวยาและลดผลกระทบของCOVID-19 ในต่างประเทศ.Retrieved from https://www.bot.or.th/Thai/FinancialInstitutions/COVID19/Documents/Measure_Foreign.pdf

Charoenmuang DA (2007) Sustainable cities in Chiang Mai: a case of a city in a valley. Chiang Mai University

Breath Council (2021) No Title. Breath Council. https://breathcouncil.org

Chiang Mai News (2020) Chiang Mai Province received public comments to solve hazeproblem - Chiang Mai News. https://www.chiangmainews.co.th/page/archives/1378849/

Chiang Mai Province Order, Appointment of Haze Committee 2020

Kamton R, Satienperakul K, Yotapakdee T, Nunthasen K (2019) Haze-relate air pollution and impacts on healthy in Chiang Mai Province. SSRN Electron J. https://doi.org/10.2139/ssrn.3462169

Kunstadter P, Chapman EC, Sabhasri S (eds) (1978). Farmers in the Forest. University of Hawai'i Press. doi:https://doi.org/10.2307/j.ctv9zck23

Leeb S, Supervisor CR, Kalling T (2004) Stakeholder collaboration in a sustainable city-a case study of San Francisco. Retrieved January 28, 2021

Mayers J (2005) Stakeholder power analysis. www.policy-powertools.org

McCarthy J (1900) Surveying and exploring in Siam. J Murray

Mitchell RK, Agle BR, Wood DJ (1997) Toward a theory of stakeholder identification and salience: defining the principle of who and what really counts. Acad Manag Rev 22(4):853–886. https://doi.org/10.2307/259247

MOTS (2021) Tourist statistics. Retrived from https://www.mots.go.th/more_news_new.php?cid=411

National Disaster Prevention and Mitigation Act B.E.2550 (2007) 124, 1

Nation TV (2018) ชาวต่างชาติวัยเกษียณ นิยมใช้ชีวิตบั้นปลายในไทยไม่ต่ำกว่า 30,000 คน.Retrieved from https://www.hurun.net/EN/Article/Details?num=670D27DA6723

Prachachart (2020) วิกฤต "หมอกควัน" เชียงใหม่ ยิ่งแก้ ! ยิ่งหนัก ! "ศก.-ท่องเที่ยว-สุขภาพ" สูญหมื่นล้าน.Retrived from https://www.prachachat.net/local-economy/news-308189

Pardthaisong L, Sin-Ampol P, Suwanprasit C, Charoenpanyanet A (2018) Haze pollution in Chiang Mai, Thailand: a road to resilience. Procedia Eng 212: 85–92. doi:/https://doi.org/10.1016/j.proeng.2018.01.012

Prakasvuthisarn, K (2019) Social movements in Chiang Mai against problems from urbanization during 1997–2008. J Soc Sci, Faculty of Social Sciences, Chiang Mai University

Sangawongse S (2009) Dynamics of land-cover/land-use in the Chiang Mai area and prediction of urbanization using the SLEUTH model. Soc Sci J 1(2552):119–169

Simachaya W (2007) Haze pollution in Nortehrn Thailand: problems and solutions, Pollution Control Department, Ministry of Natural Resources and Environment, https://www.pcd.go.th/wp-content/uploads/2020/06/pcdnew-2020-06-05_07-33-31_040770.pdf

The Secretariat of the Cabinet. (2008) Thai Cabinet Resolution. Retrieved January 22, 2021, from http://www.cabinet.soc.go.th/soc/Program2-3.jsp?top_serl=221574

Watcharasakonpong N, Thiengburanathum P, Boonthiem U (2016) Measuring the technical and scale efficiency of maize production in Thailand: the case of Mae Chaem District, Chiang Mai. J Econ Sustain Dev 7:14

Chapter 15
Greywater Treatment in Continuous Flow Solar Photocatalytic Reactor Using Graphite Supported Nitrogen-Doped TiO_2

Kumari Priyanka, Neelancherry Remya, and Manaswini Behera

Abstract The increasing water demand has been one of the major global issues for the past decades. An enormous amount of potable water is required for household, industrial and agricultural activities, which led the water authorities to look-out for suitable alternatives. Treated greywater reuse and recycling is an economically viable and attractive option for meeting a portion of future water demand. The feasibility of a continuous mode solar photocatalytic system in greywater treatment was explored in this study. The solar photocatalytic tests were employed with graphite-supported nitrogen-doped titanium dioxide (N-TiO_2). The effect of flow rate (20–70 mL/min) was investigated under pH-3, H_2O_2 dosage-1 g/L, catalyst dosage-5 g/L in a continuous reactor. These tests revealed that the maximum removal efficiency in terms of COD, TOC and NH_4-N was accomplished at 20 mL/min, while the lowest removal efficiencies were found at 70 mL/min. The removal efficiencies of COD, TOC, and NH_4-N were progressively reduced from a flow rate of 20 to 50 mL/min, followed by a sharp drop at a flow rate of 70 mL/min. The reactor operation at the lowest flowrate i.e. 20 mL/min showed the removal efficiencies of 71.8, 65.1 and 63.7% for COD, TOC and NH_4-N, respectively. The result showed that a solar photocatalytic system with GT-NTiO_2 could be effectively used for greywater treatment under continuous mode operation.

Keywords Greywater · Graphite-supported catalyst · Continuous-mode reactor · Solar photocatalysis · Pollutant degradation

15.1 Introduction

The need for consumable/non-consumable water supplies for domestic, industrial and agricultural utilization has been magnified considerably over the last decades with the rapid increase of populace and reduction in freshwater sources. To meet

K. Priyanka · N. Remya (✉) · M. Behera
School of Infrastructure, Indian Institute of Technology Bhubaneswar, Odisha 752050, India
e-mail: remya@iitbbs.ac.in

H.-Y. Jeon (ed.), *Sustainable Development of Water and Environment*,
Environmental Science and Engineering,
https://doi.org/10.1007/978-3-030-75278-1_15

this demand, the water authorities and policymakers are contributing to alternative sources of water like reused water, rainwater and greywater. Greywater accounts for 50–75% of the total domestic wastewater (Palmquist and Hanæus 2005). The domestic greywater originates from showers, kitchen sinks, laundry machines and hand washbasins but excludes wastewater from toilets. Greywater usually has lower infectious agent content and organic matter load, henceforth, its treatment and reuse are acquiring a lot of attention (Benami et al. 2016; Oteng-Peprah et al. 2018).

The treatment and reuse of greywater could dramatically reduce the demand for domestic potable water, but caution must be taken to ensure that treatment should be done without damaging public health and the environment. Some common problems associated with greywater reuse without treatment are oxygen depletion (as in eutrophication), the domination of anaerobic conditions, plant toxicity, and hygiene risks (Eriksson et al. 2002; Wiel-Shafran et al. 2006). Treated greywater has various reuse potential such as flushing toilets, cleaning floors, washing cars, and industrial cooling and cleaning applications (Al-Jayyousi 2004; Ghaitidak and Yadav 2013). The guidelines and standards for greywater reuse and recycling based on safety, sanitation, esthetics and ecological tolerance have been established by various nations (Li et al. 2009; Vuppaladadiyam et al. 2019).

Numerous greywater treatment options are applied in the past such as physical (membrane filtration), chemical (coagulation/flocculation, electrochemical process) and biological methods (constructed wetlands, rotating biological contractors) (Pidou et al. 2007). In the last decades, the utilization of advanced oxidation processes (particularly solar photocatalysis) in greywater treatment has been viewed as a potential method. In comparison to the previous greywater treatment methods, solar photocatalytic systems offer numerous merits such as (1) high efficiency in degrading emerging pollutants, (2) high stability of photocatalysts, and (3) removal or mineralization of a wide variety of aqueous pollutants (Prieto-Rodriguez et al. 2012).

In this work, photocatalytic degradation of greywater using nitrogen-doped titanium dioxide (N-TiO_2) supported on graphite is investigated in a continuous solar photocatalytic reactor. The effect of different flow rates was evaluated for treating greywater.

15.2 Materials and Methods

15.2.1 Greywater

Greywater was simulated by using analytical grade chemicals (sucrose, urea, soluble starch, ammonium chloride, potassium dihydrogen phosphate) and other ingredients (toothpaste, utensil cleaning gel and shower gel). All the chemicals in a certain amount were added to the tap water to prepare the simulated greywater. The different physicochemical parameters of greywater were analyzed and tabulated in Table 15.1.

Table 15.1 Physicochemical characteristics of greywater

	Simulated greywater characteristics									
			Solids (mg/L)		Organics (mg/L)			Nutrients(mg/L)		
Parameters	pH	Turbidity (NTU)	TDS	TSS	COD	BOD	TOC	PO_4^{3-}-P	NH_4-N	TKN
Values	7.3	6	625	102	285	142	131	19.5	22.3	51.4

15.2.2 Materials

Analytical grade titanium (IV) isopropoxide ($C_{12}H_{28}O_4Ti$, >98%), used as a precursor of titanium dioxide (TiO_2), was obtained from Sigma Aldrich. Other chemicals used for greywater preparation such as sucrose ($C_{12}H_{22}O_{11}$), soluble starch ($(C_6H_{10}O_5)_n$), ammonium chloride (NH_4Cl), potassium dihydrogen phosphate (KH_2PO_4) and urea (CH_4N_2O) were obtained from Avra Synthesis Private Ltd, Hyderabad. Emerging pollutant (Benzophenone-3, 98% purity) (BP) and standard titanium (IV) dioxide (99%) (P-25) were procured from HIMEDIA. Chemicals such as acetic acid glacial (>99.99%, Rankem, India), acetonitrile (Avra Synthesis, India), and HPLC water (Avra Synthesis, India) were obtained for the high-performance liquid chromatography (HPLC) analysis. Ethane-1,2-diyldinitrilotetraacetic acid (EDTA, $C_{10}H_{16}N_2O_8$, >99.9%), and hydrogen peroxide (H_2O_2, 30%) were obtained from Merck and Avra Synthesis, respectively.

15.2.3 Synthesis of Graphite-Coated N-Doped Catalyst

Titanium isopropoxide (TTIP) and urea were used as TiO_2precursors and nitrogen sources, respectively for the preparation of this photocatalyst as described in (Priyanka et al. 2020). To achieve a N/Ti ratio of 2:1, a certain quantity of urea and TTIP was added slowly to distilled water (about 20 mL). This mixture was stirred at 650 rpm using a magnetic stirrer for one hour. Next, the mixture was treated with ultrasonication for 30 min and then, dried at 100 °C in an oven for one day. The obtained pre-calcined powder was ground and heated at 5 °C/min upto 300 °C for 3 h in a muffle furnace. The material was then labelled as N-TiO_2.

The resulted powder N-TiO_2 was characterized with several techniques. X-ray diffraction (XRD) was performed on D8 Advance (Bruker, Germany) between 20° and 70° at room temperature with Cu-Kα radiation (voltage-40 kV, current-40 mA) and XRD patterns were identified using DIFFRACSUITE software. Surface properties were evaluated by scanning electron microscopy (SEM) (MERLIN compact, Carl Zeiss). And the elemental composition of N-TiO_2 nanoparticles was determined by electron dispersive energy spectroscopy (EDS) (51XMX 1004, Oxford Instruments). A UV–visible spectrophotometer (U-2900, Hitachi) was used to obtain spectra at a range of 200–800 nm.

Graphite was used as the substrate for the coating of N-TiO_2 particles through dip coating (Rao et al. 2012) with some changes. The pre-treatment of graphite (size-2 mm, seived) was carried out before the deposition of N-TiO_2 particles. Initially, about 1500 g of graphite was cleaned under the running tap water to get rid of the soil from the surface. Then, graphite was immersed in 1 N H_2SO_4 and kept in the shaker at 180 rpm for 12 h and rinsed again with tap water to keep neutral pH. Afterward, cleaned graphite was heated at 70 °C for 12 h. Then, the dried graphite was cooled to room temperature. 2% N-TiO_2 particles were added to the solvent solution (in a ratio

Fig. 15.1. Photographic image of GT-NTiO_2 **a** Before coating **b** After coating

of ethanol-80: water-20). The coated graphite was air-dried (<70 °C) with the help of a blow drier (HP8142/00, Philips). The same procedure was repeated for the second layer of coating with dip-coating and drying methods. Lastly, the graphite-coated N-TiO_2 material was oven-dried at 100 °C and cooled to obtain coated photocatalyst (GT-NTiO_2). GT-NTiO_2 was leached using distilled water to confirm the coating of the N-TiO_2. The graphite was weighed before and after coating to measure the actual amount of N-TiO_2 coated on it (Fig. 15.1). And it was found that about 0.8–1 g catalyst coated per 100 g of graphite.

15.2.4 2.4. Solar Photocatalytic Activity

Continuous-mode photocatalytic experiments were carried out using a tray-type solar photocatalytic reactor (Heber scientific, MODEL: HP-SLJV16254). A tungsten-halogen lamp (Heber scientific) of 150 W was employed as a visible light source with a wavelength varied from 400 to 700 nm. Tray-type solar photocatalytic reactor (25 cm × 35 cm × 8 cm) was filled with N-TiO_2 nanoparticles immobilized on graphite (as one layer uniformly). Peristaltic pump (PP-20-EX, MICLINS) and submersible water pump (WP3200, Sobo) were used for regulating flow rate (to maintain flow rate) and circulating cooling water, respectively. The flow rate was maintained between the ranges of 20–70 mL/min. The N-TiO_2 photocatalytic activity tests were carried out in the solar photocatalytic reactor (SPCR) with greywater. The initial BP concentration in greywater was 11 mg/L. The reactors were operated at optimal conditions (pH-3, H_2O_2 dosage-1 g/L, catalyst dosage-5 g/L) as provided in previous work (Priyanka et al. 2019). The schematic diagram of continuous-mode photocatalytic systems was provided in Fig. 15.2.

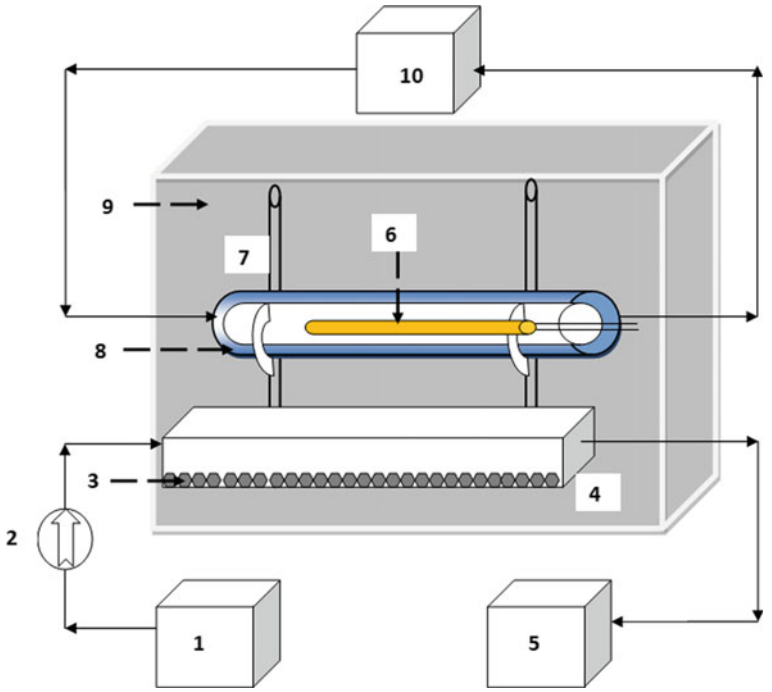

Fig. 15.2 Schematic representation of continuous solar photocatalytic reactor (1-greywater inlet tank, 2-peristaltic pump, 3-graphite coated NT-TiO_2, 4-tray-type photocatalytic reactor, 5-effluent tank, 6-visible lamp, 7-stand, 8-lamp holder, 9-protection hood, 10-cooling water tank, 11-pump for water recirculation)

15.2.5 Analytical Methods

The characteristics of the synthetic greywater samples were analysed as per the standard methods (USEPA 2012). The analytical instrument to measure the turbidity of the water sample was a turbidimeter (HACH, 2100 N (USA)). Nitrate values were assessed using a nitrate meter equipped with a nitrate probe (Thermo Scientific, EUTECH ION 2700). And pH measurement was carried out using a pH meter (ADWA Bench meter, AD800). A total organic carbon (TOC) analyzer (TOC-L, Shimadzu) was utilized for measuring TOC concentration. The total Kjeldahl nitrogen (TKN) analyzer with a digester (Kelplus, Kelvac-VA (India)) and a distillation unit (Kelplus, Classic DX VATS (E)) was used for TKN measurement. The strength of the visible lamp was calculated and noted using a photometer (HTC instruments, LX-101A).

About 1 mL sample from the continuous photocatalytic reactor was withdrawn at a different time interval. Greywater effluent was filtered through a 0.22 μm filter paper before BP measurement. BP concentration was measured in a C-18 column (250 mm × 4.6 mm) (HYPERSIL GOLD 5UM, Thermo scientific) with a UV absorbance of

287 nm using HPLC (Ultimate 3000, DIONEX, USA). Acetonitrile and 0.1% acetic acid mixture were used in a ratio of 70:30 (v/v) as mobile phase at a flowrate of 1 mL/min. BP was detected at a retention time of 6.71 min. Chromeleon 7 software was employed for processing the data of BP.

15.3 Results and Discussion

15.3.1 Characterization

The characterization of N-TiO_2 nanoparticles was discussed in our previous study (Priyanka et al. 2019). The peaks of the anatase phase were dominated in the XRD image of conventional TiO_2 (P-25) and N-TiO_2. Figure 15.3 reveals the crystalline peaks at 25.69, 38.22, 48.47, 54.52, 55.46, 63.10, and 69.15° of 2ϴ, which represented anatase phase of TiO_2 (Nguyen et al. 2018). The N-doped TiO_2 formation in the present study can be corroborated with previous findings in the literature (Sacco et al. 2018; Senthilnathan and Philip 2010). Figure 15.4a-b illustrates the SEM and EDS graphs for P-25 and N-TiO_2powders. Upon doping with nitrogen, the average grain sizes of N-TiO_2 nanoparticles were decreased from 120 to 118 nm. EDS graphs (Fig. 15.4b) confirms the doping of N into the TiO_2 structure. Further, UV-visible spectra were investigated for both P-25 and N-TiO_2 (Fig. 15.5). A remarkable redshift in N-TiO_2 nanoparticles was detected towards the wavelength of 400 to 600 nm that demonstrated an improvement of visible light absorption property.

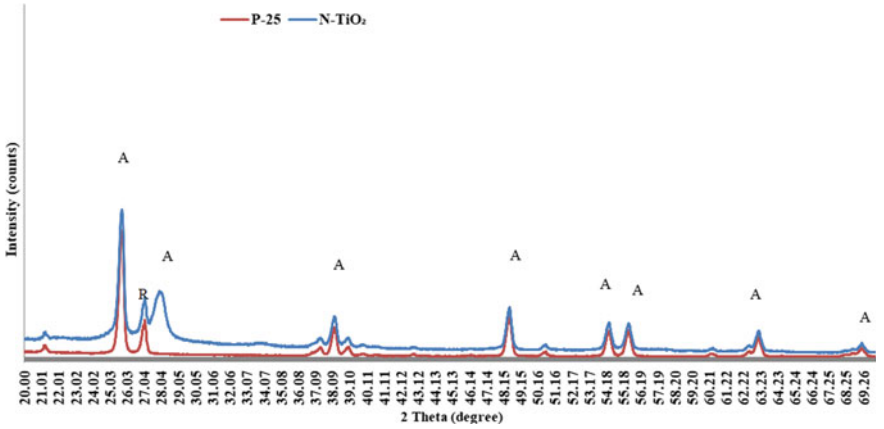

Fig. 15.3 XRD patterns of undoped TiO_2 (P-25) and N-TiO_2

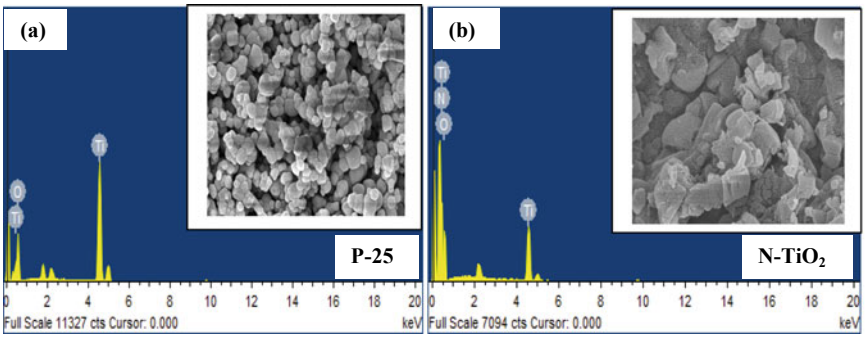

Fig. 15.4 SEM and EDS images of **a** P-25 and **b** N-TiO_2

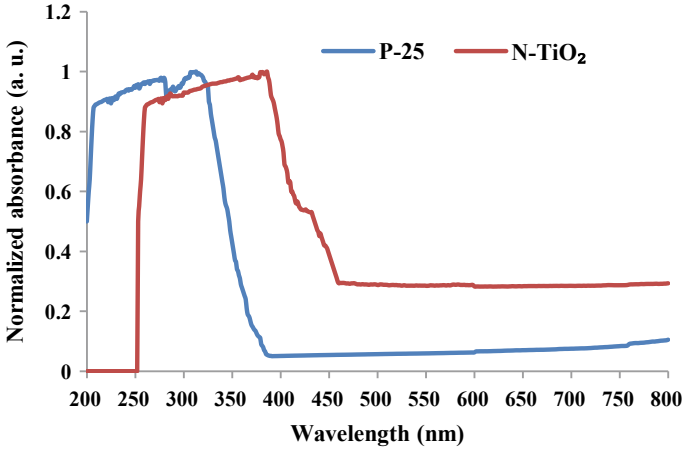

Fig. 15.5 Normalized UV visible spectra of P-25 and N-TiO_2

15.3.2 Photocatalytic Activity of Continuous Solar Photocatalytic Reactor

The treatment efficiency of the continuous solar photocatalytic reactor was evaluated in terms of COD, TOC, and ammonia. The effect of flow rates at 20, 25, 35, 50 and 70 mL/min was investigated. The flowrate was maintained up to 20 mL/min because the further decrease in flow rate would result in incomplete GT-NTiO_2 immersion.

Table 15.2 provides the continuous reactor performance for treating greywater at different flow rates. The removal efficiencies of COD, TOC and NH_4-N decreased with an increase in flow rate. From Table 15.2, it can be seen that the highest COD and TOC degradation of 71.8% and 65.1%, respectively was obtained at a flow rate of 20 mL/min. A similar trend was observed for NH_4-N removal efficiency (63.7% at 20 mL/min). The decrease in flow rate provides sufficient interaction time for the

Table 15.2. Performance of GT-NTiO$_2$ photocatalytic system operated at various flow rates

Flow (mL/min)	Hydraulic residence time (HRT)(h)	Removal efficiency (%)		
		COD	TOC	NH_4-N
20	8.33	71.8	65.1	63.7
25	6.67	62.91	60.55	59.24
35	4.75	58.76	47.24	43.62
50	3.33	44.83	33.3	39.86
70	2.38	11	8.1	16.57

pollutants with GT-NTiO$_2$ in the continuous flow reactor. Also, the reactor operating at a high flow rate (70 mL/min) showed a removal efficiency of COD (11%), TOC (8.1%) and NH_4-N (16.57%). The removal efficiencies of COD, TOC and NH_4-N were gradually decreased from 20 to 50 mL/min flowrate and next there was a sudden decrease in removal efficiencies at a flow rate of 70 mL/min. Asha et al. (2015) reported a similar study with different flowrates (60–100 mL/min) was carried out using GAC-TiO$_2$ in a continuous photocatalytic reactor. So, the optimum flow rate was found to be 20 mL/min. The graphs of COD, NH_4-N and pH variation were plotted for continuous flow reactor with respect to time (Fig. 15.6a-c). The final pH after the treatment time was obtained to be 4.9 (Fig. 15.6c). On the other hand, BP removal of 96.3% from greywater was accomplished on the completion of the treatment period.

15.4 Conclusions

In this study, a continuous flow solar photocatalytic reactor was successfully for greywater treatment with graphite coated nitrogen-doped (GT-NTiO$_2$) catalyst. Continuous mode operation displayed significant degradation of COD, TOC and NH_4-N from greywater. An enhancement in degradation efficiency in all pollutants was observed with a decrease in flowrate. The maximum reduction of COD-71.8%, TOC-65.1% and NH_4-N-63.7% was attained at the flow rate of 20 mL/min. Continuous flow solar photocatalytic reactor has proven to be an efficient system for degrading organics and nutrients from greywater. Further research work in the modification of photocatalysts such as doping with multiple elements, etc. is required to enhance the photocatalytic degradation of organics and nutrients. Additionally, the greywater effluent could be utilized for non-consumable applications (gardening, floor cleaning, cooling water in industries, etc.) with the elimination of pathogens, heavy metals, surfactants, etc.

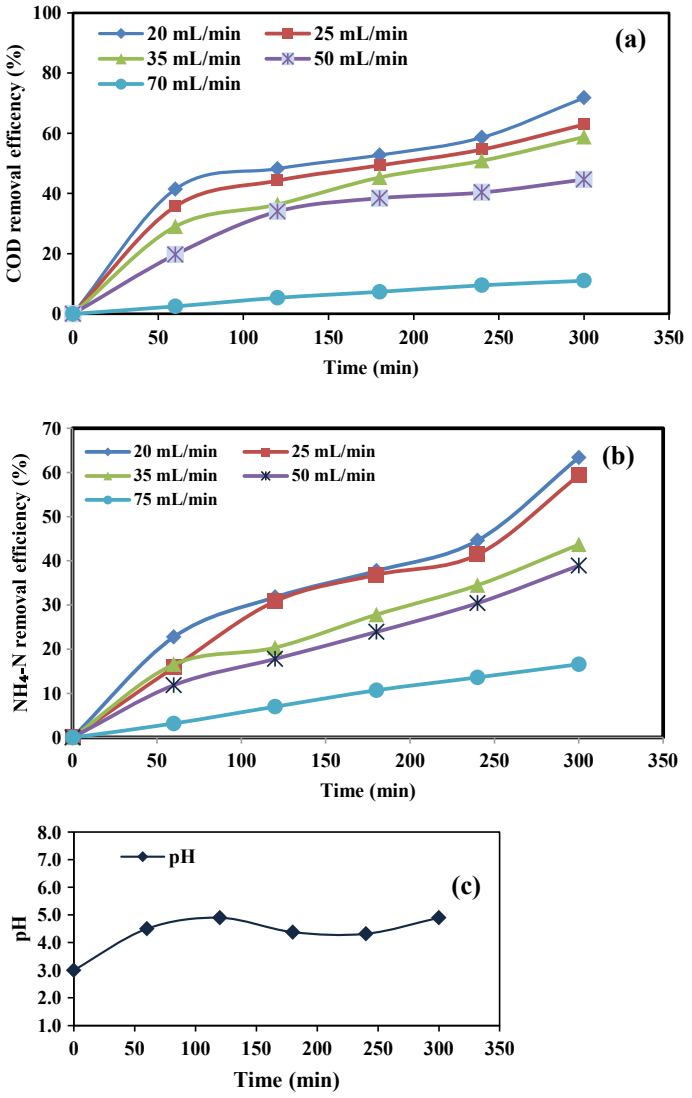

Fig. 15.6 Profiles of (**a**) COD, (**b**) NH_4-N and (**c**) pH variation for the treatment of greywater using the continuous flow solar photocatalytic reactor

References

Al-Jayyousi O (2004) Greywater reuse: knowledge management for sustainability. Desalination 167: 27–37 doi:https://doi.org/10.1016/j.desal.2004.06.110

Asha RC, Vishnuganth MA, Remya N, Selvaraju N, Kumar M (2015) Livestock wastewater treatment in batch and continuous photocatalytic systems: performance and economic analyses. Water Air Soil Pollut 226(5):1–13. https://doi.org/10.1007/s11270-015-2396-4

Benami M, Gillor O, Gross A (2016) Potential microbial hazards from graywater reuse and associated matrices: a review. Water Res 106:183–195. https://doi.org/10.1016/j.watres.2016.09.058

Eriksson E, Auffarth K, Henze M, Ledin A (2002) Characteristics of grey wastewater. Urban Water 4(1):85–104. https://doi.org/10.1016/S1462-0758(01)00064-4

Ghaitidak DM, Yadav KD (2013) Characteristics and treatment of greywater-a review. Environ Sci Pollut Res 20(5):2795–2809. https://doi.org/10.1007/s11356-013-1533-0

Li F, Wichmann K, Otterpohl R (2009) Review of the technological approaches for grey water treatment and reuses. Sci Total Environ 407(11):3439–3449. https://doi.org/10.1016/j.scitotenv.2009.02.004

Nguyen CC, Nguyen DT, Do TO (2018) A novel route to synthesize C/Pt/TiO_2 phase tunable anatase–Rutile TiO_2 for efficient sunlight-driven photocatalytic applications. Appl Catal B 226:46–52. https://doi.org/10.1016/j.apcatb.2017.12.038

Oteng-Peprah M, Acheampong MA, deVries NK (2018) Greywater characteristics, treatment systems, reuse strategies and user perception—a review. Water Air Soil Pollut 229(8):1–16. https://doi.org/10.1007/s11270-018-3909-8

Palmquist H, Hanæus J (2005) Hazardous substances in separately collected grey- and blackwater from ordinary Swedish households. Sci Total Environ 348:151–163. https://doi.org/10.1016/j.scitotenv.2004.12.052

Pidou M, Mamon FA, Stephenson T, Jefferson B, Jeffrey P (2007) Greywater recycling: Treatment options and applications. Proc Instit Civil Eng Eng Sustainability 160(3):119–131. https://doi.org/10.1680/ensu.2007.160.3.119

Prieto-Rodriguez L, Miralles-Cuevas S, Oller I, Agüera A, Puma GL, Malato S (2012) Treatment of emerging contaminants in wastewater treatment plants (WWTP) effluents by solar photocatalysis using low TiO_2 concentrations. J Hazard Mater 211: 131–137. doi:https://doi.org/10.1016/j.jhazmat.2011.09.008

Priyanka K, Remya N, Behera M (2019) Comparison of titanium dioxide based catalysts preparation methods in the mineralization and nutrients removal from greywater by solar photocatalysis. J Clean Prod 235:1–10. https://doi.org/10.1016/j.jclepro.2019.06.314

Priyanka K, Remya N, Behera M (2020) Greywater treatment using modified solar photocatalyst-degradation, kinetics, pathway and toxicity analysis. Sep Purif Technol 251: 117319. doi:https://doi.org/10.1016/j.seppur.2020.117319

Rao NN, Chaturvedi V, Li Puma G (2012) Novel pebble bed photocatalytic reactor for solar treatment of textile wastewater. Chem Eng J 184:90–97. https://doi.org/10.1016/j.cej.2012.01.004

Sacco O, Vaiano V, Rizzo L, Sannino D (2018) Photocatalytic activity of a visible light active structured photocatalyst developed for municipal wastewater treatment. J Clean Prod 175: 38–49. doi:https://doi.org/10.1016/j.jclepro.2017.11.088

Senthilnathan J, Philip L (2010) Photocatalytic degradation of lindane under UV and visible light using N-doped TiO_2. Chem Eng J 161(1–2):83–92. https://doi.org/10.1016/j.cej.2010.04.034

USEPA Standard Methods for the Examination of Water and Wastewater 22th Edition, American Public Health Association, American Water Works Association, Water Environment Federation (2012)

Vuppaladadiyam AK, Merayo N, Prinsen P, Luque R, Blanco A, Zhao M (2019) A review on greywater reuse: quality, risks, barriers and global scenarios. Rev Environ Sci Biotechnol 18(1):77–99. https://doi.org/10.1007/s11157-018-9487-9

Wiel-Shafran A, Ronen Z, Weisbrod N, Adar E, Gross A (2006) Potential changes in soil properties following irrigation with surfactant-rich greywater. Ecol Eng 26(4):348–354. https://doi.org/10.1016/j.ecoleng.2005.12.008

Chapter 16
Effect of Current and Electrodes Area to Color Removal Efficiency and Energy Consumption by Electrocoagulation Process

Bang-on Nareerob and Ponlakit Jitto

Abstract The objectives of these experiments were to investigate the effect of current and electrodes surface area on color removal efficiency and energy consumption. The result was showed that color removal efficiency was more than 95% for current apply 0.4–0.5 A, that pH increased with increasing time of electrolysis, then stabilize at close to 8–9. Amount of current density was indicate that increasing current was correspond to increase a removal efficiency that according to Faraday's law. As for, the electrode surface area with constant current, the color removal efficacy is the trend to increase. During electrolysis, larger electrodes provide higher color removal efficiency than smaller electrodes. Also, the larger electrodes can also reduce the applied voltage of the system that cause of low operation cost. For effect of current per electrode area constant but difference current and electrode area, Color removal efficiency was difference where removal efficiency was depend on the current density. The conclusion was indicated that both of current and electrode area was effect to electrocoagulation process.

Keywords Wastewater · Treatment · Electrocoagulation · Electrode area · Current

16.1 Introduction

Dyes are one of the significant toxins in the textile industry, which influences the getting climate as well as emphatically influences the wellbeing of people and creatures because of a lot of wastewater (Huynh et al. 2016). The contaminants in the outflow are colloid-dal components and dissolved organic matters, which contain chiefly by-effects, the remaining dye, acid/alkalinity, additives chemicals, and cleaning solvents. Color is a significant impurity in the textile effluent and must be eliminated prior to releasing the gushing into the aqueous ecosystem (Naje et al. 2017).

B. Nareerob · P. Jitto (✉)
Mahasarakham University, Maung Mahasarakham 44150, Mahasarakham, Thailand
e-mail: flyandaway@hotmail.com

H.-Y. Jeon (ed.), *Sustainable Development of Water and Environment*,
Environmental Science and Engineering,
https://doi.org/10.1007/978-3-030-75278-1_16

Electrocoagulation is an alternative technology for wastewater treatment (Francolins 2014) and relies upon the electrochemical dissolution of sacrificial metal electrodes (Chafi et al. 2011). Many studies have indicated the potentials of electrocoagulation in treating a variety of wastewater, such as dyes solution and textile wastewater (Abu Ghalwa and Saqer 2016; Chafi et al. 2011; El-Ashtoukhy and Amin 2010; Merzouk et al. 2009; Pajootan et al. 2012; Verma 2017), color food (Modirshahla et al. 2007), removal of pollutants from tannery (Benhadji et al. 2011; Jing-wei et al. 2007), wastewater from paint manufacturing (Akyol 2012), paper mill (Katal and Pahlavanzadeh 2011), dairy effluents (Tchamango et al. 2010, domestic wastewater (Omwene and Kobya 2018) and heavy metals (Al Aji et al. 2012). The EC technique is advantaged by its easiness, simple operation, less retention time, less or nonappearance of chemicals addition, fast sedimentation, less sludge creation, and ecological similarity when contrasted with customary techniques (Omwene and Kobya 2018).

EC operating conditions mostly depend on the current density, pH, Voltage, types of electrode, retention time, chemical constituents and concentrations containing wastewater (Mickova 2015). Generally, an increase in current causes the anode oxidation more readily, which increasing removal efficiency according to Faraday's law (Eq. 1) as described the relationship between current and the amount of anodic dissolution. Whereas the electrode surface area rarely mentions but has the advantage of a decreased time of coagulation (Ahangarnokolaei et al. 2018).

$$E = I \times T \times M / z \times F \tag{16.1}$$

where, I is current (A), T is time of electrolysis (s), M is molecular mass of electrode (g/mol), z is number of electrons transferred, F is Faraday's constant (96,487 g/mol)

EC generally refers to the electrolytic generation of coagulating metal ions, which make colloidal particles larger so they can be filtered through from the water. The gas (H_2) released at the cathode has no influence in the pollutant removal (Mickova 2015). For the most part, the EC process comprises six key processes: (i) movement to an oppositely charged electrode (electrophoresis) and aggregation due to charge neutralization;(ii) a precipitate with the pollutant forms a cation or hydroxyl ion (OH^-);(iii) to form a hydroxide, the metallic cation interacts with OH^- which has high adsorption properties that are therefore attached to the contaminant; (iv) the hydroxides, like structures, form larger lattices and sweep through the water (sweep coagulation);(v) pollutants oxidation to less toxic species;(vi) removal by electro flotation or sedimentation and bubble adhesion (Katal and Pahlavanzadeh 2011). According to the following reactions (Merzouk et al. 2009)

anode, sacrificial metal (Al):

$$Al_{(s)} \rightarrow Al^{3+} + 3e^- \tag{16.2}$$

cathode, H_2 gas and OH^- is generated:

$$3H_2O + 3e^- \rightarrow 3OH^- + 3/2\, H_2(g) \quad (16.3)$$

At low pH, aluminum anode generates the cationic monomeric species, for example, Al^{3+} and $Al(OH)^{2+}$, which at proper pH values are transformed into $Al(OH)_3(s)$ and finally polymerized to $Al_n(OH)_{3n}$ (Modirshahla et al. 2007):

$$Al^{3+}_{(aq)} + 3H_2O \rightleftarrows Al(OH)_3 + 3H^+ \quad (16.4)$$

In the EC, the predominantly formed amorphous $Al(OH)_3$ "sweep flocs" have large surface areas which are valuable for fast adsorption of soluble organic compounds and catching of colloidal particles. At last, these flocs are taken out effectively by sedimentation or flotation by H_2 (El-Ashtoukhy and Amin 2010; Omwene and Kobya 2018).

This article presents the results of the study of the laboratory scale on the removal of C.I. Acid Red 114 from water by electrocoagulation using aluminum electrodes. A detailed experimental has been done to notice the impacts of current and electrode surface areas on the efficiency of dye removal. Measurement of pH, operating time, and cell voltage for estimation of electrical energy consumption.

16.2 Experimental

16.2.1 Materials and Methods

The EC experiments were performed on Acid Red 114 (C37H28N4O10S3.2Na, C.I.:23635 MW: 830.8 g/mol, λ_{max}: 518 nm, sivasumpan Co.,Ltd.) solutions with a concentration of 400 mg/L. The batch reactor used 2 L polypropylene beaker. The aluminum electrodes with submerge surface areas range 4–100 cm^2 were used as anode and cathode with the distance of each electrodes was set 2 cm. the electrodes were submerged in HCl 15% for 30 min to remove impurities on the aluminum surface, then abraded with sandpaper and rinsed with distilled water, next and used suddenly. The DC power supply was GW Instek, GPS-3303. The experiments were performed at room temperature. The magnetic stirrer was set at 150 rpm. (see in Fig. 16.1.)

16.2.2 Experimental Procedures

The experiment was separated into 3 parts: (i) Effect of current, as testing current in range 0.05-0.5 A with fixed electrode surface area 40 cm^2. (ii) Effect of electrode surface area, 4–100 cm^2 were the different surface area studied with testing current 50, 300, and 500 mA depend on limit maximum current used. (iii) Effect of

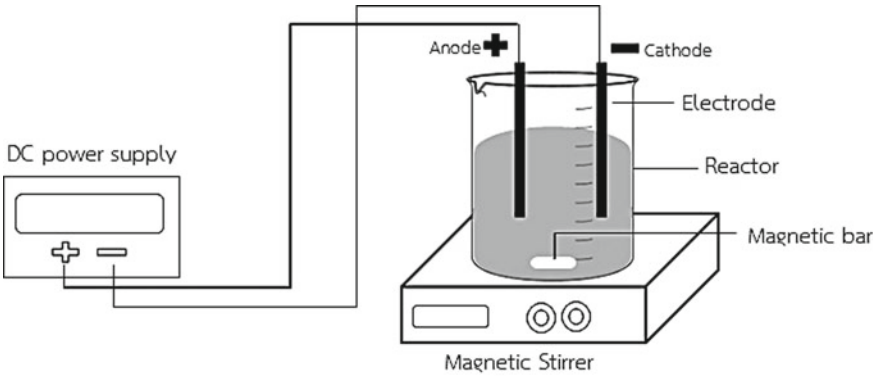

Fig. 16.1 Experimental setup for batch electrocoagulation

Table 16.1 Experimental scope

Experiment	Variation of parameters	Constant parameter
Effect of current	0.05, 0.1, 0.2, 0.3, 0.4, 0.5 A	$C_0 = 400$ mg/L, EA = 40 cm^2, d = 2 cm, pH = 6
Effect of electrode surface area	4, 10, 20, 40, 60, 80, 100 cm^2 (0.2, 0.5, 1, 2, 3, 4, 5 cm)	$C_0 = 400$ mg/L, I = 0.05-0.5A, d = 2 cm, original pH value
Effect of current/surface area constant	5 mA/cm^2 (50 mA/10 cm^2) 5 mA/cm^2 (200 mA/40 cm^2) 5 mA/cm^2 (500 mA/100 cm^2)	$C_0 = 400$ mg/L, I = 0.05-0.5A, d = 2 cm, original pH value

current density per electrode area was constant as 5 mA/cm^2 which corresponded as currents value 50, 200, and 500 mA with electrode surface areas 10, 40, and 100 cm^2, respectively. (see in Table 16.1.)

16.3 Analytical Method

In each experiment, Dye wastewaters was sampling within 0-60 min. pH was measured immediately, pH analysis using Multi-Meter. (Hach, HQ40D Portable Multi Meter). Then the sample was filtered using by filter paper.(Whatman filter paper No. 42) Determination of color removal was using UV-vis spectrophotometer (Shimadzu UV-1900), using the wavelength that provided the maximum intensity (λ_max = 518 nm). Experimentally, percentage of color removal efficiency during the treatment of dyes wastewater is determined by the expression (5):

$$\text{color removal } (\%) = [(\text{Abs}_0 - \text{Abs}_i)/\text{Abs}_0] \times 100 \tag{16.5}$$

where Abs_0 and Abs_i are the average absorbance before electrolysis and after an electrolysis time, respectively, at the maximum visible wavelength of wastewater. Expense due to electrical energy (kWh/m^3 dye solution) was determined using the following equation (Hashim et al. 2017):

$$E = I \times v \times t / Vol. \tag{16.6}$$

where E is the electrical energy consumption (kWh/m^3), I is current (A), v is the cell voltage (V), t is time of electrolysis (hr) and Vol. is the volume of dye wastewater.

16.4 Result and Discussion

16.4.1 Effect of Current

As a feature of water alkalinity, the current affects hydrolyzed metal species through pH evolution during the EC process (Hakizimana et al. 2017). Studies of differential current (I) studies of 0.05-0.5 A with dye wastewater pH initial 6 was adjusted by adding NaOH 0.5 M. The aluminum electrode area was used 40 cm^2. The result was found that the efficiency of color removal increased with an increase in current as see in Fig. 16.2a. The current was increased from 0.1 to 0.3 A, the color removal increased from 31.6% to 91.4% was observed after 22 min of operation. At the same time color removal more than 90% for current 0.4-0.5A. However, after 30 min of operation, more than 95% color removal was observed for all current above 0.3 A. Figure 16.2b it may be seen from the figure that pH increased with increasing time of electrolysis, then stabilize at close to 8–9. For the same color removal efficiency more than 80%, in current 0.1, 0.2, 0.3, 0.4 and 0.5 A. the operation time was observed 50, 40, 16, 13 and 10 min respectively. As time increases, the pH was increased. The final pH range 8–9, at a current of 0.05-0.1 A. it has a similar pH and is less than at other currents, with the final pH 7.54–7.9. For current from 0.2–0.5 A, the final pH is 8.4–8.81. It can be concluded that when the current increases, the pH changes during system operation are higher resulting in the optimum pH was rapid. That means the current increased the time of electrolysis with optimum pH (4–9) was decreased. Because of pH between 4–9, the Al^{3+} and OH^- ions generated by the electrodes react to form various monomeric species such as $Al(OH)^{2+}$, $Al(OH)_2^+$, and polymeric species such as $Al_6(OH)_{15}^{3+}$, $Al_7(OH)_{17}^{4+}$, $Al_{13}(OH)_{34}^{5+}$ that finally transform into insoluble amorphous $Al(OH)_{3(s)}$ through complex polymerization/precipitation kinetics (Merzouk et al. 2009).

Thus, the rate of ion output (Al^{3+}) on the anode rises as the current density increases. These increase the output of flocs ($Al(OH)_3$) in the solution and thus improve the efficiency of the removal of color. The fact that the dissolved coagulants (Al^{3+}) increased as improved efficiency of color removal according to Faraday's law. On the other hand, the total amount of flocs produced at a very low current was not sufficient

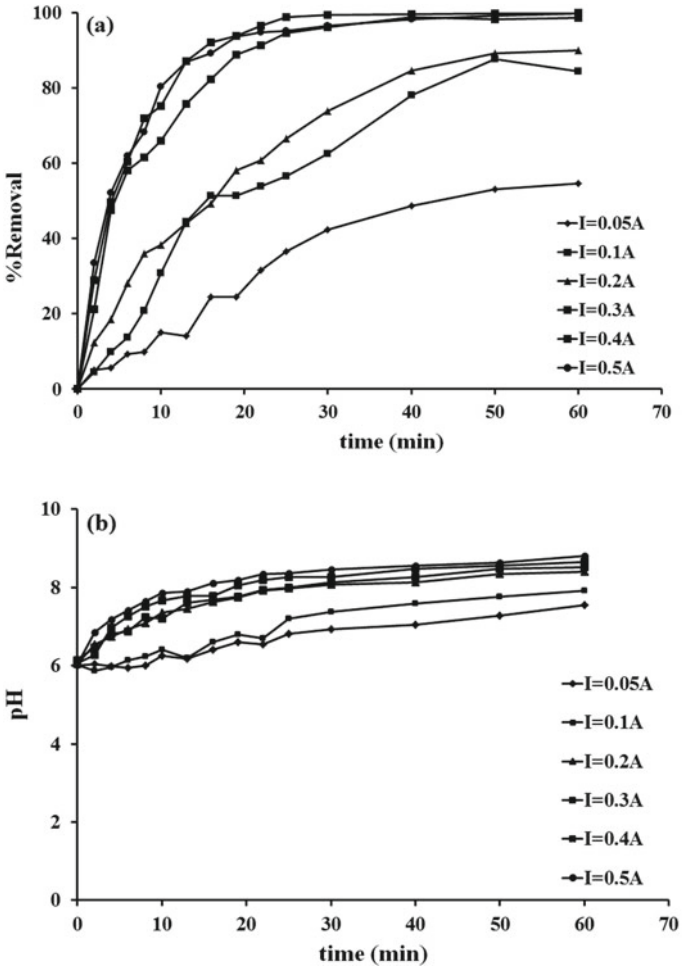

Fig. 16.2 Effect of current on the color removal efficiency with Al electrodes. Electrodes gap 2 cm. Initial pH 6 **a** color removal efficiency with different current **b** pH system

to remove all the dye molecules in the solution and more time was needed to achieve greater efficiency of color removal (Modirshahla et al. 2007; Nandi and Patel 2017). Moreover, The EC system design should consider the current and operation time which to reduce energy consumption.

16.4.2 Effect of Electrode Surface Areas

In order to investigate the effect of electrode surface areas on the efficiency of color removal, studies were carried out at different electrode surface areas of 4–100 cm^2 (width 0.2–5 cm) at fixed current min 0.05 A, current max 0.3 A (4–10 cm^2) and 0.5 A (20–100 cm^2) with original pH. Each experiment runs 60 min. According to Fig. 16.3a, demonstrate the removal efficiency of AR114 as a function of electrode surface areas. At EA 4 cm^2 (current 0.05 A) and original pH (4.09-4.28) the color removal efficiency was increased slowly. As for EA 10–100 cm^2 seems to tend was

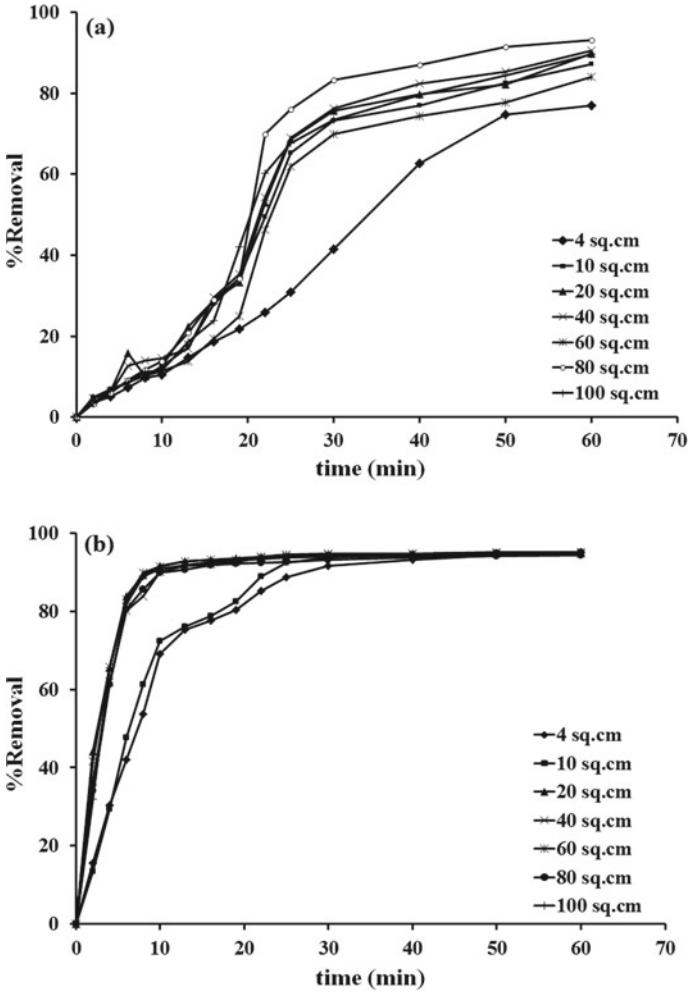

Fig. 16.3 Effect of electrode surface areas on the color removal efficiency with Al electrodes. Electrodes gap 2 cm. Initial pH 4–4.3 **a** I = 0.05 A, **b** I = 0.3–0.5 A

Table 16.2 Effect of electrode area with constant current on the electrical energy consumption (I = 0.05 and 0.5A, Al electrodes, electrodes gap 2 cm and time of experiment 60 min

Electrode surface area (cm^2)	I = 0.05 A, T = 60 min		I = 0.5 A, T = 60 min	
	Volt	KW h/m^3	Volt	KW h/m^3
4	17.1	427.50	63.1 (0.3A)	15,775
10	13	325.00	63.1 (0.3A)	15,775
20	11.5	287.50	63	15,750
40	8.8	220.00	57.6	14,400
60	6.7	167.50	45.2	11,300
80	6.2	155.00	38	9,500
100	5.2	130.00	30.6	7,650

similar. The time of experiments in range 19-25 min the color removal was changing rapidly and during electrolysis, larger electrodes provide higher color removal efficiency than smaller electrodes according to the kinetics of electrode reaction (Walsh 1992). Then, at 60 min the removal efficiency increase of 77%, 87.2%, 89.8%, 90.5%, 84%, 93.1% and 89.6%, respectively and final pH was 6.68–7.57. While various EA with maximum current test 4–10 cm^2 (0.3 A) and 20-100 cm^2 (0.5 A), for EA 4–10 cm^2 the color removal efficiency increasing less than EA above 20 cm^2 but after 40 min the efficiency seems no difference which in the range 93.3–94.6%. In addition, EA 20–100 cm^2 in 10 min the treatment efficiency is more than 90%. At the end of the experiment was observed 95.2%, 95.2%, 94.7%, and 94.9% respectively as shown in Fig. 16.3b. As initial pH before run measured 4.16–4.3, after 60 min the pH was increasing of 8–8.84.

The result indicated that an increasing of electrode surface area with constant current, the color removal efficacy is the trend to increase. During electrolysis, larger electrodes provide higher color removal efficiency than smaller electrodes. Also, the larger electrodes can also reduce the applied voltage of the system while the current constant (see in Table 16.2).

16.4.3 Effect of Current Density and Electrode Area When Current/Electrode Area Constant (CA)

Electrocoagulation process is often designed as a function of current density as the proportion current over the electrode surface (Hakizimana et al. 2017). Current density is an important factor because it determines the production rate of coagulation, bubble formation rate and hence of flocs (Naje et al. 2017). Experimental studies were carried out at fixed current density per electrode area at 5 mA/cm^2, which corresponded as currents value 50, 200 and 500 mA with electrode surface areas 10, 40 and 100 cm^2 respectively. It can be indicated from Fig. 16.4, at fixed

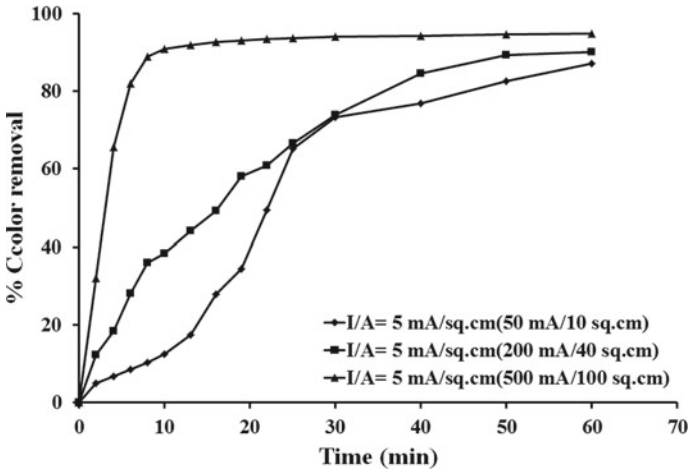

Fig. 16.4 Effect of current density on the color removal efficiency with Al electrodes. Electrodes gap 2 cm, Initial pH 4–4.3, I/A = 5 mA/cm^2

current density as various currents system was different when currents increased from 50 to 500 mA with the area of 10 cm^2 and 100 cm^2 after 10 min, the color removal efficiency increased from 12.5% to 90.9%. Although the same value of current density per electrode area ratio, it seems that currents are an important factor affecting efficiency. Other studies the current density with constant electrodes area; CA of 5-20 mA/cm^2 observed an increase in dye removal efficiency up to 98.7% with an increasing CA (Abu Ghalwa and Saqer 2016). Another study, using CA in range 100–1200 mA/cm^2, the dye removal increased from 65% to 92% (acid black 52) and 97% (acid yellow 220) with an increasing CA of 10–40 mA/cm^2, but increasing CA up to 1200 mA/cm^2 no real difference (Pajootan et al. 2012). For CA was varied between 20.8–62.5 mA/cm^2. An increase in CA from 20.83 to 62.5 mA/cm^2 the color removal efficiency increased 78–93% when CA higher than 31.25 mA/cm^2 became a small difference curve (Merzouk et al. 2009). As a result, the CA corresponded to the currents value (I), which influent to electrocoagulation efficiency. When increased CA with electrodes area was constant, the current value was increasing. In other words, seems to currents the most influential to the EC system.

16.4.4 Electrical Energy Consumption

Energy consumption regarding potential (Cell voltage; Volt), current (I; Amp), time of electrolysis and volume of dye solution that is calculated by Eq. 5. Table 16.2 represents the variation of electrical energy consumption with various electrodes areas (4–100 cm^2), current 0.05, 0.3, and 0.5 A at the time of experiment 60 min. According to observation, the cell voltage decreases by increasing the electrode

surface area due to constant current. When the electrode area increased from 4 to 100 cm^2 (I = 0.05A), cell voltage lower from 17.1 to 5.2 volts the electric energy consumption decreasing 427.5 to 130 KW hr/m^3. As for current 0.3–0.5 A the cell voltage decreased 63.1 to 30.6 volts, with the energy consumption 15,755–7650 KW hr/m^3.

In other words, at smaller electrode surface areas indeed to more potential to stabilize the current, it can be said the larger electrodes area has the least amount of energy consumption (Ahangarnokolaei et al. et al. 2018). Consequently, the electrocoagulation process design should be consider electrode surface areas.

16.5 Conclusion

Effect of current and electrodes surface area on color removal efficiency towards energy consumption with EC process using Al electrodes in the sacrificial anode and cathode with Acid red 114 dye solution. The result influent of current showed, the more color removal efficiency direct by increasing current. At the highest current 0.4–0.5 A, the color removal efficiency increases rapidly with a short time. As for the lower current 0.05–0.3 A, it required more time to achieve higher color removal efficiency and pH stabilize close 8–9. For the effect of electrodes area, it can be seen an increase in the electrodes surface areas was to increase the efficiency of color removal. Increase of current density per electrode area was correspond to increase removal efficiency The color removal efficiency indicate to depend on the current, not current density per electrode area. As for the effect of electrodes area, the smaller electrode surface areas need more voltage to stabilize the current. Consequently, the larger electrodes area uses less voltage towards reducing the amount of energy consumption. The results were concluded that both of current density and electrode area effect to electrocoagulation process. For future study will experiment to limit of electrode area in another material such iron electrode.

Acknowledgements This research was financially supported by Mahasarakham University (Grant year 2020)

References

Abu Ghalwa NM, Saqer AM (2016) Removal of Reactive Red 24 Dye by Clean Electrocoagulation Process Using Iron and Aluminum Electrodes. Journal of Chemical Engineering & Process Technology 07(01):1–7

Ahangarnokolaei MA, Ganjidoust H, Ayati B (2018) Optimization of parameters of electrocoagulation/ flotation process for removal of acid red 14 with mesh stainless steel electrodes. Journal of Water Reuse and Desalination 8(2):278–292

Akyol A (2012) Treatment of paint manufacturing wastewater by electrocoagulation. Desalination 285:91–99

Al Aji B, Yavuz Y, Koparal AS (2012) Electrocoagulation of heavy metals containing model wastewater using monopolar iron electrodes. Sep Purif Technol 86:248–254
Benhadji A, Ahmed MT, Maachi R (2011) Electrocoagulation and effect of cathode materials on the removal of pollutants from tannery wastewater of Rouïba. Desalination 277(1–3):128–134
Chafi M, Gourich B, Essadki AH, Vial C, Fabregat A (2011) Comparison of electrocoagulation using iron and aluminium electrodes with chemical coagulation for the removal of a highly soluble acid dye. Desalination 281(1):285–292
El-Ashtoukhy ESZ, Amin NK (2010) Removal of acid green dye 50 from wastewater by anodic oxidation and electrocoagulation-A comparative study. J Hazard Mater 179(1–3):113–119
Feng JW, Sun YB, Zheng Z, Zhang JB, Shu LI, Tian YC (2007) Treatment of tannery wastewater by electrocoagulation. Journal of Environmental Sciences 19(12), 1409–1415
Francolins C (2014) Effective Decolorization of Eriochrome Black T, Furschin Basic and Malachite Green Dyes from Synthetic Wastewater by Electrocoag-nanofiltration. In: The World Congress on Engineering and Computer Science on proceedings, pp. 22–24. Newswood Limited, San Francisco (2014)
Hakizimana JN, Gourich B, Chafi M, Stiriba Y, Vial C, Drogui P, Naja J (2017) Electrocoagulation process in water treatment: A review of electrocoagulation modeling approaches. Desalination 404:1–21
Hashim KS, Shaw A, Phipps D (2017) Iron removal, energy consumption and operating cost of electrocoagulation of drinking water using a new flow column reactor. J Environ Manage 189:98–108
Huynh, N.-H. T., Duong, P.-H., Yoon, Y.-S (2016) Removal of C.I. Acid Red 114 dye from wastewater by using ozonation and electrocoagulation. Jacobs Journal of Environmental Sciences 2(3), 1–9
Katal R, Pahlavanzadeh H (2011) Influence of different combinations of aluminum and iron electrode on electrocoagulation efficiency: Application to the treatment of paper mill wastewater. Desalination 265(1–3):199–205
Merzouk B, Gourich B, Sekki A, Madani K, Vial C, Barkaoui M (2009) Studies on the decolorization of textile dye wastewater by continuous electrocoagulation process. Chem Eng J 149(1–3):207–214
Mickova I (2015) Advanced Electrochemical Technologies in Wastewater Treatment Part I: Electrocoagulation. American Scientific Research Journal for Engineering, Technology, and Sciences 14(2):233–257
Modirshahla N, Behnajady MA, Kooshaiian S (2007) Investigation of the effect of different electrode connections on the removal efficiency of Tartrazine from aqueous solutions by electrocoagulation. Dyes Pigm 74(2):249–257
Naje AS, Chelliapan S, Zakaria Z, Ajeel MA, Alaba PA (2017) A review of electrocoagulation technology for the treatment of textile wastewater. Rev Chem Eng 33(3):263–292
Nandi BK, Patel S (2017) Effects of operational parameters on the removal of brilliant green dye from aqueous solutions by electrocoagulation. Arabian Journal of Chemistry 10:S2961–S2968
Omwene PI, Kobya M (2018) Treatment of domestic wastewater phosphate by electrocoagulation using Fe and Al electrodes: A comparative study. Process Saf Environ Prot 116:34–51
Pajootan E, Arami M, Mohammad N (2012) Journal of the Taiwan Institute of Chemical Engineers Binary system dye removal by electrocoagulation from synthetic and real colored wastewaters. Journal of the Taiwan Institute of Chemical Engineers 43(2):282–290
Tchamango S, Nanseu-Njiki CP, Ngameni E, Hadjiev D, Darchen A (2010) Treatment of dairy effluents by electrocoagulation using aluminium electrodes. Sci Total Environ 408(4):947–952
Verma AK (2017) Treatment of textile wastewaters by electrocoagulation employing Fe-Al composite electrode. Journal of Water Process Engineering 20(May):168–172
Walsh FC (1992) The Kinetics of Electrode Reactions: Part II—Mass Transfer and Mixed Control. The International Journal of Surface Engineering and Coating 70(2):95–99

Chapter 17
Accessing the Sustainable Developments Principle of Protection of the Mekong River's Water Resources

Thuy Hang Tran, Hong Hanh Pham, and Thanh Hoa Ha

Abstract From 2009, the Mekong River's water quantity and quality have been significantly reduced. The phenomenon happened as a result of climate change and human activities. Activities to block the flow or build dams to construct hydroelectricity or diversion in upstream countries are either the direct cause or the risk of further deterioration of the water quality and quantity of the Mekong River. The current status of the Mekong River's water resources poses serious challenges for sustainable development of the Mekong River's Basin. To cope with the problems, Agreement on the Cooperation for the Sustainable Development of the Mekong River Basin 1995 (Mekong Agreement) is the only multilateral treaty directly regulating the protection of water resources in the Mekong River. The principle of sustainable development, however, is not specified in a specific article, embodied in the Mekong Agreement through the contents of this treaty. Besides, the crucial obligations lacks an monitoring mechanism and has an unreasonable dispute solution.

Keywords Sustainable development principle · No—Harm rule · Reasonable and equitable utilisation · Mekong agreement

17.1 Introduction

The Mekong river basin in Vietnam is largely located downstream, accounting for about 8% of the basin area, including the upstream of the Nam Ron River (Dien Bien Province), the upstream of the Se Kong and Se Ba Hieng river, and the Se San and Srepok river basin and the Mekong Delta region. The Mekong River has a particularly

T. H. Tran (✉) · H. H. Pham · T. H. Ha
Faculty of International Law, Hanoi Unviersity of Law, 100000 Hanoi, Vietnam
e-mail: mrsthuyhang@hlu.edu.vn

H. H. Pham
e-mail: phamhonghanh@hlu.edu.vn

T. H. Ha
e-mail: hathanhhoa@hlu.edu.vn

H.-Y. Jeon (ed.), *Sustainable Development of Water and Environment*,
Environmental Science and Engineering,
https://doi.org/10.1007/978-3-030-75278-1_17

important role, ensuring national food security and water resources for two significant regions, Mekong River Delta and Central Highlands, contributing nearly 60% of Vietnam's total annual water volume. Every year, the Mekong River transports over 420 billion m3 (including the Mekong river tributaries' water volume that Vietnam is upstream) into the Mekong Delta. In the Mekong Delta, the Mekong River brings the fertile delta alluvium and rich natural aquatic resources. In the Central Highlands region, the Sê San and Srepok river basins' water resources have been exploited to supply water for agricultural production, domestic and hydropower development in Vietnam. With the Mekong River's special role in Vietnam, ensuring the Mekong River's water resources' sustainable development is of utmost importance.

The issue of sustainable international water resources development was mentioned very early in many treaties relating to freshwater resources, such as the 1923 Convention on Hydropower Development, Convention on the protection of Lake Geneva water from pollution sources in 1962, the Convention on the withdrawal of water from Lake Constance in 1966 with contents such as the obligation of notification, consultation, environmental impact assessment, and dispute settlement (Botchway 1919). According to the International Law Association's approach to the Berlin Rule on water law in 2004, sustainable water development is "integrated management of resources to ensure efficient use and public access. with water resources for the benefit of present and future generations, while conserving renewable resources and maintaining non-renewable resources to the extent possible "(Clause 19, Article 3) (Ministry of Natural Resources and Environment 2018). In short, the sustainable development of international water resources means that the use of international water resources must ensure benefits for all riparian states, without prejudice to meeting their countries needs current and future water countries and suitable for the adequate protection of the quantity, quality, and ecology of transboundary water resources.

Due to the close relationship between the sub-regions' natural and socio-economic conditions and the broad Mekong basin, the Mekong River's upstream activities will lead to many impacts on the environment and society to Vietnam's downstream. It is undeniable that the hydroelectric dams built in the past are among the causes of negative impacts on the Mekong River's flow and water quality in the Mekong Delta. Failure to ensure the Mekong River's sustainable development directly damages this river and seriously affects the economic and social lives of many downstream countries, including Vietnam. From a legal perspective, the current legal framework of the Mekong River Commission reveals limitations in regulating the activities of member states in the protection of Mekong water resources.

17.2 Material and Methodology

In this article, the data about the Mekong River's water level and quality was collected at the Tan Chau and Chau Doc hydrological stations, published by the Mekong Commission on the organization's official website. The Mekong Delta

region's data on a saline intrusion is evaluated based on the Vietnamese Ministry of Natural Resources and Environment reports. The data on information related to hydropower projects and hydropower projects in the Mekong is based on the report on hydropower's strategic assessment on the Mekong River submitted by the International Center for Environmental Management and reports the Ministry of Natural Resources and Environment of Vietnam.

17.2.1 The Construction of Hydroelectric Dams in the Mekong River

According to the report of MRC in July 2020, based on monitoring databases, in conjunction with other sources of monitoring, in addition to objective causes such as climate change, the performance of large hydropower dam in the mainstream, and also the tributaries of the Mekong River also contribute to reducing the volumetric flow (Ministry of Natural Resources and Environment 2020). Before that, as early as 2010, the Strategic Environmental Assessment of the Mekong mainstream hydroelectricity submitted to the Mekong River Commission indicated that when put into construction and operation, water development projects, The proposed electricity would be likely to cause transboundary impacts and international tensions in the Mekong Lower section in many ways, including the Mekong River volume water (International Law Association).

There are 13 hydropower dams in the MeKong mainstream in operation (11 upstream dams and 2 downstream dams) and 19 hydropower projects in the progress construction progress. In upstream, China's total water storage capacity of 11 dams in operation is 45,54 km^3 (Eyler, Brian and Weatherby, Courtney, 2020). Only currently operating dams in upstream have stored nearly 10% of the total average annual flow of the Mekong. In downstream, the total water storage capacity of the two operating dams is 0,4 km3, in which the water storage capacity of the Xayaburi Dam is 0,37 km^3 and the Don Sahong Dam is 0,03 km^3 (International Centre for Environmental Management 2010). Nine other hydropower dam projects are planned, including five projects in Laos, two projects in Cambodia and two projects across the Laos-Thai border. The total water storage capacity of these nine hydropower dams and two current dams is 11,43 km^3.

Water storage in hydropower dams with large reservoir capacity will potentially cause change in the Mekong River's water level. In fact, the Chinese dams in Yunnan. Province have already induced noticeable changes in water levels at Chiang Saen at a daily time (International Centre for Environmental Management (ICEM) 2010). The retention times of these dam chains cause water to flow back to the Mekong Delta very late. During the rainy season, dams upstream will reduce runoff energy by 70–100%; some dams have the ability to block flows for 2–3 weeks in the dry season and 1–2 weeks in the wet season, some dams have a retention time of up to 1 month

during drought years like the Sanakham dam in Laos (Mekong River Commission 2020).

17.2.2 A Decline in Water Resources of the Mekong River in the Basin Part of Vietnam

From November 2020 to early February 2021, the Mekong River's water level measured at Tan Chau station was lower than the average water level in the period 1961-2019. Specifically, in the last two months of 2020, the lowest measured level is 1.32 m (7 December), while the average at the corresponding period 1961-2019 is 2.01 m. Similarly, in the first two months of 2021, the lowest measured level was 0.31 m (4 February), while the average water level at the corresponding period 1961-2019 was 0.98 m (MeKong River Commission 2018).

In 2020, the MRC's Hydrological Observation and Reports also showed that the Mekong River's water level was low in some areas. The water level in the dry season that flows on the Mekong mainstream in June and July 2020 is described as "exceptionally low." (Office of the National Assembly 2017). At Tan Chau and Chau Doc stations, the maximum water level at the end of September 2020 at Tan Chau station is still 1.2 m lower than the average and 1.25 m lower than the level 1 flood alarm. Tan Chau and Chau Doc's total water flow in the second half of September 2020 tend to decrease, reaching only 59% of the average and 37% lower than the same period in 2019. Water level and total flood volume to the Mekong Delta in the second half of September 2020 remained the lowest level in 10 years (Vietnam Mekong River Commission Standing Office 2020).

In 2019, due to the Mekong River's low flood peak at the Tan Chau 2.5 m and Chau Doc station of the low 2.2 m, the total flow in the Mekong River's upstream to the Mekong Delta region was much less than the average many years. The MRC data shows that the water level in Tan Chau in the last six months of 2019 and the first five months of 2020 is at a low level, nearly coinciding with the historical deadline of 2015–2016. Even in the period defined as the rainy season, the water level in 2019 is lower than in previous years (Table 17.3). At Tan Chau and Chau Doc stations, the water level started to drop lower than average from 18 June. In July, the water level at these two stations is usually 0.8–2.3 m lower than the average water level. Similarly, Tan Chau and Chau Doc's flow is also lower than the average flow by 14,000 m^3/s, a 75% reduction in the average flow in the same period in July at these two stations.

Along with the decline in water volume, the river water level falls low, causing salt to penetrate deeply into the estuary. Specifically, since November 2019, drought is seriously affecting the Mekong Delta, increasing between March and April. Saline boundary 4% (4ppt) on Vam Co Tay river (at times over 125 km), Cua Tieu, Cua Dai, Ham Luong penetrated deeper than 2016 from 3 to 7 km, greatly affecting production and domestic of the Mekong Delta provinces. As of April 2020, the Mekong Delta's dry season has lasted for nearly six months, causing about 96,000 households in the

Table 17.1 Information on some of China's hydropower dams in the upper Mekong basin (Lancang River) (stage 1) (*From upstream to the China-Laos border*)

No.	Hydroelectric dam projects	Basin acreage (10^{3+} km^2)	Water reservoir acreage (ha)	Capacity (10^6 m^3)	Output Capacity (MW)
1	Gongguoqiao Dam	97,2	343	120	750
2	Xiaowan Dam	113,3	3.712	9.900	4.200
3	Manwani Dam	114,5	415	250	1.500
4	Dachaoshan Dam	121,0	826	280	1.350
5	Nuozhadu Dam	144,7	4.518	12.300	5.500
6	Jinghong Dam	149,1	510	310	1.500
7	Guanglanba	151,8	12	110	150
8	Manson	160,0	58	140	600

Source Ministry of Natural Resources and Environment (2018), Thematic Information - Water resources and issues in ensuring national security

Table 17.2 Information on 11 Hydropower Projects in the Lower Mekong Basin

No.	Hydroelectric dam projects	Power capacity (MW)	Reservoir Area (km^2)	Length (m)	Height (m)
1	Pakbeng	1200	87	943	76
2	Luang Prabang	1,100	55.9	1,106	68
3	Xayaburi	1,280	55.9	810	32
4	Paklay	1,320	108	630	35
5	Sanakham	700	81	1,144	38
6	Pakchom	1,079	74	1,200	55
7	Ban Kum	1,872	74	780	53
8	Latsua	686	13	n/a	Na
9	Don Sahong	240	0.29	1,820-720-2,730	10.6-8.2-8.3
10	Stung Treng	900	211	10,884	22
11	Sambor	2,600	620.5	18,002	56

Source ICEM, MeKong River Commission, Strategic environment assessment of hydropower on the MeKong mainstream. https://icem.com.au/documents/envassessment/mrc_sea_hp/SEA_Final_Report_Oct_2010.pdf

Table 17.3 Water level of the Mekong River at Tan Chau and Chau Doc stations in the second half of June 2019 compared to some years ago

Name of stations	2016	2017	2018	2019
Tan Chau Station	1.05	9.18	6.53	0.38
Chau Doc Station	1.5	8.39	5.66	−0.25

Source Mekong River Commission- Regional Flood Management and Mitigation Centre, *Weekly Flood Situation Report for the Mekong River Basin*

area to lack domestic water, five provinces must publish natural disasters. The highest salinity intrusion level at saline intrusion points in the Mekong Delta from 1/1/2020 to 20/4/2020 are: (i) 7.3 g/l (Dong Tam), 1.9 g/l (Vinh Binh), 6.49 g/l (Monitoring station 285 Binh Dien), 20.13 g/l (New Ca Bridge – Binh Dien), 10.61 g/l (Vam Bon Bot), 13.56 g/l (Dai Ngai), 13.65 g/l (Outside Can Chong Gate), 23.51 g/l (Vam Don Chau), 22.64 g/l (Lang Chim Bridge), 27.2 g/l (Ban Trai), 13.5 g/l (Huong My), 29.5 g/l (An Thuan), 28.2 g/l (Son Doc), 29.2 g/l (Binh Dai), 25.4 g/l (Vam Kenh), 21.1 g/l (Cau Noi), 14.1 g/l (Ben Luc) (Can Tho University 2020). The damage of agricultural production is minimized due to seasonal adaptive measures, but lack of domestic water or water for irrigation for orchards and serious lack of freshwater has become the largest concern during the salty drought season (Ministry of Natural Resources and Environment 2020).

17.3 Discussion on the Legal Framework of Protection Mekong's Water Resource

There are currently more than ten cooperation mechanisms in the Mekong region, such as the Mekong River Commission (MRC), the Mekong-Trade Cooperation (LMC), the Lower Mekong Initiative (LMI), the Mekong-Japan Cooperation. One of the most prominent cooperation mechanisms is the Mekong Commission, which was established based on the 1995 Agreement on Cooperation for the Sustainable Development of the Mekong River Basin (the Mekong River Agreement) and the Protocol for Implementation, which has the functions of an international agency in the protection of Mekong water resources, including implementing the contents of the Agreement. The Mekong Agreement is the only regional multilateral treaty directly regulating legal issues related to the Mekong River water resources' use and protection. The goal of sustainable development of the Mekong water resource, as stated in the Mekong Agreement, together with Procedures and several Technical Guidelines adopted by the Mekong River Commission, is expressed through the legal contents of the obligation to maintain minimal flow, management of water transfer between basins, monitoring of water used in the Mekong River, monitoring of water quality of the Mekong River, environmental impact assessment, no - harm obligation.

The situation as mentioned above of the Mekong River's water source shows that the exploitation and use of the Mekong River water resource of other countries, particularly hydropower activities, do not ensure the principle of sustainable development in the protection of Mekong water resources while being and will cause adverse effects on the quantity and quality of the Mekong water. Water loss, in addition to saline intrusion, is affecting agricultural activities in the Mekong Delta region. At least 50% of arable land in the Mekong Delta will be affected by the loss of sediment and nutrients from hydroelectric facilities. If adding the cascade effect of 11 mainstream hydroelectric projects downstream of the river basin and the Mekong river tributary hydropower projects, the total annual sediment and sediment volume decreases by 80%. A preliminary calculation of a hydropower project's cumulative impact on the mainstream and the Mekong River's main river hydropower steps could reduce nutrient sources (nitrogen and phosphorus) by 6–10%'s delta. Accordingly, crop yield is forecasted to decrease by 0.6-1 ton/ha (Ministry of Natural Resources 2020). Nowadays, only four of six MeKong riparian states are part of the MeKong Agreement. In the legal aspect, since China and Myanmar are not members of this Agreement, there is no legal obligation to comply with the Agreement's provisions and other documents adopted by the MRC, especially the regulations on prior consultation before building hydropower dams. Moreover, the Mekong Agreement still has many shortcomings in terms of and implementation mechanism towards this goal of sustainable development of global water resources.

First of all, the inconsistency of member states on the minimum natural flow determination. The regulation of minimum natural flow on the mainstream ensures the Mekong River water quantity on these flows, thereby preventing water resources degradation and depletion. However, the member countries have not yet agreed with each other in determining minimum natural flow on the mainstream. Although the Mekong Agreement provides for three levels of natural flow maintenance on mainstream, the hydrological thresholds for determining the behavior need to be taken is still for reference only to member states.

Secondly, the undetailed provision on obligation of reasonable and equitable utilization. The obligation to Reasonable and equitable utilization is briefly defined by the Article 5. But, The Mekong Agreement and other MRC documents do not define or list what factors are considered "relevant circumstances and conditions". Article 6 of the 1997 Convention on the Law of the Non-Navigational Uses of International Watercourses recognizes many factors influencing reasonable and equitable uses. However, only Vietnam joined this Convention, so it is impossible to invoke the Convention to explain which factors are the circumstances and conditions involved in fair and equitable use of the Mekong River water resources.

Thirdly, non-legally binding regulations on environmental impact assessments. Within the MRC's cooperation framework, the Draft Guidelines for transboundary environmental impact assessment in the lower Mekong River are the only documents that directly document the contents related to environmental impact assessment in the Mekong basin. After the MRC submitted the latest draft on 25 September, 2018, the member states continue to affirmed that this document is not legally binding,

so even if the final guidance is passed, the environmental impact assessment content will only bring recommendations for the parties.

Fourthly, lack of specific provisions on prior consultation obligation. Provisions on consultation obligation before undertaking operations on main stream, including dam construction, are convered in the Notification, Prior Consultation and Agreement Procedures (PNPCA) and Guidelines. However, the current content of this obligation still has a number of issues that have not been clearly specified, including time to notify, "available" and "relevant" data and information on project must be submitted to other parties and time to conduct consultation. For example, regarding to time to notify, the MeKong Agreement only stipulates such notification should be "timely". Although PNPCA Guidelines further suggested that submission to the MRC Join Committee must be at least six months prior to commencement of project implementation, it also regulated that: "In actual practice, it is likely that projects for proposed water use falling within the 'prior consultation' category would be submitted far in advance of the intended start-up date because they are long-term large scale projects requiring considerable technical, economic, social and impact analysis". The lack of specific regulations makes the implementation this obligation heavily depend on the country where the project is going to be implemented.

Fifthly, the limitation of current regulation on dispute settlement mechanism. Article 35 of the Mekong Agreement only recognizes that dispute settlement measures include direct negotiations and a third party through a country or an organization to which the disputing parties mutually agree. In other words, the Mekong Agreement excludes the application of dispute settlement mechanism through international tribunals. If the parties cannot resolve the dispute through direct negotiation, an action through a third party provided in Article 35 cannot fully resolve the conflict since the third parties' opinions are also only recommendations. Furthermore, this Article stipulates that if disputes cannot be settled within a certain time by agencies regulated in the Mekong Agreement, the disputes will be directly resolved by the parties. But, it does not specify how long is "certain time". Due to the lack of specific deadline, this can affect the promptness and timeliness of the dispute settlement process when a member of above agencies intentionally delay in resolving dispute.

Lastly, regarding the implementation assurance mechanism, the Mekong Agreement and the documents passed by the MRC do not provide a legal means to ensure the implementation. As for water use procedures, there is no standard mechanism to guarantee the fulfillment of an obligation to modify, minimize or suspend inter-basin water transfers for a specified period during the dry season to meet the requirements of MRC procedures when required by the Joint Committee. There is no mechanism for the notification and consultation procedures to guarantee the performance of obligations if the MRC fails to fulfill the Joint Committee's notification obligation. Similarly, for maintaining minimum flows, there is no mechanism to ensure the fulfillment of the obligation to report flow data to Member States' MRC Secretariat. For the post-dispute settlement phase, the Mekong Agreement stipulates member states' commitment to directly notify the Council's results for this agency to take the necessary action. Still, it does not specify the mechanism to supervise the compliance of dispute settlement methods.

17.4 Recommendation and Conclusion

Over the past decade, water resources have become increasingly scarce. The shortage of water will lead to a medical crisis, an agricultural crisis, an economic crisis, and even a political crisis. The above potential catastrophic phenomenon underscores the importance of establishing legal frameworks at different levels, from regional to global, to regulate countries' behavior of exploitation and to use international water resources in a sustainable, reasonable, and equitable manner. The protection of international water resources towards sustainable development ensures that all countries, especially downstream countries, can enjoy international water sources' benefits equally. Therefore, the Mekong Agreement's legal contents must create a complete legal framework to maintain the Mekong River's water resources for the next generations' supply.

Some legal solutions to improve the international legal basis for sustainable development in the protection of Mekong water resources are recommended by the authors as follows:

Firstly, enact minimum natural flow rules on main streams. This rule serves as a basis for determining the "threshold" for legal interventions to be conducted against the causes of water degradation and depletion. Violation of the obligation to maintain minimum flow is a violation of the obligation to use the Mekong River's equitable and fair use of water resources as a basis for the dispute settlement process among member states. Secondly, define the factors affecting to reasonable and equitable utilization of the Mekong River. The parties may refer the 1997 Convention on the Law of the Non-navigational uses of International watercourse to list these factor, such as geography, hydrology, ecology and the country's economic and social needs.

Thirdly, unify the regulations on transboundary environmental impact assessment the Mekong River's downstream, recognizing the binding legal validity for these guidelines in place of the only recommendation.

Fourthly, guide on specific prior consultation obligation regarding notification timing, the threshold for specifying "available" and "relevant" of information on project and grounds for the country having project to eliminate the consultation process.

Fifthly, amend the dispute settlement regulations. The dispute settlement clauses should be re-defined to supplement dispute settlement through international tribunals, including courts and arbitration. This content may include recognizing the settlement of disputes by international tribunals in general international law. In the future, the parties may agree in detail on establishing separate arbitral tribunals to resolve disputes arising from the Agreement's implementation.

Lasty, Supplement the provisions on mechanisms to ensure the fulfillment of obligations related to water use, notification, consultation and reporting flow data. Accordly, Member States should regulate the MRC to impose the enforced measures in the event that a concerned state fails to fulfill its obligations under the Agreement.

References

Botchway FN (2013) The Context of Trans-Boundary Energy Resource Exploitation: The Environment, the State, and the Methods", Colorado Journal of International Environmental Law and Policy, No.1919, p 209–337

Can Tho University (2020) Institute for Climate Change, Current map of saline intrusion in the Mekong Delta to March 2020

International Law Association, The Berlin Rules on Water Resources https://unece.org/fileadmin/DAM/env/water/meetings/legal_board/2010/annexes_groundwater_paper/Annex_IV_Berlin_Rules_on_Water_Resources_ILA.pdf, accessed 5 January 2021. https://www.mrcmekong.org/assets/Publications/Situation-report-Jan-Jul-2020.pdf

International Centre for Environmental Management (ICEM) 2010, Strategic Environmental Assessment of Hydropower on the Mekong Mainstream, http://www.mrcmekong.org/assets/Publications/Consultations/SEA-Hydropower/SEA-FR-summary-13oct.pdf. accessed 2 Januarry 2021

Ministry of Natural Resources and Environment, Study on the Impact of hydroelectric dams on the Mekong Mainstream (2018)

Ministry of Natural Resources and Environment, Review report on water pollution in some big rivers and propose mitigation measures, pp. 10–13, p.20 (2020)

Mekong River Commission, Situation Report Hydrological Conditions in the Lower Mekong River Basin in January–July 2020 (2020)

MeKong River Commission, Gulines for Transboundary Environmental Impact Assessment in the Lower Mekong Basin (2018). http://www.mrcmekong.org/assets/Publications/TbEIA-Guidelines-Final-version-25–9-2018.pdf, last accessed at 2/1/2021

Office of the National Assembly, Topic Information - Water security in the Mekong Delta: Current situation and solutions, p. 16 (2017)

Vietnam Mekong River Commission Standing Office, Newsletter on water resources development to the Mekong Delta, October 2020

Chapter 18
Key Technology and Economic Analysis of Using Fujiang River Water as the Cooling and Heating Sources for Air Conditioning System

Zhang Wei, Fu Daoyou, Yao Mingqiang, and Gan Shiyuan

Abstract In order to use the river water, a new renewable energy, as the cooling and heating sources for the air conditioning system, the temperature, quality and quantity of water in the downstream of Fujiang River is analyzed; it is believed that it is suitable to use the properly processed river water as the cooling and heating sources for the air conditioning system. The floor area ratio in the riverside is relatively high and the building coverage ratio is large, and its horizontal and vertical distances to Fujiang River are short; therefore, those favorable conditions contribute to the application of the river water source heat pump air conditioning system. With a residential community in downstream of Fujiang River as the research object, the system mode and water intake method for the water resource heat pump air conditioning system are analyzed; it is believed that it is advantageous to adopt the open system and direct water intake method; referring to the existing performance model of the heat pump unit, the operation of the water resource heat pump system is optimized with the aim of high energy efficiency; it is further believed that the energy efficiency ratios in the heating and cooling seasons reach 4.12 and 4.42 respectively. Compared with the conventional air conditioning system, the energy cost saving rate for adopting the river water source heat pump unit is 23.78%. The harmful gas emission reductions are as follows: CO_2: 3450.09t/a, SO_2:14.58t/a, NO_2:5.73t/a, smoke dust: 100.12t/a, with reduction amplitudes of 66%, 54%, 55% and 53% respectively. The application of river water source heat pump unit for water intake and discharge in the downstream of Fujiang River has little influence on water in Fujiang River. The research provides reference for the application of river water source heat pump air conditioning system in the downstream of Fujiang River.

Z. Wei (✉) · G. Shiyuan
Chongqing Technology and Business Institute, Chongqing 400052, China

F. Daoyou
Chongqing Sino-French Energy Services Co., Ltd, Chongqing 400020, China

Y. Mingqiang
Chongqing Hechuan Minqi Construction Engineering Co., Ltd, Chongqing, China
e-mail: 108047161@qq.com

H.-Y. Jeon (ed.), *Sustainable Development of Water and Environment*,
Environmental Science and Engineering,
https://doi.org/10.1007/978-3-030-75278-1_18

Keywords River water source heat pump · Air conditioning system · Key technology · Economic analysis

18.1 Introduction

Building energy consumption takes a great proportion in the total energy consumption in the whole society and it turns on a trend of increase year by year, while air conditioning electricity consumption is 40–50% of the building electricity consumption. Building heating and air conditioning not only brings the environmental pollution problems to China but also contributes to the greenhouse effect. The application of river water, a new kind of renewable energy, in the heat pump system can ease this situation to a certain degree.

Many scholars have conducted a large quantity of investigations and researches on the suitability for application of surface water source heat pump in Yangtze River Basin has been studied in a flood of literatures such as literatures (Zhang 2012; Zhu and Xiang 2007) in which it is believed that it is of advantages to apply the water source heat pump system in Yangtze River Basin. Specific to the problem that the river water in China is subject to pollution of different degrees, detailed water quality analysis is conducted in literatures (Fu et al. 2007) and (Zhao 2006) to figure out propose corresponding water treatment methods; in literature (Li and Wang 2006), different water inlet methods are proposed specific to different water qualities and water temperatures. As for the technical and economic analysis on the application of river water source heat pump system, the cooling and heating energy efficiency of the river water source heat pump unit & ice storage solution for Shanghai Shiliupu District Integrated Reconstruction Project is 5.1 and 3.6 (Zhu and Xiang 2007), the cooling primary energy ratio (PER) is 1.79 and the heating PER is 1.26. In literatures (Huang et al. 2008; Xie et al. 2011) the operating conditions of a Yangtze River water source heat pump pilot project in Chongqing in Summer and Winter are tested respectively, and the heating and cooling energy efficiencies of the water source heat pump unit are 4.72 and 5.09 respectively.

It can be inferred from the above literatures that differences exist in hydrology and water quality of different waters; for the suitability of low-grated hot source of heat pump air conditioning system, separate analysis shall be done to different water bodies. Currently, there are few research literatures and engineering applications relevant to the utilization of water in Fujiang River as the cooling and heating sources for the heat pump system. Based on this fact, relevant technical and economical indexes such as the suitability of using water in downstream of Fujiang River as the cooling and heating sources of the air conditioning system, application technology solution and system energy efficiency, economical efficiency and environmental protection benefit etc. are analyzed with a riverside building community at downstream of Fujiang River as the research object, to provide reference for similar engineering practices.

18.2 Materials and Methods

18.2.1 Current Hydrological Situation for Water in the Downstream of Fujiang River

With a full length of 670 km, Fujiang River has the drainage area of 36400 square meters and it is also the largest right bank branch of Jialing River which is a branch of Yangtze River. According to the long-term monitoring data at the measuring point, it is found that the water temperatures in winter varies from 8.9 °C to 11.3 °C and the average temperature is 9.9 °C; in summer, the water temperature varies from 22.1 °C to 29.9 °C, and the average water temperature is 26.4 °C; moreover, the varying patterns for temperatures of river water and air temperature are consistent. The varying pattern for the monthly average temperature of river water is shown in Fig. 18.1.

The water quality in Fujiang River is classified as water quality category III, especially with high contents of microorganisms and suspended solids in summer. In addition, the yearly average sediment concentration in Fujiang River ranges from 1.2 kg/m^3 to 1.33 kg/m^3 in many years and the sediment mainly appears in the flood season from June to September, accounting for more than 95% of the sediment in all the year round. The yearly average flow in Fujiang (Xiaoheba) is 458.9 m^3/s; the flow varies greatly within a year; the minimum monthly average runoff during the cooling in Fujiang River area is about 300 m^3/s in May; and the average flow during the main flood season during July and September is 1083 m^3/s; the above mentioned period is also the period with the maximum building cooling load; the runoff during the cooling season from December to February of the next year is the minimum, which is 131.9 m^3/s in winter and 207.7 m^3/s in spring (Wang et al. 2014).

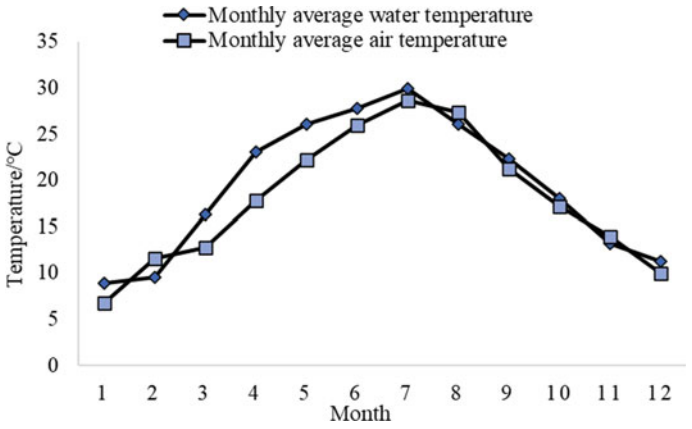

Fig. 18.1 Annual variation curve for the water temperature and air temperature in Xiaoheba, Fujiang

18.2.2 Current Situation for the Application of Air Conditioning System in a Building Community in Downstream of Fujiang River

The total floor area of this residential community is 209800 m^2 and the floor area ratio is 2.38, the community has buildings such as residence, hotel, kindergarten, commercial buildings, and service and office buildings etc. The absolute elevation of the community floor is 221.2 m and the elevation of the ground floor of the double-floor underground garage is 211.6 m. The south of the community is closely neighboring Fujiang River and the horizontal distance between the community and the surface of the river is about 80 meters. DeST building energy analysis software is adopted for the simulation calculation of cooling and heating loads of each building; and meanwhile, it is considered to use a coefficient 0.7 to calculate the design cooling and heating loads of the buildings in the whole community, which are 9807.39 kW and 5678.76 kW respectively; and the cumulative values of heating load are 11187221.13 kWh and 7128845.71 kWh respectively. If the conventional cooling water unit + gas boiler system is adopted in this community and the energy efficiency ratio of the water chilling unit is considered to be 3.39, then the electricity consumption in the cooling season is 3300065.23 kWh; considering the heating efficiency of the gas boiler to be 0.9 and the low-grade heat value for the gas in Chongqing City to be 34942 kJ/m^3, the gas consumption in the heating season is 734469.82 m^3.

18.2.3 Research Methods

Qualitative Analysis. qualitative analysis on the advantages and disadvantages of the open and closed system modes as well as the suitability is conducted in this research. In addition, as for the selection for water intake methods and water treatment solutions, qualitative analysis is also adopted for the research.

Quantitative Analysis. Quantitative analysis is adopted for analysis on technical economic indexes of river water source heat pump air conditioning system such as operation energy consumption, energy saving, economical efficiency, environmental protection benefit and the influence on water environment etc.

Comparative analysis. The technical and economic indexes of the air conditioning system using water in downstream of Fujiang River as the cooling and heating source of the air conditioning system and the conventional water chilling unit + gas boiler air conditioning system are analyzed respectively for comparison.

18.3 Results

18.3.1 Analysis on Suitability of Using Water in Downstream of Fujiang River as the Cooling and Heating Resources of the Air Conditioning System

Suitability of river water. The temperature of river water directly affects the working energy efficiency of the water resource pump system and the main device; appropriate temperature control is essential to condition for determining the system design. As per Fig. 18.1, the temperature of water in downstream of Fujiang River in winter ranges from 8.9 °C to 11.3 °C and the average temperature is 9.9 °C; in summer, the temperature ranges from 22.1 °C to 29.9 °C and the average temperature is 26.2 °C; moreover the variation rules for river water temperature and air temperature are consistent and it is suitable to use water in downstream of Fujiang River as the cooling and heating source of the air conditioning system.

Considering the parameters for water in downstream of Fujiang River, the water quality in downstream of Fujiang River in summer cannot meet with the requirements of heat pump air conditioning system on water quality so that the water body will cause some wear, corrosion and blockage, which also affects the heat-exchanging effect and the energy efficiency of the unit. Desanding, filtration and necessary chemical treatment are adopted for river water treatment; by enhancing the near-wall disturbance in the fluid and adopting regular cleaning method to enhance the heat-exchange and scale removal for the heat exchanger so as to solve the problem of water quality.

The weight of water in water bodies has direct influence on the heat exchange amount and the bearing capacity for cool and heat loads. The relationship between the heat exchange amount and the water intake amount is as follows:

$$Q = C_{pw} \cdot V \cdot \rho_w \cdot \Delta t \tag{18.1}$$

where V represents flow of chilled water, m^3/h; Q represents heat exchanger design heat exchanging amount of the heat exchanger, W; C_{pw} represents constant-pressure specific heat of the chilled water, kJ/kg·°C (4.2 kJ/kg °C); ρ_w represents density of chilled water, kg/m^3 (1000 kg/m^3); Δt represents temperature difference in supply and return water system, °C.

In the standard Surface Water Source Heat Pump System Design Standard (DBJ50-115-2010), the restrictions in water intake in flowing water systems such as rivers are described and it is required that the maximum water intake shall be less than 20% of the water system's flow. According to formula 1, the maximum heat exchange amount is 1.76×10^7 kW in summer and the heat exchange amount reaches 2.51×10^6 kW in winter, as shown in Fig. 18.2.

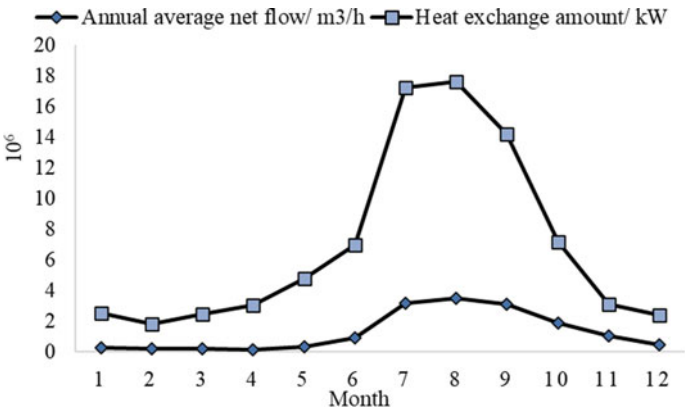

Fig. 18.2 Annual variation curve for the runoff and exchangeable heat amount in Xiaoheba, Fujiang

From the above, the application of the river water source heat pump air conditioning system in downstream of Fujiang River is suitable after proper treatment on water quality.

Suitability of the building community. Judging from the relative position between this community and Fujiang River, the horizontal distance between this community and Fujiang River is near, the vertical altitude differences are 26.4 m and 24.2 m, relatively not too large.

In addition, this community is a residential center integrated with commercial and high-level buildings, hotels and service, with high floor area ratio and large building coverage ratio, which is suitable for centralized cooling and heating.

18.3.2 Key Technology Analysis on Utilizing Water in Downstream of Fujiang River as the Cooling and Heating Sources of the Air Conditioning System

Water intake and water treatment modes. In this project, floating pontoon water intake is of little significance as the constant water level during water storage in the dam in the downstream, dry season and rainy season is only 2.2 m; although the quality of water intake with the filtration method is good, the cost is too high, and the construction is of great difficulty; therefore, it is usually used for water intake in water works and cannot meet with the economic requirements on cooling and heating for the heat pump system; as for direct water intake, an intake head is usually equipped as the content of sand in the river water is high; the intake head must go under the perennial low water level so as to meet with the requirements for water intake, which might affect the safe navigation access to a certain degree and the water

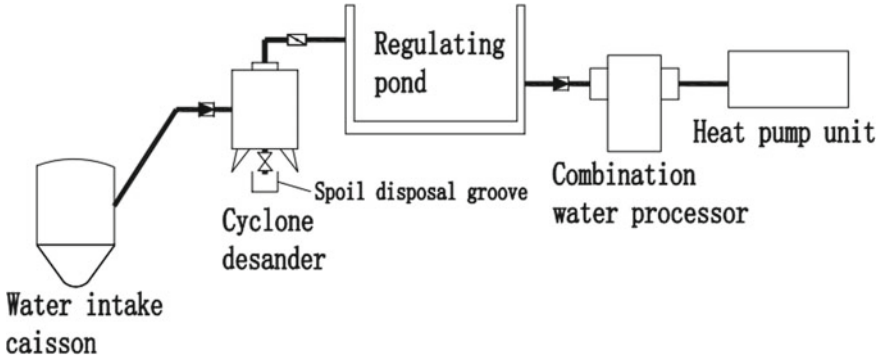

Fig. 18.3 Water treatment flow diagram

quality is poor; the water shall be properly treated if it directly goes into the water source heat pump unit; however, the cost for water intake is lower.

After comprehensive consideration, direct water intake method is preferentially considered in this project; the water treatment solution is as follows: primary filtration for the source water by the intake head—desanding treatment by the rotational flow desander—refined filtration by whole range water processor, as shown in Fig. 18.3; meanwhile, automatic in-place cleaning system is adopted to clean the heat exchange pipe to avoid deposit accumulation on the surface of the heat exchanger. This solution is low in cost, convenient in maintenance and management, and the quality of water being treated can meet with the operation requirement of the water source heat pump.

Unit selection for river water source heat pump air conditioning. The unit types of water source heat pump system most commonly used are screw-type and centrifugation type. The efficiency of the screw-type heat pump unit is high when it is under part load conditions; however, the capacity per unit and speed are lower than those of the centrifugation type unit; the noise produced by the screw-type unit with large capacity is higher than that of the centrifugation type unit. However, the centrifugation unit has large capacity per unit and high EER value, but surging phenomenon will appear in single-step compressor with low load, with fast decrease in efficiency when the operating condition deviates from the design operating condition.

In view of the above features of these two kinds of units, the centrifugation type of unit with large capacity per unit is selected for this project; on the basis that the primary model selection for the centrifugation type of heat pump unit is completed, an additional screw-type heat pump unit with relatively small capacity is provided to meet with the requirements for residual cooling and heating load, so that the advantage of high energy efficiency in the centrifugation unit under high load rate and that of relatively high efficiency of screw-type unit with partial load can be fully developed and supplemented for each other. From the above, a centrifugation type water chilling unit with cooling capacity of 2285 kW and 3 screw-type heat pump units with cooling/heating capacity of 1281 kW/1542 kW (type 1–400 A) and 2 screw-type heat pump units with cooling/heating capacity of 447 kW/525 kW (type

1–130 A) are for stage I; an additional centrifugation type water chilling unit with cooling capacity of 2285 kW and 1 screw-type unit B are provided during the stage II.

Unit operation optimization and energy consumption. The building thermal load is changing dynamically and the time proportion of low load is large so that the units are operating under part load ratio at most of the time; moreover, the temperature of river water is also changing. As a result, figuring out the energy efficiency operating rules of the units under different load rates and temperatures of river water plays an important role for the high-efficient operation of the units.

The performance models for the screw-type and centrifugation heat pump units are proposed In literatures (Huang et al. 2013; Fan 2010) on this basis, the original models are modified by the author considering the sample parameters of the heat pump units selected for this project to obtain the relationship between the energy efficiency of each unit and the load rate under the heating and cooling operating conditions, as shown in Fig. 18.4.

During the heating process, priority shall be given to ensure that the units have high load rate during the operation under the same operating conditions; when the load rates are similar, priority shall be given to the operation of units with larger capacities. During the cooling process, the variation amplitude of the screw-type unit is small when EER $\geq$ 3.62($\varepsilon \geq 0.5$); the cooling capacity of the centrifugation water chilling unit is 639.8 kW when EER = 3.62, in case the cooling load is higher than 639.8 kW, the energy efficiency of centrifugation water chilling unit is higher and the unit shall be preferentially started; when the cooling load is lower than 639.8 kW, the energy

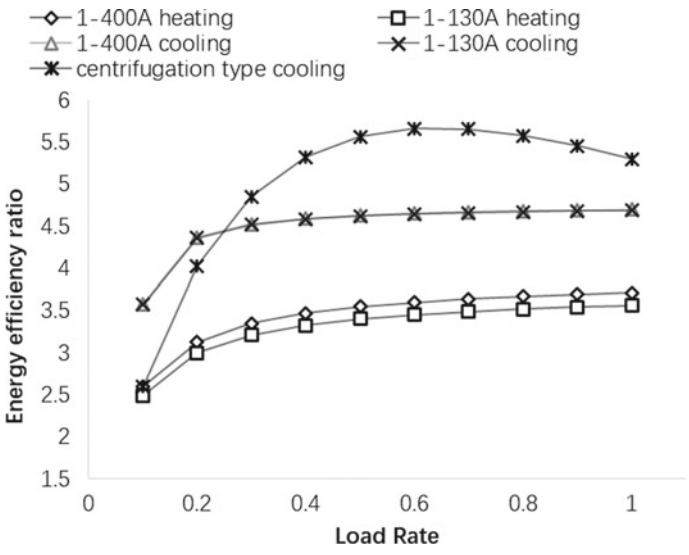

Fig. 18.4 Performances of units under heating and cooling operating conditions

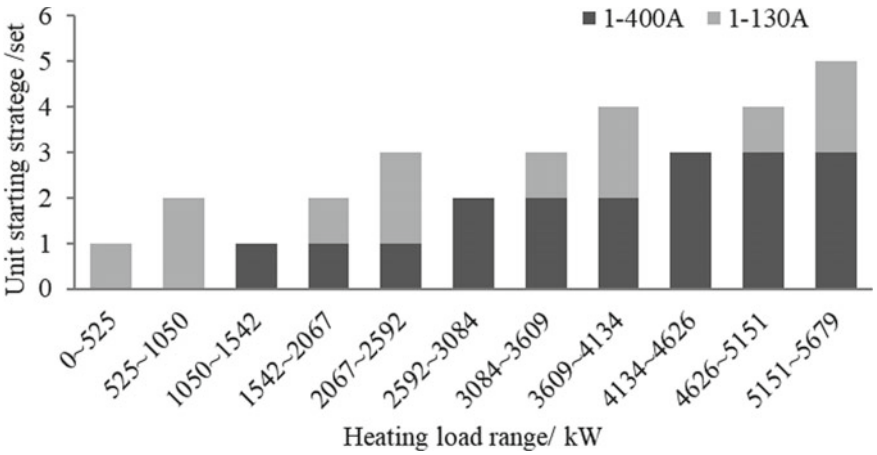

Fig. 18.5 Unit starting strategy under different heating load

efficiency of screw-type unit is higher, and the energy efficiency of operating two screw-type units B is higher than operating one screw-type unit A.

Through the above analysis, the unit operating strategies in the heating and cooling seasons are determined as shown in Figs. 18.5 and 18.6.

Differences in temperatures of supply and return water at riverside for the water source heat pump during both the heating and cooling seasons are considered to be 5°C; during the cooling season, the supply and return water temperatures at the load side are 5 °C/13 °C; during the heating season, the supply and return water temperatures are 47 °C/39 °C. Under the above operation strategy, the total heating and cooling energy consumption of the cool and heat source unit during winter and summer are 1739502.49 kWh and 2531954.36 kWh respectively; the seasonal energy efficiency of the unit are 4.12 and 4.42 respectively.

18.3.3 Economic Analysis

Energy-saving analysis. Thresholds for Public Buildings Air Conditioning Engineering Design Energy Efficiency Ratio (Trial) issued by Chongqing Municipal Construction Committee specifies that the energy efficiency ratio threshold for screw-type water chilling unit is 3.39; compared with this threshold, the cooling energy efficiency ratio of the river water source heat pump unit is 30.38% higher; it is calculated by analysis in literature (Xie et al. 2011) that the average heating energy efficiency ratio of air source heat pump unit of several famous brands is 3.65; compared with this value, the heating energy efficiency ratio of the river water source heat pump unit is 12.88% higher. Taking the power supply efficiency of the power plant as 30.1% and the transmission efficiency of the power grid as 92%, the primary energy utilization

rates of the river water source heat pump unit during the cooling and heating seasons are 1.22 and 1.14 respectively.

Economic Analysis. The current prices for gas and electricity in Chongqing City are 2.66Yuan/m^3 and 0.848Yuan/kWh; the cost for energy consumption by the river water source heat pump units in this community is 3.6222 million Yuan/a; the cost for the conventional water chilling unit + gas boiler system energy consumption is 4.7521 million Yuan/a. and the saving rate for the energy consumption cost of the river water source heat pump unit is 23.78%.

Emission reduction analysis. CO_2 generated by each cubic meters of gas combustion is 1.89 kg, SO_2 0.10 g, NO_2 0.63 g and smoke dust 0.24 g; according to the average thermal power generation level at the current stage, 0.36 kg standard coal is averagely consumed to generate 1kWh of electricity, and, at the same time, 1.17 kg CO_2, 8.23gSO_2, 2.99 g NO_2 and 56.71 g smoke dust are generated. The emission of 1 m^3 gas is equal to that of 1.2143 kg standard coals; compared with the conventional air conditioning system, the harmful gas emissions of the river water source heat pump project are as follows: CO_2 is 3450.09t/a, SO_2 is 14.58t/a, NO_2 is 5.73t/a, smoke dust is 100.12t/a, with reduction amplitudes of 66%,54%,55% and 53%.

Analysis on the influence on water environment. According to the heating and cooling loads of the buildings and temperatures of inlet and outlet water at the riverside, design water withdrawal for the river water source heat pump system can be obtained; taking the extra coefficient as 1.2, the design water withdrawal are 245.74 m^3/h and 687.21 m^3/h respectively; compared with the runoff of river water in winter and summer, the proportions are extremely small. As a result, the influence of water intake in this project on water environment of Fujiang River can be ignored.

18.4 Conclusions

Using river water as the low-grade cool and heat source of heat pump air conditioning system is new energy utilization technology. In order to study the application effect of river water source heat pump technology in downstream of Fujiang River, the suitability for using water in downstream of Fujiang River as the cool and heat source of the heat pump air conditioning system, suitability for applying the heat pump air conditioning system in the riverside building community as well as the system mode and water intake methods are analyzed using the method of qualitative analysis, with a riverside building community along the downstream of Fujiang River as the research object; the method of quantitative analysis is adopted to analyze the technical and economic indexes such as operation energy consumption, energy saving performance, economic performance, environment protective benefit and the influence on water environment for the river water source heat pump air conditioning system. The method of comparative analysis is adopted to analyze and compare the technical and economic indexes of the air conditioning system in which water in the

downstream of Fujiang River is used as the cool and heat source of the air conditioning system, and the conventional water chilling unit + gas boiler air conditioning system. The conclusions drawn in this paper are as follows:

(1) Being properly treated, Fujiang River water can be used as the cooling and heating source for heat pump system; direct water-intaking method shall be adopted.
(2) The energy efficiency ratio of the river water source heat pump unit with operation optimized during the cooling season is higher than the threshold of the energy efficiency ratio of the local water chilling unit; during heating season, the energy efficiency ratio is higher than that of the air source heat pump; the water source heat pump unit has a good energy efficiency ratio.
(3) Compared with the conventional water chilling unit + gas boiler system, the saving rate for the energy consumption cost of Fujiang River water source heat pump unit might exceed 23%; the reduction of harmful gas emission might exceed 50%.
(4) Water intake and drainage by river water source heat pump unit in downstream of Fujiang River exerts little influence on Fujiang River.

Compared with conventional air conditioning system, using water in downstream of Fujiang River as the cool and heat source of the air conditioning system has significant economic and environmentally protective advantages; however, there are few applications of heat pump air conditioning system along downstream of the Fujiang River; therefore, the promotion and application of river water source heat pump air conditioning system in this district is extremely urgent; and this paper can provide some reference for the application of river water heat pump air conditioning system along the downstream of Fujiang River.

Acknowledgements The study was supported by Hechuan science and technology plan project of Chongqing Hechuan science and Technology Bureau of China (Grant No. 2019-26), and the Science and Technology Research Program of Chongqing Municipal Education Commission of China (Grant No. KJQN201804003).

References

Fan, Y.Q. 2010. Character analysis and program design of lake water-source heat pump system. Chongqing: Master Degree Thesis of Chongqing University, China

Fu SD, Liu JX, Lu GL et al (2007) Analysis of common problems in earth' s surface water heat pump. Refrigeration, Air Conditioning & Electric Power Machinery 28(1):64–66

Huang Z, Liu XY, Huo JH et al (2008) Water-source heat pump system using water from Yangtze River in Chongqing. HV&AC 38(2):101–104

Huang GQ, Lu J, Wang L et al (2013) Transient condition model of heat pump unit with screw compressor based on data fitting. HV&AC 43(7):82–86

Li Y, Wang ZW (2006) Research on ways of water system of open–loop water source heat pump. Coal and Carbon Process 2006(8):95–97

Wang GQ, Li M, Jin JL et al (2012) Variation trend of runoff in Fujiang River catchment and its responses to climate change. Journal of China Hydrology 32(1):22–28

Wang Y, Xu HM, Cheng BY et al (2014) Impacts of precipitation change on the runoff change in the Fujiang River basin during the period of 1951-2012. Progressus Inquisitiones de Mutatione Climatis 10(22):127–134

Xie, H.L., Liu, X.Y. and Lin, X.S. 2011.Testing and discussion on Yangtze River water-source heat pump air conditioning project of Chongqing in winter conditions. HV&AC, 41(11):74–76;91

Zhang JY (2012) Based on the numerical simulation of river water source heat pump system of the technology of tail water discharge. Chongqing: Master Degree Thesis of Chongqing University, China

Zhao QC (2006) Application prospect of the water- source- based heat- pump and some problems needing attention. Sci- tech Information Development & Economy 16(16):245–247

Zhu JM, Xiang PZ (2007) Application of river water-source heat pump in the Shanghai Shiliupu reconstruction project. HV&AC 37(2):88–93

Chapter 19
Highly Effective Magnetic Silica-Chitosan Hybrid for Sulfate Ion Adsorption

Sukamto, Yuichi Kamiya, Bambang Rusdiarso, and Nuryono

Abstract The contamination of sulfate ions leading to corrosion is a severe problem in the aquatic environment, and adsorption is an effective method to remove this contaminant. In this study, magnetic silica-chitosan hybrids (MP@SiO_2/CPTMS/Chi) prepared by the sol-gel method have been used for adsorbing sulfate ions from an aqueous solution. The maximum adsorption capacity (Q_{max}) of the adsorbent for sulfates was 108.50 mg g^{-1} at pH 3. The MP@SiO_2/CPTMS/Chi can be easily magnetically separated (completely separated less than 5 min) from the solution after the adsorption process. High adsorption capacity and easily magnetic separation make MP@SiO_2/CPTMS/Chi a prospective candidate adsorbent for removing sulfates from wastewater.

Keywords Magnetic silica-chitosan hybrid · Sol-gel · Sulfate · Adsorption

19.1 Introduction

Sulfate is generally found in the water surface and industrial waste, including mining, printing, dyeing waste, and pharmaceuticals. Naturally, sulfates can be formed due to the chemical dissolution and oxidation of minerals containing sulfur (Fernando et al. 2018). Sulfate ions are generally considered non-toxic to humans, but sulfate ions are potentially harmful to the living organism and the environment. The presence of sulfate ions in high concentrations in water causes an imbalance in the ecosystem's sulfur cycle. Besides that, sulfate ions may accelerate the corrosion rate of building materials containing metal (Runtti et al. 2016). Therefore, it is essential to find an effective method to remove sulfate ions from water.

Sukamto · B. Rusdiarso · Nuryono (✉)
Department of Chemistry, Faculty of Mathematics and Natural Sciences, Universitas Gadjah Mada, Bulaksumur, Yogyakarta 55281, Indonesia
e-mail: nuryono_mipa@ugm.ac.id

Y. Kamiya
Faculty of Environmental Earth Science, Hokkaido University, Kita 10 Nishi 5, Sapporo 060-0810, Japan

H.-Y. Jeon (ed.), *Sustainable Development of Water and Environment*,
Environmental Science and Engineering,
https://doi.org/10.1007/978-3-030-75278-1_19

Various methods, including electrocoagulation (Omwene and Kobya 2018), ion exchange (Du et al. 2018), adsorption (Ma et al. 2019), have been used to remove sulfate ions from wastewater. Among them, adsorption is considered one of the best methods for the pollutants' removal from wastewater because of its excellent efficiency, effectiveness, and low energy demand (Xiong et al. 2011). However, adsorption method suffers from adsorbent lost after the adsorption process and cause the formation of secondary pollutant (Narita et al. 2019).

Chitosan is a biopolymer obtained from the deacetylation of chitin from crustacean (Zhang et al. 2015). The chitosan-based adsorbent has been widely used to remove pollutants in the wastewater because of its availability, biodegradable, and low impact on the environment (Zhang et al. 2018). The presence of abundant amine and hydroxyl groups on chitosan structure can be used to support its application for removing pollutants from the environment, including heavy metal and organic matters. However, chitosan has poor mechanical stability and readily dissolves under acidic conditions, leading to a decrease in adsorption capacity (Huang et al. 2017). Chitosan has been modified with various modifiers to overcome this drawback, such as silica (Kelechi et al. 2018), La(III)-bentonite (Xu et al. 2020), and calcite (Pap et al. 2020). Chitosan combined silica, known as hybrid material, shows excellent characteristics such as large surface area, high porosity, and high mechanical stability (Juan-Diaz et al. 2016).

Silica-chitosan hybrid materials can be synthesized by using a sol-gel method with the presence of a crosslinker. One of the crosslinking agents used to prepare silica-chitosan hybrid is 3-chloropropyltrimethoxysilane (CPTMS). Even though CPTMS is not the most reactive silane agent, this organosilane is one of the most widely used organosilanes for surface modification because it is easily handled, and the alcohol by products is not volatile corrosive. On the other hand, CPTMS facilitates the formation of covalent bonds between the chitosan and the silica network to enhance the chitosan's stability.

In this study, we report silica-chitosan hybrid preparation using 3-chloropropyl trymethoxysilane as the crosslinker and introducing the magnetic property to the hybrid using natural magnetic particles (MP) separated from iron sand. The materials resulted were used to remove sulfate ions from the solution. The effect of ionic strength, solution pH, adsorption time, initial concentration, and adsorbent dosage were investigated to evaluate the adsorption characteristics of sulfates. The adsorption mechanism is predicted by applying appropriate kinetics and isotherm models.

19.2 Methods

19.2.1 Materials

The iron sand sample was taken from Bugel Beach, Kulon Progo, Yogyakarta. Chitosan (>90% DD) was purchased from cv. Chemix (Yogyakarta). Sodium silicate

solution (10.6% Na_2O and 27% SiO_2), 3-chloropropyl trymetoxysilane (CPTMS), hydrochloric acid (HCl 37%), ammonium hydroxide (NH_4OH 25%) were purchased from Merck. Potassium dihydrogen phosphate ($KH_2PO_($), hydrochloric acid (HCl 0.1 mol/L), sodium hydroxide (NaOH), glacial acetic acid (CH_3COOH) were obtained from Wako Pure Chemical Industries. Ltd (Osaka, Japan).

19.2.2 Preparation of Magnetic Particles

Iron sand was dried under sun radiation for 24 h and separated from non-magnetic components with an external magnet. Dried magnetic sand was ground to pass 200 mesh in size. The magnetic particles (100 g) were washed using 250 mL distilled water with sonication for 10 min. Washing was repeated three times, and then the magnetic particles were dried in an oven at 70 °C for 24 h.

19.2.3 Synthesis of Magnetic Silica-Chitosan Hybrids (MP@SiO_2/CPTMS/Chi)

Magnetic silica-chitosan hybrids were synthesized by the sol-gel method. Magnetic particles (MP) 0.5 g and 1 mL of HCl 1 M were placed into a beaker glass. The mixture was allowed to stand for 15 min at 25 °C. MP was then separated from HCl with an external magnet. Na_2SiO_3 solution (1 mL, 3.0 mmol) and distilled water (3 mL) were mixed to the MP, and HCl (1 M) was added dropwise until pH 10. Furthermore, the obtained mixture was stirred with a mechanic stirrer for 30 min. The mixture of chitosan (2 g, 4 mmol) and CPTMS with certain volume/mmol was added to the previous mixture. The mixture was stirred with a mechanic stirrer for 5 h. After mixing, NH_4OH solution (0.5 M) was added dropwise until pH 7.0 and gel was formed. The obtained gel was aged for one night at room temperature (25 °C). The gel was then washed using distilled water and dried in an oven at 60 °C for 24 h. The analog works were carried out with various mol ratios of CPTMS to chitosan, as shown in Table 19.1.

Table 19.1 Various mol ratios of CPTMS to chitosan

CPTMS	The mol ratio of CPTMS:chitosan	Hybrid code
0.00 mL (0 mmol)	0:4	MP@SiO_2/Chi
0.18 mL (1 mmol)	1:4	MP@SiO_2/CPTMS1/Chi
0.36 mL (2 mmol)	2:4	MP@SiO_2/CPTMS2/Chi
0.54 mL (3 mmol)	3:4	MP@SiO_2/CPTMS3/Chi
0.72 mL (4 mmol)	4:4	MP@SiO_2/CPTMS4/Chi

19.2.4 Adsorption Experiment

An adsorption experiment was conducted in a batch system. Adsorbent 0.2 g was mixed with 25 mL of sulfate solutions, and the pH was adjusted at a certain value. The mixture was shaken in a shaker (VBR-36; TAITEC Co., Ltd.) for a certain time. The adsorbent was separated magnetically by applying an external magnet, and the sulfate ion concentration in the supernatant with Ion chromatography 2001. The amount of sulfate ion per gram adsorbent in the equilibrium state (q_e, mg g^{-1}) was determined using Eq. 19.1.

$$q_e = \frac{(C_o - C_e).V}{m} \tag{19.1}$$

where C_0 is the initial concentration (mg L^{-1}), and C_e is the equilibrium concentrations of sulfate ion (mg L^{-1}), V is the volume of the solution (L), and m is the mass of adsorbent (m).

Variables investigated included pH, adsorption time, initial concentration, ionic strength, and adsorbent dosage. The solution pH effect was investigated by adjusting the initial pH in the range of 2-7 using HCl (0.1 M) and NaOH (0.1 M). The effect of adsorption time was evaluated by varying contact time from 20 to 180 min. The experimental data was then analyzed using pseudo-first order (PFO) and pseudo-second-order (PSO) kinetics. The effect of initial concentration was evaluated by varying the concentration of sulfate ion 10, 30, 50, 70, and 100 mg L^{-1}, and the experimental data were analyzed with Langmuir and Freundlich models to predict the possible adsorption mechanism. NaCl concentration and adsorbent mass were varied in the range of 0-05 M and 10-100 mg, respectively, at the optimum pH and adsorption time to investigate the effect of ionic strength and adsorbent dosage,

19.3 Result and Discussion

19.3.1 Adsorption Experiments

19.3.1.1 Effect of Initial Solution pH

The initial solution pH plays an essential role in the adsorption of sulfate ions on the adsorbent surface. The pH of a solution influences the adsorption efficiency and affects the charge density on magnetic silica-chitosan hybrids' surface. The effect of pH on sulfate's adsorption into MP@SiO_2/Chi and MP@SiO_2/CPTMS1/Chi was investigated at pH ranging from 2 to 7 (Fig. 19.1). As shown in Fig. 19.1, sulfate adsorption of MP@SiO_2/Chi and MP@SiO_2/CPTMS1/Chi reached the maximum efficiency at pH 3.0 and decreased with the increasing pH value.

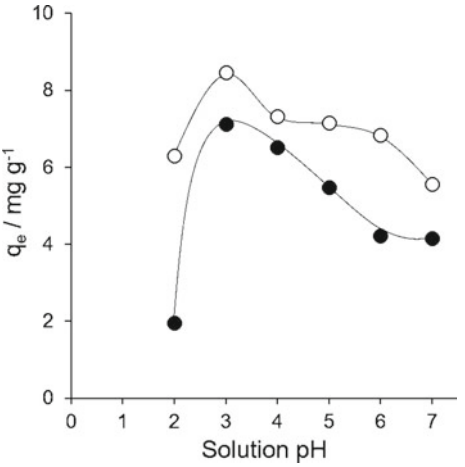

Fig. 19.1 Effect of initial pH solution on sulfate ion adsorption over (●) MP@SiO_2/Chi and (○) MP@SiO_2/CPTMS1/Chi (Conditions: sulfate ion concentration 10 mg L^{-1}; solution vol. 25 mL; adsorbent 0.02 g; temperature 30 °C; and contact time 2 h.)

The effect of the initial pH solution on the sulfate adsorption of MP@SiO_2/Chi and MP@SiO_2/CPTMS1/Chi can be explained by the point of zero charges (pH_{pzc}). The zero charge point (pH_{pzc}) for MP@SiO_2/Chi and MP@SiO_2/CPTMS1/Chi were 7.35 and 7.2, respectively (Nuryono et al. 2020). Pure silica reached the point of zero charges at pH 2, while chitosan has a positive surface charge (zeta potential) at pH lower than 6 (Anal et al. 2008). The surface of MP@SiO_2/Chi and MP@SiO_2/CPTMS1/Chi can be positively charged at pH lower than 7.35 and 7.2 due to the protonation of amine groups into ammonium groups. Therefore, the adsorption of sulfate might be attributed to the intensively electrostatic interaction between anionic sulfate species and the stable ammonium groups on the surface of materials. OH- species donate negative charge to the adsorption solution under the alkaline condition, which repulsed anionic species sulfate electrostatically. Thus, because of the electrostatic repulsion between OH^- and anionic species of sulfate, the MP@SiO_2/Chi and MP@SiO_2/CPTMS1/Chi showed low adsorption activity at pH higher than 3.

19.3.1.2 Effect of Adsorption Time and Kinetics Study

The influence of adsorption time on sulfate ion removal by MP@SiO_2/Chi and MP@SiO_2/CPTMS1/Chi can be observed in Fig. 19.2. The sulfate adsorption rate was significantly faster for the first 20 min due to an abundant active site favoring the sulfate ion adsorption. The adsorbent's active sites decreased by the increase of time and caused slower adsorption before reached equilibrium. The role of CPTMS on the structure of adsorbent also can be observed by comparing the adsorption rate between MP@SiO_2/Chi and MP@SiO_2/CPTMS1/Chi. The high density of amine groups on

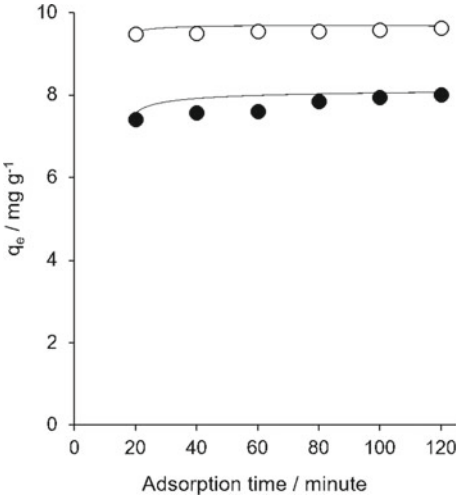

Fig. 19.2 Effect of adsorption time on the sulfate adsorption of (●) NMP@SiO_2/Chi and (○) NMP@SiO_2/CPTMS1/Chi (Conditions: sulfate ion concentration 10 mg L^{-1}; solution vol., 25 mL; adsorbent, 0.02 g; temp., 30°C; and contact time, 2 h.)

MP@SiO_2/CPTMS1/Chi promotes more vacant active sites, which increase electrostatic interaction between sulfate ion species and amine groups during adsorption time.

The sulfate adsorption mechanism was examined by applying pseudo-first-order and pseudo-second-order kinetics model to the experimental data. The pseudo-first-order kinetic model can be expressed in Eq. (19.2) as follows:

$$q_t = \mathrm{q_e} * (1 - \exp(-k_1 * t)) \tag{19.2}$$

Equation 19.2 is a nonlinear form that can be linearized in Eq. (19.3) as follows:

$$l_n(q_e - q_t) = l_n q_e - (k_{1*} t) \tag{19.3}$$

The pseudo-second-order kinetic model can be expressed in Eq. (19.4) as follows:

$$qt = (K_2 * q_{(e*)}^2 t)/(1 + (q_e * k_2 * t)) \tag{19.4}$$

Equation 4 is a nonlinear form that can be linearized in Eq. (19.5) as follows:

$$\frac{t}{q_t} = \left(\frac{1}{k_2 * q_e^2}\right) + \frac{t}{q_e} \tag{19.5}$$

$\mathrm{q_e}$ and $\mathrm{q_t}$ (mg g^{-1}) are the amounts of adsorbed sulfate ion at equilibrium, and time t, $\mathrm{k_1}$ (min^{-1}), and $\mathrm{k_2}$ (g mg^{-1} min^{-1}) is pseudo-first and second-order rate constant. The parameters obtained from pseudo-first order and pseudo-second order kinetics model for sulfate adsorption are summarized in Table 19.2.

Table 19.2 The pseudo-first and pseudo-second-order kinetic model for sulfate

Kinetics	Parameters	MP@SiO_2/Chi	MP@SiO_2/CPTMS1/Chi
Pseudo-first order	q_e^a	0.852	0.704
	k_1^b	0.014	0.063
	R^2	0.912	0.823
Pseudo-second order	q_e^c	10.225	12.106
	k_1^d	0.031	0.144
	R^2	0.9995	1

[a] q_e in mg. g^{-1} [c] q_e in mg. g^{-1}
[b] k_1 in min^{-1} [d] k_2 in mg. g^{-1}. min^{-1}

The correlation coefficient (R^2) (Table 19.2) calculated from the pseudo-first-order kinetic model shows unsuitable results between experimental and pseudo-first-order kinetic models due to the lower R^2 value. In contrast, pseudo-second-order obtained a higher R^2 value. The product exhibited that the sulfate adsorption follows PSO kinetic model. The introduction of chitosan to silica surfaces formed active layers containing hydroxyl and amine groups as active sites. The active sites, including hydroxyl and amine groups, can be easily accessed by sulfate species. Hydrogen bonding and electrostatic interaction may promote the adsorption rate of sulfate.

19.3.1.3 Effect of Initial Concentration and Isotherm Study

The adsorption profile of sulfate on MP@SiO_2/Chi, MP@SiO_2/CPTMS1/Chi, MP@SiO_2/CPTMS2/Chi, MP@SiO_2/CPTMS3/Chi, and MP@SiO_2/CPTMS4/Chi as the function of initial concentration increased significantly for the initial sulfate concentration from 10 to 70 mg L^{-1}. In contrast, the adsorption capacity increased steadily at 100 mg L^{-1} (Fig. 19.3).

The higher concentration of sulfate ions promotes the effective collision between sulfate ions and the adsorbent's active sites. The increasing of adsorption capacity demonstrates that the adsorbents have sufficient active sites which competent for accommodating a high gradient of sulfate ion. However, the materials' adsorption capacity steadily increased when the initial sulfate concentration is 100 mg L-1, which causes by the saturation of the adsorbent's active sites under a high concentration of adsorbate. The detailed investigation shows that the materials' adsorption capacity decreased by increasing CPTMS concentration on the material structure. MP@SiO2/CPTMS2/Chi achieves the highest adsorption capacity. The rise of crosslinker concentration on the magnetic silica-chitosan hybrid materials decreases the chitosan's active site due to the crosslinker's reaction with the nitrogen atom of the chitosan, which forms a denser polymer network inside the material (Osifo et al. 2008).

The mechanisms of sulfate adsorption have been investigated by applying Langmuir and Freundlich isotherm models. The maximum adsorption

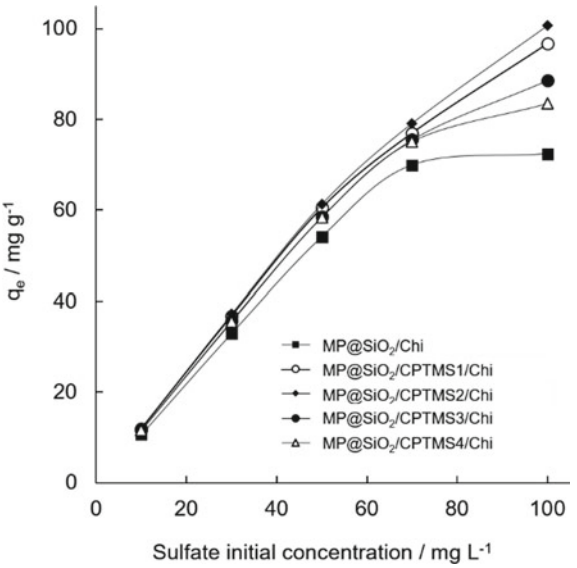

Fig. 19.3 Effect of initial sulfate concentration (Conditions: solution vol., 25 mL; adsorbent, 0.02 g; temp., 30 °C; and solution pH, 6 and 3)

capacity of MP@SiO_2/Chi, MP@SiO_2/CPTMS1/Chi, MP@SiO_2/CPTMS2/Chi, MP@SiO_2/CPTMS3/Chi, and MP@SiO_2/CPTMS4/Chi and other isotherm parameters were obtained by plotting experimental data to the isotherm models.

Langmuir model assumes the adsorption process occurred in a monolayer of the material surface where the active sites presented on the surface are identic and have equivalent energy (Naiya et al. 2009). The nonlinear Langmuir isotherm model can be expressed in Eq. (6) as follows:

$$q_e = \frac{Q_{max} K_L C_e}{1 + K_L C_e} \tag{19.6}$$

Equation 19.6 can be linearized in Eq. (19.7).

$$\frac{C_e}{q_e} = \frac{1}{bQ_{max}} + \frac{C_e}{Q_{max}} \tag{19.7}$$

Q_{max} (mg g^{-1}) is adsorbent maximum adsorption capacity, K_L (L mg^{-1}) is Langmuir isotherm constant. The value of Q_{max} and K_L can be obtained by fitting linear Langmuir isotherm or plotting C_e/q_e versus C_e.

The value of Gibbs free energy ($\Delta G°$) can be calculated by using K_L (units of liters per mole). According to the adsorbate charges characteristic, adsorbates studies can be divided into two groups: charged species and neutral species. The value of $\Delta G°$ for neutral species or adsorbate with weak charge can be calculated by using Eq. (19.8).

$$\Delta G^{O} = -RT \ln\left[K_L\left(1 mol L^{-1}\right)\right] - RT \ln K_L \tag{19.8}$$

In terms of ΔG° calculation, K_L must be changed to a dimensionless constant by multiplying the K_L value by 55.5 (mol water per liter). The proposed value of ΔG° was calculated by using Eq. (19.9) (Milonjic 2007).

$$\triangle G^{O} = RT \ln(55.5) K_L \tag{19.9}$$

According to Freundlich isotherm, the adsorbent surface has heterogeneous energy distribution of the active sites and the adsorption occurred by the multilayer formation on it. Nonlinear Freundlich isotherm model can be stated in Eq. (19.10) as follows:

$$q_e = K_F C_e^{\frac{1}{n}} \tag{19.10}$$

Equation (19.10) can be linearized in Eq. (11) as follows:

$$log q_e = log K_F + \frac{1}{n} log C_e \tag{19.11}$$

K_F (mg g^{-1}) is the Freundlich model's adsorption constant, and 1/n is the adsorption intensity. The value of K_F and 1/n can be determined with log q_e vs. log C_e plotting. The fit result of experimental data with linear Langmuir and Freundlich isotherm model can be observed in Fig. 19.4, and the obtained parameters are summarized in Table 19.3.

Sulfate adsorption on the magnetic silica-chitosan hybrid materials indicated better fitting to the Langmuir model with Q_{max} of 108.50 mg g^{-1}. The

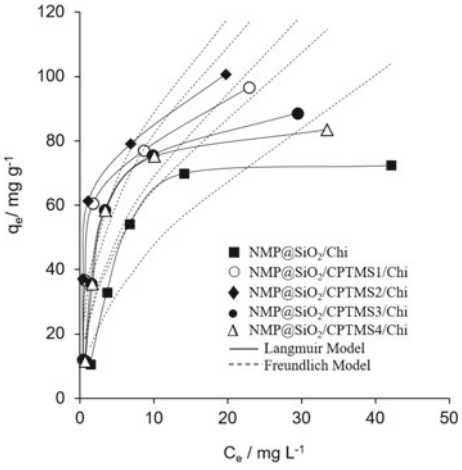

Fig. 19.4 Linear plotting of Langmuir and Freundlich isotherm model

Table 19.3 Sulfate ion adsorption parameters

Adsorbent	Langmuir			Freundlich		
	Q_{max}	K_L	R^2	n	K_F	R^2
MP@SiO_2/Chi	84.50	0.171	0.974	1.814	13.223	0.799
MP@SiO_2/CPTMS1/Chi	104.20	0.484	0.990	2.381	31.361	0.754
MP@SiO_2/CPTMS2/Chi	108.50	0.564	0.985	2.538	36.181	0.672
MP@SiO_2/CPTMS3/Chi	99.66	0.289	0.990	2.019	22.035	0.801
MP@SiO_2/CPTMS4/Chi	91.90	0.329	0.990	2.116	21.829	0.780

Table 19.4 Comparison of MP@SiO_2/CPTMS/Chi to other sulfate adsorbents

Adsorbent	Q_{max} (mg g^{-1})	References
Ni-Al	45.2	Sadeghalvad et al. (2016)
ZrBC	35.2	Ao et al. (2020)
Activated carbon from rice straw	56.49	Farahmand et al. (2015)
MP@SiO_2/CPTMS/Chi	109	Present study

MP@SiO_2/CPTMS/Chi has a higher Q_{max} than other materials, which can be summarized in Table 19.4. The comparison with other sulfate adsorbents indicated that MP@SiO2/CPTMS/Chi exhibits excellent adsorption activity toward sulfate ions.

The R_L value for sulfate ion adsorption by magnetic silica-chitosan hybrids ranged from 0.0648-0.1539. The Langmuir isotherm is conformable if the R_L lies between 0 and 1, while values higher than unity suggest an unfavorable adsorption system. Moreover, it can be confirmed by the negative $\Delta G°$ values, which shows that sulfate adsorption is spontaneous. The value of $\Delta G°$ for sulfate ion adsorption by magnetic silica-chitosan hybrid can be seen in Table 19.5. We conjecture that the silica surface was homogeneous, with the amine group as the most dominant active sites based on the Langmuir model. The proposed adsorption mechanism of sulfate by silica-chitosan hybrid materials can be shown in Fig. 19.5.

Table 19.5 Adsorption energy ($\Delta G°$) and separation factor (R_L) for sulfate adsorption

Adsorbent	K_L	$\Delta G°$	R_L
MP@SiO_2-Chi	0.1709	−5670.14	0.1539
MP@SiO_2/CPTMS1/Chi	0.4842	−8294.92	0.0648
MP@SiO_2/CPTMS2/Chi	0.5640	−8679.42	0.0565
MP@SiO_2/CPTMS3/Chi	0.2893	−6996.83	0.1011
MP@SiO_2/CPTMS4/Chi	0.3287	−7318.64	0.0908

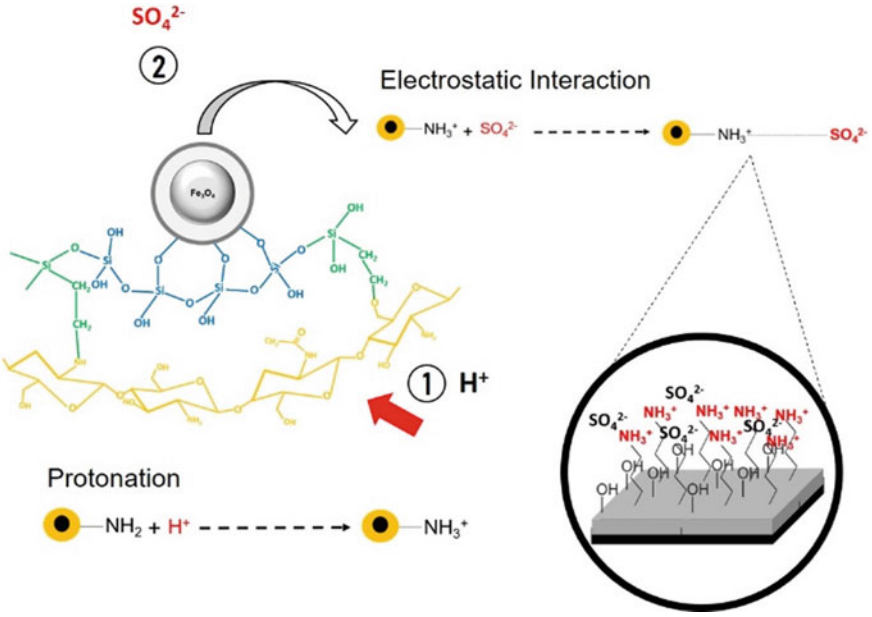

Fig. 19.5 Proposed adsorption mechanism of sulfate by silica-chitosan hybrid

19.3.1.4 Effect of Ionic Strength

The adsorption process of pollutants by an adsorbent can be caused by various interactions between adsorbate species and the adsorbent's active site. Electrostatic interaction is one of the most interactions that occurred in charged adsorbate species in the adsorption process. Most adsorption process which caused by electrostatic interaction is influenced by confounding ions. Thus, the effect of confounding ions on sulfate ion adsorption must be investigated. As shown in Fig. 19.6, the amount of adsorbed sulfate was decreased due to sodium chloride in the adsorption system. The decrease of adsorbed sulfate was caused by competitive effects between sodium ion and ammonium species on the adsorbent surface. It shows that sulfate ion adsorption by silica-chitosan hybrid materials is primarily driven by electrostatic interaction.

19.3.1.5 Effect of Adsorbent Dosage

The adsorbent dosage has a significant impact on sulfate ion adsorption. The correlation between adsorbent dosage and the adsorption capacity of the material is shown in Fig. 19.7.

The increasing of adsorbent dosage causes the increased efficiency of sulfate removal. Adsorbent dosage contributes to the increase of surface area and offers

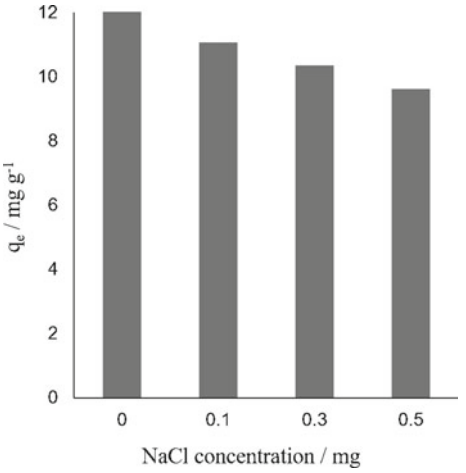

Fig. 19.6 The effect of ionic strength on sulfate adsorption (Conditions: sulfate ion concentration, 10 mg L^{-1}; solution vol., 25 mL; adsorbent, 0.02 g; temp., 30 °C; and solution pH of 3)

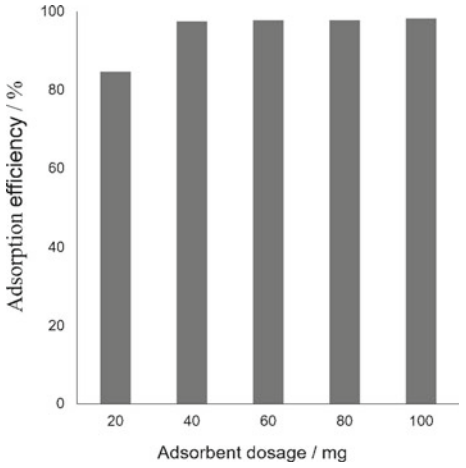

Fig. 19.7 Effect of adsorbent dosage on sulfate adsorption (Conditions: sulfate ion concentration, 10 mg L^{-1}; solution vol., 25 mL; temp., 30 °C; and solution pH of 3)

more vacant active sites, which increase the electrostatic interaction between sulfate species and active sites of the materials (Mohammadi et al. 2019).

19.4 Conclusions

In this study, the magnetic silica-chitosan hybrids synthesized from sodium silicate and chitosan using the 3-chloropropyl trimethoxysilane (CPTMS) sol-gel method were effective adsorbent for sulfate ions. The introduction of magnetic property to the silica-chitosan hybrids using natural magnetic particles produced highly magnetical separable adsorbents. It was quickly removed from the solution after the adsorption

process by applying an external magnet within less than 5 min. The effect of CPTMS addition on the adsorption showed that CPTMS at a lower concentration increased the adsorption capacity. However, at higher concentrations, the ability tended to be reduced. The mole ratio of CPTMS to chitosan 2:4 was the optimum composition to give the highest adsorption capacity of sulfate ions (108.50 mg g^{-1}). This performance makes the material produced to be prospective candidate adsorbent for removing sulfate ions from wastewater. Further research is recommended to characterize the adsorbent materials for analyzing the physical and chemical properties of materials and determine the adsorbent selectivity towards sulfate ions with various ions.

Acknowledgements The first author acknowledged the Ministry of Finance, the Republic of Indonesia for the Indonesia Endowment Fund for Education (LPDP) scholarship. This research was also financialized by the Ministry of Research and Technology/National Research and Innovation Agency through the Magister Thesis Research (PTM) Grant with the contract number: 2033/UN1/DITLIT/DIT-LIT/PT/2020.

References

Anal AK, Tobiassen A, Flanagan J, Singh H (2008) Preparation and characterizationof nanoparticles formed by chitosan–caseinate interactions. Colloids Surf B 64:104–110

Ao H, Cao W, Hong Y, Wu J, Wei L (2020) Adsorption of sulfate ion from water by zirconium oxide-modified biochar derived from pomelo peel. Sci Total Environ 708:

Du H, Lung CYK, Lau T-C (2018) Efficient adsorption, removal and recovery of phosphate and nitrate from water by a novel lanthanum(iii)-Dowex M4195 polymeric ligand exchanger. Environ Sci Technol 4:421–427

Farahmand E, Rezai B, Ardejani FD, Tonekaboni SZS (2015) Kinetics, equilibrium, and thermodynamic studies of sulfate adsorption from aqueous solution using activated carbon derived from rice straw. Bulg. Chem. Commun. 47:72–81

Fernando WAM, Ilanko IMSK, Syed TH, Yellinshetty M (2018) Challenges and opportunities in the removal of sulphate ions in contaminated mine water: a review. *Miner. Eng.* 117, 74–90

Huang R, Liu Q, Huo J, Yang B (2017) Adsorption of methyl orange onto protonated crosslinked chitosan. Arab. J. Chem. 10:24–32

Juan-Díaz MJ, Martínez-Ibánez M, Lara-Sáez I, da Silva S, Izquierdo R, Gurruchaga M, Goni I, Suay J (2016) Development of hybrid sol–gel coatings for the improvement of metallic biomaterials performance. Prog Org Coat 92:45–51

Kelechi E, Elvis OA, Kanayo AK (2018) Synthesis and Characterization of Chitosan–Silica Hybrid Aerogel using Sol-Gel Method. J. King Saud Univ. Sci. 32:550–554

Ma H, Wang M, Zhang J, Sun S (2019) Preparation mechanism of spherical amorphous $ZrO(OH)_2$/AlOOH hybrid composite beads for adsorption removal of sulfate radical from water. Mater Lett 247:56–59

Milonjic S (2007) A consideration of the correct calculation of thermodynamic parameters of adsorption. J. Serbian Chem. Soc. 72:1363–1367

Mohammadi E, Daraei H, Ghanbari R, Athar SD, Zandsalimi Y, Ziaee A, Maleki A, Yetilmezsoy K (2019) Synthesis of carboxylated chitosan modified with ferromagnetic nanoparticles for adsorptive removal of fluoride, nitrate, and phosphate anions from aqueous solutions. J Mol Liq 273:116–124

Naiya TK, Bhattacharya AK, Das SK (2009) Adsorption of Cd(II) and Pb(II) from aqueous solution on activated alumina. J Colloid Interface Sci 333:14–26

Narita Y, Sakti SCW, Akemoto Y, Tanaka S (2019) Ultra-rapid removal of cationic organic dyes by novel single- and double-stranded DNA immobilized on quaternary ammonium magnetic chitosan. J. Environ. Chem. Eng. 7:

Nuryono, Miswanda, D., Sakti, S.C.W., Rusdiarso, B., Krisbiantoro, P.A., Utami, N., Otomo, R., Kamiya, Y (2020) Chitosan-functionalized natural magnetic particle@silica modified with (3 chloropropyl)trimethoxysilane as a highly stable magnetic adsorbent for gold(III) ion, Mater. Chem. Phys., 255, 123507 (2020)

Omwene PI, Kobya M (2018) Treatment of domestic wastewater phosphate by electrocoagulation using Fe and Al electrodes: A comparative study. Process. Saf. Environ. 116:34–51

Osifo PO, Webster A, van der Merwe H, Neomagus HWJP, van der Gun MA, Grant DM (2008) The influence of the degree of crosslinking on the adsorption properties of chitosan beads. Bioresour Technol 99:7377–7382

Pap S, Kirk C, Bremner B, Sekulic MT, Shearer L, Gibb SW, Taggart MA (2020) Low-Cost Chitosan-Calcite Adsorbent Development for Potential Phosphate Removal and Recovery from Wastewater Effluent. Water Res 173:

Runtti H, Luukkonen T, Niskanen M, Tuomikoski S, Kangas T, Tynjälä P, Lassi U (2016) Sulphate removal over barium-modified blast-furnace-slag geopolymer. J Hazard Mater 317:373–384

Sadeghalvad B, Azadmehr A, Hezarkhani A (2016) Enhancing adsorptive removal of sulfate by metal layered double hydroxide functionalized Quartz-Albitophire iron ore waste: preparation, characterization and properties. RSC Adv. 6:67630–67642

Xiong J, Qin Y, Islam E, Yue M, Wang W (2011) Phosphate removal from solution using powdered freshwater mussel shells. Desalination 276:317–321

Xu X, Cheng Y, Wu X, Fan P, Song R (2020) La(III)-bentonite/chitosan composite: A new type adsorbent for rapid removal of phosphate from water bodies. Appl Clay Sci 190:

Zhang B, Chen N, Feng C, Zhang Z (2018) Adsorption for phosphate by crosslinked/non-crosslinked chitosan-Fe(III) complex sorbents: Characteristic and mechanism. Chem Eng J 353:361–372

Zhang J, Chen N, Tang Z, Yu Y, Hu Q, Feng C (2015) A study of the mechanism of fluoride adsorption from aqueous solutions onto Fe-impregnated chitosan. Phys Chem Chem Phys 17:12041–12050

Chapter 20
Statistical Analysis of Water and Sediment Research in Heilongjiang River Basin

Ning Yu, Lei Zhang, Jun Li, and Yousheng Wang

Abstract To understand the development history and variation of research focused on water and sediment in the Heilongjiang River Basin, statistical analysis was conducted based on the databases in Web of Science. Aspects including the number of publications, countries, institutes, subject categories, words in the title, and article adoptions were analyzed, which could provide a basis for future research directions. The results show that the development history can be divided into three stages: the early stage from 1943 to 2001, the rapid development stage from 2002 to 2013, and the current stage of 2014 to present, where the number of publications per year is relatively large. China and Russia pay the highest attention to this field because Heilongjiang is a boundary between the two countries. Correspondingly, most number of publications are from the Russian Academies of Science followed by the Chinese Academies of Science, which are followed by the universities and institutes in the northeast of China which account for the third largest number of publications to the tenth largest number. Furthermore, it was found that international cooperation is scarcer than domestic cooperation. As for the subjects, the number of publications under the subject of ecological environment ranks first; attentions paid to water and sediment movement and riverbed evolution are low. The results of title word frequency for all publications show that the word "water" ranks first which is much higher than "sediment;" "soil," which is related to agriculture and forestry, ranks second. Currently, research on characteristic analysis is at the forefront, model development is next, and the theoretical studies are relatively scarce. Our research is of immense significance since the results of our study can identify research hotspots and trend changes, and hence, can provide references for research in the same field.

N. Yu
Heilongjiang Water Conservancy Investment Group Co Ltd., Harbin, China

L. Zhang (✉) · Y. Wang
State Key Laboratory of Simulation and Regulation of Water Cycle in River Basin China, Institute of Water Resources and Hydropower Research, Beijing, China
e-mail: lei207b@163.com

J. Li
Heihe Water Conservancy Research Institute, Heihe, China

H.-Y. Jeon (ed.), *Sustainable Development of Water and Environment*,
Environmental Science and Engineering,
https://doi.org/10.1007/978-3-030-75278-1_20

Keywords Heilongjiang data · Analysis · Water · Sediment · Research state

20.1 Introduction

As the world's sixth-longest river, the Heilongjiang River (also known as the Amur River in Russia) is an important international river that flows through China, Russia, and Mongolia. On the side of China, it covers 902,400 km^2, accounting for approximately 48% of the total basin area. Its main stream has a length of 2821 km, and its 1861-km-long upper and middle stream is a border between China and Russia. One of the important tributaries of the Heilongjiang River is the Wusuli (Ussuri) River, whose main stream along the border is 494 km in length. Together, the border sections of the Heilongjiang main stream, the Wusuli River, and the Argun River form the world's longest boundary river (Dai et al. 2015). The changes in water and sediment in the main stream and tributaries of Heilongjiang influence its stability, thereby affecting the life and property safety of the Chinese and Russian people, social stability, and economic development on both sides. However, as one of the world's largest rivers and a border river between China and Russia, Heilongjiang has not received appropriate attention for its status and importance. Compared with the Yellow River and Yangtze River, the existing research results related to Heilongjiang are relatively limited (Dai et al. 2015).

Under the influence of climate change, over-utilization and development of rivers, and other intense human activities in recent years, the water and sediment of major rivers worldwide have undergone significant changes, which has attracted widespread attention from scholars both at home and abroad. As a boundary river between China and Russia, the impact of human activities on Heilongjiang is relatively small. Its change intensity is weaker than those of the Yellow River, Yangtze River, and other river basins. However, according to a survey and comparative analysis of topographic maps, the length of river bank erosion along the upper and middle stream of Heilongjiang has reached approximately 1,100 km, and the bifurcating river section with central bars is as long as 1,108 km. The severe river bank erosion, large cutting area of low shallow beaches, and frequent swing of the main stream have posed a serious threat to the river channel stability. Therefore, it is urgent to research the water and sediment changes in the river basin. Scholars have conducted many studies to address this urgency and have presented a series of results, but these results have not been well sorted and analyzed.

This paper presents a statistical analysis of publications on water and sediment changes in the Heilongjiang River Basin using the bibliometric method to understand the research status quo and hotspots in this field. Bibliometric analysis is an important branch of library and information science research used to quantitatively analyze the current state and predict the future trend of academic development through mathematical statistics. It exhibits significant objective and quantitative characteristics (Qiu and Wang, 2008; Tian and Chang, 2012) and can capture macro-research trends, such as the development dynamics of subject categories (or fields of research) and

research hotspots. It has been widely used in the research of many subjects and fields (Fu et al. 2010; Abramo et al. 2011; Liu et al. 2011, 2019; Niu et al. 2014; Zhang et al. 2016; María et al. 2019). It is also an important tool for assessing the development trend of subject journals (Ning et al. 2010, 2015; Wang et al. 2017). In the field of water and sediment research, Zhang et al. (2016) applied the bibliometric method to analyze the history and hotspot changes in research on Lake Taihu. Niu et al. (2014) analyzed the global development trend of sediment-related research in earth science. They found that the heat of research on "water," "soil(s)", "evolution", and "model" was consistent and that research on "erosion", "sediment transport", and "dynamics" was growing rapidly. Based the current research landscape, the bibliometric method was used in this study to conduct a quantitative analysis of the literature related to water and sediment in the Heilongjiang River Basin. The specific aspects of analysis covered in this study include the numbers of publications, journals, subject categories, and titles. The research outcomes are expected to identify research hotspots and trend changes, thereby providing references for research in the same field.

20.2 Data Sources

The Web of Science databases were used as the data sources, and the "subject" search field was used for the queries. In the literature related to Heilongjiang, there are different spellings and expressions related to water and sediment; therefore, the following specific search terms were used: "runoff", "run-off", "hydro", "hydrology", "hydrological", "streamflow*", "fluvial", "flood", "floods", "floodwater", "storm", "downpour", "intense fall", "river channel*", "water*", "sediment*", "bedload", "bed-load", "suspended load", "suspensate", "suspended sediment", "suspended particles", "wash load", "total load", "alluvia", and "alluvium". The basin was searched as to "Amu", "Wusuli", and "Heilongjiang". A total of 4,249 publications were retrieved, of which 3838 were journal articles, accounting for 90.33%. There were 988 News, Letter, Abstract, and other types of documents, accounting for the remaining 9.67%. The bibliometric analysis presented in this paper was performed based on the retrieved 4,249 publications.

20.3 Results Analysis

20.3.1 Variation in the Number of Publications

The annual variations of publications on water and sediment research in Heilongjiang are shown in Fig. 20.1. It can be seen that the earliest publication on this research topic appeared in 1943. The research in this field can be divided into three stages: (1) 1943–2001, (2) 2002–2013, and (3) 2014–present. Stage (1) represents the slow early

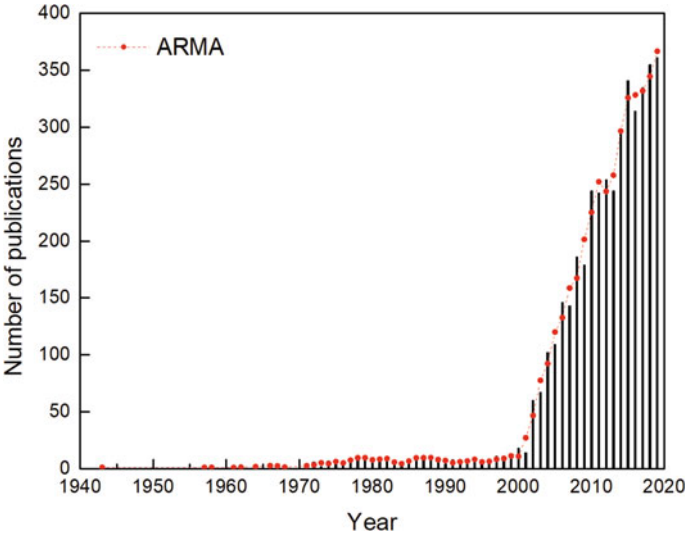

Fig. 20.1 Variation in the number of publications published per year

stage of research in this field, during which the number of publications was relatively small at approximately 10 per year. In stage (2), which is the rapid development stage, the number of publications exhibited an overall trend of rapid growth. In stage (3), the number of publications is close to or above 300 per year, and the most publications were retrieved for the year 2019. In recent years, the number of publications on water and sediment research in Heilongjiang has remained at a relatively high level and has shown continued growth trend, reflecting a lasting research heat in this field.

20.3.2 Statistics of Countries

The numbers of publications in various countries are compared in Fig. 20.2. It can be seen that the number of publications by Chinese scholars (up to 3,500) is the highest, accounting for 83.17% of the total. Russia ranks second with 611 publications, accounting for 14.38%. The number of publications in other countries is relatively low, accounting for less than 10%. Because Heilongjiang is a border river between China and Russia, it is reasonable that scholars from the two countries have paid the greatest attention to it. Statistics were collected on the annual volume of publications in China, Russia, United States, Japan, and Germany since the year 2000, and the results are shown in Fig. 20.3. It can be seen that China has been researching water and sediment changes in the Heilongjiang River Basin in recent years, and the number of publications has increased year by year, reaching approximately 300 articles per year. Russia's publication volume has also shown an increasing trend year by year, from approximately 10 articles per year in 2000 to approximately 50

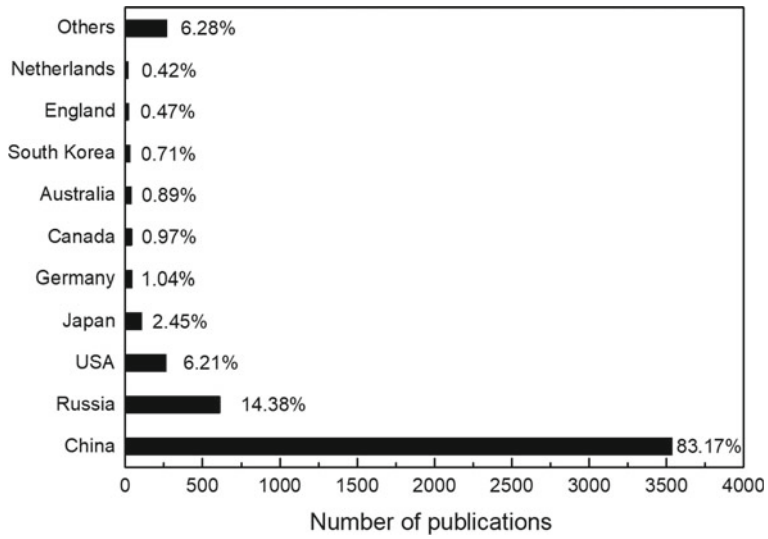

Fig. 20.2 Proportions of publications from different countries

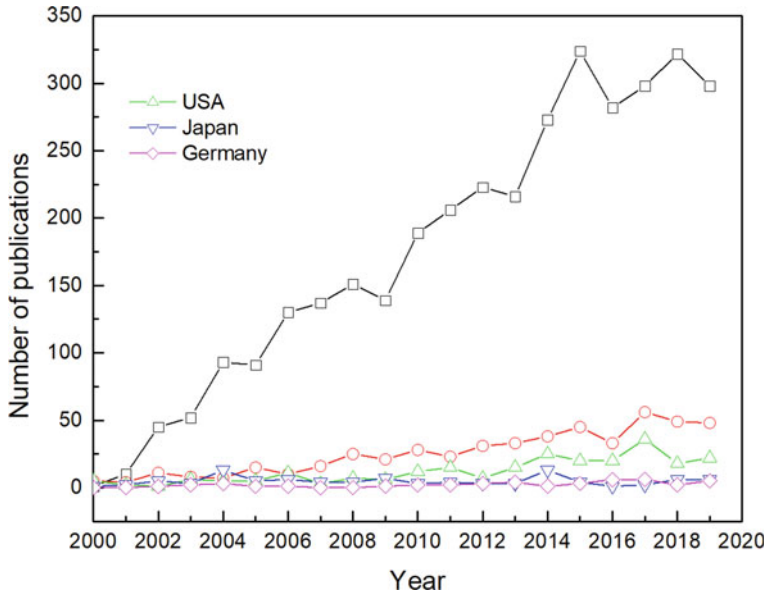

Fig. 20.3 Annual statistics on the numbers of publications by China, Russia, United States, Japan, and Germany

per year in recent years. It is worth noting that the United States has also significantly increased its attention on the Heilongjiang River Basin, from less than 5 articles per year in 2000 to 20–30 articles per year in recent years. There have been no significant changes in the numbers of publications in Japan and Germany.

20.3.3 Statistics of Research Institutes

The top ten research institutes in terms of the number of publications on water and sediment research in the Heilongjiang River Basin are listed in Fig. 20.4. These institutes have published 3,029 papers, accounting for 71.29% of the total number of retrieved documents. Among them, the Russian Academy of Sciences ranks first with 848 publications, followed by the Chinese Academy of Sciences with 764 publications. The institutes ranked third to tenth are all Chinese research institutes, exhibiting an obvious regional relationship. Because Heilongjiang is located in the northeast, universities and research institutes in the northeast are the main research force. Northeast Agricultural University, Northeast Forestry University, Harbin Institute of Technology, and Jilin University rank third to sixth, respectively. From the perspective of university characteristics, agricultural, forestry, and normal universities accounted for the majority. It can thus be inferred that the changes in water and sediment in Heilongjiang are closely related to the development of agriculture and forestry.

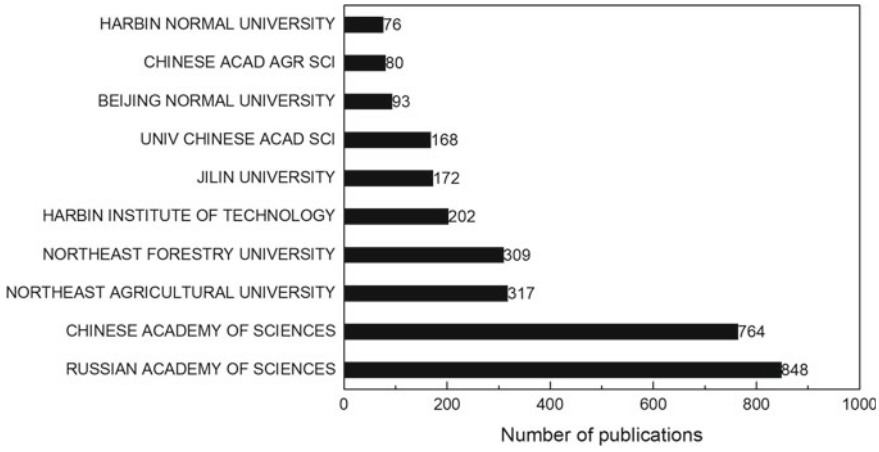

Fig. 20.4 Number of publications by different institutes

20.3.4 Statistics of Subject Categories

The statistics of the top 15 subject categories with the highest numbers of publications on water and sediment research in the Heilongjiang River Basin are listed in Fig. 20.5. The results show that the subject of environmental sciences and ecology ranks first with 1,905 publications, accounting for 44.83% of the total. The subjects ranked second to fifth are agriculture, water resources, zoology, and marine freshwater biology, which account for 31.73%, 16.52%, 15.39%, and 15.16%, respectively. For water conservancy and sedimentation-related subjects—except for water resources, which ranks third—the subjects of geology and engineering rank seventh and fourteenth, accounting for 14.62% and 9.11%, respectively. It can be seen through comparison that the current research on water and sediment in the Heilongjiang River Basin is mainly concentrated on the ecological environment and agricultural development, and the attentions paid for water-sediment movement and river bed evolution are relatively low.

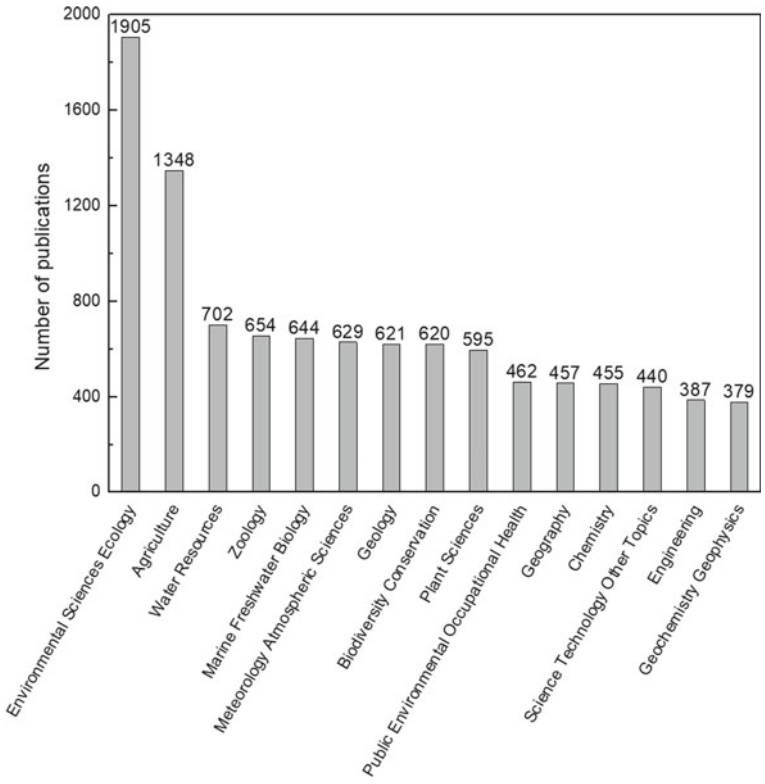

Fig. 20.5 Numbers of publications in different subjects

20.3.5 Statistics of Subject Categories Research Hotspot Analysis

The title of an article is a high-level summary of its content, methods, conclusions, etc. Thus, the research hotspots and trends related to the Heilongjiang River Basin can be identified from the changes in high-frequency words found in titles. In this study, all retrieved publications were divided into four time intervals: before 1990, 1991–2000, 2001–2010, and 2011–2020. The frequency of each word in the titles was counted, and the top ten words in the two stages of 2001–2020 and 2011–2020 are shown in Fig. 20.6. It should be noted that insignificant words, such as "of" and "a/an" were not included in the statistics. The following can be seen from the figure:

(1) The word "water" ranks first, which is directly related to the set search keyword. Another search keyword, "sediment", ranks sixth in the statistical results. This indicates that the current research in the Heilongjiang River Basin focuses more on water changes, and the attention paid to sediment is relatively lower.

(2) The word "soil" ranks second. This is because both agriculture and forestry in the Heilongjiang River Basin are related to soil, and there are relatively more related studies.

(3) The words "effect", "analysis", and "characteristic" rank fourth, fifth, and sixth, respectively; the word "assessment" ranks ninth. These words indicate that the current research on water and sediment change in Heilongjiang is mostly focused on qualitative analysis of characteristics, effects, and assessments, which addresses the impact factors and characteristics of water and sediment. The word "model" ranks

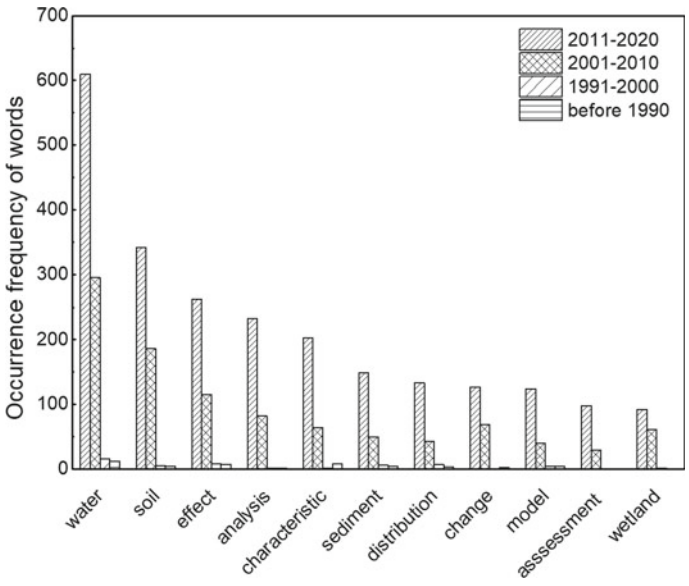

Fig. 20.6 Statistical results of top ten most frequent words used in titles

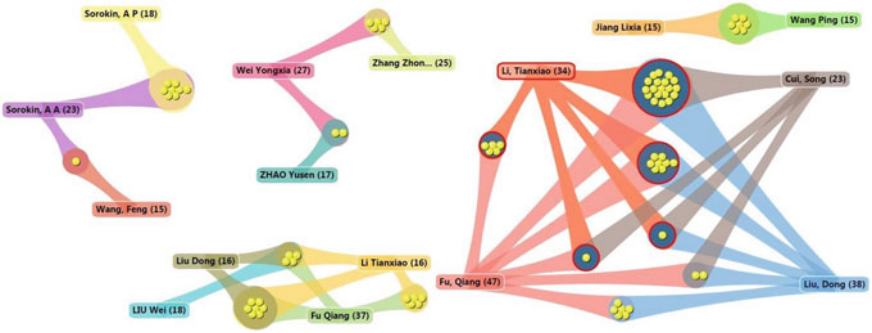

Fig. 20.7 Core inter-institutional collaboration network of authors

seventh, and "theory" only appeared 11 times. Thus, it can be inferred that the research status quo on water and sediment in the Heilongjiang River Basin is dominated by characteristic analysis, followed by model development, and is relatively weak on the theoretical side.

(4) Because there were relatively fewer articles published before 2000, the frequency of each word in the titles is also lower. A comparison between the two stages of 2001–2010 and 2011–2020 shows that the top ten high-frequency words have changed. For 2011–2020, the word "change" ranks eighth, but during 2001–2010, it ranks fifth; the word "wetland" ranks seventh for 2001–2010, but it is outside the top ten for 2011–2020. The word "assessment" is not in the top ten for 2001–2010 and ranks tenth for 2011–2020.

20.3.6 Analysis of Author Collaborations

The collaborations between authors with more than 15 publications were analyzed, and the results are shown in Fig. 20.7. It was found that there is currently little international collaboration in water and sediment research in the Heilongjiang River Basin. The dominant collaborations are among different domestic scholars, who have formed three different research groups. Among them, "Fu, Qiang", "Liu, Dong", and "Li, Tiantao" have formed close connections; they have collaborated with each other as well as other scholars and have published many articles.

20.3.7 Analysis of Article Citations

The 4,249 retrieved publications have been cited 36,754 times, with an average of 8.65 citations per article and an h-index of 68. The top ten cited publications are listed in Table 20.1. It can be seen that the current research hotspot is climate change, and the

Table 20.1 Statistics of the top ten most cited publications

No.	First author	Title	Journal	Times Cited
1	Nijssen, B	Hydrologic sensitivity of global rivers to climate change	Climatic Change	357
2	Wang, CK	Biomass allometric equations for 10 co-occurring tree species in Chinese temperate forests	Forest Ecology and Management	304
3	Zhou, JB	The crustal accretion history and tectonic evolution of the NE China segment of the Central Asian Orogenic Belt	Gondwana Research	303
4	Wan, ZM	New refinements and validation of the collection-6 MODIS land-surface temperature/emissivity product	Remote Sensing of Environment	250
5	Nohara, Daisuke	Impact of climate change on river discharge projected by multi-model ensemble	Journal of Hydrometeorology	238
6	Hulata, G	Genetic manipulations in aquaculture: a review of stock improvement by classical and modern technologies	Genetica	232
7	Peng, SB	Improving nitrogen fertilization in rice by site-specific N management. A review	Agronomy for Sustainable Development	223
8	Smith, SV	Humans, hydrology, and the distribution of inorganic nutrient loading to the ocean	Bioscience	196
9	Qin, F	Effects of low-molecular-weight organic acids and residence time on desorption of Cu, Cd, and Pb from soils	Chemosphere	189
10	Lu, AX	Time effect on the fractionation of heavy metals in soils	Geoderma	188

two related publications are ranked first and fifth, respectively. The other publications are related to forestry, agriculture, soil, and geology. Publications on the subject of water conservancy and engineering are not in the top ten.

20.4 Conclusions

In this study, a statistical analysis was performed on the research status quo of water and sediment in Heilongjiang using the bibliometric method. The main findings of this study are as follows: (1) The number of publications in this field has been increasing year by year and has reached approximately 300 articles per year in recent years, reflecting that related research has attracted more attention from scholars. (2) Heilongjiang, as an international river, still receives the most attention from China and Russia at present, especially the universities and research institutes in the northeast of China, which continue to pay close attention to the Heilongjiang River Basin. (3) It can be seen from the statistics of subject categories and article citations that the current research related to water and sediment in the Heilongjiang River Basin is mainly in relation to the ecological environment, agriculture, and forestry. Relatively less attention has been paid to water and sediment transport and river bed changes in conventional water and sediment research. (4) Compared with the Yellow River and Yangtze River basins, the Heilongjiang River Basin has a relatively low sediment content. Therefore, the current related research mostly focuses on water changes. The research content is mainly concentrated on characteristic analysis, followed by model development, and theoretical research is relatively weak.

Acknowledgements This work was supported by the National Key Research and Development Program of China (2018YFC0407304), and the Basic Research Project of China Institute of Water Resources and Hydropower Research (SE0145B702017).

References

Abramo G, Ciriaco Andrea D'Angelo, Viel F. The field-standardized average impact of national research systems compared to world average: the case of Italy. Scientometrics, 88(2), pp. 599–615, 2011

Baoying Ning, Guojun Chen, Lianhua Xue et al (2015) Publication trends of Acta Sedimentologica Sinica in 3 decades: Results and Enlightenment based on Bibliometric Analysis. Acta Sedimentol Sin 033(001):1–9

Changlei Dai, Sicong Wang, Zhijun Li et al (2015) Review on hydrological geography in Heilongjiang River Basin. Acta Geogr Sin 070(011):1823–1834

Fu HZ, Ho YS, Sui YM et al (2010) A bibliometric analysis of solid waste research during the period 1993-2008. Waste Manag 30(12):2410–2417

Junping Qiu (2008) Wang Yuefen. Beijing Library Press, Content Analysis on Bibliometrics

Marín-Carrillo et al (2019) María de las Mercedes Capobianco-Uriarte, María del Pilar Casado-Belmonte, A Bibliometric Analysis of International Competitiveness (1983–2017). Sustainability, 2019, 11

Liu X, Zhang L, Hong S (2011) Global biodiversity research during 1900–2009: a bibliometric analysis. Biodivers Conserv 20(4):807–826

Liu Z, Yang J, Zhang J et al (2019) A Bibliometric Analysis of Research on Acid Rain. Sustainability, 11

Ning B, He Quang, Shen Y et al (2010) Publication Current of the Journal of Glaciology and Geocryology in 1979–2009: Results and Enlightenment Based on Bibliometric Analysis. Journal of Glaciology and Geocryology, 32(6), pp. 222–231

Niu B, Hong S, Yuan J et al (2014) Global trends in sediment-related research in earth science during 1992–2011: a bibliometric analysis. Scientometrics 98(1):511–529

Wang S, Qing X, Wang J et al (2017) Analysis of competitiveness of international geographic institutes based on bibliometrics. Acta Geographica Sinica, 72, 9, pp. 164–178

Yaping Tian, Hao Chang (2012) Bibliometric Analysis of Research Progress on Ecological Vulnerability in China [J]. Acta Geogr Sin 067(011):1515–1525

Zhang Y, Yao X, Qin B (2016) A critical review of the development, current hotspots, and future directions of Lake Taihu research from the bibliometrics perspective. Environ Sci Pollut Res 23(13):12811–12821

Chapter 21
Empowering Citizens' Resilience—The FLOODLABEL

P. Meier, H. Meyer, A. Schüttrumpf, and G. Johann

Abstract Floods and heavy rain events are on the rise, fostered by climate change. They cause damage in the same order of magnitude, but heavy rain can fall anywhere, irrespective of rivers or creeks and therefore affect everyone. The larger infrastructural measures taken by governmental authorities must be supplemented by private precautions taken by citizens themselves. The Floodlabel is a multi-stage concept that explains to homeowners their flood risk and provides instruction as to how to structurally secure their property against damage caused by floods, heavy rain, sewer backwater and groundwater. If these personal provision measures are implemented by sufficient numbers of citizens, this will strengthen the resilience of the community to these events. As this is a topic of international relevance, the Floodlabel developed in Germany and recommended by the climate protection portal of the German federal government is now being further developed for international use and is currently being adapted within two research projects for the special needs and conditions on the ground in Ghana and Iran.

Keywords Heavy Rain · Flood · Private Precaution · Resilience · Protection · Home · Ghana · Iran

21.1 Introduction

It is widely acknowledged that fluvial and pluvial flooding are now responsible for many deaths every year and cause billions of euro worth of damage. This development is attributable to climate change, the increase in population density and economic values. Recent flood events with catastrophic consequences have brought the challenges that people currently face back into the spotlight with dramatic effect.

P. Meier · H. Meyer · A. Schüttrumpf · G. Johann (✉)
HochwasserKompetenzCentrum (Flood Competence Center), Ostmerheimer Straße 555, 51109 Cologne, Germany
e-mail: georg.johann@hkc-online.de

H.-Y. Jeon (ed.), *Sustainable Development of Water and Environment*,
Environmental Science and Engineering,
https://doi.org/10.1007/978-3-030-75278-1_21

Analyses of flood events from recent years show that pluvial flooding causes similarly high levels of damage as large river floods, but heavy rain events can occur anywhere and therefore affect everyone.

Public authority adaptation measures can reduce the scope of potential damage, but they can be only one part of the solution. These—often large-scale—measures must be accompanied and supplemented by small-scale risk prevention measures on the part of citizens aimed at protecting individual buildings, in order to secure and increase the resilience of society. This requires that the associated risks be communicated to the population (Johann 2020). Pointing out the risks is insufficient, however; information on the options available to protect oneself must also be provided. Often, cost-effective measures can reduce—or even prevent entirely—larger-scale damage to buildings.

When developing a resilient society, the activation of "hidden" community strengths is a key factor (Höppner et al. 2010). Private precautions or the lack thereof impact not only individual citizens, but also the public at large. If house owners or residents take measures and thereby protect their property, they thus avoid or reduce potential damage and require no or at least little support in acute situations from neighbours, fire department, municipal authorities etc. If, however, private precautionary measures are not taken or were insufficient, their ability to handle the crisis will be woefully lacking and they will be dependent on support.

If the coping capacities of several affected persons at the same time, this can, lead to the coping capacities of those who are attempting to help no longer being sufficient. Then new actors have to be brought in, e.g., the fire department from neighbouring municipalities and/or higher administrative levels. Each time the coping capacities of an actor or an administrative level are exceeded, the involvement of further actors or higher administrative levels is required, and the crisis can, in the extreme case, end up being escalated from the municipality to national level. On the other hand, public authorities have the option of promoting—through information, motivation, incentives or regulations—private precautions to be taken by individuals, thus ultimately promoting the resilience of the community (Fig. 21.1).

21.2 The FLOODLABEL

In Germany, there are flood hazard and risk maps, in accordance with the EU Flood Directive; however often these are not sufficiently understood or correctly interpreted by all citizens (Fekete 2012). Information on measures that house owners can take are not included. Risk communication tailored to the specific needs of people can however influence the risk awareness of people and encourage them to adapt their behaviours (Haer et al. 2016; Handmer 1980).

The concept of the Floodlabel, an initiative of the HochwasserKompetenzCentrum (HKC—Flood Competence Center), a non-profit organisation, aims to motivate and empower citizens, through information and consultancy, to protect their property by taking private precautions and thus to contribute to the resilience of the community.

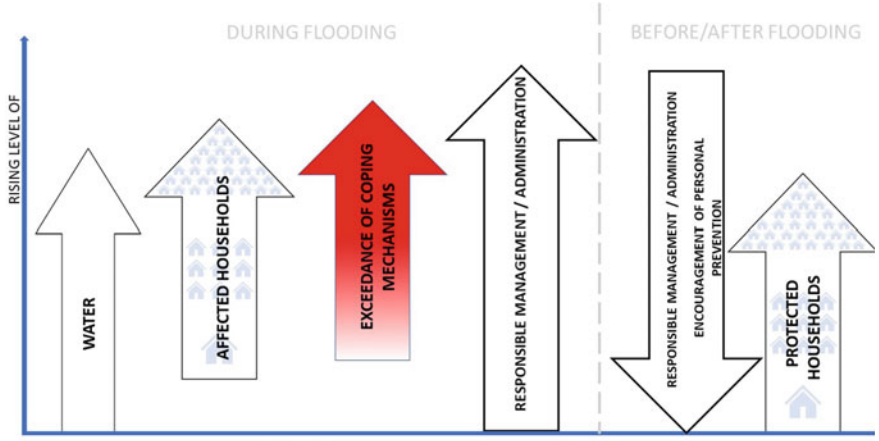

Fig. 21.1 Schematic representation of the change in responsibilities

Citizens can gain insight into the flood risks to which they themselves are exposed. To this end, the website, www.floodlabel.com provides the most important and useful information on possible flood risks in a manner that is understandable for citizens. If the layperson then consults with an expert, she/he will receive with the Floodlabel certificate (Fig. 21.2) a comprehensive risk assessment for their house or building along with tailor-made recommendations as to how the flood risk can be reduced by private measures.

Furthermore, the Floodlabel serves as evidence as to how at risk of flooding the property is and the measures taken to secure against this or adapt to it, which can be an important issue for insurance. It enables citizens and industry to operate active precautionary measures against damage caused by river flooding, heavy rain (pluvial flood), sewer backwater and groundwater n four steps:

Addressing the problem of flooding. The homepage of the HKC website provides essential information in layman's terms. The HKC also maintains an 'Info-Mobile' for example, which provides information at events and thereby reaches people who are not actively looking for information.

Evaluation of the property. Trained experts evaluate the building. In addition to the topography of the environment, other features are factored in including the hydrological conditions, location with respect to bodies of water, the mode of construction, materials and much more. The property owner receives a document for the property which sets out the risk assessment for the building by categorising it using a traffic light system.

Recommendation of measures. Independent precautionary measures tailored to the property are recommended by the experts; after successful implementation, the property can be re-categorised into a lower risk category.

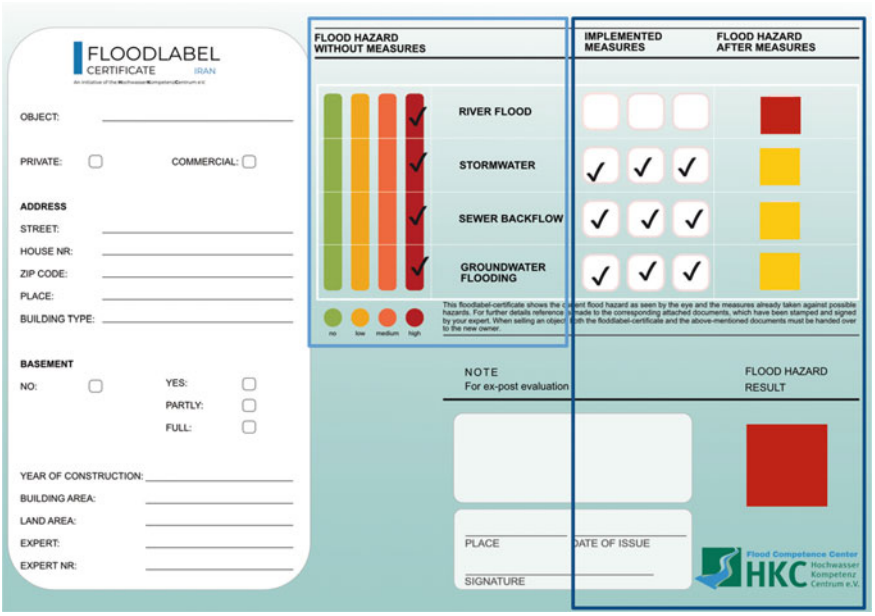

Fig. 21.2 Floodlabel certificate, Categorization of risks of a house to flooding—light blue frame: vulnerability of house without protection measures, dark blue frame: Realized protection measures and vulnerability of house with protection measures

Implementation by the citizens. The recommended measures are implemented voluntarily, furthermore the concern for operational capability is important. This presumes both the technical operability and also the competence of the user, if e.g., an emergency seal must be applied.

21.3 FLOODLABEL International

21.3.1 Transfer to Other Countries

As flooding and heavy rain occur worldwide and therefore private precautions are also of international interest as a building block for the resilience of a population, the Floodlabel is to be adapted for international use. The successful transfer of the above-described concept requires much more than just a simple linguistic translation. Comprehensive analyses and adaptations must be performed for the implementation of the described stages.

At times, circumstances internationally can vary significantly. For example, we should note the quantity and quality of available data, the stipulations from authorities and how implementation is controlled, urban planning and the actual development,

the different construction methods and materials and the lifetime of buildings. In addition, information that is adapted to the needs of the population is to be compiled and the means and channels of communication adjusted to local and cultural norms. The principles of risk assessment must be set down by trained personnel—where they are not already present—by performing large-scale analyses with respect to the hydrological conditions, topography etc.. Decision support systems must be developed to assess the risk of flooding of properties. Moreover, sensible precautionary measures are to be identified. Training materials for the education of experts must be developed and/or adjusted. The area of application of the Floodlabel can therefore only be expanded by embedding it in larger cooperative projects and can now, after the JPI Urban Europe Project, be implemented via PARADeS for Ghana and HoWaMan for Iran.

21.3.2 Adaptation to Unforeseen Conditions

During the initiation phase of the projects, the boundary conditions were significantly different from those currently prevailing: research visits were planned to gather data regarding house construction types, residents were to be surveyed about their own experiences and their personal risk assessment, networks were to be created and similar. These visits are now impossible for the foreseeable future due to COVID-19-related travel and contact restrictions, but this situation is being used to develop methods for adapting the Floodlabel that are as transferable internationally as possible.

To this end, digitally available data is used in the new context; thus, for example, information is obtained from satellite images about the type and density of buildings. This is then compared with statistical data which together with further research and, if required, surveys including those by partners on site offers information about representative house types.

An online questionnaire, that had already been designed with a view to international use and can be distributed via various information channels, provides additional information, and reveals possible communication channels that can be used later for information provision. The results of the online survey must be critically reviewed but, in this context, they already offer many insights into the particular needs of the various user groups. By making contact in this way, the issue of private precautions is already addressed, and it is communicated and represented visibly together with the partners on site, making it possible to start already at this early stage with the implementation of important components of the Floodlabel concept, despite the current special circumstances.

21.4 FLOODLABEL in Ghana

Ghana is already one of the most flood-affected countries in West Africa and the frequency and intensity of flood events will increase in the coming years due to climate change (Almoradie et al. 2020; World Bank 2011; IPCC 2012). From 1950 to 2020, more than five million people in Ghana were affected by flooding. On average, each flood in this period impacted 200,000 people and each flood event caused average economic damages in the amount of US$ 5.2 million (Centre for Research on the Epidemiology of Disasters 2020). The increasing number of floods and the rising number of those affected, of damages and of deaths correlate, which is why the development of prevention and coping strategies is required to increase the resilience of the population. $\text{Floodlabel}_{\text{GHANA}}$ aims to contribute here to strengthening personal provision. The three project regions were selected taking into consideration the flood risk and the water supply and sanitation infrastructure (Fig. 21.3).

The most southernly project region, the catchment area of the Odaw River, stretches from the Aburi Mountains in the Eastern Region to the Korle Lagoon in Accra. The region is at risk from pluvial, fluvial and coastal flooding (Centre for Research on the Epidemiology of Disasters 2020; Karley 2009; Water Research Institute (WIR) 2011; Ansah et al. 2020). The south-westerly region around Kumasi is criss-crossed by rivers and streams. The river basins are largely flood plains. Along with fluvial flooding, Kumasi is also at risk of pluvial floods. The third project region is the catchment area of the White Volta River in the northern regions. In Northern Ghana, heavy rains and overflow from the Bagre Dam upriver in Burkina Faso lead to extensive flooding upriver in Burkina Faso (Armah et al. 2010).

The climate in Ghana is influenced by monsoon winds and is tropical year-round (Portal 2020). In Accra more than 50% of precipitation falls in the main rainy season from May to July. The rainy season in Kumasi reaches its high point in June and July. It is in these months that most flood events in the region are recorded (Campion and Venzke 2013). The north has a unimodal rainy season (May to September), with peak values at the end of August and the start of September (Armah et al. 2010; United Nations Office for the coordination of humanitarian affairs (UNOCHA) 2007).

In Accra, in particular, population pressure and the housing shortage mean that 25% of the population live in flood-prone areas, whereby almost half the city is considered at risk of flooding (Karley 2009) and flood protection measures are underdeveloped. Low-income areas in Ghana, particularly in Accra, are frequently impacted by flooding (Douglas et al. 2009; Amoani et al. 2012; Codjoe et al. 2014) (Fig. 21.3). Despite this, studies show that the population in flood-prone areas of Accra has increased steadily since 2000 due to informal urbanisation (Ghana Statistical Service United Nations fund for population activities (GSS UNFPA) 2005; Accra Metropolitan Assembly (AMA) 2011). In informal settlements, in particular, the overall concept of the Floodlabel should improve information supply and thus has great potential to increase the resilience of the population. Even people who do not own a house or property can benefit from precautionary information. They can

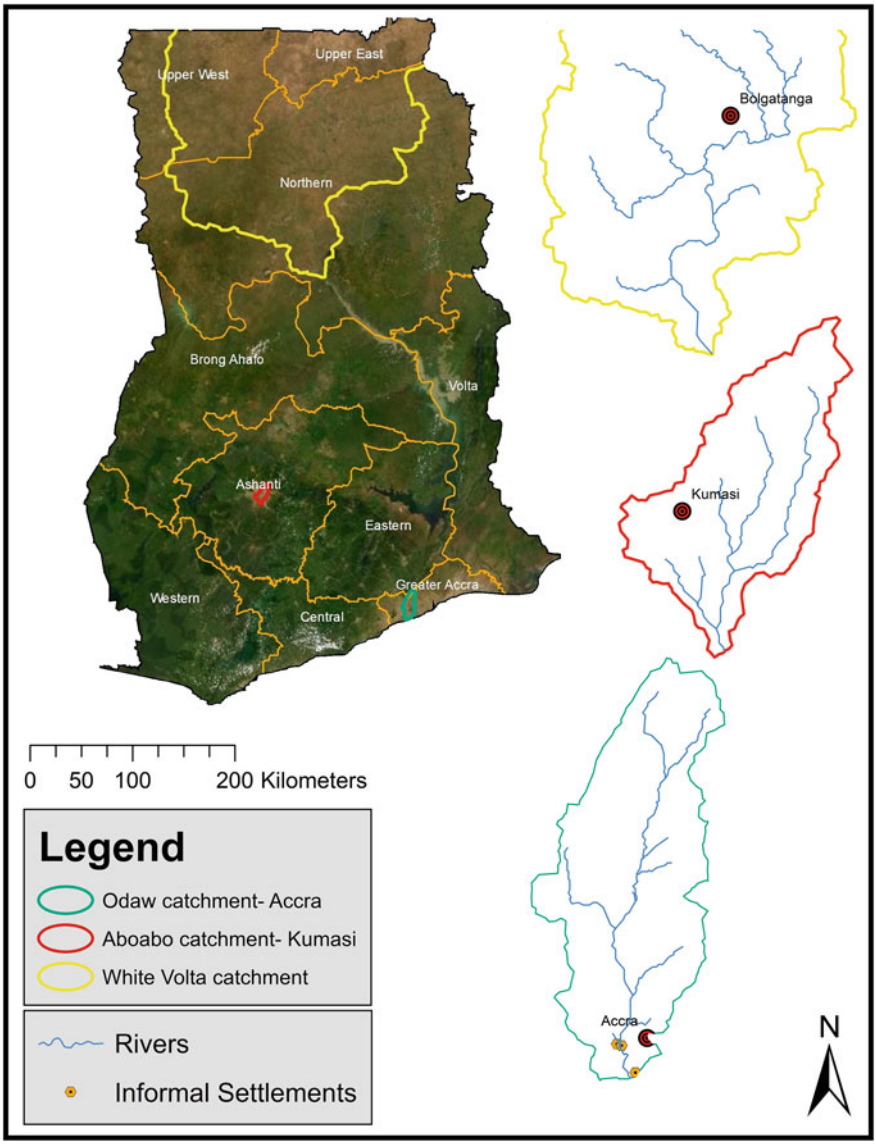

Fig. 21.3 Overview map of the project regions in Ghana

obtain information about the risk status of their accommodation and, if required, protect their property and find safe escape routes and/or places to stay.

For the conceptual design of the Floodlabel, it is critical that, in addition to population trends and development structure, an awareness of flood hazards on the part of the population and their risk perception be taken into consideration. For Ghana, an online

questionnaire was created, the results of which are to form the first data basis for the elaboration of the Floodlabel. The population can access and participate in the survey via an online link using any available Internet-capable end device. The questionnaire is being disseminate in close cooperation with the Ghanaian project partners, the Water Resources Commission (WRC) and the National Disaster Management Organization (NADMO), who are using their extant communication channels and contacts to disseminate the questionnaire, and thus visibly represent the topic. In addition to an information basis regarding the personal risk assessment, experience with flooding, the development structure and the building construction, insights are also gained into the existing supply of information and actor-specific means and channels of communication. By comparing the distribution channels of the online questionnaire link, conclusions are drawn regarding the understanding of the communication means, via which the population in its diversity with respect to age, education, gender etc. in all parts of Ghana can and want to be reached.

The results from the online questionnaire are supplemented in a second step by an on-site survey of the population in the areas under examination, so that representative results from all three project regions are available and it is ensured that even those people who do not have access to the Internet or an end device are taken into consideration. The on-site survey also serves to validate the online questionnaire. Based on the results and further studies, the comprehensive concept of the Floodlabel, taking into consideration the otherness of the natural risks and the construction method of houses, is adapted to the social and cultural circumstances, transferred to Ghana and implemented.

21.5 FLOODLABEL in Iran

Given its location in an arid and semi-arid region, Iran is facing a very particular set of challenges. The low probability of occurrence of flood events compared to humid regions, and their stronger spatial and temporal fluctuations lead to a low risk awareness regarding flooding on the part of both the public authorities and residents. The combination of flood events, an unprepared civilian population and limited capacity to act on the part of the public institutions can lead to significant consequences. There have already been floods in the past following heavy rainfall, which at times have caused serious damage to local infrastructure. One example is the flooding of the Tehran subway system in 2012, which caused damages in the order of US$ 21 million (Taghizadeh et al. 2013).

According to Hooshyaripor et al. (2020), Yazdi et al. (2013) and (Nezammahalleh and Tali 2013) the number of floods in Iran in recent years has increased. According to an evaluation of data by the “Centre for Research on the Epidemiology of Disasters” (Centre for Research on the Epidemiology of Disasters 2020) there were 93 significant floods in Iran in the period between 1950 and 2020 with total economic damages both direct and indirect of almost US$ 13 billion. In the same period, 8,169 people lost their lives due to flooding while 14,329,120 were impacted. In contrast to

the previously named sources however, no clear trends can be derived from the data. The number of flood events, deaths, persons affected and economic damage further display a strong variance between the years and decades, which is typical of a semi-arid climate, and could thus explain the low risk awareness among the population. Moreover, according to (Bundesministerium für Verkehr und digitale Infrastruktur (BMVI) 2020), floods and heavy rain events could increase in Iran in the future, driven by climate change, leading to a worsening of consequences.

Infrastructural measures taken by governmental authorities and flood risks communication could reduce the potential damage experienced by residents. Compared to Germany, however, there are neither defined measures to reduce flood damage nor any risk information. Private action to reduce possible damages caused by floods thus has a high priority and great potential in Iran. At this point the Floodlabel can help by conveying information on flood risks and potential risk reduction measures with the aim that these will be implemented by residents as private precautionary measures.

In Iran, the river basin of the Kan (Fig. 21.4) is a representative example of a catchment area in which historically numerous flash floods have occurred due to its steep mountain terrain, sparse vegetation and short hydrological times of concentration. The considerable population growth in the twentieth and twenty-first centuries, due to modernisation, centralisation and internal migration, has further led to a high level of urbanisation of Tehran, whose metropolitan area now covers large parts of the Kan catchment area. The development history of the city is evidence of the low risk awareness of flooding on the part of the population, in that scant regard has been given to the natural characteristics of the catchment area. The changes that have been brought about have changed the runoff behaviour of the Kan, which is expressed in an increased flood risk (Yazdi et al. 2018; Nezammahalleh and Tali 2013; Masnavi et al. 2016).

In order to increase the resilience of the population, a Floodlabel is needed that is adapted specifically to the needs of the residents, including:

- Local flood risks,
- Vulnerability of buildings,
- Measures to enhance private precautions, and
- Conceptual design of the Floodlabel – taking into consideration the cultural and institutional circumstances.

Against the backdrop of the Covid-19 pandemic, alternative approaches have been required at times to procure data for the Floodlabel adaptation. In addition to hydrological and hydraulic modelling methods, literature reviews have been performed for the analysis and evaluation of flood risks in Floodlabel. To identify weaknesses in buildings with respect to the risks, analyses of the development structure using GIS-based methods have been performed with remote sensing data and verification using the literature. The derivation of vulnerabilities from the development structure and the identification of effective private precautionary measures are only possible to a limited extent, however, and must be supplemented by surveys developed specifically to this end, and by expert interviews. Given the cultural, institutional and political

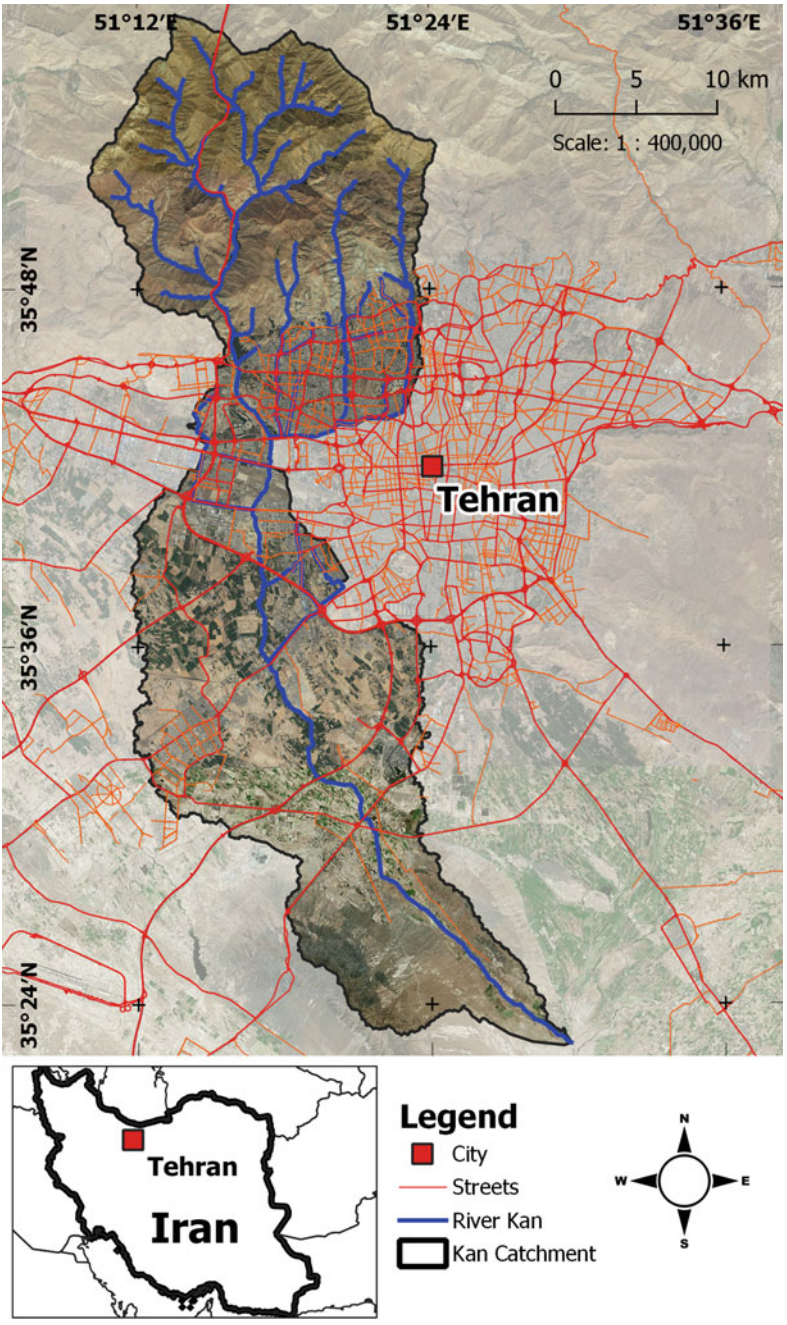

Fig. 21.4 Overview map of the project regions in Iran

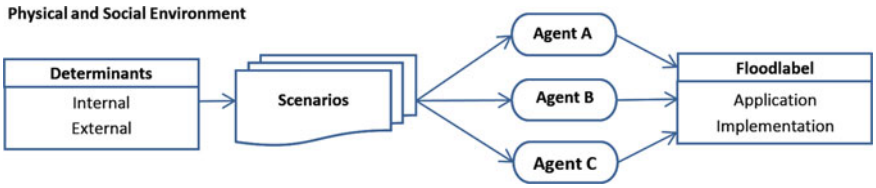

Fig. 21.5 Agent-Based Modelling (AMB)—Conceptual Framework

circumstances, research into and the trialling of effective communication channels is also required here. To enhance general acceptance and understanding of the interplay between actors and effective implementation of the Floodlabel, innovative methods such as Agent-Based Modelling (ABM) should be used. ABM is a new technique of microscopic modelling, used to understand the dynamics of complex systems from the characteristics and behaviour of autonomous and interactive agents within an environment (World Bank 2011; IPCC 2012;). As Fig. 21.5 shows, a conceptual experiment set-up aims to examine the consequences and relationships of the main actors in the Floodlabel procedure, the "agents".

The agent classes are set up within the physical and social environment and connected in a defined geographical space. Relevant determinants, i.e. internal and external factors, are identified and their impact on the behaviour of individual agents, and thus their decision to use the Floodlabel and implement private precautionary measures, is analysed. Factors should be varied in different scenarios, with the aim of finding efficient strategies to implement the Floodlabel and thus come closer to achieving the goal of a flood-resistant society.

21.6 Outlook

A resilient society is a joint effort. Ways must be found to optimally complement the protection measures of the public sector with private prevention measures. It needs to be clearly shown where the limits of large-scale public infrastructure measures are and where sensible personal preventions need to be realized. Further research is needed on this particular issue. The concept of the Floodlabel must be adapted to the specific conditions of the country where it is to be applied. Means of transferability of such concepts should therefore be explored in the future. Research should aim to provide tools and recommendations on how the Floodlabel can be efficiently and easily adapted to local conditions, i.e. which existing flood hazards, building structures, cultural and institutional characteristics are given, and what kind of guidance on the necessary data required for the adaptation of the Floodlabel depending on availability and scope of implementation is needed for each of the regions.

Focus must be especially placed on people who live under vulnerable conditions and hence are limited in their capability to adapt to the recommendations given in order to be able to protect them sustainably. The development of cost-effective

flood protection measures for the private sector needs to be further investigated. To ensure that private measures actually increase resilience, it goes without saying/is compulsory is imperative that a public institution promotes and manages the implementation of the Floodlabel. It is necessary to conduct a detailed examination of the awareness of the population towards private flood precautions, and how perception of the issue can be increased and strengthened. Investigations should also be conducted to ascertain if the willingness to take precautions increases through the promotion of external factors such as incentive mechanisms (e.g. financial support, insurances and subsidies), capacity building or regulations and which factors have the greatest impact.

With climate change and rapidly growing urbanization the increasing level of flood risk, being fluvial or pluvial, becomes an increasingly severe challenge all over the word. Therefore, the Floodlabel together with the measures and studies listed are not only urgently needed, in addition they will also pay off at the flood events to come to achieve a flood resilient society.

Acknowledgements The HKC is a partner in the projects "Participative Flood Prevention and Adapted Coping Strategies in Ghana—PARADeS" and "Sustainable Strategies and Technologies for Flood Risk Management in Arid and Semi-Arid Regions—HoWaMan" in Iran. The cooperative projects are supported as part of the dissemination of "International Catastrophe and Risk Management—IKARIM" project of the BMBF (Federal Ministry for Education and Research) and within the framework of the Federal government's programme "Research for Civil Security". The PARADeS project is coordinated by the Geographical Institute of the Rheinische Friedrich-Wilhelms-Universität in Bonn. The HoWaMan project is run by the Institut für Wasserbau und Wasserwirtschaft (IWW) at RWTH Aachen.

References

Accra Metropolitan Assembly (AMA) & United Nations Human Settlements Programme (UN-Habitat): participatory slum upgrading and prevention. Millennium City of Accra, Ghana (2011)

Almoradie A, Brito Md, Evers M, Bossa A, Lumor M, Norman C, Yacouba Y, Hounkpe J (2020) Current flood risk management practices in Ghana: gaps and opportunities for improving resilience. J Flood Risk Manag

Amoani KY, Appeaning-Addo K, Laryea WS (2012) Short-term shoreline evolution trend assessment. A case study in Glefe, Ghana. J Disaster Risk Stud 4(1):1–7

Ansah SO, Ahiataku MA, Yorke CK, Otu-Larbi F,Yahaya B, Lamptey PNL, Tanu M (2020) Meteorological analysis of floods in Ghana. Adv Meteorol

Armah PNL, Yawson DO, Yengoh GT, Odoi JO, Afrifa EKA (2010) Impact of floods on livelihoods and vulnerability of natural resource dependent communities in Northern Ghana. Water 2:120–139

Bundesministerium für Umwelt, Naturschutz und nukleare Sicherheit, KLIVO—DEUTSCHES KLIMAVORSORGEPORTAL. https://www.klivoportal.de/SharedDocs/Steckbriefe/DE/HochwasserPass/HochwasserPass_steckbrief.html. Last Accessed 13 Oct 2020

Bundesministerium für Verkehr und digitale Infrastruktur (BMVI), GOVDATA Das Datenportal für Deutschland, Raster der Wiederkehrintervalle für Starkregen (Bemessungsniederschläge) in Deutschland (KOSTRA-DWD)–ASCII. https://www.govdata.de/suchen/-/details/raster-der-

wiederkehrintervalle-fur-starkregen-bemessungsniederschlage-in-deutschland-kostra-dw. Last Accessed 30 Oct 2020
Campion BB, Venzke JF (2013) Rainfall variability, floods and adaptations of the urban poor to flooding in Kumasi. Ghana Nat Hazards 65(3):1895–1911
Centre for Research on the Epidemiology of Disasters—CRED, EM-DAT The International Disaster Database. https://www.emdat.be/. Last Accessed 24 July 2020
Codjoe NAS, Owusu G, Burkett V (2014) Perceptions, experiences and indigenous knowledge of climate change and variability. The case of Accra, a sub-Saharan African city. Reg Environ Chang 1:369–383
Douglas I, Alam K, Maghenda M, McDonnel Y, McLean L, Campbell J (2009) Unjust waters: climate change, flooding and the urban poor in Africa. Environ Urban 20(1):187–205
Fekete A (2012) Safety and security target levels: opportunities and challenges for risk management and risk communication. Int J Disaster Risk Reduct 67–76
Ghana Statistical Service & United Nations fund for population activities (GSS & UNFPA): Population Data Analysis Report: policy implications of population trends. Ghana Statistical Service (2005)
Haer T, Botzen WJW, Aerts JCJH (2016) The effectiveness of flood risk communication strategies and the influence of social networks—Insights from an agent-based model. Environ Sci Policy 44–52
Handmer JW (1980) Flood hazard maps as public information: an assessment within the context of the Canadian flood damage reduction program. Can Water Resour J 4:82–110
Hooshyaripor F, Faraji-Ashkavar S, Koohyian F, Tang Q, Noori R (2020) Evaluation of the probable annual flood damage influenced by El-Niño in the Kan River Basin. Iran Nat Hazards Earth Syst Sci 20(10):2739–2751
Höppner C, Buchecker M, Bründl M (2010) Risk communication and natural hazards. CapHaz-Net WP5 report. Swiss Federal Research Institute WSL, Birmendsdorf, Switzerland
IPCC: managing the risks of extreme events and disasters to advance climate change adaptation. The World Bank, Washington DC (2012)
Johann G (2020) Die App FloodCheck—einfache und direkte Information zur Hochwasser- und Starkregengefahr vor Ort [The FloodCheck app - Simple and direct information on flood and heavy rain risks on site]. Korrespondenz Wasserwirtschaft 7:350–351
Karley NK (2009) Flooding and physical planning in urban areas in west Africa: situational analysis of Accra, Ghana. Theor Empir Res Urban Manag 4(13):25–41
Masnavi MR, Ghobadi M, Farzad Behtash MR, NeginTaji MR (2016) Restoration and reclamation of the river valleys' landscape structure for urban sustainability using FAHP process, the case of Northern Tehran-Iran. Int J Environ Res 10(1):193-202
Nezammahalleh AM, Tali MG (2013) Urban flooding management by using the natural ddrainage system: case study Tehran captial of Iran. Floods Risk Oppor IAHS Publ 357:174–180
Portal CCK, The World Bank Group. https://climateknowledgeportal.worldbank.org/. Last Accessed 12 Nov 2020
Taghizadeh AO, Soleimani SV, Ardalan A (2013) Lessons from a flash flood in Tehran subway. PLOS Current Disasters, Iran
United Nations Office for the coordination of humanitarian affairs (UNOCHA): Ghana Floods Flash Appeals (2007)
Water Research Institute (WIR): prevention of hydro-hazard disaster in Ghana: update of flood phenomenon in Ghana—draft report. UNESCO Cluster Office, Accra
World Bank (2011) Disaster risk management programs for priority countries. The World Bank, Washington DC
Yazdi J, Mohammadiun S, Sadiq R, Neyshabouri SS, Gharahbagh AA (2018) Assessment of different MOEAs for rehabilitation evaluation of urban stormwater drainage systems—case study: eastern catchment of Tehran. J Hydro-Environ Res 76–85

Yazdi J, Neyshabouri SS, Niksokhan M, Sheshangosht S, Elmi M (2013) Optimal prioritisation of watershed management measures for flood risk mitigation on a watershed scale. J Flood Risk Manag 372–384

Chapter 22
Sustainable Environmental Planning of a Tourist Destination Bulgaria—State and Trends

Elenita Velikova

Abstract The research object is Bulgaria as a tourist destination. Research subject is sustainable environmental planning for tourism purposes. The competitive usage of the territory imposes the search of possibilities for carrying out a few different and sometimes mutually excluding activities. Careful environmental planning is needed, and in order for it to be sustainable, it must not violate the right of future generations to use this territory as well. The tourism is a spatial phenomenon and is a very important sector of the Bulgarian economy. Its sustainable development is a priority for the government of the country. The Ministry of tourism is developing a targeted policy towards establishing the field and is trying to introduce some relieves so it can help the tourist companies in overcoming the current crisis. Significant progress in the development of tourism provides the division of the territory into nine tourist regions, which aim to stabilize the tourist supply in Bulgaria. The publication aims to analyse the development of regulations in the field of spatial planning, to show the progress made in terms of tourism environmental planning and on this basis to outline trends in the future development of the destination Bulgaria.

Keywords Tourism · Sustainable environmental planning · Bulgaria · Tourist regions

22.1 Introduction

The accelerated development of the tourism industry in the modern world has led to increased interest in the process of sustainable destination planning. This interest is dictated by the reduction in the growth of industrial production and the sustainable progress of the tourism industry until 2019. The implementation of local policy in the global market further intensifies the trend. The gradual increase in available revenues in the industrialized western economies, combined with the increased mobility, leads

E. Velikova (✉)
University of National and World Economy, Sofia 1000, Bulgaria
e-mail: evelikova@unwe.bg

H.-Y. Jeon (ed.), *Sustainable Development of Water and Environment*,
Environmental Science and Engineering,
https://doi.org/10.1007/978-3-030-75278-1_22

to the achievement of new horizons in the tourism industry at geographical, demographic and cultural level. This creates new problems in the field of economic, social and environmental management.

Although the crisis caused by the Corona virus has had a significant impact on the tourism industry, the outlook for the sector is not so bad. In historical context, tourism is characterized by significant resilience to crises and shows a rapid recovery within tactical periods of time. That is why the issues that are essential for its future development should not be diverted from the focus of attention. This gives us a reason in this publication to focus on the opportunities for sustainable environmental planning in Bulgaria for tourism. The availability of research on the issue is not a prerequisite for finding adequate solutions, and achieving sustainable development in most cases is impossible. In territorial terms, Bulgaria is developing chaotically as a tourist destination, without a strategy and plan for the future. In our opinion, the traditional models and processes of spatial planning for the purposes of tourism have exhausted their applicability, which is why they need to be reconsidered.

The research object in the publication is a tourist destination Bulgaria, and the research subject is the state and trends in sustainable spatial planning of tourism. The thesis is defended that sustainable planning of the tourism territory is a prerequisite for overcoming the crisis and the future better development of tourism in Bulgaria.

22.2 State of the Problem and Literature Review

In the literature on environmental tourism planning there is ambiguity regarding the normative and positivist approach both in relation to the description and analysis of the studied categories and in the application of the rational and practical approach (Burns 1999). To be sustainable, the planning process must be studied and analysed in a social and ecological context (Vasileva and Nikolov 2018). This is partly due to the complexity and diversity of tourist activities. The specific legislation in the country has an additional influence on the establishment of the key factors and the connections determining the final result (Nikolov and Botseva 2018). First of all, we must have in mind that the process of tourism planning is subjective. This process is considered to depend on the relationship between the rational and technical context of the different levels of decision-making, as well as the political and symbolic context according to which these decisions are taken and implemented. Secondly, the planning process should be seen as an ongoing reconciliation of the different and sometimes mutually exclusive interests of the company and industrial benefits, as well as environmental issues (Velikova 2010).

The answer to the growing challenges for tourism in territorial terms can be given by the planning science. However, this does not mean taking planning action against an individual guest house, hotel, tourist resort or business. Centralized coordination of actions across the country or even a region (e.g. the Balkans) is needed. The goals to be achieved are to ensure the achievement of an optimal tourism development (Botseva et al. 2020). Only in this way can the respective tourist region achieve what

the other competing regions cannot. Unexpected situations force countries to be in different situations and uncertain environment which are accompanied by different obstacles and are characterized by complexity and dynamism hence they need a planning (Bogomilova 2020).

Planning has been involved in tourism literature for a long time (almost 90 years). Naturally, each element of which the tourist product is composed, considered as a result of the total tourist activity, is subject to planning. Planning for the future, setting goals and making decisions about their realization is a relative measure that helps to achieve such results, which are part of our daily lives. Sustainable environmental planning is aimed at coordinating the planning activities of all participants located within a limited territorial structure. Its objects are the economy, social and cultural life, infrastructure, housing conditions and the structure of the local population, local organizations and institutions, the natural environment of the territory and others (Velikova 2010).

Therefore, the study of the environment is interdisciplinary and contains both applied and fundamental aspects. The object of knowledge are parts of the earth's surface (more precisely the geosphere) at various levels of scale (e.g. cities, regions). The purpose of the study of the territory is the registration, description and explanation of structures, processes and ways of functioning of space-related problems between man (in particular the tourist) and the environment (Velikova 2017). The acquisition of this knowledge aims to achieve sustainable development of space.

Environmental planning is the totality of all planning means used in the development, compilation and implementation of the structural and spatial order of a given territorial unit. The system to be developed, i.e. the spatial plan is inextricably linked with the fact that the order and development of space should not be an end in itself, but a means and part of the policy for the society development (Müller 1990). Environmental planning is more than the layout of a village, workplace, educational institution or a resort. It is part of the daily formation of the social relationships that define our lives.

Environmental planning requires a study of society (in all its activities), the economy, ecology, settlement structure and geographical location in their functional relationship. As a result, structural plans are being developed and should be implemented. In this process, the separation of the study of space from its planning is conditional, because the study of the territory (as an initial stage), local, regional, settlement, etc. planning represent the stages of implementation of environmental planning (Evrev 1999).

One of the main tasks of environmental planning is the correct allocation of the respective spatial resource for different, in most cases competing, use. Environmental planning of tourism is the spatial level of planning of the functional direction tourism in the unified process of spatial planning, which creates a territorial basis for the optimal tourism development (Evrev 1999). The planning of the territory is also related to the quality of the subsequently offered tourist product. In tourist regions, it is not only the quality of the services offered by enterprises, but also the quality of the environment in which they are produced and consumed and in which the reproduction of human resources takes place, as well as the other environmental

conditions necessary for the functioning of each enterprise (Velikova et al. 2017). The possibilities of the tourist product to satisfy the consumer needs also depend on the quality and variety of the elements in the territory, representing resources for the implementation of the tourist activity or attraction.

In addition, determining the places for tourist use is also a task of environmental planning, i.e. environmental planning of tourism is the basis for the development of any type of tourism. Allocation should be done efficiently, which means sparingly using (public) goods to maximize positive and minimize negative effects (Velikova 2010). Among the positive effects of tourism, we must first mention the economic benefits, such as the improvement of the balance of payments (in international tourism), additional income, increased employment and tax revenues (Velikova et al. 2017). In addition, tourism acts as a catalyst for the development of other sectors in the territory. It also contributes to the preservation of cultural heritage and natural landmarks, for which there are often insufficient funds. The sector creates leisure, cultural and economic opportunities for both tourists and locals (Velikova 2019). It is no coincidence that in the current situation, all countries are making efforts to save the tourism sector, because the eventual bankruptcy will have consequences in many other sectors.

However, tourism also causes a number of problems, such as economic distortions (rising property prices in tourist regions), destruction of the environment, loss of cultural identity and integrity, as well as the strengthening of existing prejudices against other nationalities (UNEP 2021). Effective planning and policy measures need to be taken to optimize the benefits in an appropriate way and to reduce the disadvantages. In particular, sustainable environmental planning of tourism is imposed because of the following reasons: (1) Tourism is a complex system that interacts with other systems and sectors (agriculture, trade, transport, etc.). Coordinated planning and development is needed to integrate these areas into both tourism and public use. (2) The tourism industry sells a product that is compared to certain previous events or previously provided services, depending on experience. This requires an accurate analysis of tourism preferences and the individual decision-making process, without, however, neglecting the objectives related to environmental protection and cultural and historical heritage. (3) Tourism has both positive and negative impacts in the field of socio-economic development. Sustainable environmental planning can help create development strategies that minimize mistakes. (4) The development of tourism opportunities, as well as the activities of tourists in the narrow sense, have both positive and negative impacts on the environment. Careful planning is absolutely necessary to develop the type of tourism and to such an extent that do not lead to disturbance of the ecological balance in the environment. (5) Environmental planning of tourism must comply with the principles of sustainable development. Natural and cultural-historical resources should not be destroyed, but should be preserved for future generations. (6) The application of sustainable environmental tourism planning also requires specialized organizational structures, marketing strategies and legal provisions (Velikova et al. 2017).

The specific objectives of sustainable environmental tourism planning, in turn, can be summarized as follows: economic success, environmental protection, sustainable

development and local integration, i.e. acceptance by the local population. Planning activities must ensure the functioning of the tourism system that does not harm the environment and does not destroy it. In addition, companies operating in the tourism market achieve economic success both for their own benefit and for the benefit of the national economy and society as a whole (Velikova 2019). There is a need for such exploitation of the available resources, which combines the principles of preserving the cultural wealth, of maintaining the ecological and economic balance, without harming the future generations. Last but not least, it is necessary to integrate the local population in tourism activities, which, on the one hand, contributes to its financial prosperity and, on the other hand, to increase its cultural and educational level.

22.3 Research and Results

Sustainable environmental planning cannot happen without the intervention of the institutions. Their main role is to build an appropriate regulatory framework to distribute uneven demand and competitive use of territorial resources. The study provides a basis for assessing progress and gaps. To establish the current state in sustainable environmental planning of a destination Bulgaria, the historical, normative, expert and method of observation are used. This study includes the entire territory of the country with the opportunity to offer tourism. Expert analysis based on available data, observation and personal experience is attached. The research methods are based on general scientific principles and main achievements of economic theory, global regionalism and modelling of economic processes, which are carried out in the field of tourism. The methodological fundamental is based on the methods of abstraction, dialectics, logic, retrospection, structural and systematic approach to analysis, expert research. We examine the regulations for spatial planning and subsequently the tourist experience and the models for planning and management of the tourist territory.

22.3.1 Retrospective Analysis of the Territory Uses in Bulgaria

In Bulgaria, the first step in the field of territorial organization of settlements is the development of the Kingdom of Bulgaria (1897), which affects only settlements (blocks of at least 50 houses located in one place). At the same time, the preparation of a plan-record of street plans, regulation plans and vertical planning is envisaged. The next actions on the subject of the Law on the Improvement of Settlements (1941) are: envisaging the development of general plans as a basis for the transformation and development of the city and its surroundings. The law regulates rules and norms for

building the development of human settlements. It also provides for supervision over the activity of construction and observance of the rules and norms, which are carried out by the local municipal and state technical bodies (Ministerstvo na regionalnoto razvitie i blagoustroĭstvo, Istorichesko razvitie na administrativno-teritorialnoto ustroĭstvo na teritoriyata na Bŭlgariya 2021).

Political, social and economic changes in the 1990s necessitated the creation of a new law in this area. This is the Spatial Planning Act (2001), which is currently in force. According to him, the state is obliged to create a comprehensive planning scheme on the country territory (National Scheme for Integrated Development), as well as for administrative regions (district development schemes). The local government is obliged to create general and detailed development plans (Zakon za ustroĭstvo na teritoriyata 2021).

In the 80 s, in the period of centralized planning, Bulgaria had a plan for unified territorial development of the entire national territory. After the democratic changes in Central and Eastern Europe during the 1990s, the planning process was abandoned and neglected. Even before 1998, when the practice of planning was restored, the way to a decentralized approach was opened on a new, much broader basis. The planning process is carried out in connection with the implementation of the Regional Development Act (1999). In addition, a National Regional Development Plan and regional development plans are being developed (Velikova et al. 2017).

The Spatial Planning Act provides for the development of regional development schemes, but work in this area has not yet begun. In accordance with the Regional Development Act, the process of developing regional development plans is underway. It is recommended that these plans must be coordinated with the regional development schemes (Zakon za ustroĭstvo na teritoriyata 2021). The successful results of this initiative will depend both on amendments to the Regional Development Act and on its harmonization with the Spatial Planning Act. The development of municipal development plans is hampered by financial deficits. According to the Spatial Development Act, this is the responsibility of the municipalities (UNEP 2021). However, under the Regional Development Act, many municipal development strategies and action plans have been developed during the period 1999–2000. The forthcoming update must take into account municipal development plans so that a territorial basis for economic and social planning is provided.

Finally, it should be noted that local planning practices have been developed and municipalities have more planning experience and skills, including public participation in meetings and municipal forums. To a large extent, tourist activities are carried out at the municipal level. Therefore, the achieved sustainable planning at this level is a good prerequisite for the future development of tourism.

22.3.2 The Tourist Experience

At national level the tourism in Bulgaria is managed by the Ministry of Tourism. It was created by the National Assembly in 2014. The management of the sector was given to

different institutions since 1989, and before the establishment of the current ministry was prerogative of the Ministry of Economics, Energy and Tourism. The Ministry of Tourism works closely with the private sector and other stakeholders as well as collaborates with regional and local tourism bodies listed in the National Tourism Register. At the regional level, authorities develop and implement tourism strategies and programs in line with national tourism and regional development strategies. The Tourism Act regulates the co-ordination associated with the interaction of the State and municipalities in the implementation of activities related to tourism, as well as the participation of not-for-profit legal entities. The Tourism Act makes provisions for local authorities to adopt tourism development programs according to local resources and need, and establishes an Advisory Council on Tourism and a Municipal Commission to oversee the development of tourism related facilities (Ministerstvo na turizma 2021) (Figs. 22.1 and 22.2).

Recent legislative changes have led to the establishment of Regional Tourism Management Organizations. The members of these include tourism associations, regional and municipal administrations, institutes, museums, scientific bodies and tourism schools. The Regional Tourism Management Organizations are responsible for regional tourism product development and marketing of the nine identified tourist regions in Bulgaria (Kontseptsiya za turistichesko raĭonirane na Bŭlgariya 2021). Concept for tourism regions was created. Nine tourism regions that cover the whole country were devised in 2015. For every region a city-centre was chosen in which an organization for management should be established. Every region has main and additional tourism specialization. The regions are the following:

According to the Ministry of Tourism, the tourist regions must reflect the realities of the tourist potential and of the modern tourist development, incl. and existing organizational structures. To define a tourist area, it is necessary to have significant attractions that provide a wide enough range of opportunities for tourists, attract significant number of tourist and allow longer stay (Kontseptsiya za turistichesko raĭonirane na Bŭlgariya 2021). The tourist area must be large enough to be able to present itself on the international market as a stand-alone, recognizable tourist product. Tourist areas must be territorially complete, not overlap and ensure the supply of a complex tourist product. They must comply with the municipal division (one municipality should not be divided) and take into account the territorial scope of the already established voluntary regional tourist associations (Kontseptsiya za turistichesko raĭonirane na Bŭlgariya 2021) (Table 22.1).

The main criteria that form the decision-making process of the Ministry of Tourism for the tourist zoning are geographical location; natural, socio-economic and cultural features; resource potential (existing attractions or opportunities for their development); regional identity (a specific set of natural, cultural and social characteristics that create a sense of regional identity); transport connectivity of the different parts of the region; accommodation base (volume, structure); opportunities for effective creation of the necessary services (hotel, restaurant, medical, communication, information services, etc.); technical, social and tourist infrastructure; tourist flows (volume, structural characteristics, spatial behaviour); appropriate spatial combination between attractions (resources), transport and axes and available or potential

Table 22.1 Touristic regions of Bulgaria

No	Region name	City-centre
1	Danube	Ruse
2	Stara Planina	Veliko Tarnovo
3	Sofia	Sofia
4	Trace	Plovdiv
5	Rose Valley	Kazanlak
6	Rila-Pirin	Blagoevgrad
7	Rhodopi	Smolyan
8	Varna	Varna
9	Burgas	Burgas

Source Concept for tourist zoning of Bulgaria (Kontseptsiya za turistichesko raĭonirane na Bŭlgariya 2021)

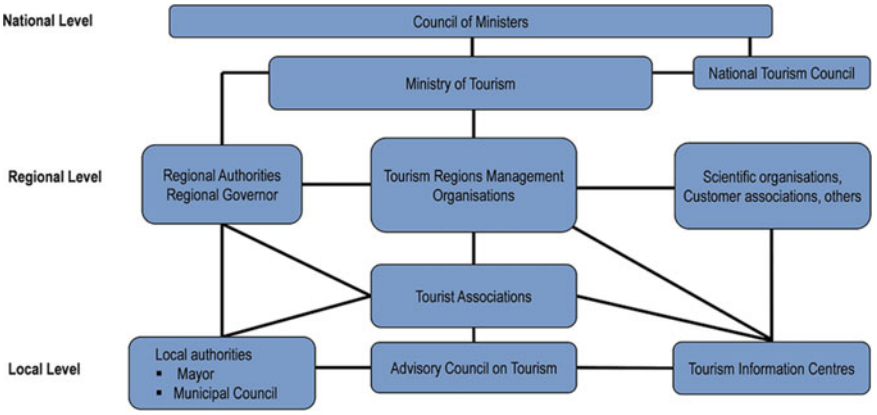

Fig. 22.1 Levels of tourism management. *Source* OECD, adapted from the Ministry of Tourism, 2020

services; possibility to present as complete destinations (products); territorial scope of the existing organizational structures (regional and local tourist associations); labour resources (including daily work trips) (Kontseptsiya za turistichesko raĭonirane na Bŭlgariya 2021). The organizations for management of tourism regions are registered as legal entities during 2018–2019 period. As of the current moment their management structure is the following: Representative (have the function of chairman of the board of directors) and members of Board of directors (usually representatives of the municipalities in the region). The process of participation of the regions in the tourism policy and initializing marketing activities via OMT is still insignificant (Kontseptsiya za turistichesko raĭonirane na Bŭlgariya 2021).

Fig. 22.2 Tourist regions in Bulgaria. *Source* Concept for tourist zoning of Bulgaria (Kontseptsiya za turistichesko raĭonirane na Bŭlgariya 2021)

22.3.3 Trends in Tourist Environmental Planning

It is important for the future development of tourism in Bulgaria to observe the trends that will dominate tourist travel after overcoming the crisis. We believe that their combination with strategies for ensuring sustainable development is a guarantee for future prosperity. In our opinion, they can be summarized as follows: tourists would avoid the visitation of big hotels, "all-inclusive" resorts and loud mainstream resorts; the concepts for sustainable development of tourist resorts rely on the establishment of ecological modes of transport; outdoor activities will be necessary to a large extent—walks, outdoor sports, rock climbing, hiking, etc.; technologies and innovations also can help the sustainable development in the tourist destinations; epidemiological measures will establish the pools as a preferred and sought form for sports, healing and recreation; corporate social responsibility will be established through the search for "eco-friendly" travel companies. New models of tourist accommodation and catering will be established, providing greater independence and isolation (Velikova 2020).

The whole planning process is in itself a closed cycle in rights (from the development of strategies to certain operational plans to the implementation and control) and feedback (from the report of the results implemented by the plan to their reformulation). The plan includes key indicators for the activities to be achieved at the end of a given period. Tourism support plans are required to be developed in the context of the socio-economic life of the territory (insofar as tourism is an integral part of

it) (Natsionalna strategiya za ustoĭchivo razvitie na turizma v Republika Bŭlgariya 2014–2030 g 2021). On the other hand, the plans for the development of the individual elements in the tourism system (for example, the hotel industry) must be linked to a calculation, as well as to a master plan for the location of the sites and infrastructure of tourism in the specific recreation areas. Uncoordinated plans can contribute to disaster development (transport problems, environmental pollution, limited access to water and lack of water, insufficient level of education of people employed in tourism, insufficient flexibility in the formation of the package of services, strong seasonality, inadequate performance of the industry, etc.). Experience shows that environmental tourism planning achieves the best results with the joint participation and close cooperation of the sector with the government, as well as other industries developing in the territory. The plans will be very well implemented and sustainable, when all stakeholders (entrepreneurs, public organizations, the population) have been involved in their preparation.

Tourism planning is carried out at macro, national, regional to micro local level. Each level focuses to a different degree on the detailing and processing of planning decisions, taking into account the specifics of each level. The ideal development process is bound to develop from the general to the private, as the general levels provide guidance for the preparation of private plans. At the international level, the main connections are transport, travel and directions of tourists in different countries, international marketing strategies and advertising campaigns. This level of planning depends on the interactions of the individual countries and is expressed in the support of international organizations with sponsorship of regional tourism projects (Velikova et al. 2017).

At the national level, the essence of planning is to identify and define the areas of tourism development, containing one or another tourist attraction. In addition, it is necessary to develop a national tourism policy, plans and programs to achieve the desired state of tourism development and the formation of investment policies, tourism legislation, marketing campaign, development of strategic and tactical methods for implementing tourism policy. The tourism policy of the country finds its reflection in conceptions about creating and realization of the national tourist product. The policy is also obliged to create a basis for the integration of environmental planning in the tourism product.

The essence of regional tourism planning is reflected in the development of regional policies, programs and plans for tourism development by anticipating the specific conditions of the territory (Natsionalna strategiya za ustoĭchivo razvitie na turizma v Republika Bŭlgariya 2014–2030 g 2021). Local planning concerns a specific area. It designs in detail the location of tourist sites, as well as park areas, landscape architecture and infrastructure facilities used for tourism. Such detailed planning can be carried out both at the state level and in the private sector, but the plans created must meet the local criteria and development standards established by the local administration (Velikova et al. 2017).

As a rule, several levels of planning are taken into account within the development and implementation of a project. The preparation of regional concepts and plans for the priority areas can be used as a national concept for tourism development. In

addition, the tasks for the development of tourism and the creation of modern tourist complexes must be considered in a broad context and in public policy and must be included in the medium and long-term plans of the tourism development program.

22.4 Conclusion

In conclusion, we could say that environmental planning aims to harmonize spatial requirements at different levels (neighbourhood, city, region, province, country, continent) in relation to the different aspects (transport, environment, population, economy, tourism). This should lead to conflict resolution, as well as take care of (future) spatial functions and use in advance. In that sense environmental planning strives for sustainable development of space, bringing into harmony the social, economic, legal and environmental claims in space. It is also necessary to guarantee the free development of the individual, protection of the natural preconditions of life and its development, ensuring the economic development of the space, as well as commitment to appropriate monitoring, maintaining open long-term possibilities for layout, strengthening the diversity of the individual parts, the creation of equal living conditions in all areas and promoting the unification of Europe.

Of interest for future research are the processes of climate change, which will strongly influence the future development of tourism in Bulgaria. Global warming will significantly change the tourist offer. On the one hand, it will have a positive effect on summer sea tourism in the direction of extending the season. On the other hand, it will negatively affect winter ski resorts. This requires a rethinking of the supply in these territories and re-planning of the territory in order to offer other types of tourism. The sustainable ecological development of tourism in Bulgaria requires the study of these processes as well.

References

Bogomilova E (2020) Upravlenie v usloviyata na izvŭnredna situatsiya. Biznes Posoki 27(2020):9–13

Botseva D, Tsolov G, Tanakov N (2020) Key factors for accessible tourism in South East Europe. University Euro-Balkan, Skopje, Republic of Macedonia, pp 53–63

Burns P (1999) Paradoxes in planning: tourism elitism or brutalism? Ann Tour Res 26(2):330–332

Evrev P (1999) Teritorialnoustroĭstveno planirane na otdikha i turizma, UI „Sv. Kliment Okhridski", Sofiya, pp 13–23

Kontseptsiya za turistichesko raĭonirane na Bŭlgariya. https://www.tourism.government.bg/bg/kategorii/strategicheski-dokumenti/koncepciya-za-turisticheskо-rayonirane-na-bulgariya. Last Accessed 17 Feb 2021

Ministerstvo na regionalnoto razvitie i blagoustroĭstvo, Istorichesko razvitie na administrativno-teritorialnoto ustroĭstvo na teritoriyata na Bŭlgariya. https://www.mrrb.bg/bg/administrativno-teritorialno-ustrojstvo/. Last Accessed 17 Feb 2021

Ministerstvo na turizma. https://www.tourism.government.bg/. Last Accessed 17 Feb 2021

Müller G (1990) Raumplanung, Akademie für Raumforschung und Landesplanung (HG): „Handwörterbuch der Raumforschung und Raumordnung", Hannover, pp 2542–2553
Natsionalna strategiya za ustoĭchivo razvitie na turizma v Republika Bŭlgariya 2014–2030 g. https://www.tourism.government.bg/bg/kategorii/strategicheski-dokumenti/nacionalna-strategiya-za-ustoychivo-razvitie-na-turizma-v/. Last Accessed 17 Feb 2021
Nikolov G, Botseva D (2018) Role and importance of government policies and strategies for long-term economic development. Synth Sci Soc Solving Glob Probl 34
UNEP (United Nations Environment Program), Impacts of Tourism. http://www.uneptie.org/pc/tourism/home.htm. Last Accessed 17 Feb 2021
Vasileva E, Nikolov G (2018) Adapting to climate change in the focus of regional development policy. In: Regional economy and sustainable development, conference proceedings 2017 (No. 2). Research Institute, University of Economics-Varna
Velikova E (2020) Sustainable planning and development of the mountain resorts in Bulgaria. J R Estate Prop Bus 4(2):81–90
Velikova E, Yaneva M, Portarska, V (2017) Prilozhni aspekti na planiraneto i upravlenieto na turisticheskite destinatsii, „Avangard Prima", Sofiya, pp 15–96
Velikova E (2019) Methodological guidelines for the sustainable development of the Bulgarian touristic resorts through reducing the harmful impact of transport. In: E3S Web of Conferences 101, 01004 (ICESD 2019)
Velikova E (2010) Planirane na teritoriyata v turizma, Nauchno spisanie "Aktualni problemi na infrastrukturata i komunikatsiyata", Godina 1, fevruari 83–89
Velikova E (2017) Trends in the planning and construction of tourist destinations. J R Estate Prop Bus I 1:41–55.
Zakon za ustroĭstvo na teritoriyata. https://www.lex.bg/laws/ldoc/2135163904. Last Accessed 17 Feb 2021

Chapter 23
Analytical Approach for Sustainable Multi-Objective Management of Sediment-Algae Dynamics

Hidekazu Yoshioka and Saya Hashimoto

Abstract We propose an analytical framework for sustainable management of sediment-algae dynamics in dam-downstream river environment. The problem considered in this short paper is an optimization of the dynamics by sediment replenishment schemes having multiple objectives: cost-efficient sediment supply and prevention of the bloom of nuisance benthic algae. We apply an Ergodic long-run stochastic control model to this problem, and show that it can be solved analytically being different from many other multi-objective optimization models. The sediment storage and algae population dynamics follow ordinary differential equations perturbed randomly by the sediment replenishment. We show that the most cost-efficient policy, namely the optimal sediment replenishment policy, is of a threshold type that is implementable in the real world. We analytically lead to a practical sustainability criterion that is based only on the biological and physical parameters, which can be specified prior to implementing a replenishment scheme. Our model is simple, but can give useful and practical insights into sustainable river environmental management.

Keywords Mathematical approach · Ergodic stochastic control · Sustainable river environmental management

H. Yoshioka (✉) · S. Hashimoto
Shimane University, Nishikawatsu-cho 1060, Matsue 690-8504, Japan
e-mail: yoshih@life.shimane-u.ac.jp

S. Hashimoto
e-mail: aa174037@matsu.shimane-u.ac.jp

H.-Y. Jeon (ed.), *Sustainable Development of Water and Environment*,
Environmental Science and Engineering,
https://doi.org/10.1007/978-3-030-75278-1_23

23.1 Introduction

River environmental management should be cost-efficient as well as sustainable so that humans and aquatic ecosystems can coexist in long-run. In addition, such a management problem contains several objectives that should be concurrently optimized. It is therefore a multi-objective problem whose resolution requires an application of appropriate computational methods that are sometimes black-box for decision-makers (Cioffi and Gallerano 2012; Mohammad-Azari et al. 2020; Seifi et al. 2020). The conventional multi-objective models are undoubtedly powerful tools for tackling river environmental management problems, but their complicated nature hinders us from deeply understanding their detailed optimization mechanisms. An analytically tractable model, if it exists, would be helpful for better understanding the underlying optimization mechanisms in the multi-objective problems. However, such an approach is still rare except for some economic models (Marsiglio and Torre 2018; Marsiglio and Privileggi 2019). In this short paper, we show that an analytically tractable model applicable to environmental management exists.

The main objective of our contribution is to propose a simple conceptual model for analyzing sustainability of a multi-objective problem of the sediment and algae dynamics in a dam-downstream river. The problem structure is simple. Creating a dam across a river cross-section stops sediment transport, especially bedload transport toward downstream, which potentially triggers a variety of disutilities including the bloom of nuisance benthic filamentous green algae (Flinders and Hart 2009). Sediment replenishment into dam-downstream rivers has been considered as an effective strategy to suppress the algae bloom by the high shear stresses of sediment-laden flows (Ock et al. 2013); however, its optimization has only been recently analyzed theoretically by the authors (Yoshioka 2020; Yoshioka and Yaegashi 2020), and its multi-objective nature has not been explored in detail. This is the main motivation of the multi-objective model considered in this paper.

Our multi-objective optimization model is based on the single-objective models (Yoshioka 2020; Yoshioka and Yaegashi 2020), mathematically rigorous, and has a clear connection to sustainable environmental management. The underlying mathematics is sophisticated as it is based on a modern theory of nonlinear integro-differential equations, but is not presented in this paper to avoid too much mathematical presentations. The model is tractable and its application does not encounter significant technical difficulties. This model would be useful for better understanding management aspects of coupled sediment-algae dynamics.

23.2 Mathematical Model

23.2.1 Sediment Storage Dynamics

We explain our mathematical model in this section. See, also the conceptual figure (Fig. 23.1). The amount of lumped sediment storable in a downstream reach of a dam is denoted as $\bar{S} > 0$. The amount of lumped sediment stored at time t is denoted as S_t. The range of S_t is therefore $\Omega = [0, \bar{S}]$. The sediment discharge along the river is denoted as $Q > 0$, which should be replaced by 0 when the lumped sediment is depleted ($S_t = 0$). The sediment discharge can be evaluated using an available empirical formula (Pähtz and Durán 2020).

Following Yoshioka (Yoshioka 2020), the physically-based sediment decrease is formulated as

$$\frac{\mathrm{d}S_t}{\mathrm{d}t} = \begin{cases} -Q & (0 < S_t \leq \bar{S}) \\ 0 & (S_t = 0) \end{cases}. \tag{23.1}$$

This equation does not consider sediment replenishment, which is incorporated into our model as follows. We assume that the sediment replenishment can be carried out discretely and sometimes irregularly in time (Yoshioka 2020) as in real problems, following a Poisson process with the mean jump interval $T > 0$. This is the simplest model of replenishment timing having a characteristic time scale, which is identified as T in our model. At each jump time $t = \tau$, the environmental manager of the river, the decision-maker, chooses whether he/she replenishes the sediment as

$$S_\tau \to S_\tau + \eta_\tau, \tag{23.2}$$

where η_τ represents the amount of replenished sediment at the time $t = \tau$. This η_τ is chosen from $\left\{0, \bar{S} - S_\tau\right\}$ because S_t should be constrained in Ω.

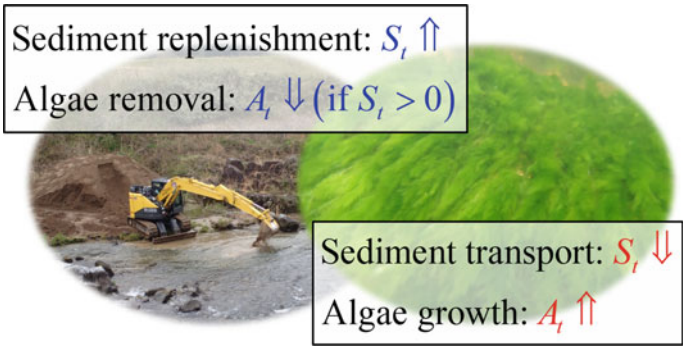

Fig. 23.1 Conceptual figure of the mathematical model

23.2.2 Algae Growth Dynamics

We also consider population dynamics of filamentous green algae whose biomass in the reach at time t is denoted as A_t. We assume a logistic model with the decay due to bed shear stresses by the sediment transport in a simplified form (Boulêtreau et al. 2006):

$$\frac{\mathrm{d}A_t}{\mathrm{d}t} = rA_t\left(1 - \frac{A_t}{\bar{A}}\right) - \alpha(S_t)A_t, \tag{23.3}$$

but any other growth models can be utilized because what is important in our model is the behavior near the state $A_t = 0$ as demonstrated in the next sub-section. Here, $r > 0$ is the intrinsic growth rate, $\bar{A} > 0$ is the carrying capacity, and $\alpha(S_t)$ is the detachment coefficient depending on the sediment transport. By the experimental finding that the algae detachment is not significant if there is no sediment transport (Hamagami and Yoshioka 2020), we can set the simple relationship

$$\alpha(S_t) = \begin{cases} \bar{\alpha} & (0 < S_t \leq \bar{S}) \\ 0 & (S_t = 0) \end{cases} \tag{23.4}$$

with a constant $\bar{\alpha} > 0$.

We focus on suppressing the algae bloom, which can be achieved if the equilibrium point $A_t = 0$ of the Eq. (23.3) is stable. Considering the linearized equation of (23.3) at $A_t = 0$:

$$\frac{\mathrm{d}A_t}{\mathrm{d}t} = (r - \alpha(S_t))A_t, \tag{23.5}$$

the no-population equilibrium $A_t = 0$, which is the desired state, is said to be stable if

$$\lim_{t\to+\infty} \frac{1}{t} \ln A_t = \lim_{t\to+\infty} \left(r - \frac{1}{t}\int_0^t \alpha(S_u)\mathrm{d}u\right) < 0. \tag{23.6}$$

Namely, $A_t = 0$ is stable if the time-averaged growth rate at this point is negative. Because the sediment is replenished randomly, assuming that the probability density function p of the sediment storage exists, the condition (23.6) is satisfied if

$$r - \bar{\alpha}\int_{(0,\bar{S}]} p(s)\mathrm{d}s < 0. \tag{23.7}$$

This is an important inequality explicitly characterizing the condition to suppress the algae bloom by the sediment replenishment, meaning that checking the condition reduces to finding the probability density function p.

23.2.3 Optimization Problem

The optimization problem here has the two objectives. The one is to replenish the sediment in a cost-efficient manner so that it is not depleted. We assume that sediment replenishment at each jump time $t = \tau$ requires a fixed cost (labor cost) $d > 0$ and a proportional cost $c\eta_\tau$ with $c > 0$. Summing up them yields the total cost $C(\eta_\tau) = d + c\eta_\tau$ if $\eta_\tau > 0$, and $C(0) = 0$ because there should be no replenishment cost if there is no replenishment. In addition, we set a penalization function

$$P(S_t) = \begin{cases} 0 & (0 < S_t \leq \bar{S}) \\ 1 & (S_t = 0) \end{cases}, \tag{23.8}$$

which is activated when the sediment is depleted. The other objective is to suppress the algae bloom so that the state $A_t = 0$ is stable in the sense of (23.6), and we employ the inequality (23.7) as a constraint.

We are interested in sustainable management policies of the sediment-algae dynamics, and therefore consider an Ergodic control formulation as in Arapostathis et al. (Arapostathis et al. 2012) that explores policies optimizing an objective function in long-run. In our case, the objective function to be minimized is

$$\phi = \lim_{u \to +\infty} \frac{1}{t} \mathbb{E}\left[\int_0^t P(S_u) \mathrm{d}u + \sum_{k \geq 1, \tau_k \leq t} C\left(\eta_{\tau_k}\right) \middle| S_0 = s \right], \tag{23.9}$$

where $\mathbb{E}$ represents the expectation, $s \in \Omega$ is the initial condition of the lumped sediment storage, and τ_k $(0 < \tau_1 < \tau_2 < ...)$ is a sequence of jump times of the Poisson process at which the sediment may be replenished.

The objective function ϕ has to be minimized with respect to each η_{τ_k} so that the constraint (23.7) is satisfied. This is a multi-objective optimization problem. The minimized value of ϕ is denoted as H. We simply set $H = +\infty$ if the constraint (23.7) is not satisfied. For example, we get $H = +\infty$ if $r \geq \bar{\alpha}$. Hereafter, we assume

$$r < \bar{\alpha}, \tag{23.10}$$

meaning that the algae bloom is possibly suppressed by the sediment replenishment. Otherwise, the problem is clearly not sustainable and is out of the interest.

23.3 Sustainability Analysis

23.3.1 Policy Without the Inequality Constraint

The multi-objective optimization problem posed in the previous section is resolved as follows. Notice that we have exactly the two cases: the constraint (23.7) is satisfied or not. We tackle this issue in the following two steps. Firstly, we solve the optimization problem without the constraint and derive an optimal policy minimizing the objective function ϕ. Secondly, we check that whether the derived policy satisfies the constraint (23.7) or not.

An advantage of this two-step approach is that we can directly utilize the existing results of the single-objective stochastic control problems (Yoshioka 2020; Yoshioka and Yaegashi 2020). We then find that the quantity H is a positive constant, and the optimal policy is of the threshold-type: at each jump time τ, based on the observed value S_τ, replenish the sediment following the threshold-type policy

$$\eta(S_\tau) = \begin{cases} \bar{S} - S_\tau & (0 \le S_\tau \le F) \\ 0 & \left(F < S_\tau \le \bar{S}\right) \end{cases} \tag{23.11}$$

with a threshold F found below. This is a kind of feed-back control. For convenience, set $f = F\bar{S}^{-1}$ and $K = \bar{S}Q^{-1}T^{-1}$. Following the dynamic programming argument (Yoshioka 2020), the normalized threshold f is determined from the nonlinear equation

$$(1 - f)\exp(-Kf) = \frac{dQ\bar{S}^{-1}}{1 - cQ\bar{S}^{-1}}. \tag{23.12}$$

A straightforward analysis with the help of an intermediate value theorem shows that the Eq. (23.12) has a solution $0 < f < 1$ if and only if the condition $c + d < \bar{S}Q^{-1}$ is satisfied (Yoshioka 2020). The threshold F is then found using this f as $F = f\bar{S}$. In addition, we find H, although not used in this paper, as a byproduct:

$$H = Q\bar{S}^{-1}\left(c + \frac{d}{1 - f}\right). \tag{23.13}$$

If $c + d = \bar{S}Q^{-1}$, then $f = 0$. In addition, if

$$c + d > \bar{S}Q^{-1}, \tag{23.14}$$

then doing no replenishment is optimal, which is clearly not a desirable management policy. Therefore, the condition (23.14) has to be avoided for the sustainable environmental management; namely, the cost should not be too large.

A remarkable point of the optimal policy (23.11) is that it is implementable once the threshold F is found from the Eq. (23.12). The condition (23.14) means that the threshold-type policy is optimal if the cost is small and/or the sediment discharge relative to the amount of storable sediment is not large. It is interesting to see that the condition (23.14) is free from the mean observation interval T.

23.3.2 Optimal Policy and Its Sustainability

Based on the previous work (Yoshioka 2020), the optimal policy without considering the inequality constraint (23.7) was presented in the previous sub-section. We then incorporate (23.7), which is considered for the first time in this paper, into the optimization problem. A key finding for facilitating the analysis is that the probability density function p under the threshold-type control satisfies the relationship (Yoshioka and Yaegashi 2020)

$$p(0) = \delta_0 \times \frac{\exp(-Kf)}{1 + K(1 - f)}, \tag{23.15}$$

where δ_0 is the Dirac's Delta function concentrated at $s = 0$. In this way, considering the conservation of probability, we find

$$\int_{(0,\bar{s}]} p(s)\mathrm{d}s = 1 - \frac{\exp(-Kf)}{1 + K(1 - f)}. \tag{23.16}$$

Consequently, we can rewrite the constraint (23.7) as

$$r\bar{\alpha}^{-1} < 1 - \frac{\exp(-Kf)}{1 + K(1 - f)}. \tag{23.17}$$

The right-hand side of (23.17) is immediately computed once we find f by solving (23.12).

23.3.3 Sustainability Analysis

One can analyze sustainability of the optimal policy (23.11) using the mathematical results above. A possible algorithm of the analysis is explained below.

1. Set the parameter values.
2. Check that (23.14) is not satisfied.
3. Solve (23.12) to find f (or equivalently F).

4. If (23.17) is satisfied, then the policy is sustainable. Otherwise, it is not sustainable.

The third step may require some numerical method to solve the nonlinear Eq. (23.12). One can apply a Picard iteration when necessary. The other steps can be carried out purely analytically.

The analysis above suggests that we can also work with normalized parameter values $K = \bar{S}Q^{-1}T^{-1}$, $L = cQ\bar{S}^{-1}$, $M = dQ\bar{S}^{-1}$, and $N = r\bar{\alpha}^{-1}$ if necessary. Consequently, the policy is sustainable if

$$L + M \leq 1 \text{ and } N < 1 - \frac{\exp(-Kf)}{1 + K(1-f)} \text{ with } (1-f)\exp(-Kf) = \frac{M}{1-L}. \tag{23.18}$$

Notice that the first condition can be used to restrict the parameter space prior to the sustainability analysis.

We are not intended to fully analyze the sustainability condition for arbitrary cases, but present one critical case that gives a unified result applicable to the other cases. In the model, the laziest potentially sustainable case occurs in the most costly case $L + M = 1$ leading to $f = F = 0$. This policy is actually a reasonable one because it says that replenishing the sediment is optimal if and only if the sediment has been depleted at the observation. By (23.18), this policy is sustainable if

$$N < \frac{K}{1+K} \text{ orequivalently } r\bar{\alpha}^{-1} < \frac{\bar{S}}{QT + \bar{S}}. \tag{23.19}$$

By (23.19), the mean observation interval T should be chosen sufficiently small:

$$T < \bar{T} = \left(\frac{\bar{\alpha}}{r} - 1\right)\frac{\bar{S}}{Q}. \tag{23.20}$$

This is a clear design criterion of the sustainable policy in the laziest case. Notice that the right-hand side of (23.20) is determined only by the biological and physical quantities that are factorized as the two different terms, and is not based on the parameters of the objective function. Furthermore, the right-hand side of the second inequality in (23.18) is increasing with respect to f. The condition $T < \bar{T}$ therefore applies to generic $0 < f < 1$ as well. This kind of simple, clear, and practical criterion has not been found in the literature.

Finally, we briefly apply the estimate (23.20) to an on-going case of O dam in H River in Japan (Yoshioka 2020). In this river, a sediment replenishment scheme with $\bar{S}$ (m^3) of 100 to 1,000 (m^3) is being considered at a downstream reach of O dam. Assume the river width of 20 (m) and the slope of 0.001 and consider the well-known Meyer-Peter–Müller formula (Ancey 2020). The historical data of hourly discharge (From April 1 2016 to May 31 2020) with the sediment having

the diameter of 0.005 (m) and the density of 2,600 (kg/m^3) gives the averaged unit-width sediment discharge of 4.3×10^{-5} (m^2/s). We then get $Q = 73.1$ (m^3/day). Assume $\bar{S} = 200$ (m^3). Further, assume that $\bar{\alpha} r^{-1}$ is at the order of 10^1 based on the previous research (Hamagami and Yoshioka 2020; Yoshioka et al. 2020); for example, setting $\bar{\alpha} r^{-1} = 10$ gives $\bar{T} = 24.6$ (day), meaning that a monthly or more frequent observations to making the decision of the sediment replenishment is recommended based on the proposed model.

23.4 Conclusion

We presented a simple mathematical framework for analyzing sustainability of a multi-objective optimization problem of sediment-algae dynamics in a dam-downstream river. The model is tractable and the sustainability criterion to accommodate both replenishing sediment cost-efficiently and supressing nuisance benthic algae bloom was found analytically. Our contribution would highlight a new connection between mathematical sciences and sustainable environmental management.

It should be noted that a simple mathematical model is not always beneficial because it may be too simple. For analyzing a real-world problem of environmental management, one would have to utilize a mathematical model having a larger degree-of-freedom whose resolution requires some numerical method. Nevertheless, the presented mathematical model can be employed as a benchmark for verifying such numerical methods.

A possible direction of future research would be finding a least complex verifying method for sustainability of sediment replenishment schemes under more general conditions of river flows and constraints. Optimal sizing of the storable sediment $\bar{S}$, which was assumed to be a fixed value in this paper, is also an important future research topic.

Acknowledgements JSPS Research Grant 19H03073, Kurita Water and Environment Foundation Grant No. 19B018 and No. 20K004, and a grant from MLIT Japan for management of seaweed in Lake Shinji support this research.

References

Ancey C (2020) Bedload transport: a walk between randomness and determinism. Part 1. State Art J Hydraul Res 58(1):1–17

Arapostathis A, Borkar VS, Ghosh MK (2012) Ergodic control of diffusion processes. Cambridge University Press, UK

Boulêtreau S, Garabétian F, Sauvage S, Sánchez-Pérez JM (2006) Assessing the importance of a self-generated detachment process in river biofilm models. Freshw Biol 51(5):901–912

Cioffi F, Gallerano F (2012) Multi-objective analysis of dam release flows in rivers downstream from hydropower reservoirs. Appl Math Model 36(7):2868–2889

Flinders CA, Hart DD (2009) Effects of pulsed flows on nuisance periphyton growths in rivers: a mesocosm study. River Res Appl 25(10):1320–1330

Hamagami K, Yoshioka H (2020) Chapter 3. Hydraulic control of the benthic alga Cladophora glomerata. In: Yoshioka H (ed) Ayu and river environment in Hii River, Japan-research results from 2015 to 2020. Laboratory of Mathematical Sciences for Environment and Ecology, Shimane University, Matsue, Japan. https://www.hiikawafish.jp/date/200300ayutokankyo.pdf. Last Accessed 18 Aug 2020 (in Japanese)

Marsiglio S, La Torre D (2018) Economic growth and abatement activities in a stochastic environment: a multi-objective approach. Ann Oper Res 267(1–2):321–334

Marsiglio S, Privileggi F (2019) On the economic growth and environmental trade-off: a multi-objective analysis. Annals of operations research. https://doi.org/10.1007/s10479-019-03217-y (in press)

Mohammad-Azari S, Bozorg-Haddad O, Loáiciga HA (2020) State-of-art of genetic programming applications in water-resources systems analysis. Environ Monit Assess 192(2) (Paper No.73)

Ock G, Sumi T, Takemon Y (2013) Sediment replenishment to downstream reaches below dams: implementation perspectives. Hydrol Res Lett 7(3):54–59

Pähtz T, Durán O (202) Unification of aeolian and fluvial sediment transport rate from granular physics. Phys Rev Lett 124(16) (Paper No. 168001)

Seifi A, Ehteram M, Soroush F (2020) Uncertainties of instantaneous influent flow predictions by intelligence models hybridized with multi-objective shark smell optimization algorithm. J Hydrol 587 (Paper No. 124977)

Yoshioka H, Tsujimura M, Hamagami K, Yoshioka Y (2020) A hybrid stochastic river environmental restoration modeling with discrete and costly observations. Optimal control applications and methods. https://doi.org/10.1002/oca.2616 (in press)

Yoshioka H (2020) River environmental restoration based on random observations of a non-smooth stochastic dynamical system. arXiv:2005.04817

Yoshioka H, Yaegashi Y (2020) Stochastic impulse control of non-smooth dynamics with partial observation and execution delay: application to an environmental restoration problem. arXiv:2006.16034

Chapter 24
From Convergent to Ecological Transition—Challenges for the Management and Regional Development of Bulgaria

Georgi Tsolov and Nikola Tanakov

Abstract Many complex challenges have marked Europe's transition to Economy 4.0 and Society 5.0. One of them, considered at all possible levels of government, is implementing EU environmental policy. The consensus in principle in this area does not always lead to the achievement of strategic environmental goals. The reasons are rooted in the objective comprehensiveness of the ecological transition. We argue that it is evolving far beyond the complicated governance structure of the Union. An additional condition is an undeniable and very close connection between the national and integrated economy with global and regional trends. The transformation to Bulgaria's environmentally friendly economy was preceded by a socio-economic transition, culminating in the country's integration into the EU and a convergent transition, which we will say is only in its infancy. Therefore, we are faced with assessing Bulgaria's potential to mobilize its available resources (managerial, spiritual, cultural, material, financial, and integration) to develop the most effective available "environmental" tools. Environmental policy should not be implemented only with the tools for management and administrative control but should also be added to the available scientific, financial, and technical means.

Keywords Environmental management · Ecological transition · Convergent transition · Regional development · Green economy · EU policy · Environmental objectives · GDP per capita · Region

24.1 Introduction

The European Union (EU) faces one of its most severe challenges during the current period of the EU's Multiannual Financial Framework (MFF for 2021–2027)—the implementation of a truly "common" environmental policy. Although one of the

G. Tsolov (✉) · N. Tanakov
University of National and World Economy (UNWE), Student Town, Sofia 1700, Bulgaria
e-mail: georgi.tsolov@unwe.bg

H.-Y. Jeon (ed.), *Sustainable Development of Water and Environment*,
Environmental Science and Engineering,
https://doi.org/10.1007/978-3-030-75278-1_24

most comprehensive legislative frameworks is already in place in the field of environment, and numerous institutions and organizations working in this direction have proclaimed their current strategies, today the management of the processes of creating and maintaining sustainable development, the effective use of renewable resources, and the expansion of the low-carbon economy, there are more questions than proven useful answers.

Already in the process of Bulgaria's accession to the Union, the negotiating government experts, through the instrument of the so-called "Structured dialogue", expressed their belief that environmental policy in the context of integration will automatically lead to the imposition of high environmental standards, will encourage "green innovation", will lead to "green growth" and environmental entrepreneurship. However, under pressure from the market and competition, we now realize that lagging or "catching up" economic systems within the EU (such as Bulgaria) tend to "cool" their enthusiasm for ambitious environmental goals, and more they often tend to put their signature in the background. This fact is explained by political governance's aim to achieve economic and social results in a short time due to their urgency and to consider environmental results as the object of "better times".

Structurally and functionally, this trend has been supported by a significant constraint on the Europe 2020 strategy—its headline environmental objectives have not been met by binding European legislation. Optional in nature, these goals are deprived of effective implementation by national governments in times of economic and political crisis (COM(2014) 130—European Commission), although it is to them that the Strategy assigns the most crucial role (COM(2014) 130).

At the beginning of the third decade of the millennium, negative global trends (European semester—thematic information document) (inefficient use of resources; unbearable pressure on the environment; climate change) not only transform space and territory but are about to cross boundaries beyond which human communities could not prevent irreversible consequences. For its part, the EU is pursuing sustainable economic growth, which is only seen as possible if environmental constraints are considered. Legislatively and institutionally, the Union emphasizes that, in the context of this condition, a green and circular economy can provide solutions for the environment and the economy and society as a whole (COM(2015) 614).

In the conditions of three-time horizons in front Bulgaria and the EU—the Multiannual Financial Framework (MFF 2021–2027); The European Strategic Framework 2030 and the Green Deal, we will look at the results of the environmental transition as a consequence of management action or inaction.

24.2 Convergent Basis of Ecological Development of the Society and the Economy

Suppose the report did not focus on the specific environmental context of contemporary national, regional and European development. In that case, we could assume that

Convergence means similarity or approach to a specific value, norm, or benchmark, or to a particular state characterized by balance. However, this is incompatible with the dynamics and regional specifics of environmental processes and the urgency of the tasks posed by environmental problems.

The EU Member States interact through the management of various macroeconomic indicators, and they usually participate in the review of the dynamics of the convergence criteria. According to the Maastricht Treaty, these criteria are highly interdependent. Each Member State of the Union must meet all the criteria to join the euro area.

According to the EC and the ECB's Convergence Reports until 2018, Bulgaria continues to meet the economic criteria for price stability, debt, deficit, and long-term interest rates. Regarding the criterion for exchange rate stability, Bulgaria is not part of the Exchange Rate Mechanism II (ERM II), but the Bulgarian lev is pegged to the euro at the so-called "hard" exchange rate.

At the beginning of June 2020, the European Commission (EC) and the European Central Bank (ECB) published a Convergence Report for 2020, where the numerical criteria for Bulgaria take into account the first adverse effects of the COVID-19 pandemic (COM(2015) 614—European Commission). Profound shocks affect all socio-economic systems, and as noted above, post-crisis recovery actions can significantly ignore environmental issues.

To overcome this management deficit and for Bulgaria to successfully make its ecological transition, we believe that we need to pay attention to another aspect of Convergence—the technological one. It suggests that transformations, progress, and sustainability are possible only when society is aware of the technological step's essential characteristics on which its economic core is based. We want to emphasize that, in essence, this approach is evolutionary and, as such, does not imply skipping technological steps. Undoubtedly, the countries in Europe with a well-developed convergent economy have demonstrated effective practices and models based on state participation (Nikolov 2016). Nevertheless, other regions, including Bulgaria, face some objective convergent challenges of a geographical, economic, demographic, or political nature. While the EU15 countries have acted regionally and globally on issues such as: reorganizing the European energy market; diversification of energy sources; reduction of energy dependence; achieving resource efficiency, and others, the Bulgarian agenda was determined by the efforts in the direction of overcoming the results of the inefficient model of privatization of polluting industrial sectors; increasing the competitiveness of energy and resource-intensive SMEs; combating higher levels of poverty and/or unemployment, and others.

Bulgaria's current development and its six regions for economic planning at the NUTS 2 level are incredibly resource-intensive. When we look at it through the prism of environmental issues, we must agree that this shortcoming is characteristic of both the sphere of national production and the sphere of consumption. The adopted administrative approach of management, mostly looking for environmental responsibility in production and consumption (traditions, market attitudes, consumer culture, and others), is rarely associated with the prerequisites for the emergence or deepening of environmental problems in our country. Our country has not yet reached the required

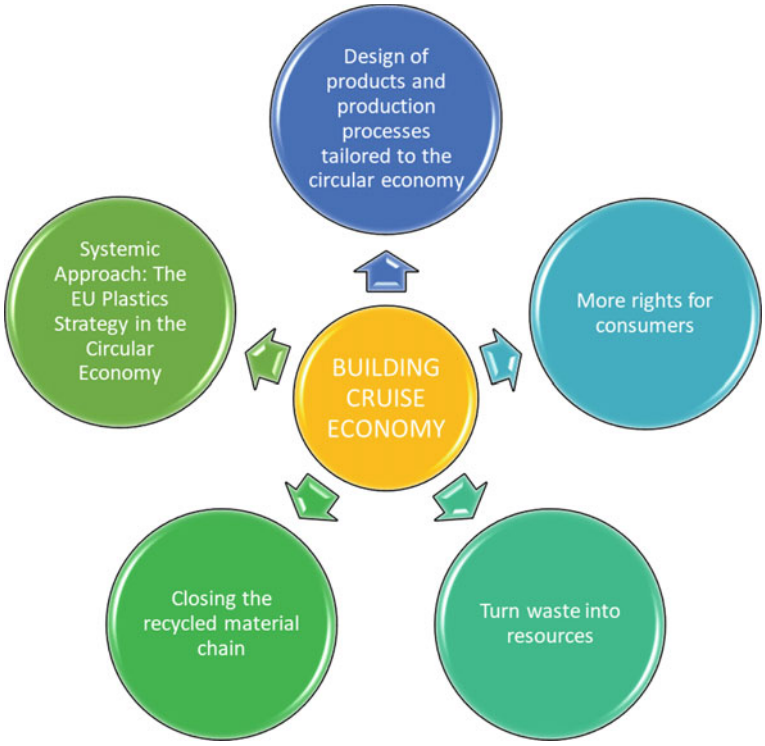

Fig. 24.1 Main directions of building a circular economy. *Source* Authors adaptation according to the available information on the researched issues on the official website of the EU—https://europa.eu/european-union/index_bg

level of convergence (technology), and one of the main reasons for this is rooted in the fact that the principles of the "circular economy" require qualitatively new investments (Figs. 24.1 and 24.2).

24.3 Regional Approach to the Ecological Transition

The values of macroeconomic convergence indicators can measure the transition to a green economy in Bulgaria (see Table 24.1), but they have somewhat indicative and comparative value due to the slow pace of technological progress and vast regional differences and disparities in areas such as investment, innovation, research and development (R&D). In attempting to assess the environmental potential of individual regions of the country, we rely on the proven link between EU cohesion policy (Petre 2015) and Member States' convergent efforts and their local and regional authorities.

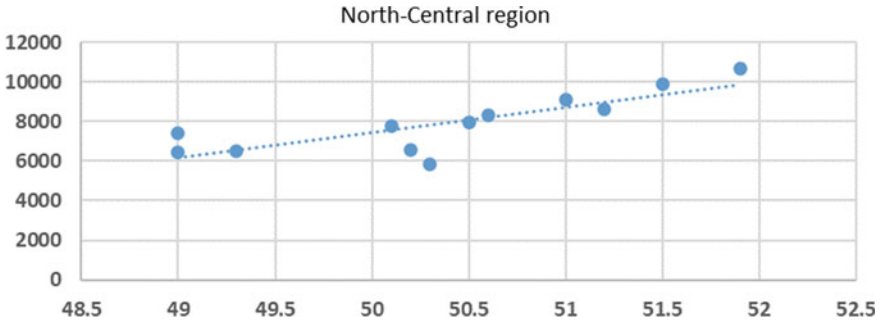

Fig. 24.2 Dynamics of the active population in the region. *Source* Authors adaptation according to the available information on the researched issues on the official website of the EU—https://europa.eu/european-union/index_bg

Table 24.1 Convergence criteria from Maastricht

Economic purpose Macroeconomic policy	Indicator	Criterion
Stability of public finances	Government debt Budget deficit	<60% of GDP <3% of GDP
Price stability (inflation)	Harmonized indices of consumer prices (HICP)	<1.5% above the average level of the three best countries
Sustainable convergence	Long-term interest rates	<2% above the average level of the three best countries
Exchange rate stability	Deviation from a certain level	Participation in Monetary Mechanism II (ERM II) for a period of 2 years without serious deviations

Source Authors adaptation according to the available information on the researched issues on the official website of the EU—https://europa.eu/european-union/index_bg

With the support of the EU and through the principles of solidarity, cooperation, and partnership, Bulgaria, within the three strategic periods outlined above, can alleviate environmental pressures and turn it into a competitive advantage for a socially just, green transition of local communities and regional economies. To this end, it is necessary to increase the efficiency of the management of critical indicators, such as the resource efficiency index, which includes many indicators—resource productivity; domestic consumption of materials; water use; water productivity; greenhouse gas emissions; energy productivity; share of renewable energy in total final energy consumption; recycling of household waste; urban air pollution; innovation capacity and costs of R&D companies. As a result of some interim assessments (Nikolov 2016) covering these indicators' dynamics, a significant distance of Bulgaria is still reported—for example, compared to other countries in the last category of "modest

innovators," having integrated limits below 50% of the EU average (Interim evaluation of the implementation of the Innovation Strategy for Smart Specialization). Such smart/intelligent strategy has to consider the urban development and the dimension it creates regarding the demographic challenges, globalization, scientific and technological change, climate and environmental risks, development of green economy, poverty and risk of social exclusion. Nowadays, however, the policies for social and economic development of cities are still highly fragmented and there is no sustainable enough response provided to ensure the successful and efficient implementation of long term growth strategies (Botseva 2019).

Among the essential factors in Bulgaria that can positively influence the environmental activity at the level of individual enterprises, regional economy, and national economy are the current national operational programs (OP). However, due to their management's segmented approach, we believe that they show weakness in reporting on environmental performance as a factor in socio-economic progress. Although within the strategic period 2021–2027, it is planned to continue implementing the Operational Program "Environment" (OPE), it is noted that the indicators used for the implementation of operational programs in our country differ and are not integrated into environmental monitoring and evaluation indicators (Vasileva 2019). Especially in regional development and related environmental issues, some of the OP indicators serve the government to summarize information at the macroeconomic level without being accurate in terms of their scope and impact. Their overall positive impact is undeniable, but let us not forget that these instruments should play a supporting and complementary rather than a key role in the context of deepening convergence.

Due to budgetary constraints, Bulgaria is characterized by:

- Lagging in the process of transforming its economy from linear to circular;
- Efforts to build a comprehensive environmental risk management system do not yield satisfactory results due to development management fragmentation through national OPs. Their intensity, financial resources, and nature of intervention are too small;
- The main elements of environmental prevention and management are not yet widely integrated into specific legislation in crucial economic sectors.

24.3.1 Ecological Perspective of Regional Development

Bulgaria's management practice has brought out the regional policy and its ecological elements as one of the most dynamic spheres of development in the last few years after our country accedes to the EU. With the implementation of the European environmental legal norms, a normative framework and institutional structure have been created, which is still gaining positive experience in planning and coordination between the individual sectors. The adoption and gradual amendment of the Regional Development Act and the related by-laws have created real preconditions for conducting a modern regional policy in Bulgaria (Law on Regional Development 2008). We mentioned that adopting the administrative approach to environmental

and regional policy (which has leading pan-European importance) has commenced preparing many strategies and development plans, but with a low degree of integrity. They were initially summarized in the National Development Plan (2007–2013), upgraded through the National Development Program: Bulgaria 2020 in force until 2020, and today should be adapted to the new strategic conditions with a horizon of at least 2030.

Applying a Systematic and Functional Approach to Regional Development Policy, we believe that it is determined not only by the principles of cohesion, territorial solidarity, and competitiveness. The principles of sustainability, fair working, and living conditions in different parts of the country are also crucial. The existence of "unified" strategic documents does not automatically lead to overcoming the existing disparities and differences (demographic, economic, environmental, cultural, and others) in the regions and between them. Specific problems accumulate forces that cause social and economic shocks and can quickly reflect on the national economy with which they are closely linked.

On the other hand, market forces alone cannot ensure a balanced ecological transition and regional sustainability. The conceptual nature of environmental and regional development in the new conditions aims to stimulate and diversify economic activities, stimulate investment in the private sector, and reduce unemployment. These are concepts that should lead to an increase in the standard of living of the population. The scientific interest and the practical results show that modern regional development can be realized only through conscious activity and society's effective participation (Nikolov 2019).

24.3.2 Theoretical Formulation of the Research

The official data of economic and social nature (National Statistical Institute) show that there is an urgent need for a comprehensive state environmental policy in Bulgaria in the current convergent situation. It should further focus on the tools for targeted regional development support. This gives grounds to analyze the relationship between the centrally conducted socio-economic policy in the country and individual regions' financial results represented by the GDP per capita indicator. Through the rich research tools, the authors of the report aim to support the assessments of the prospects for the introduction of effective measures and guidelines for increasing GDP per capita in the six regions in Bulgaria.

The starting point is that to track trends over time in a geographical area (region), the calculations are usually based on real GDP (chain-linked volumes), excluding inflation. Calculations are usually based on GDP, expressed in common values—purchasing power, unemployment rate, investment, and others to compare the regions. The subject of this analysis is the impact of two main categories of human resources—"active population" and "unemployment rate" on GDP. The impact was tested in the six different NUTS 2 regions of the country. The relationship between

the variables is examined by analyzing the official national statistics data for a 12-year period (from 2007 to 2018), which were initially processed based on a multiple regression model:

$$Y_i = \beta_0 + \beta_1 X_{1i} + \beta_2 X_{2i} + u_i$$

where

Y_i—GDP per capita for the *i*-th region; X_{1i}—active population in the *i*-th region;

X_{2i}—unemployment rate in the *i*-th region; u_i—random component;

This model allows us to assess each of the factors (X) on the result (Y).

After a correct check of the models in the different regions, it turned out that the factor "unemployment rate" shows statistical significance in none of them. The authors removed this factor from the analysis, and it is now based on the following one-factor model:

$$Y_i = \beta_0 + \beta_1 X_{1i} + u_i$$

where

Y_i—GDP per capita for the *i*-th region;

X_{1i}—active population in the *i*-th region;

u_i—random component;

Under these objective conditions, the research task set by the authors is to derive the main problems marked by the negative or positive processes in the dynamics of the active population by regions and their effects on the GDP per capita.

The hypothesis is that by avoiding attempts to influence the macroeconomic indicators listed in Table 24.1, regional sustainable development efforts will lead to environmental convergence due to qualitative changes in regional GDP.

24.3.3 Empirical Formulation of the Study

Our initial intention to clarify the impact of the factors "unemployment rate" and "active population" on a critical indicator for regional policy—the region's GDP-was guided by making several assessments of governance policy. The correct statistical processing of the data led to the need for a more specific analysis of the data on the population's regional economic activity and its impact on GDP per capita. We assume that a systematic connection has been established between economic activity and the state of the environment as elements of the regions' development. Therefore, both elements will be reflected in the increase in GDP. The empirical study covers

Table 24.2 Baseline data for the North-Central region of NUTS 2 of Bulgaria. *Source* www.nsi.bg—official site of the National statistical institute

Years	Unemployment rate (%)	Active population (%)	GDP per capita (in BGN)
2007	10,7	50,3	5 848
2008	8,5	50,2	6 577
2009	8,4	49,3	6 523
2010	11,6	49	6 435
2011	12,8	49	7 416
2012	14,3	50,1	7 779
2013	15,3	50,5	7 925
2014	13,2	50,6	8 336
2015	10,6	51,2	8 635
2016	9,3	51	9 129
2017	6,9	51,5	9 865
2018	6,7	51,9	10 654

the dynamics of activity in different periods of economic growth and regional development crises, and the national economy. The results for the different regions are considered separately following the example of the first of them:

A. North-Central region*—The estimated model shows that with a one percent increase in the active population, GDP per capita would increase by BGN 1,275* (Table 24.2).

After processing with statistical software SPSS, the best model here is the quadratic model (Rsquare = 0.702). However, to ensure the adequacy of the evaluated relationships, the authors choose to apply the straight-line model, according to the rule that the best model exceeds the linear one with more than 10% explanatory power (Goev et al. 2018), should be chosen (Rsquare = 0.664). The straight-line model is adequate (Sig. = 0.001) and has the following graphic image and estimated shape:

$$\mathbf{Y_{north-central}} = \mathbf{-56297} + \mathbf{1257.X_{inorth-central}}$$

The constant (Sig. = 0.003) and the parameter (Sig. = 0.001) are statistically significant and interpreted.

In unison with the above:

B. Northeastern region*—The estimated model shows that with a one percent increase in the active population, GDP per capita would increase by BGN 1,076.*

C. Southeastern region*—The estimated model shows that with a one percent increase in the active population, GDP per capita would increase by BGN 1,270.*

D. South-Central Region*—The estimated model shows that with a one percent increase in the active population, GDP per capita would increase by BGN 612.*

E. Northwestern and Southwestern regions—In these two regions, the authors did not find a statistically significant relationship between the "active population" factor and the GDP per capita indicator. None of the 11 models tested turned out to be adequate to describe their relationship.

Comparing the obtained empirical results, we conclude that in the regional plan, the active population has the most significant effect on GDP per capita in the North-Central region and the smallest effect in the South-Central region. The very fact that the statistical models used in the study did not work in the two regions located at the endpoints of the socio-economic pendulum (the richest and the poorest) leads us to assume that the chosen approach is adequate.

24.4 Conclusion

Without claiming absolute completeness and comprehensiveness, the above assessments of the effect of the dynamics of the active population on GDP per capita in the individual regions in Bulgaria, and interregional comparisons, allow us to conclude the necessary management measures to support the implementation of the concepts of regional development and ecological transition of society and the economy. The authors of the report recommend that the following conclusions be taken into account:

1. Shortly, the regions will develop their economic and environmental potential without much connection with the unemployment level. This is due to the mass introduction of new technologies in producing goods and services for final consumption and the replacement of human labor with machine labor.
2. Social capital in the regions will be assessed to the greatest extent according to its quality indicators. these are education, skills, competencies, creativity, and "green" innovation.
3. The management of spatial and territorial processes can be effective only if it engages the public's attention on environmental issues. People determine the region's economic needs and environmental priorities, and the state creates the conditions to accumulate the necessary resources to meet them. Regional and environmental policy cannot be based only on the budget but should stimulate the creation of effective self-developing instruments—regional funds, free industrial zones, guaranteed municipal and regional loans, the possibility of issuing bonds, and others.
4. Achieving sustainable employment in the regions should become a key priority. The approach used shows that despite the conventions that emerged from the analysis, there is a relationship between the percentage of the active population in the regions and the regional GDP size.

   In the context of the environmental challenges identified through the three strategic periods covered by the report's structure, we can expect the EU to reduce convergence to the micro-level to achieve economic, social, and environmental results. New instruments such as the Fair Transition Fund will help to

adapt to the green economy. Completing technological convergence is essential to unleash the potential of the green economy fully.

Notes:

(1) For example: The cyclical energy and oil crises of the second decade of the twenty-first century; The global financial crisis after 2009; The war with ISIL; The Covid-19 pandemic and others.

(2) European Semester—thematic information document. Resource efficiency, 2018.

(3) Report 2020 notes that while according to the assessment of 2018, Bulgaria has met the requirements for price stability with inflation of 1.4 percent, by April 2020, inflation is 2.6 percent, and officially our country no longer meets this criterion. https://tbk.bg/%D0%B4%D0%BE%D0%BA%D0%BB%D0%B0%D0%B4-%D0%B7%D0%B0-%D0%BA%D0%BE%D0%BD%D0%B2%D0%B5%D1%80%D0%B3%D0%B5%D0%BD%D1%86%D0%B8%D1%8F-2020-%D0%B8-erm-ii/, last accessed 2021/02/26.

(4) The mid-term evaluation methodology of implementing the "Innovation Strategy for Smart Specialization 2014–2020" covers the following groups of countries-innovators in descending order—leading innovators; strong innovators; moderate innovators; modest innovators.

(5) From the beginning of 2019, the current information on the Operational Program "Environment" (OPE) is published in the Single Information Portal of the European Structural and Investment Funds www.eufunds.bg.

References

Botseva D (2019) Smart specialization on local level—a new dimension for integrated urban development. In: International scientific conference—regional development and cross-border cooperation. Serbia, Pirot, pp 523–528

COM(2014) 130—European commission, review of the results of the Europe 2020 strategy for smart, sustainable and inclusive growth

COM(2015) 614—European commission, communication from the commission to the European parliament, the council, the European economic and social committee, the committee of the regions and the European investment bank: closing the cycle—an EU circular economy action plan

EEA Report No 1/2017, Climate change, impacts and vulnerability in Europe 2016. An indicator-based report. https://www.eea.europa.eu/publications/climate-change-impacts-and-vulnerability-2016. ISSN 1977–8449

European semester—thematic information document. Resource efficiency. https://ec.europa.eu/info/sites/info/files/file_import/european-semester_thematic-factsheet_resource-efficiency_bg.pdf. Last Accessed 26 Feb 2021

Goev V, Boshnyakov V, Tosheva EK, Haralampiev K, Bozev V (2019) Statisticheski analiz v sociologicheski, ikonomicheski I biznes izsledvaniq, IK–UNSS, Sofia, p181

Interim evaluation of the implementation of the innovation strategy for smart specialization 2014–2020. https://www.mi.government.bg/files/useruploads/files/innovations/smartstrategyactivityreport%E2%84%961.pdf. Last Accessed 26 Feb 2021

Law on Regional Development, in force since (2008). Last amended and supplemented in SG. Issue 21 March 13, 2020
Nikolov G (2016) Darzhavni politiki I strategii za regionalno razvitie. IK-UNSS, Sofia, pp 7–9
Nikolov G (2019) Innovations as a factor for regional growth. In: International Scientific Conference–trends in regional development and security management. Publishing Complex - UNWE, Sofia, pp 7–15
Petre A (2015) Trends and challenges of cohesion and convergence in the European union. Int J Econ Pract Theor 5:7–8
Vasileva E (2019) Biznes sreda I ustoychivo razvitie na regionite. IK-UNSS, Sofia, pp 17–19
www.nsi.bg—official site of the National statistical institute.
https://europa.eu/european-union/index_bg—official website of the EU

Chapter 25
Comparison Methods of Carbon Oil Sorbents Hardening

Elena Ushakova, Liliya Soloveva, and Andrey Ushakov

Abstract Oil sorbents based on carbon-containing waste of coal, woodworking enterprises and active sludge of biological treatment facilities were developed at the Department of Chemical Technology of Solid Fuel T. F. Gorbachev Kuzbass State Technical University. These sorbents performed well for water cleaning from oil, but they have low strength. Hardening methods of the developed granules are proposed and their influence on the characteristics of oil sorbents, such as moisture, ash content, density, volatile yield substances, compressive strength, as well as moisture and oil capacity were studied in this article.

Keywords Oil sorbents · Spills · Hardening methods

25.1 Introduction

For many years, surface waters is a subject of industrial harmful effects, especially oil producing, transporting and refining. The anthropogenic loads on many river reservoirs is significantly exceeds the water self-purification ability (Blais 2015).

A large number of effective water treatment methods have been developed. Sorption method is the most widely used; it is used for water purification from oil and petroleum products, as well as for the treatment of weakly concentrated wastewater and water containing several substances.

Peat (Kitaeva 2015), sawdust, agricultural waste (Hu 2010), clays of various kinds, sand, zeolites, etc. are used as the starting material for the sorbents creation. However, not all of them have the required quality: high sorption capacity for petroleum products and buoyancy, low moisture capacity, sufficient availability, etc. (Björklund and Li 2016).

Oil sorbents based on carbon-containing waste of coal, woodworking enterprises and active sludge of biological treatment facilities are developed at the Department of

E. Ushakova (✉) · L. Soloveva · A. Ushakov
T. F. Gorbachev Kuzbass State Technical University, Vesennyaya str. 28, 650066 Kemerovo, Russia
e-mail: brels@list.ru

H.-Y. Jeon (ed.), *Sustainable Development of Water and Environment*,
Environmental Science and Engineering,
https://doi.org/10.1007/978-3-030-75278-1_25

Chemical Technology of Solid Fuel T. F. Gorbachev Kuzbass State Technical University (Kvashevaia et al. 2017). These sorbents performed well for water cleaning from oil, but they have low strength.

There are many methods for harden carbon granules preparing:

I. Introduction of Additional Components:

(a) Molasses—syrupy liquid of dark brown color, having a specific smell. It gives strength to the granules due to the formation of calcium saccharide (Clarke 2003).

(b) Lignosulfonate—a product of technological processing of vegetable wood raw materials in pulp and paper production. It gives strength to the pellet due to the film formation in the mixture due to highly dispersed hydrate phases.

(c) Urea–formaldehyde resin—polycondensation product of urea with formaldehyde, having a high density of 1200 kg/m^3 (Paul et al. 2014).

(d) Difurfurilidenacetone increases the strength and yield of the carbon product due to its constituent vinyl and carbonyl groups that form mesh spatial structures (Lemes et al. 2010).

(e) Mineral additive—kaolinite (Bentz et al. 1999), montmorillonite (Runliang et al. 2016), illite (May et al. 2019).

Kaolinite ($Al_2O_3 \cdot 2SiO_2 \cdot 2H_2O$) is a substance characterized by a relatively dense and fixed structure of the crystal lattice with the smallest distance from the naturally recurring ions groups. Therefore, it is not able to attach and retain a large amount of water. The introduction of kaolin (as part of clay) in the sorbent leads to a decrease in moisture capacity and an increase in the density of granules.

Montmorillonite ($Al_2O_3 \cdot 4SiO_2 \cdot H_2O \cdot nH_2O$) has a relatively high cation exchange capacity. Its characteristic feature is the ability to adsorb various ions and ion exchange.

The crystal structure of Illite (hydroslude) ($K_2O \cdot MgO \cdot 4Al_2O_3 \cdot 7SiO_2 \cdot 2H_2O$) is a loosened laying of mica parts with a lack of kations in the interlayer gap and in the gibbsite octahedral layer. Water molecules occupy the interlayer space, freed from kations. Its characteristic properties are flexibility and elasticity. Its hardness is 1–2, and the density is slightly lower than 2.829 g/cm^3.

II. Carbon deposition on sorbent surface during thermal processing of hydrocarbon gases and liquid.

Gases and liquid hydrocarbons pyrolysis occurs at temperatures from 600–700 °C and close to atmospheric pressures. All pyrolysis reactions can be classified into two gropes.

Primary grope is characterized by the cleavage of paraffin and naphthenic compounds to hydrocarbons with a lower molecular weight. At the same time, the lower the molecular weight of the hydrocarbon, the higher the temperature required for its decomposition (for example, methane decomposes at 900 °C, ethane from 600 °C, propane about 500 °C).

Secondary reactions is occurring in the late stages of the pyrolysis process. As a result of the passage of secondary reactions, aromatic, aromatic polynuclear hydrocarbons are formed, as well as solid carbon compounds.

Same pyrolysis parameter is influenced on the formation of carbon.

Reducing pressure inhibits the formation of carbon. The longer the residence time of hydrocarbons in the high temperature zone, the higher the carbon yield (Kugatov et al. 2016). An increase in temperature above the optimal value increases the rate of hydrocarbons decay to hydrogen and carbon, so accompanied by intensive graphitization. An increase in the content of heavy hydrocarbons in the raw materials can allow a high yield of carbon (Kuvshinov 1999).

The aim of the work is to study the effect of mineral additives to the properties of carbon sorbents (derived from wood processing waste and excess activated sludge of biological treatment facilities), as well as the study of combined hardening method (introduction of mineral additives and carbon deposition on the finished product surface).

25.2 Methods

The main raw materials in this research work were sawdust (carbon-containing waste of woodworking enterprises), dehydrated excess activated sludge of biological treatment facilities, clay (mineral additives), and propane (gaseous hydrocarbon to produce carbon) (Clarke 2003).

There are characteristics of the raw materials in Table 25.1.

Liquefied propane (GOST 20,448–90) was used as a hydrocarbon gas (Bannov et al. 2012).

Sorbents production contain the four following stages.

Stage 1. Granulation of raw materials

Mixture containing 20% sawdust (as filler), 80% anaerobically treated excess sludge (as binder) is pre-prepared previously. In the case of granules hardening with mineral additives, dry clay is introduced into the initial mixture for granulation in amount 5% of the mass. The finished mixture was loaded into a drum-type granulator, where

Table 25.1 Characterization of raw materials

Characteristic	Sawdust	Excess sludge	Clay
Moisture, %	5–6	92–95	2–8
Ash content, %	5–7	35–37	–
Density, kg/m^3	105–117	1195–1205	850–900
Particle size	0.5–2 mm	–	less 5 mkm
Volatile yield, %	75–78	85–89	–
pH	–	6.3–7.3	–

spherical granules are formed due to the 'rolling' mode. The sizes of granules and density were regulated by the rotation speed of the drum.

At the end of granulation, the obtained granules were sorted to separate the 0.5–1 cm fraction. Remaining granules were destroyed and re-sent to the granulator.

Stage 2. Drying of the granules

Moisture removal was carried out in an infrared box at a temperature of 60ºC for 12 h.

Stage 3. The pyrolysis of the granules

Pyrolysis was carried out in a laboratory tubular electric furnace (Figs. 25.1, 25.2) without air access at a slow gradual heating to a temperature of 600 ± 50ºC for 60 min. Vapor–gas mixture consisting of water and resin vapors, as well as hydrocarbon gases, was removed from the retort.

Stage 4. Pyrolysis

Pyrolysis of hydrocarbon gases with carbon deposition on the surface of the sorbent (graphitization).

In the case of sorbent hardening by carbon deposition on the surface, propane was passed through the retort at a temperature of 800 ± 50ºC for 1–1.5 h. The volume flow rate of propane was 30 ml/min.

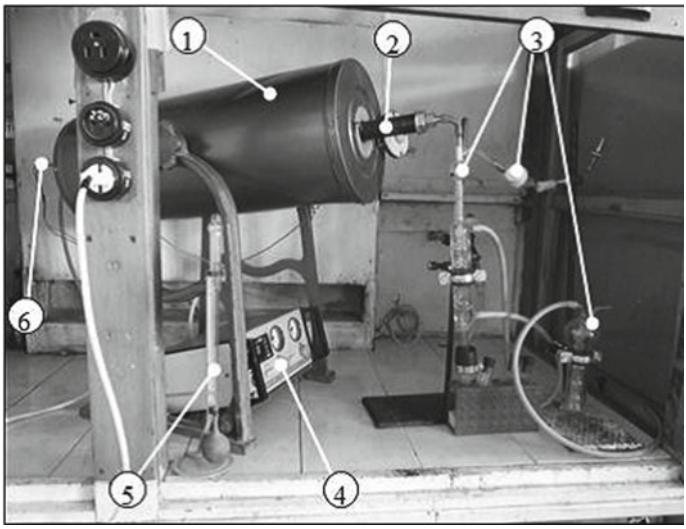

Fig. 25.1 Experimental pyrolysis plant for oil-sorbent preparing: 1—tube furnace; 2—pyrolyser reactor; 3—cooling and gas cleaning system; 4—control unit; 5—foam flowmeter; 6—temperature sensor

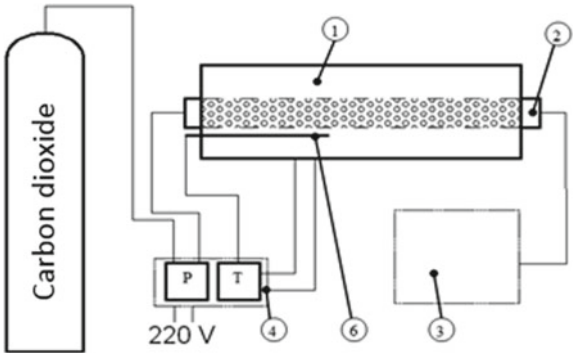

Fig. 25.2 Scheme of experimental pyrolysis plant for oil-sorbent preparing: 1—tube furnace; 2—pyrolyser reactor; 3—cooling and gas cleaning system; 4—control unit; 5—foam flowmeter; 6—temperature sensor

Stage 5. Cooling of the sorbent

Inert gas (CO_2) was passed through the retort for gradually reduce the temperature of the sorbent to 200 °C; further cooling was carried out in air.

The obtained sorbents were analyzed for moisture, ash content, density, volatile yield substances, compressive strength, as well as moisture and oil capacity.

Determination of moisture was carried out according to GOST 12,597 (Sorbents 2021), ash content—GOST 11,022 (Solid mineral fuels 2021), volatile yield—GOST 6382, water adsorption—GOST 21,290 (Coal briquettes 2021).

The granules density was determined by the calculation method according to the equation:

$$\rho = \frac{6m}{\pi d^3} \tag{25.1}$$

ρ granules density of, kg/m^3;
m granule weight, kg;
d average diameter in three dimensions, m.

The determination method of moisture and oil capacity is in detail described in the work (Ushakova et al. 2018).

Sorbent samples were placed in a container with petroleum products. Every 5 min, the sorbent was extracted and weighed. The mass of the adsorbed oil product was determined by the formula:

$$M = m_x - m_s \tag{25.2}$$

M mass of the sorbed oil product.
m_x sorbent mass with the adsorbed oil product, g;
m_s sorbent mass, g.

If the mass of the adsorbed oil product remains unchanged for 10 min, the test is stopped. The oil capacity of the sorbent was calculated:

$$OC = \frac{M_{max}}{m_s} \tag{25.3}$$

OC oil capacity, g/g;
M_{max} maximum mass of the adsorbed oil product, g;
m_s mass of the sorbent, g.

25.3 Results and Discussion

Oil sorbents obtained with the use of mineral additives did not differ externally from sorbents obtained without additives. In turn, the oil sorbents treated with propane pyrolysis products had a distinctive metallic luster.

The averaged characteristics of the obtained carbon oil sorbents are presented in Table 25.2.

As the results, if mineral additives of clay is introduced into the composition of oil sorbents the effect on increasing the strength of the obtained sorbents by 2 times and reducing their moisture capacity by 2 times is positive. These phenomena are a consequence of sintering clay with particles of raw materials. As a known, clay becomes durable and moisture-resistant material when firing, and therefore gives these properties to the finished sorbent.

At the same time, the phenomena of increasing the ash content of the product by 2 times can be considered unfavorable; it is great importance when disposing of spent oil sorbent. Increasing the density may adversely affect the buoyancy of the oil sorbent and lead to higher costs of product transportation.

However, the main negative consequence of the introduction of mineral additives is a decrease in the oil capacity of the oil sorbent (from 3.5 to 1.55 g/g).

Further deposition of carbon on the surface and pores of the sorbent allows increasing the granules strength up to 3 kg/granule. If the oil sorbent sating with

Table 25.2 Results of oil sorbents analysis

Characteristic	Oil sorbent type		
	Without mineral additives	With mineral additives	With mineral additives and after graphitization
Moisture, %	2.00 ± 0.32	1.12 ± 0.15	2.05 ± 0.19
Ash content, %	22.40 ± 0.12	57.41 ± 2.05	40.17 ± 1.56
Density, kg/m^3	195 ± 25	516 ± 32	731 ± 28
Volatile yield, %	35.20 ± 0.90	14.69 ± 0.32	11.58 ± 0.30
Compressive strength, kg/granular	0.40 ± 0.05	1.02 ± 0.23	3.20 ± 0.26
Oil capacity, kg/kg	3.50 ± 0.13	1.55 ± 0.09	1.55 ± 0.09
Moisture capacity, kg/kg	2.10 ± 0.60	0.03 ± 0.01	0.05 ± 0.01

carbon the ash content of the product and the yield of volatile are reducing, the density of the sorbent is increasing.

25.4 Conclusion

The mineral additives afford to increase the strength of carbon oil sorbents, but it is necessary to increasing the initial oil capacity. Carbon deposition on the surface and in the pores of oil sorbents can further increase the granules strength, but this method has shown effectiveness only in the case of introduction of mineral additives into the sorbent. Therefore, it is necessary to find the optimal content of mineral additives in the composition of oil sorbents, so that the graphitization process gives the strengthening, but the oil capacity of the product decreases slightly. It is also necessary to further study the effect of the different mineral additives on the graphitization process in sorbent.

The experiments revealed a decrease in the oil capacity of the sorbent with an increase in strength, so the main task of further research will be to find and study methods for increasing the oil sorption activity.

References

Bannov A, Varentsov V, Chukanov I, Gorodilova E, Kuvshinov G (2012) Comparative analysis of methods of oxidative modification of carbon nanofibers. Prot Met Phys Chem Surf 48:199–206

Bentz D, Garboezi E, Haecker C, Jensen O (1999) Effect of cement particle size distribution on performance properties of portland cement-based materials. Cem Concr Res 29(10):1663–1671

Björklund K, Li L (2016) Estimation of rock physics properties from seismic attributes. Water Sci Technol 4:35–53

Blais JM, Rosen M, Smol JP (2015) Environmental contaminants, 18th edn. Springer, Netherlands

Clarke M (2003) Encyclopedia of food sciences and nutrition, 2nd ed. Springer Academic Press

Coal briquettes. Method for the determination of water absorption homepage. http://docs.cntd.ru/document/1200024248. Last Accessed 06 Mar 2021

Ghiurea M, Dima S, Turcanu A, Fierascu R, Nicolae C, Trica B, Oancea F (2010) Carbonaceous nanostructures obtained by hydrothermal conversion of biomass. Proceedings 22:813–828

Hu B et al (eds.) (2010) Carbonaceous nanostructures obtained by hydrothermal con-version of biomass, Adv Mater 22:813–828

Kitaeva N, Bannova E, Alekseeva M, Merkov S, Llicheva N (2015) Adsorption properties of carbon sorbents based on carbonized peat. Biosci Biotechnol Res Asia 12(3):2393–2403

Kugatov P, Bashirov I, Zhirnov B (2016) Production of a mesoporous carbon adsorbent from carbon black and petroleum pitch by high-temperature roasting and steam activation. Coke Chem 59(9):345–348

Kvashevaia E, Ushakova E, Ushakov A (2015) Carbon-containing waste of coal enterprises in magnetic sorbents technology. In: The second International innovative mining symposium 2015, vol 21. Springer, Kemerovo, pp 1–7

Kuvshinov G et al (eds) (1999) Comparative analysis of methods of oxidative modifi-cation of carbon nanofibers. Carbon 37:1239–1246

Lemes P, Soto-Oviedo M, Waldman W, Innocentini-Mei L, Duran N (2010) Effect of lignosulfonate on the thermal and morphological behavior of poly(3-hydroxybutyrate-co-3-hydroxyvalerate). J Polym Environ 18:250–259

May H, Kenichiro N, Sohei N (2019) Durability index for quality classification of cover concrete based on water intentional spraying tests. Cement Concr Compos 104:54–67

Paul A, Ezeh E, Gimba E, Arthur D (2014) Comparative study of phenol formaldehyde and urea formaldehyde particleboards from wood waste for sustainable environment. Int J Sci Technol Res 3(9):53–61

Runliang Z, Qingze C, Qing Z, Yunfei X, Jianxi Z, Hongping H (2016) Adsorbents based on montmorillonite for contaminant removal from water: a review. Applied Clay Sci 123:239–258

Solid mineral fuels. Methods for determination of ash homepage. http://docs.cntd.ru/document/gost-11022-95. Last Accessed 06 Mar 2021

Solid mineral fuel. Methods for determination of volatile matter yield homepage. http://docs.cntd.ru/document/1200029223. Last Accessed 06 Mar 2021

Sorbents. Method for determination of moisture fraction of total mass in activated carbons and catalysts on their base homepage. http://docs.cntd.ru/document/1200017238. Last Accessed 06 Mar 2021

Ushakova E, Kvashevaya E, Ushakov A (2018) Innovative environment-saving technology using magnetic sorbents based on carbon-containing waste from coal. In: IIIrd international innovative mining symposium 2018, vol 41. Springer, Kemerovo, pp 36–40

Chapter 26
Integration of Experimental and Numerical Methods to Investigate the Effect of Hydraulic Retention Time on Ultrafiltration Membrane Fouling

Meng Yao, Ting Chen, Zhilin Ran, Xiaoqing Dong, and Guosheng Wang

Abstract The floc formation, breakage and regrowth processes were investigated by numerical simulation to explore the effect of hydraulic retention time on ultrafiltration membrane (UF) fouling. Using a numerical method, the floc average size, fractal dimension and porosity under various coagulation conditions were investigated. The standardized flux and invertibility of membrane fouling were also investigated. Results illustrated that flocs formation under shorter flocculation time (10 min) had a small value of fractal dimension, which readily generated a larger pores and shaggy cake layer on the surface of membrane. An initial simplified breakage model based on DLA model was proposed, which demonstrated that the broken flocs afforded more opportunities for diffused particles to access deeper-lying flocs uniformly packed around the aggregated core. Flocs became increasingly compact with increased time of stirring after breakage. Therefore, shortening of stirring time, whether during flocculation or recovery process, could enhance the permeability of membrane.

Keywords DLA model · Numerical simulation · Hydraulic retention time · Flocculation and ultrafiltration · Membrane fouling

26.1 Introduction

As the alternative within the drinking water treatment process, membrane technology could provide high quality drinking water, which can meet much stricter water quality regulations (Yu et al. 2010). But, fouling remains the primary shortcoming of membrane ultrafiltration process. Fouling results in a decline of flux leading to higher water treatment cost and a degenerating of the membrane (Jarvis et al. 2005).

M. Yao (✉) · Z. Ran · X. Dong · G. Wang
School Key Laboratory of New Technology of Urban Water Environment, School of Transportation and Environment, Shenzhen Institute of Information Technology, Shenzhen 518000, People's Republic of China
e-mail: ym808766@163.com

T. Chen
Guangdong GDH Water Company Limited, Shenzhen 518021, People's Republic of China

H.-Y. Jeon (ed.), *Sustainable Development of Water and Environment*,
Environmental Science and Engineering,
https://doi.org/10.1007/978-3-030-75278-1_26

Pre-coagulation treatment before UF, the membrane fouling is significantly reduce particularly by "in-line" chemical coagulation (Zhao et al. 2011; Yu et al. 2012). The influences of pre-coagulation on membrane permeability primarily relate to the coagulation conditions, such as coagulants species, dosages and mixing mode (Wei et al. 2009; Xu et al. 2014). Choi and Dempsey (2004) found the alum concentration was key factor to impact the polyethersulfone flat-sheet UF membrane fouling, and indicated that "in-line" coagulation increase the hydraulic removal of filter cake. In addition, compared with under the sweep floc condition, the flocs formation under charge neutralization condition have lower hydraulic resistance. Significantly, the characters of aggregates formed by various coagulations can affect membrane fouling (Yao et al. 2014; Yu et al. 2015). It should be noted that the configuration of particle aggregates is correlated with the flocculation time in the coagulation/flocculation process.

Rossini and Garrido proved that the effect of the rapid mixing time on final coagulation efficiency, and indicated that a short time of rapid mixing was beneficial for producing lesser residual turbidity (Rossini et al. 1999). Nevertheless, little interest has been taken in the influence of flocculation time on the performance of the coagulation UF process. Therefore, this deserved more attention to understand the morphology of flocs under different reaction times.

A pathbreaking fractal growth model, the diffusion-limited aggregation (DLA) model, was initially proposed to describe aggregating properties of inorganic particles, (Parkinson et al. 1999). The DLA model which applying simple growing rules, is able to represent a more realistic phenomenon of fractal which can provide particular information to allow deep investigation of the structure of aggregation. Although much recent research has studied on the DLA model, the majority attention has posed on the and properties of aggregation and physical growth mechanism (Yao et al. 2014; Higashitani et al. 2001; Zhao et al. 2013). Several past studies have found that the shear force compel dispersed particles moving in the orthokinetic regime, indicating that all particles shift in the same direction (Hopkins and Ducoste 2003; Mpofu et al. 2003). To study approaches to grow single floc during flocculation treatment, the present study proposed that random motion of particles is the primary account behind the fractal structure of floc, while the rotation in uniform direction of each particle was neglected. On account of this assumption, the two dimensional (2D) DLA model was applied to illustrate the development program of single floc under a shear flow field. In addition, a parameter representing time was included in DLA model to simulate the growth process of individual floc under various reaction times. Furthermore, we modified this classic model to allow for the study of complex mechanism of flocs in practice, and we expect that this method could aid improved understanding of the changes in flocs shape during the breakage process. Based on model modification, the DLA model was used to analyze the morphological characteristics of flocs settled on the surface of UF membrane. The impact of different flocculation times during coagulation process was investigated to provide an improved process understanding of aggregate properties on membrane fouling in the subsequent UF process. The main research were the effects of flocs size, structure and characteristics of floc surface on the UF membrane process with pre-coagulation. Besides, the

invertibility of membrane fouling was also studied. An improved 2D DLA model, which extended the maximum motion steps, was applied to predict the floc growth. The model provided an analysis of the influence on floc property under different flocculation times on membrane fouling. The modified comprehending of this process could provide significant additional cognition in the field of UF membrane fouling natural and the coagulation of organic matter (NOM).

26.2 Materials and Methods

26.2.1 Stock Solution and Coagulant

The Kalolin clay concentration was 100 mg L^{-1} by dissolving the clay (Tianjin, China) in tap water. The suspension was consisted of 100 mg L^{-1} kaolin and 2 mg L^{-1}humic acid. The final turbidity of suspension was about 100 NTU, measured by an online turbidity meter (700AQ, WTW, Germany).

The basicity of Polyaluminum chloride (PACl) (28% quality calculated as Al^2O^3), was 72.3%. By dissolving 5 g of reagent in 500 mL deionized water, the concentration of PACl remained to 1% (Yu et al. 2017). This solution was used directly, without prior preparation.

26.2.2 Coagulation and UF Procedure

Concurrent with the addition of the optimal dosage of PACl (approximately 0.08 mM Al) to the reactor, the test water sample was rapidly mixed at 400 rpm ($G \approx 175\ s^{-1}$) for 60 s to destabilize particles. Two modes of flocculation process were conducted to indicate the evolution of floc morphology with various HRT. The first mode was set to have a slow stirring at 94 rpm min − 1 ($G \approx 20\ s^{-1}$) for 10 min, 15 min, 20 min and 25 min, respectively. The second mode was set to have a slow stirring at 94 rpm min^{-1} for 20 min and 400 rpm min^{-1} for 1 min to break the flocs, following which the stirring speed returned to 94 rpm min^{-1} for 5, 10, 15 and 20 min to recover flocs. In addition, during this process, the condition of average size and fractal dimension of flocs were measured by on-line monitoring devices.

After implementing different flocculation times and a slow stirring speed, the effluent was slowly tripped to the unit of dead-end filtration and filtered by a UF membrane without sedimentation. This dead-end batch UF unit, which consisted by a 400 mL- capacity cylindrical beaker (Amicon 8400, Millipore, US) was used for UF experiments, with Fig. 26.1 illustrating the process followed. The UF membrane (Mosu, Shanghai, China) with a cutoff molecular weight (MWCO) of 100 kDa was applied for UF. The material of membrane used was polyethersulfone (PES). What is more, the effective membrane area could reach 50.24 cm^2. In every UF experiment,

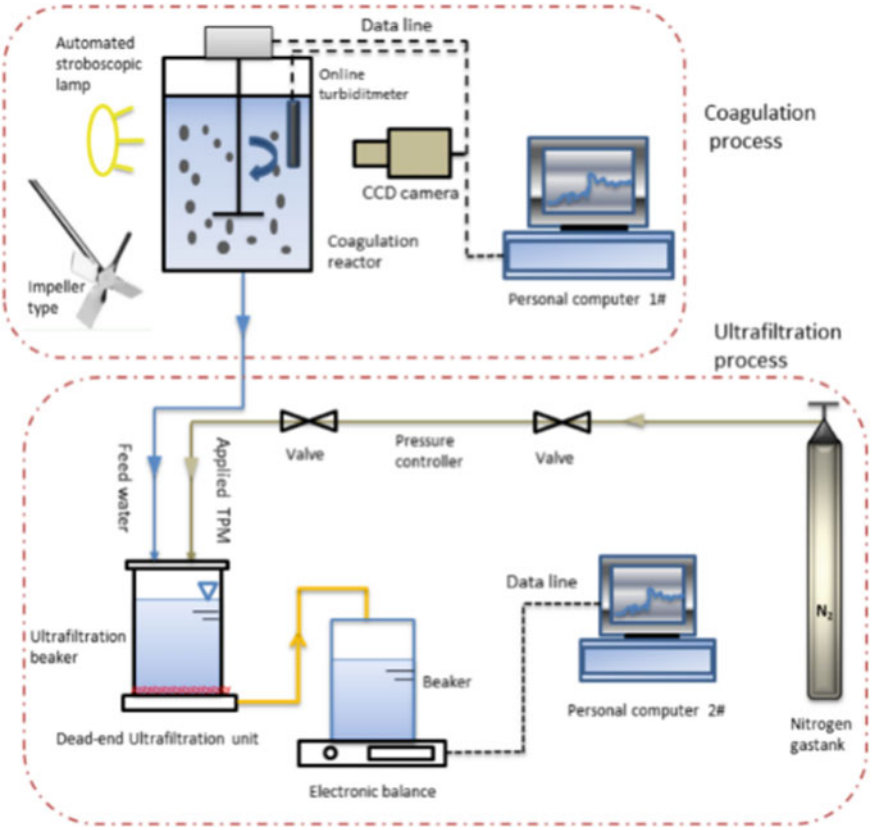

Fig. 26.1 Flow chart of pre-coagulation/UF experiments

a fresh section of membrane was adopted. The nitrogen gas was applied to maintain the constant pressure of 0.15 MPa. The electronic balance was used for measuring the instantaneous mass of cumulative permeate (SI-2002, Denver Instrument, China) and the data were uploaded to a personal computer.

Every UF test contains three periods, with each in turn includes three steps. Reversible fouling (RF) was defined as the pollutant, which was removed by backwash process. Whereas contaminants inside the membrane holes and remaining on membrane surface and were classed as irreversible fouling (IF). The two kinds of fouling collectively comprise total fouling (TF). The calculation formulas of RF, IF and TF were as follows:

$$IF_n = \frac{J_{p(n-1)} - J_{p(n)}}{J_{p(0)}} \tag{1}$$

$$TF_n = \frac{J_{p(0)} - J_{f(n)}}{J_{p(0)}} \tag{2}$$

$$RF_n = TF_n - IF_n \tag{3}$$

26.2.3 Modified Version of the 2D DLA Model

26.2.3.1 Underlying Mechanism of the DLA Model

The Matrix Laboratory (MATLAB) software was used for Off-lattice simulations of the 2D irreversible aggregation processes. The original DLA algorithm was implemented by placing a seed particle in the center of the cube. A new monomeric particle was then released far from the seed, which moved randomly on the lattice at a constant step size in each direction until it collides with the seed particles and sticks. A particle was removed from the model if during the course of the movement it crossed the lattice boundary. A new particle was then generated, and the process repeated. The development of a DLA cluster was caused by the agglomeration of particles. Simulations could be sped up by increasing the step sizes or returning rather than escaping.

The preset parameters of M are introduced into the 2D-DLA model to denote the free particles total motion step length from emergency state to hold or escape/destruction, indicating the influence of time on development of virtual floc. The maximum motion step (abbreviated to MS) of monomeric particles was firstly imported into this model, which was applied for blocking the free particles moving time. Besides, when the M was larger than that of the presetting MS, the free particle was removed or kept away from the cubic system. Besides, in the feasible tests, the hydraulic residence time (HRT) is equivalent the MS in the numerical modeling process, which facilitated the dynamic simulation of floc morphological properties in the modeling method. The maximum motion steps was added into the aggregation and regrowth process as MSA and MSR to simplify this model. The influence of aggregation and time of regrowth on the characteristics of simulated flocs could be efficiently studied varies with the value of MS.

26.2.3.2 Simple Breakage Model

The surface erosion and mass fragmentation were considered as two typical modes of floc broken (Jarvis et al. 2005; Mikkelsen and Keiding 2002). As typical flocs strength models, Rumpf and Kendall(K) were used to conduct the simplified method of floc breakage, namely MSA and MSR, which are able to attain a visualization prediction of floc aggregation, breakage and regrowth processes (Kendall et al. 1986).

The gyration radius of simulated floc was calculated using the following equation (Serra et al. 1997):

$$R_g = \left[\sum_{i=1}^{N} r_i^2\right]^{1/2} = \left[\frac{1}{N}\sum_{i=1}^{N}\left((x_i - x_0)^2 + (y_i - y_0)^2\right)\right]^{1/2}, \quad (4)$$

where R_g is the gyration radius of virtual floc and r_i is the distance between the ith particle (x_i, y_i) and the centroid of the virtual floc (x_0, y_0).

The coordinates of the centroid were calculated according to Eq. (5):

$$x_0 = \frac{1}{N}\sum_{i=1}^{N} x_i y_0 = \frac{1}{N}\sum_{i=1}^{N} y_i \quad (5)$$

where x_i and y_i are the abscissa and ordinate of the number i particle, respectively.

The fractal feature of simulated flocs also used the boundary fractal dimension as mentioned above. In addition, the ratio of the number of particles in the formed flocs to the number of grids in the rotating radius region is denoted as the porosity of the simulated flocs. As the porosity ratio, S, the following expression may be obtained:

$$\mathrm{S} = 1 - \pi * \gamma^2 N\left(R_g\right)/R_g^2, \quad (6)$$

where r is the particle radius pre-set as 0.5 and (Rg) is the particle number in the gyration radius.

26.3 Results and Discussion

26.3.1 Effect of MSA on Virtual Floc

The final configurations of flocs simulated by the improved 2D DLA model using various MSA values are exhibited in the first row of Fig. 26.2. In each sub-image the symbol at lower left indicated the porosity ratio and Df of simulated flocs. When the least aggregated steps (MSA = 200) was adopted, the fractal feature of virtual flocs was not obviously observed. With the slightly longer time of aggregation, the simulated flocs gradually grew in the prominent direction and the irregular branches shown. When MSA = 1000, the increase of the branches of simulated flocs in every direction was observed. With the increase of aggregated time, the increase of flocs size in the coagulation process was obtained, which was similar to the actual experiment results. The DLA numerical simulation illustrated that particles usually grow towards the strong branches without breakage during the procedure. Because of the more opportunities to intercept suspended particles of the long and robust branches, the growth of branches was inhibited by that. This shielding effect also constrained the movement of free particles into the inner part of virtual flocs.

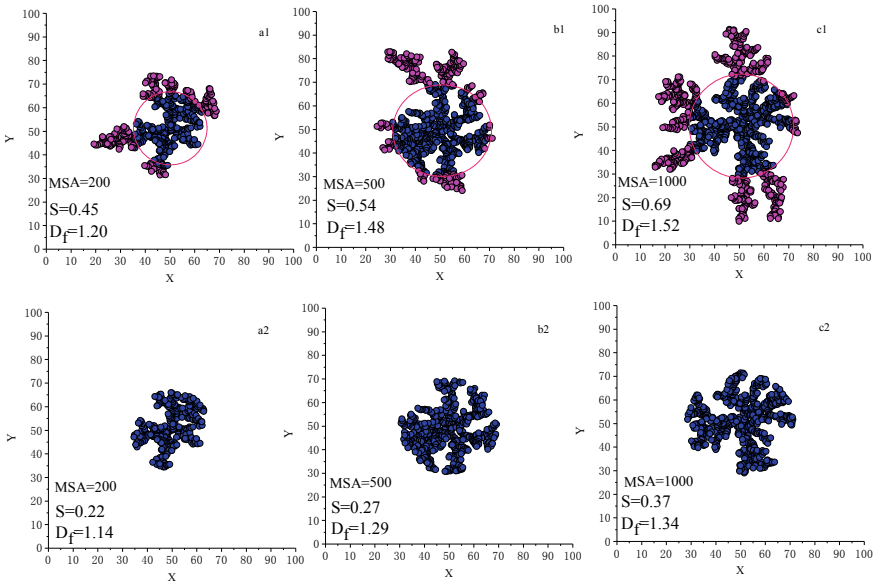

Fig. 26.2 Morphological characteristics of original and broken virtual flocs under different MSA

Although flocs with 200 MSA appear compact, the value of D_f was only 1.2. This implies that floc structure was not yet fully developed leading to a larger number of small particles and micro-flocs are expected in this system. As reaction time extended (500 MSA), free particles readily adhered to the developed branches of virtual floc, thereby promoting the growth of flocs to follow a pattern of increased branches and roughness. A fractal structure of flocs gradually appeared as D_f increased to 1.45, whereas porosity of flocs also grew larger than 200 MSA. The Carman–Kozeny Equation has been described as the cake resistance of porous materials and indicates a direct correlation between hydraulic resistance and cake porosity. It can be assumed that a relatively porous polyhedral structure can be generated in this case, resulting in a looser cake layer on the membrane surface with lower resistance. A feasible control of MSA is significant for the production of flocs with the desired structure and characteristics and to further migrate membrane fouling during the UF process.

26.3.2 Effect of Flocculation Time on Membrane Flux

The UF experiments were performed by filtering the pre-coagulation suspensions under different flocculation times. The normalized permeate fluxes ($J/J_{P(0)}$) versus filtration volume are shown in Fig. 26.3.

According to our previous study (Yao et al. 2015), the same raw water was applied and the standardized permeate fluxes reduced dramatically from 1 to 0.4 by the end

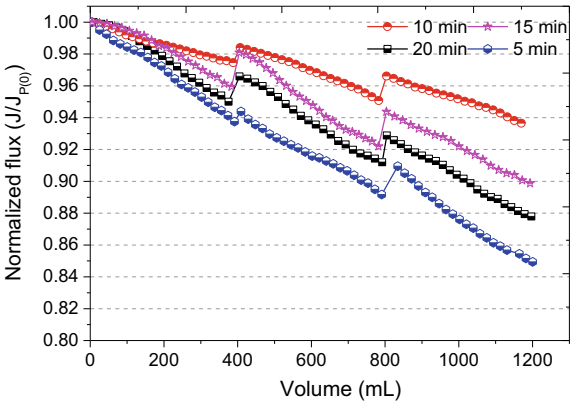

Fig. 26.3 Normalized ultrafiltration permeate flux profiles of different flocculation times

of the experiment. In contrast, it could be found that the permeate fluxes were significantly improved by pre-coagulation, independent of flocculation time. Specifically, with the increase in flocculation time, flux was improved. Under slow stirring for 5 min, the final value of $J/J_{P(0)}$ was approximately 0.85, whereas the final normalized flux increased to 0.93 at 10 min under slow stirring. Inversely, this value tended to be declined with further increases in flocculation time. This implies that flocculation time is able to influence the performance of UF. Coagulation effluents, the feed water of UF, contained floc of different sizes formed under various flocculation times. Thus, the membrane fouling could be impacted by the characteristics of flocs developed in the former coagulation process. This result in the 2D DLA model illustrated that there was insufficient opportunity for the particle to aggregate with a reduced aggregation time. Small particles remained in the system, and it is difficult to remove those particles by sedimentation. In addition, both fractal dimension and porosity of virtual flocs are increased with an increase in MSA (Fig. 26.2). The flocs external structure became increasingly mature, whereas the internal structure gradually loosened. Fractal dimension is positively correlated to the density of formed flocs as well as the density of the cake layer formed by flocs (Yu et al. 2015). Due to the superior settleability in the subsequent settling unit, the flocs with higher effective densities are suitable for the traditional coagulation process. Nevertheless, such aggregates were readily compressed by outer pressure and the buildup of a tight cake layer results in a higher specific resistance to water flow.

26.3.3 Effect of Different Flocculation Times on Reversibility of Membrane Fouling

Previous studies have shown that particle sizes < 3 nm resulted in minimal membrane fouling (Ma et al. 2014). The RF and IF, which occurred during filtration under different membrane flocculation times, are shown in Fig. 26.4.

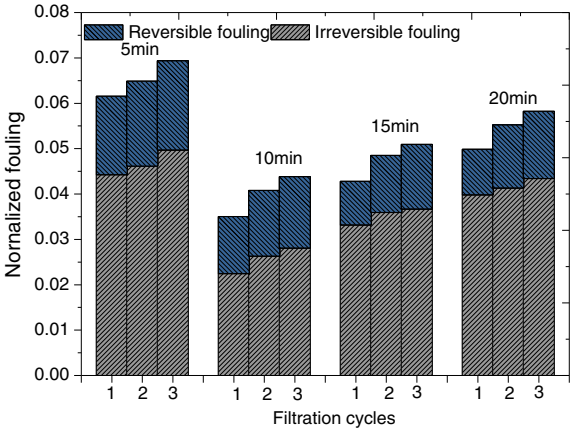

Fig. 26.4 Effect of different flocculation times on the reversibility of membrane fouling

Under different MSA values of a1, b1 and c1, the differences were 12.16, 11.37 and 17.6, respectively shown in Table 26.1. Corresponding with MSA values, the broken flocs diversity always become similar. This phenomenon provided a stronger indication of the presence of a critical point at which flocs structure transforms from isotropic to anisotropic. In addition, the results also implied the inhibition of branch growth strengthens. The flocs formed before breakage are characterized by a larger number of abnormal branches. However, the number of broken flocs branches, which do not appear to follow any pattern, started to decrease. After breakage, there were significant reductions in S and D_f of broken flocs. Particularly under slowly stirring for 5 min, the permeability of the cake layer decreases because of incomplete particle aggregation and a higher number of residual small particles. The removal of smaller particles by backwash is difficult, which resulted in further severe IF.

26.3.4 Effect of MSR on Virtual Flocs

Some studies has shown through experiment that broken flocs will recovery under suitable hydraulic conditions (Zhao et al. 2013; Barbot et al. 2010). A modified simulation with the specific operations was performed for visualizing the restructure of broken flocs under various MSR, and shown in Sect. 2.3.2. The improved study of the relationship between flocs structure and UF membrane fouling was achieved by numerical simulation. By considering broken flocs as aggregated cores, the regrowth process occurred between small clusters and scattered particles in this simulated aggregated system. The final shape of re-aggregated virtual flocs under various values of MSR are shown in Fig. 26.5.

The characteristic length of regrown simulated flocs become more uniform than that of flocs before breakage, indicating that free particles have a similar chance of capture by the branches. Furthermore, it is noteworthy that the configuration

Table 26.1 Characteristic lengths of virtual flocs for each direction

Characteristic length	a1	a2	a3	a4	b1	b2	b3	b4	c1	c2	c3	c4
Positive direction of x	18.71	12.79	21.02	23.41	25.39	19.34	25.91	25.29	33.97	21.35	26.71	30.12
Positive direction of y	23.40	15.94	22.65	23.11	26.01	19.26	25.06	28.04	40.03	21.03	23.01	28.92
Negative direction of x	30.70	15.36	19.03	25.21	21.16	19.17	27.58	29.21	23.64	21.115	29.40	31.40
Negative direction of y	18.54	15.64	23.08	27.86	32.89	19.10	23.41	27.63	41.24	21.44	24.37	32.83

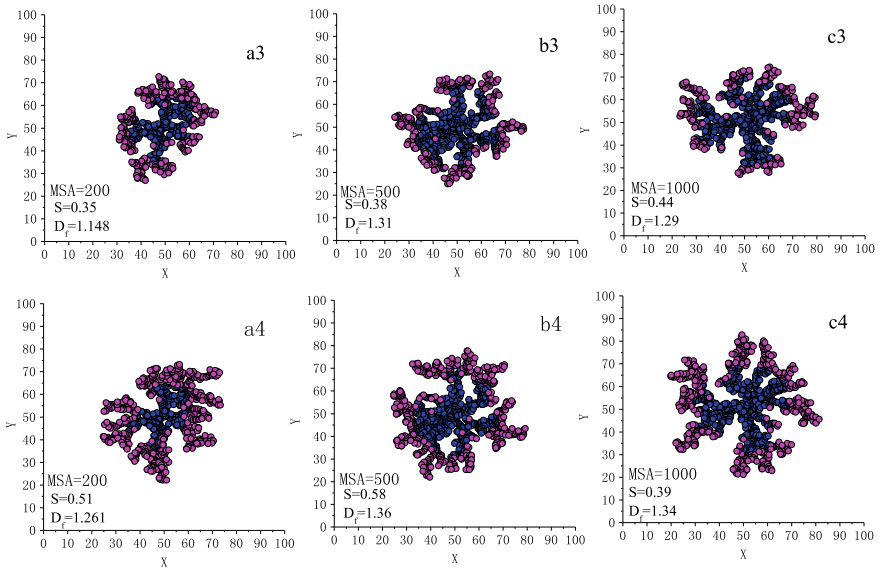

Fig. 26.5 Morphological characteristics of regrown virtual flocs under different MSR

of broken flocs effected on the feature of regrown flocs. A comparison between characteristic lengths of simulated regrown flocs under the same MSR showed that a higher number of flocs existed with the increase of MSA. Compared with large MSA, it is obviously observed that formation of broken flocs under smaller MSA have less potential connection points for regrowth. Despite this, the values of S and Df of original flocs were higher than regrown flocs. This results indicated that the breakage and regrowth processes could improved the properties of flocs. In addition, comparing the characteristic features of regrown flocs produced under various values of MSR showed that a slightly larger amount of compacted flocs formed under a greater MSR. This indicates that a slightly longer regrowth time could compress flocs on the surface of membrane and further result in serious fouling of membrane. A strategy of shortening the regrowth stirring time could relieve membrane fouling, provided that particles have sufficient opportunity to collide.

26.3.5 Effect of Regrowth Time on Membrane Filtration

Coagulation under various regrowth times was conducted to study the influence of various slow stirring conditions on UF performance. In addition, the associated normalized permeate fluxes with filtration volume are plotted in Fig. 26.6. In particular, because of the largest eventual permeate flux, the improved flux was most effective by regrowth time of 10 min. The regrowth time of 5 min contributed to the smallest increase of membrane flux.

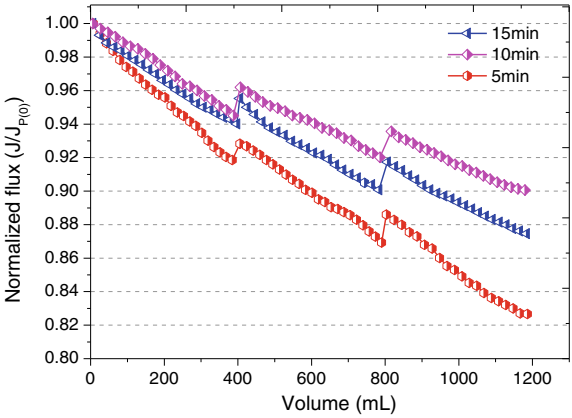

Fig. 26.6 Normalized ultrafiltration permeate flux profiles under different regrowth times

Though the average size of floc formed with 10 min regrowth time was smaller than those under regrowth times of 15 and 20 min, 10 min was sufficient for the collision and aggregation of dispersed particles. It is obviously from the Fig. 26.5 indicated a more compact floc structure could be obtained. According to previous study, the loose aggregates produced less resistance for membrane UF. On the contrary, the tight flocs caused a cohesively structured cake layer which was able to augment UF resistance and reduce aggravate the flux declines (Wang et al. 2009). Therefore, the application of 10 min regrowth provides more significant results and meaning.

26.3.6 Effect of Regrowth Time on the Reversibility of Membrane Fouling

Both RF and IF occurred under various slow stirring speeds, as presented in Fig. 26.7. Significant increase in RF and IF were evident with the increase of stirring time after the breakage procedure. This can likely be attributed to a mild stirring after breakage resulting in the cementing of small particles to produce floc aggregates. Besides, a smaller number of small-sized aggregates are deposited in membrane pores. The higher values of fractal dimension implies the enhancement of effective density, resulting in the increase of floc settling velocity. Flocs with lower densities were able to form a higher porosity cake layer. However, because of the more compression of regular-shaped flocs by external pressure, the flocs with higher values of fractal dimensions leaded to more serious fouling (Choi and Dempsey 2004; Barbot et al. 2010; Kim 2015). In the present study, shortening the stirring time after breakage could produce loose and porous flocs, which decreased IF. IF was strengthened under a regrowth time of 5 min. These results indicate that the morphology of flocs is key factor to effect the reversibility of fouling. A shorter time of the mixing stage after breakage could effectively limit TF and IF through the UF process.

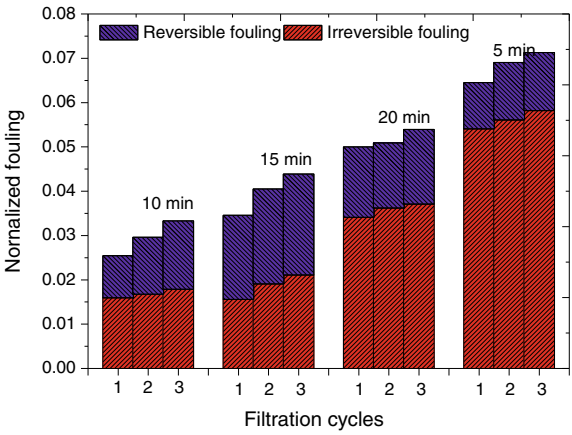

Fig. 26.7 Effect of different regrowth times after flocs breakage on the reversibility of membrane fouling

26.4 Conclusion

The dynamical variation of floc structure under various HRTs in flocculation process has been studied by experimental and simulated analysis to investigate the impact of hydraulic retention time on UF membrane fouling. The HRTs significantly affected floc structure and UF membrane fouling. Therefore, the adoption of a shorter slow stirring time (10 min) was more appropriate to reduce membrane fouling. According to the model, the exposure of the breakage and vacant adhesion destroyed the sites peripheral branches of virtual flocs, which resulted in the production of isotropic floc pieces. Free particles have more chance of entering inner flocs, and are uniformly packed around the aggregated core with increased regrowth times, which comprised available flocs with a high density. Therefore, the adoption of an appropriately shortened and slow stirring time (10 min) appeared to effectively enhance the permeability of membrane.

References

Barbot E, Dussouillez P, Bottero JY, Moulin P (2010) Coagulation of bentonite suspension by polyelectrolytes or ferric chloride: floc breakage and reformation. Chem Eng J 156:83–91

Choi KYJ, Dempsey BA (2004) In-line coagulation with low-pressure membrane filtration. Water Res 38:4271–4281

Higashitani K, Iimura K, Sanda H (2001) Simulation of deformation and breakup of large aggregates in flows of viscous fluids. Chem Eng Sci 56:2927–2938

Hopkins DC, Ducoste JJ (2003) Characterizing flocculation under heterogeneous turbulence. J Colloid Interf Sci 264:184–194

Jarvis P, Jefferson B, Gregory J, Parsons SA (2005) A review of floc strength and breakage. Water Res 39:3121–3137

Kendall K, Alford NMcN, Tan SR, Birchall JD (1986) Influence of toughness on Weibull modulus of ceramic bending strength. J Mater Res 120–123

Kim H-C (2015) In-line coagulation with quaternary amine polymer prior to microfiltration of humic-rich water. J Colloid Interf Sci 459:151–159
Ma B, Yu W, Liu H, Qu J (2014) Effect of low dosage of coagulant on the ultrafiltration membrane performance in feedwater treatment. Water Res 51:277–283
Mikkelsen LH, Keiding K (2002) Physico-chemical characteristics of full scale sewage sludges with implications to dewatering. Water Res 36:2451–2462
Mpofu P, Addai-Mensah J, Ralston J (2003) Investigation of the effect of polymer structure type on flocculation, rheology and dewatering behaviour of kaolinite dispersions. Int J Miner Process 71:247–268
Parkinson J, Brechet Y, Gordon R (1999) Centric diatom morphogenesis: a model based on a DLA algorithm investigating the potential role of microtubules. Biochem Biophys Acta 1452:89–102
Rossini M, Garrido JG, Galluzzo M (1999) Optimization of the coagulation–flocculation treatment: influence of rapid mix parameters. Water Res 33:1817–1826
Serra T, Colomer J, Casamitjana X (1997) Aggregation and breakup of particles in a shear flow. J Colloid Interf Sci 187:466–473
Wang Y, Gao B-Y, Xu X-M, Xu W-Y, Xu G-Y (2009) Characterization of floc size, strength and structure in various aluminum coagulants treatment. J Colloid Interf Sci 332:354–359
Wei J, Gao B, Yue Q, Wang Y, Li W, Zhu X (2009) Comparison of coagulation behavior and floc structure characteristic of different polyferric-cationic polymer dual-coagulants in humic acid solution. Water Res 43:724–732
Xu W, Gao B, Du B, Xu Z, Zhang Y, Wei D (2014) Influence of shear force on floc properties and residual aluminum in humic acid treatment by nano-Al-13. J Hazard Mater 271:1–8
Yao M, Nan J, Chen T (2014) Effect of particle size distribution on turbidity under various water quality levels during flocculation processes. Desalination 354:116–124
Yao M, Nan J, Li Q, Zhan D, Chen T, Wang Z, Li H (2015) Effect of under-dosing coagulant on coagulation-ultrafiltration process for treatment of humic-rich water with divalent calcium ion. J Membr Sci 495:37–47
Yu WZ, Gregory J, Campos L (2010) Breakage and regrowth of al-humic flocs - effect of additional coagulant dosage. Environ Sci Technol 44:6371–6376
Yu W, Hu C, Liu H, Qu J (2012) Effect of dosage strategy on al-humic flocs growth and re-growth. Colloids Surf A Physicochem Eng Asp 404:106–111
Yu W, Gregory J, Campos LC, Graham N (2015a) Dependence of floc properties on coagulant type, dosing mode and nature of particles. Water Res 68:119–126
Yu W-Z, Qu J-H, Gregory J (2015) Pre-coagulation on the submerged membrane fouling in nano-scale: effect of sedimentation process. Chem Eng J 262:676–682
Yu W, Graham N, Liu T (2017) Effect of intermittent ultrasound on controlling membrane fouling with coagulation pre-treatment: significance of the nature of adsorbed organic matter. J Membr Sci 535:168–177
Zhao YX, Gao BY, Shon HK, Wang Y, Kim JH, Yue QY (2011) The effect of second coagulant dose on the regrowth of flocs formed by charge neutralization and sweep coagulation using titanium tetrachloride (TiCl4). J Hazard Mater 198:70–77
Zhao YX, Gao BY, Qi QB, Wang Y, Phuntsho S, Kim JH, Yue QY, Li Q, Shon HK (2013) Cationic polyacrylamide as coagulant aid with titanium tetrachloride for low molecule organic matter removal. J Hazard Mater 258–259:84–92

Chapter 27
Using Electrodialysis to Recycle Chemical Polishing Agent from Anodizing Industry

Jih-Hsing Chang, Mohanraj Kumar, and Shan-Yi Shen

Abstract In this study, we use the electrodialysis technique (ED) to recycle chemical polishing agents, including the removal efficiency of aluminum ions and water quality variation. Finally, the electricity consumption of the ED technique for separating aluminum ions was estimated. The ED system was composed of a cation exchange membrane, anion exchange membrane, and graphite electrode. With a current of 1.0 A and an average voltage of 70 V, the treatment time was 60 min. The results showed that variation of pH and conductivity in the wastewater has a stable status. The aluminum ion concentration was rapidly decreased from about 11,056 to 2,512 mg/L in the wastewater chamber within 30 min, and the removal efficiency reached 78%. The variation of concentration indicated that the high concentration of aluminum ion is rapidly adsorbed on the cation exchange membrane under the ion permeation in the early stage of operation, resulting in a significant decrease in the aluminum ion concentration. After the adsorption was saturated, the aluminum ion became movable from the cation exchange membrane to the cathode under electromigration. With the operating time, the concentration of aluminum ions gradually increased at the recovery chamber. The electricity consumption shows that the ED can effectively separate aluminum ions in the wastewater and recycle chemical polishing agents.

Keywords Electrodialysis · Aluminum ions · Chemical polishing agents · Ion exchange membrane

27.1 Introduction

Surface chemical polishing used in the anodizing industry is an essential process for metal surface treatment, the reflection, heat reflection, and corrosion resistance can be improved. The chemical polishing agent's function is to achieve a smooth and flat substrate (Wang et al. 2005; Huang et al. 2019). The chemical polishing agent is a mixture of strong acids, consists of phosphoric acid 40%, nitric acid 30%,

J.-H. Chang · M. Kumar · S.-Y. Shen (✉)
Department of Environmental Engineering and Management, Chaoyang University of Technology, Wufeng 41349, Taiwan

H.-Y. Jeon (ed.), *Sustainable Development of Water and Environment*,
Environmental Science and Engineering,
https://doi.org/10.1007/978-3-030-75278-1_27

hydrochloric acid 10%, and sulfuric acid 10%. Among them, phosphoric acid is the main component of chemical polishing agents, and the cost is expensive. The amount of chemical polishing agents used in the anodizing process is large, and the concentration of the aluminum ion in the polishing agent was increased with the number of polishing. The polishing agent cannot be used continuously when containing a high concentration of aluminum ions. Polishing wastewater has not easy to recycle, and the high concentrations of metal ions will cause environmental pollution. Traditional methods are costly, operation complicated and challenging to recycle. Inappropriate treatment will cause damage and pollution to the human body and environment. So far, it isn't easy to treat this type of wastewater. Therefore, most polishing agent wastewater can only be outsourced for treatment and purchase polishing agents, but the polishing agents are imported from abroad and expensive.

Since a high concentration of aluminum ions was produced after the polishing agent uses, resulting in the polishing performance is reduced. It makes the polishing agent unable to be used for a long time. Therefore, it is urgent to find a practical and cost-effective wastewater treatment technique to recover polishing agent wastewater. The ED technique has advanced in recent years, mainly used in seawater desalination, food industry, heavy metal recovery in the chemical industry, and wastewater treatment (Doornbusch et al. 2021; Xu et al. 2020; Bdiri et al. 2018; Smara et al. 2007; Abou-Shady 2017; Jiang et al. 2018). The main advantages of ED with a small treating space and fast separation of metal ions, and it is an environmentally friendly wastewater treatment technique. The ED mechanism is to drive ions in water to penetrate through ion exchange membranes with selective permeability by electric energy, which promotes the migration of ions in different polar directions to separate ions in water (Al-Amshawee et al. 2020; Canas and Benavente 2001). The cation exchange membranes (CEM) have selective permeability to positive charge ions and repel negatively charged ions; the opposite is true for anion exchange membranes (AEM). By this mechanism, the AEM and CEM are placed in the electrodialysis system and arranged alternately. Under the applied electric field, the cations will move to the cathode. The anions will move to the anode and penetrate the membrane to achieve the role of wastewater concentration and desalination. In addition to its high separation efficiency, the ED does not require chemicals during the treatment process. The ED can also be combined with solar power and can become an efficient and no sludge wastewater recycling technique (Bouchekima 2003).

The ED has an excellent performance in the removal of metal ions. Some researchers have used it to treat wastewater of copper, lead, and nickel (Chang et al. 2017; Wang et al. 2021; Gherasim et al. 2014). The results showed that the treatment efficiency could reach more than 70%. Since the chemical polishing wastewater only contains aluminum ions and polishing agents and its main components are expensive. If aluminum ions can be effectively separated from the polishing agent wastewater, the chemical polishing agent can be recycled to achieve the goal of reuse and to solve the environmental issues for chemical polishing agent wastewater treatment difficult and expensive. Therefore, this study focused on using the ED to recover chemical polishing agents from anodizing industry, explore the separation efficiency of aluminum ions, and find the appropriate operating parameters for ED operation.

27.2 Materials and Methods

27.2.1 Chemicals and Equipment

This study's sample was polishing agent wastewater after anodizing to separate aluminum ions in the wastewater to achieve the recycling of polishing agent. The wastewater chamber, the recovery chamber, anode chamber, and the cathode chamber were real wastewater, pH 2 sulfuric acid solution (Purity of 97%; Riedel-de Haen), and 0.5 M sodium sulfate solution (Purity of 99%; Merck), respectively. A flame atomic absorption spectrometer (FAAS, PerkinElmer AAnalyst 400) was used to analyze the aluminum ion concentration. The cation exchange membrane (CEM-7001) and anion exchange membrane (AM1-7001) used in this study will be cleaned with an ultrasonic oscillator (DELTA DC400H) to remove impurities on the surface of the membrane. The aerator improves the solution's uniformity, and the DC power supply (GPR-35H20D) provides an external electric field for ED operation.

27.2.2 Electrodialysis System

The ED treatment system for treating the polishing agent wastewater is shown in Fig. 27.1. It includes a set acrylic model, cathode plate, anode plate, peristaltic motor, power supply, and other devices. The acrylic model size is 60 cm × 20 cm × 10 cm (length × width × height). There are four chambers in the electrodialysis reactor. From left to right, they are anode chamber, wastewater chamber, recovery chamber,

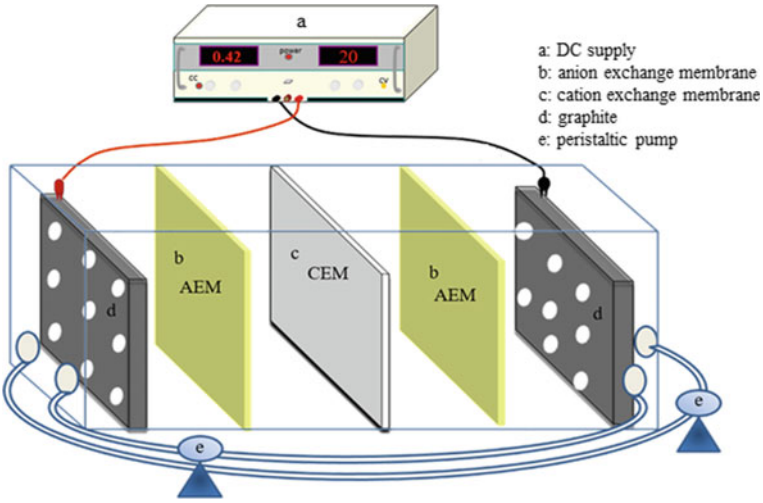

Fig. 27.1 Electrodialysis reactor for treating the real wastewater from anodizing

and cathode chamber, respectively. In the middle of the ED axial, a cation exchange membrane was used to divide the wastewater chamber and recovery chamber. An anion exchange membrane was placed on the left and right sides to separate the anode chamber and the cathode chamber. Both the anode and cathode materials were graphite plates with a size of 20 cm × 10 cm × 0.5 cm (length × width × thickness). The peristaltic pump (Rocker 300) allows the electrolyte from the cathode chamber to flow back to the anode chamber to stabilize the wastewater pH and conductivity.

27.2.3 Electrodialysis Test of Polishing Agent Wastewater

Beginning of operation, putting the polishing agent wastewater and pH 2 sulfuric acid solutions into the wastewater chamber and the recovery chamber. Then, pour the 0.5 M sodium sulfate solution into the anode chamber and the cathode chamber, respectively. The volume of the solution in the four chambers was 300 mL. Finally, the ED operation was performed with a fixed current of 1.0 A from the DC power supply. In order to obtain the appropriate conditions for the recovery of the chemical polishing agent, this experiment uses an electrodialysis reactor (EDR) and a simply-designed reactor (SDR) for testing. The EDR was shown in Fig. 27.1, including a CEM, two AEM, and a reflux device; the SRD has only a CEM, without AEM and reflux device. The treatment time is 60 min, with sampling once every 10 min for analysis. During the operation, aeration was performed at the wastewater chamber and recycling chamber to maintain the solution's uniformity.

27.3 Results and Discussion

27.3.1 Variation of pH and Conductivity

Figure 27.2 shows the pH variation of polishing agent wastewater in the wastewater chamber and the recovery chamber under the SDR with the treatment time. It can be seen that the pH of the wastewater chamber was maintained below pH 1 within 60 min, while the pH of the recovery chamber was increased with time, from the initial pH 2 rising to 5.2. The pH variation gradually leveled off after 40 min. Figure 27.3 shows the pH variation of polishing agent wastewater in the four chambers under the EDR with the treatment time. It can be seen that the pH value of the wastewater chamber was about 1.5 at the beginning, and it remained almost stable after 60 min of treatment. The recovery chamber was a sulfuric acid solution of pH 2, which had the same pH trend as the wastewater chamber. The anode chamber's pH gradually decreases from pH 6 to pH 5 within 30 min, while the cathode chamber's pH gradually increases from pH 6 to pH 6.8. After 30 min, the two chambers' pH tended to be flat, and the variations were almost the same; the pH value was about 5.8.

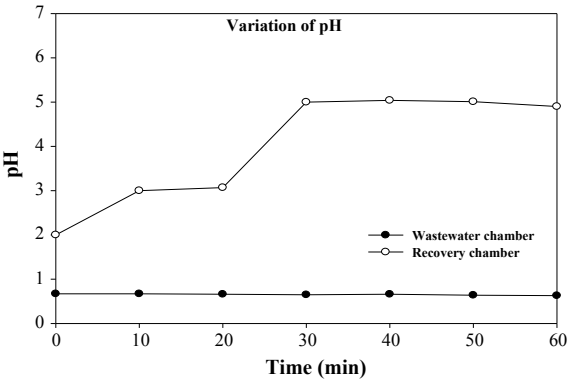

Fig. 27.2 The pH variation of polishing agent wastewater under the SDR system

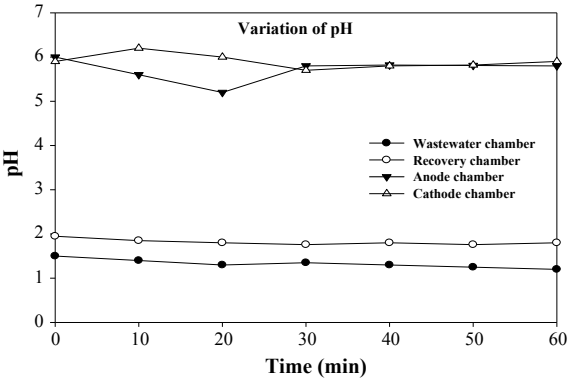

Fig. 27.3 The pH variation of polishing agent wastewater under the EDR system

In general, the acid and alkali will be generated at the anode and cathode, respectively, during the electrolysis process. Therefore, it generated hydroxide ions at the cathode resulting in a pH increased in the recovery chamber under the SDR system. In contrast with the SDR system, the reflux design of electrolytes at the anode and cathode chambers under the EDR system enables the pH of the solution to be neutralized. Therefore, the pH of the anode and cathode chambers can be kept relatively stable. In addition, since the wastewater chamber is mainly an ion transfer reaction and is affected by the AEM, the generated hydrogen ions in the anode chamber cannot penetrate the AEM to the wastewater chamber, with this has not caused a significant change in the pH. There are no produce hydroxide ions at the recovery chamber and partitioned by an AEM. The hydroxide ions at the cathode chamber will quickly flow back to the anode chamber remains pH stable. It is known from the pH variation that the reflux device and an anion exchange membrane can effectively control the wastewater pH, which is beneficial to the system's stable operation.

Figure 27.4 shows the conductivity variation of polishing agent wastewater under the SDR system with treatment time. The result indicates that the wastewater chamber's conductivity gradually increases with the treatment time, from 77

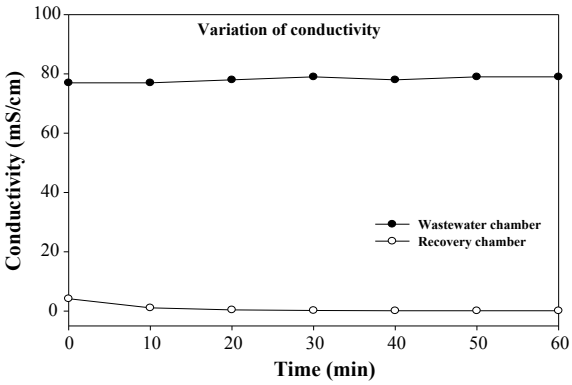

Fig. 27.4 The conductivity variation of polishing agent wastewater under the SDR system

to 79 mS/cm, and then tends to be flat. On the contrary, the recovery chamber's conductivity decreases significantly, from 4.18 to 0.11 mS/cm. The conductivity is related to the change of the pH value of the solution. For the SDR system, the wastewater pH is kept below pH 1, leading to relatively stable conductivity. The hydrogen ions at the recovery chamber react with the hydroxide ions continuously generated at the cathode to form H_2O, thereby decreasing conductivity. Figure 27.5 shows the conductivity variation of polishing agent wastewater in the four chambers under the EDR system with treatment time. The wastewater chamber's conductivity dropped from the initial 80 to 76 mS/cm, and the recovery chamber was significantly increased from 5 to 38 mS/cm. The conductivity of the anode chamber and cathode chamber were relatively stable. For the EDR system, the variation of aluminum ions concentration at the wastewater chamber is more significant than the change in pH, resulting in a slight drop in the wastewater chamber's conductivity. The increase in the recovery chamber's conductivity is attributed to the effective penetration of aluminum ions through the CEM. Due to the reflux device, the anode and cathode

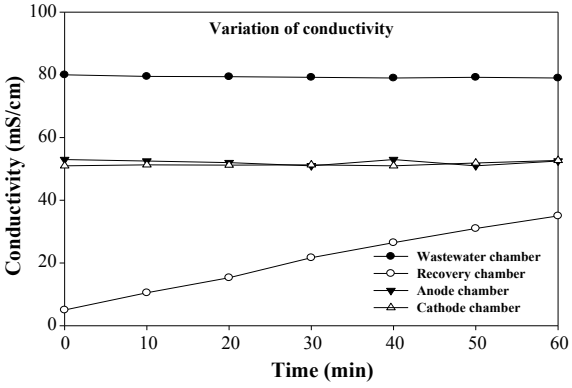

Fig. 27.5 The conductivity variation of polishing agent wastewater under the EDR system

chambers' conductivity changes relatively stable and can maintain a nearly constant conductivity value in the later stage of operation.

27.3.2 Variation of Aluminum Ions Concentration

Figure 27.6 shows the variation of aluminum ion concentration from aluminum polishing agent wastewater with the SDR system's treatment time. The result shows that the aluminum ion concentration at the wastewater chamber decreases with the treatment time. The removal efficiency reached 42.6% within 50 min, which is reduced from the initial 12,532 to 7,185 mg/L. The concentration of the aluminum ions in the recovery chamber was maintained below 30 mg/L. Figure 27.7 shows the variation of aluminum ions concentration from polishing agent wastewater with the treatment time under the EDR system. It is clearly found that the aluminum ion concentration at the wastewater chamber decreased significantly within 30 min. The concentration dropped from 11,056 to 2,512 mg/L, and the removal efficiency as high as 78%. The concentration of aluminum ions in the recovery chamber remained

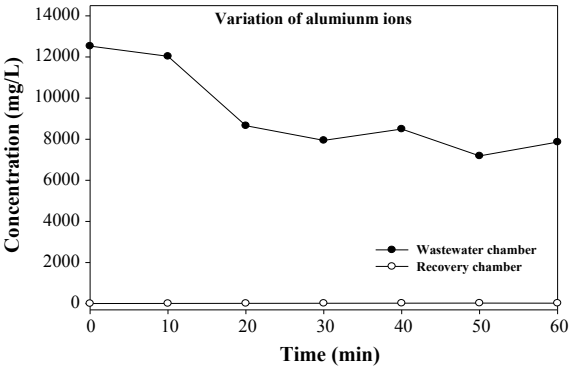

Fig. 27.6 The concentration variation of aluminum ion from polishing agent wastewater under the SDR system

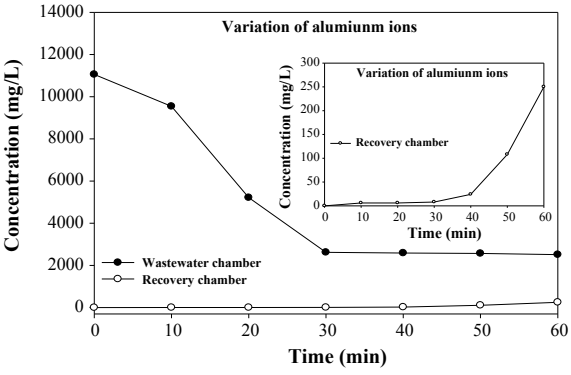

Fig. 27.7 The concentration variation of aluminum ion from polishing agent wastewater under the EDR system

stable before 30 min and then gradually increased. After 60 min of treatment, the recovered concentration of aluminum ion was about 250 mg/L. According to the variation of aluminum ion concentration, the removal efficiency and recovery efficiency of the EDR system were higher than the SDR system.

The pH and conductivity of the EDR system are relatively stable, the aluminum ions concentration at the wastewater chamber continues to decrease before 30 min. At 30 min of treatment time, the aluminum ion's separation efficiency under the EDR system is about that of 2 times for the SDR system (78 and 36%). Under an electric field operation, aluminum ions quickly move to the CEM and are adsorbed on the membrane. When aluminum ions' adsorption saturation was reached, the recovery chamber's pH value was in acidic conditions. The aluminum ions were gradually moving toward the cathode chamber and staying at the recovery chamber. Therefore, the concentration of aluminum ions at the recovery chamber was gradually increased after 30 min.

According to the variation of aluminum ion concentration, aluminum ions' movement is divided into two stages. At the beginning of the operation, the ion penetration happens on the high concentration of aluminum ions and the cation exchange membrane, leading to aluminum ions are quickly adsorbed on the cation exchange membrane. This is the separation stage of aluminum ions; when the aluminum ions in the membrane reach adsorption saturation, the aluminum ions will move gradually to the recovery chamber under an electric field. This is the recycling stage of aluminum ions. Therefore, the chemical polishing agent wastewater can be recycled and reused under EDR, and the recovered aluminum ions can be used as materials for other resource utilization such as flocculants. However, due to the high concentration of aluminum ions in the real wastewater, the aluminum ion was rapidly adsorbed on the cation exchange membrane in a short time, resulting in the membrane fouling problem still occurs. The concentration of aluminum ions stables gradually after 30 min of treatment time. In future practical applications, when the cation exchange membrane has been used for a period of time, the membrane can use the cleaning process by strong acid to solve the problem of fouling. According to the concentration variation of aluminum ions, the reflux device and anion exchange membrane will significantly affect aluminum ions' reaction rate.

Depending on the variation of aluminum ion concentration, the treatment time can be reduced and to improve the performance of EDR in the future. Also, it can explore the impact of various current operations for the recovery of aluminum ions. For practical application, a new polishing agent wastewater can be added to the wastewater chamber after aluminum ions concentration is reduced to a certain level, in which to continuously separate and recover aluminum ions to achieve the goal of polishing agent recycle.

27.3.3 Electricity Consumption of Electrodialysis

In this study, the ED with a current of 1.0 A and an average voltage of 70 V was applied to recycle the chemical polishing wastewater. ED's electrical consumption was evaluated during the treatment process, with KWh (kilowatt-hour) as a measurement unit. Based on the following equation (Costa and Olivi 2009), the electrical consumption of the ED under such operational conditions was calculated.

$$EC = UIt / V \quad (1)$$

where U is the average voltage during the electrocatalytic process (V), I is the applied current (A), t is the treatment time (h), and V is the wastewater volume (L).

The electricity consumption of ED was evaluated under 70% removal condition. According to the EDR result, the removal efficiency of 70% for aluminum ions occurs in the 30-min with 0.3 L wastewater. Therefore, the electricity consumed of EDR was 0.12 KWh (70 V * 1.0 A $*10^{-3}$ * 0.5 h/0.3 L). Moreover, the operation cost of removing the aluminum ions could be obtained through the NT$ 3.0 for each-KWh consumed. Considering the cost of purchasing chemical polishing agents, this study's results can provide a reference for the ED technique to recycle the polishing agent wastewater from anodizing. More research will be discussed further.

27.4 Conclusion

Based on experimental results, several conclusions can be drawn:

1. The EDR recycles the chemical polishing agent wastewater has stable pH value and conductivity, which is beneficial to the system operation.
2. The removal efficiency of aluminum ions at the wastewater chamber can reach 78% within 30 min, from about 11,056 mg/L decreased to 2,512 mg/L.
3. The concentration of aluminum ions at the recovery chamber gradually be increased after 30 min of treatment time, and recovery concentration was 250 mg/L after 60 min.
4. The EDR has the potential to recycle the chemical polishing agents in the anodizing industry, and the electrical consumption for the operation was 0.12 KWh.
5. A new polishing agent wastewater can be added to the wastewater chamber after aluminum ions concentration is reduced to a certain level, in which to continuously separate and recover aluminum ions to achieve the goal of polishing agent recycle.

References

Abou-Shady A (2017) Recycling of polluted wastewater for agriculture purpose using electrodialysis: perspective for large scale application. Chem Eng J 323:1–18

Al-Amshawee S, Yunusa MYBM, Azoddein AAM, Hassell DG, Dakhil IH, Hasan HA (2020) Electrodialysis desalination for water and wastewater: a review. Chem Eng J 380:

Bdiri M, Dammak L, Chaabane L, Larchet C, Hellal F, Nikonenko V, Pismenskaya ND (2018) Cleaning of cation-exchange membranes used in electrodialysis for food industry by chemical solutions. Sep Purif Technol 199:114–123

Bouchekima B (2003) Solar desalination plant for small size use in remote arid area of south algeria for the production of drinking water. Desalination 156:353–354

Canas MJ, Benavente AJ (2001) Characterization of active and porous sublayers of a composite reverse osmosis membrane by impedance spectroscopy, streaming and membrane potentials, salt diffusion and X-ray photoelectron spectroscopy measurements. J Membr Sci 183:135–146

Chang JH, Huang CP, Cheng SF, Shen SY (2017) Transport characteristics and removal efficiency of copper ions in the electrodialysis process under electroconvection operation. Process Saf Environ Prot 112:235–242

Costa CR, Olivi P (2009) Effect of chloride concentration on the electrochemical treatment of a synthetic tannery wastewater. Electrochim Acta 54:2046–2052

Doornbusch G, Wal M, Tedesco M, Post J, Nijmeijer K, Borneman Z (2021) Multistage electrodialysis for desalination of natural seawater. Desalination 505:

Gherasim CV, Krˇivcˇík J, Mikulášek P (2014) Investigation of batch electrodialysis process for removal of lead ions from aqueous solutions. Chem Eng J 256:324–334

Huang J, Gu QM, Yang F, Tang K, Gou SF, Zhang ZL, Shen Y, Zhang JL, Wang LJ, Lu YC (2019) Growth and properties of CdZnTe films on different substrates. Surf Coat Technol 364:444–448

Jiang C, Chen H, Zhang Y, Feng H, Shehzad MA, Wang Y, Xu T (2018) Complexation electrodialysis as a general method to simultaneously treat wastewaters with metal and organic matter. Chem Eng J 348:952–959

Smara A, Delimi R, Chainet E, Sandeaux J (2007) Removal of heavy metals from diluted mixtures by a hybrid ion-exchange/electrodialysis process. Sep Purif Technol 57:103–110

Wang XQ, Jie WQ, Li Q, Gu Z (2005) Surface passivation of CdZnTe wafers. Mater Sci Semicond Process 8:615–621

Wang C, Li T, Yu G, Deng S (2021) Removal of low concentrations of nickel ions in electroplating wastewater by combination of electrodialysis and electrodeposition. Chemosphere 263:

Xu H, Ji X, Wang L, Huang J, Han J, Wang Y (2020) Performance study on a small-scale photovoltaic electrodialysis system for desalination. Renew Energy 154:1008

Chapter 28
Methodological Aspects of Strategic Regional Planning for Achieving Sustainable Development in Bulgaria

Georgi Nikolov, Elka Vasileva, and Desislava Botseva

Abstract The publication explores the possibilities for integrating the global goals for sustainable development in Bulgaria's strategic regional planning process. The authors consider the concept of achieving sustainable development in its strategic aspect. The scholars' thesis is that strategic planning plays a crucial role in the regions' future and is a reliable tool in their transition to sustainable development. The integration of sustainable development goals begins at the planning stage at national, regional, and local levels. In the study, the authors examine the United Nations Agenda 2030—Sustainable Development Goals and the new European consensus on the development 'Our World, Our Dignity, Our Future.' The author's team also studies the legal framework and institutionalization of sustainable development in Bulgaria at the beginning of the XXI century. Current strategic documents for regional development are assessed for their compliance with the Global Sustainable Development Goals. To this end, the research team investigates the current strategic framework for regional development and conducts it, focusing on the environmental dimension of sustainability. The effective use of sustainable development opportunities is a proper perspective for regional policy in achieving maximum dynamics for socio-economic development in Bulgaria and its participation in building a competitive European economy based on knowledge and innovation.

Keywords Regional development · Environmental protection · Sustainable development · Water · Agenda 2030

28.1 Introduction

Sustainable development's strategic goal is to satisfy human material and spiritual needs, aspirations, and dreams for a better life and prosperity. Achieving this goal requires the maintenance of such consumption standards that fit within the limits of environmental capabilities and are accessible to all economic and social processes.

G. Nikolov · E. Vasileva · D. Botseva (✉)
University of National and World Economy, Student Town, UNWE, Sofia 1700, Bulgaria
e-mail: d_botseva@unwe.bg

H.-Y. Jeon (ed.), *Sustainable Development of Water and Environment*,
Environmental Science and Engineering,
https://doi.org/10.1007/978-3-030-75278-1_28

An essential requirement is the exploitation of resources, the direction of technological development, and changes in institutions to be in harmony and to increase both current and future opportunities to meet objective human needs.

The United Nations Agenda 2030: Sustainable Development Goals, adopted by world leaders in 2015, is a global framework for sustainable development that sets 17 quantitative and qualitative goals for sustainable development. The 2030 agenda is based on a global partnership involving all stakeholders and requires the mobilization of all means of implementation and sound monitoring, and a review mechanism to ensure progress and accountability.

The Millennium Development Goals' evolution towards Sustainable Development Goals reflects the changing approach to world development. The new program and its advanced sustainable development objectives are universal and apply to all parties at all development stages, relying on national ownership and overall responsibility. Partnerships with different stakeholders are crucial to meeting sustainable development goals.

In November 2016, the European Commission presented its strategic approach to implementing the Program by 2030, including sustainable development goals (European Commission, Strasbourg 2016). The new European consensus on development "Our world, our dignity, our future" (EN Official Journal of the European Union, p. 210/1, 30.6.2017) expresses the European Union's (EU) sustainable development policy, in line with The United Nations Agenda 2030: Sustainable Development Goals.

The strategic approach to regional development planning makes it possible to analyze and forecast development trends and support efficient and effective targeting of resources where they are most needed. The strategies set out a vision, goals, and priorities and anticipate development risks, including expected economic and social development crises. The creation of conditions and preconditions for accelerating the Bulgarian regions' sustainable development transition (Velikova 2019) requires forming a framework package of long-term regional goals in the economic, social, and environmental dimensions.

This study aims to examine the degree of integration of global sustainable development goals in strategic regional planning for Bulgaria, focusing on the environmental dimension of sustainability. The authors agree that strategic planning plays a crucial role in the regions' future and is a reliable tool in their transition to sustainable development.

The study's complex nature requires an integrated use of a set of traditional research approaches and methods such as historical approach, comparative analysis, expert assessment, inductive and deductive method. Information from the National Statistical Institute, the Ministry of Finance, the Ministry of Regional Development and Public Works, the National Association of Municipalities, and others is analyzed. Analytical papers, opinions, and studies were also used by European Union institutions such as the European Commission, European Parliament, Committee of the Regions, and others.

28.2 Harmonization of the Legal Framework and Institutionalization of the Sustainable Development Concept

At the beginning of the 21st century, Bulgaria's legislation evolved harmonizing with European norms and standards direction (Human rights and the goals of sustainable development. United Nations Society in Bulgaria, Sofia (2017)).

Firstly, Bulgaria ratified several necessary international legal instruments in environmental protection and sustainable development and participated in many international forums on sustainable development issues. International treaties and conventions are part of the domestic law of the country.

Secondly, the institutional foundations for managing and implementing the sustainable development process have been built. The coordination of the overall process of implementing sustainable development principles in the country involves many institutions at different levels and spheres (state and non-governmental, national, regional, and local).

Thirdly, the concept of sustainable development is gaining more and more popularity among the political elite and the state administration and the representatives of the academic community, non-governmental organizations, and businesses. We could argue that the necessary knowledge and experience in sustainable development is already available, which is a prerequisite for a more dynamic and practical application of its principles.

Fourthly, many projects at the national, regional, and local levels related to the sustainable development process have been implemented. International organizations have attracted significant financial resources, and internal resources have been mobilized to implement these projects. Essential is the fact that the number of these projects has increased significantly in recent years, expanding their scope.

Fifthly, the Law on Regional Development's adoption (Transforming our world: the 2030 Agenda for Sustainable Development 2015) marks the beginning of a new stage in the country's regional policy. The philosophy of the law is completely subordinated to the principles of sustainability. According to Article 2 of the law, "the state policy for regional development creates conditions for balanced and sustainable integrated development of the regions and municipalities and covers a system of normatively regulated documents, resources, and actions of the competent authorities."

The transitional and final provisions of the law also define the characteristics of regional development. "Sustainable integrated regional and local development" is the preservation, development, and implementation of targeted changes in living and working conditions in the regions through interrelated actions in the economic and social spheres in compliance with environmental protection requirements and protection against all forms of discrimination. The system of strategic documents for regional and local development regulated by law is crucial for creating a comprehensive long-term regional development policy based on a balance of national, regional, and local interests and priorities (The Bulgarian Law on Regional Development).

28.3 The European Consensus on Sustainable Development and Regional Development Policy in Bulgaria

The European Consensus on Development reflects a change in the model of development cooperation under the 2030 Agenda in response to the increasingly complex and interconnected challenges facing the world today.

The policy paper proposes a shared vision and framework for all EU institutions and all Member States. Sustainable development has long been at the heart of the European project. The EU has a solid foundation for sustainable development and is determined to play a leading role with its Member States in implementing the UN Agenda 2030. Regional development policy is an integrated policy based on social, economic, and infrastructural development and regional economic mechanisms at European, national and regional levels. Figures 28.1, 28.2, and 28.3 present the authors' generalized view of the system's main components and interrelations for sustainable and integrated regional development in terms of content and procedure.

The implementation of regional development policy is a process of coordination of sectoral policies on a country's territory. It requires implementation through a system of strategies, forecasts, programs, and spatial plans, developed and approved in a particular order and procedure. The integration of the sectoral policies and their inclusion in a joint regional model of development presupposes the application of the regional government bodies' consistent actions for coordination and joint work of all interested institutions in elaborating, adopting, and implementing the adopted regional development policy. The combination of natural, human, material, and financial resources mobilizes the territorial potential, and regional development occurs in an oriented development policy.

However, the regional development policy does not repeat the sectoral policies' goals but sets out its own, taking into account the specific characteristics of the respective territorial communities. In the general case, these goals and priorities relate to their sustainable balanced and integrated development and reduce their intra-regional and inter-regional differences.

At the beginning of the third decade of the 21st century, regional development policy implementation needs to be reconsidered and improved. This is necessary to meet European requirements and, at the same time—to contribute to the realization of national goals for achieving sustainable development of Bulgarian regions. The challenges are related to better and effective coordination and coherence between the structure-determining policies, the regional policy, the policy for spatial development, and the country's administrative-territorial organization.

At the national level should be preserve, the government's responsibility for the formulation of the state regional policy, the methodological guidance in its implementation, the coordination of regional aid, the strategic monitoring and evaluation of the policy's implementation. Regional development legislation continue expanding decentralization and subsidiarity in the management of regional development, increasingly engaging the regional level in the implementation of regional development policy.

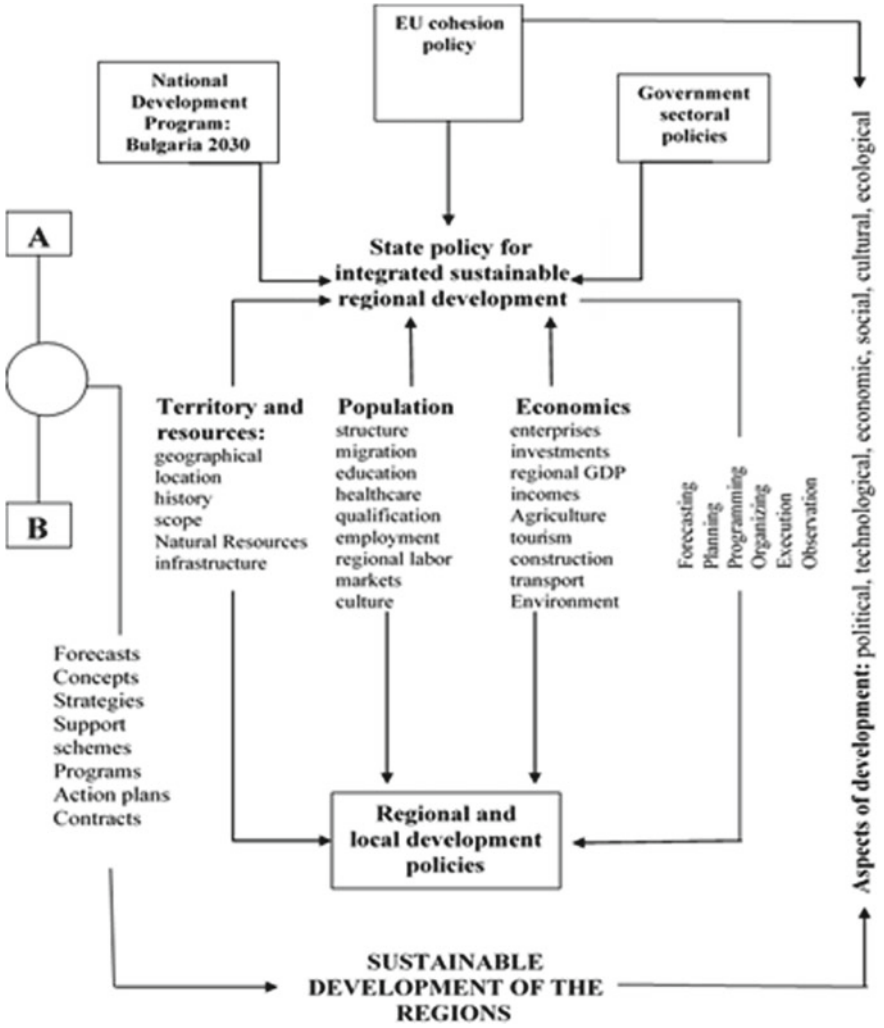

Fig. 28.1 Sustainable development of the regions—policies and indicators. *Source* author's graphics

Non-profit structures such as development agencies, clusters, technology transfer centers, local financial companies, and others support regional development. The partnership at the regional and local level is represented by universities, research centers, associations of producers and traders, foundations, foreign trade organizations, and others. All these organizations, through their activities, create an attractive localization environment for investors and intensify the process of economic, social, and cultural development for the region. Organizations are characterized by input

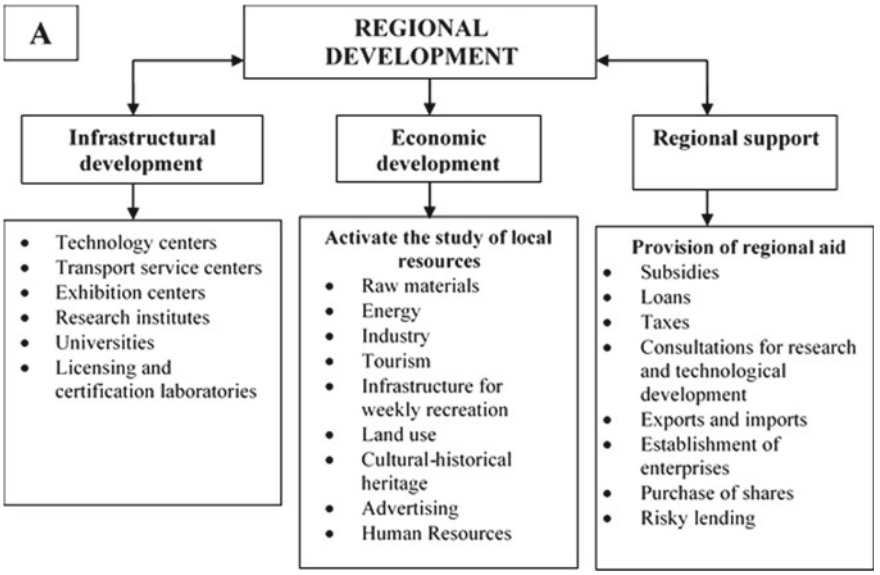

Fig. 28.2 Potential centers for regional development (Adapted from: analytical materials of the Center for the Study of Democracy, Sofia, 1996)

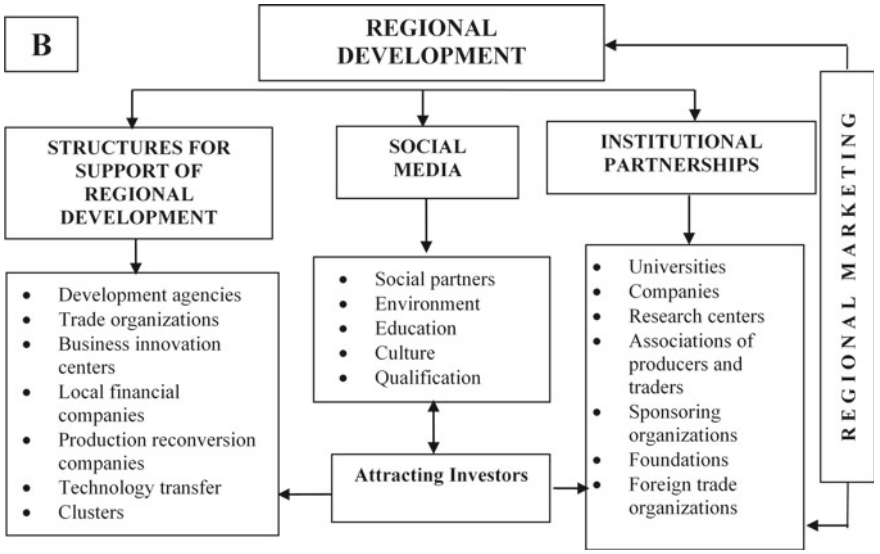

Fig. 28.3 Regional development—institutions and partner (Adapted from: analytical materials of the Center for the Study of Democracy, Sofia, 1996)

and output resources, transformation processes, feedback, and the external environment. Incoming resources are associated with human, financial, material, information resources and those used to produce goods and services (Tsolov 2018).

Strategic planning of regional development is of paramount importance in the formulation and selection of goals and priorities for Bulgaria's sustainable development. Bulgaria's natural wealth and the diverse physical-geographical conditions create opportunities for green business development, which is the basis for achieving socio-economic development through sustainable and smart growth (Tanakov 2018). The emphasis is on the integrated approach in the planning and implementation of regional development policy by applying sustainable development principles, namely the combination of socio-economic development goals and those in the field of environment. Sustainable development is a key objective of the EU and Bulgaria should not lag behind in terms of the essential indicators for its achievement (Velikova 2019).

28.4 Integration of Global Goals for Sustainable Development in the Process of Strategic Regional Planning

World development is expanding its scope to include more and more new participants. Each country has the primary responsibility for its own economic and social development, but the 2030 Agenda for Sustainable Development must be implemented by all countries and all stakeholders in the partnership.

Achieving most of the Sustainable Development Goals depends very much on local and regional authorities' active participation. The EU will support reforms for transparency, accountability, and decentralization to give regional and local authorities opportunities for better governance and a better impact on development and find better solutions to tackling inequalities within countries. The pyramid of the two interrelated processes of the strategic planning of Bulgaria's regional and spatial development, following the current normative framework, is presented sequentially in Fig. 28.4. With the amendments to the Regional Development Act of March 2020, the current system of documents for strategic planning of regional and spatial development has been optimized and covers:

1. National concept for regional and spatial development; 2. Integrated territorial strategies for development of the level 2 planning regions; 3. Plan for integrated development of the municipality.

These documents fulfill several common goals and tasks: identify the current problems, needs, and potentials for development of the regions, municipalities, and settlements, considered in the development of investment programs and financial instruments, including co-financed by the European Union funds; identify projects contributing to the achievement of national goals and priorities for regional and local development; plan and implement integrated approaches for territorial and urban development; coordinate sectoral and horizontal policies at territorial level, taking

Fig. 28.4 Pyramid of the strategic regional planning process

into account their territorial dimensions; ensure the coherence of implementing the state policy for regional development with the national level's strategic documents.

To prepare the development of the package of strategic documents in the field of regional and local development, in fulfillment of its normative commitments, the Minister of Regional Development and Public Works approves the relevant methodological guidelines related to the development of integrated regional development strategies for planning at level 2, as well as those for the creation of plans for integrated development of municipalities for the period 2021–2027 (EU document 2017).

The subject field of the National Strategy for Regional and Spatial Development has a multi-purpose and multifunctional character. The development of the specific territory is reflected in both the external conditions and the state's macroeconomic policy and sectoral policies. These policies do not have as a specific object the development of the regions and the reduction of interregional differences. However, the policy for regional development must focus on them and offer integrated measures that will contribute to achieving the country's long-term development goals. Territorial growth factors must also consider these measures.

For this reason, the developed strategy is a summary document that covers all critical elements of future regional development. Some of the proposed measures are implemented in partnership with sectoral policies, and others are subject only to regional policy. It is important to emphasize that the set actions are related to the mandatory participation of regional and local authorities and local socio-economic partners, so they become a subject of regional policy.

The Integrated Territorial Strategy for the Development of Level 2 Planning Regions is a strategic document. It defines the medium-term goals, priorities, and perspectives for sustainable integrated regional and local development on the respective planning region's territory. The goal setting is in line with the National Concept's provisions for Regional and Spatial Development and other sectoral and horizontal policies. The connections with other level 2-planning regions in the country and

the neighboring countries in the macro-region are also considered (Methodological guidelines, Ministry of Regional Development and Public Works 2020). Integrated Territorial Development Strategies for Level 2 Planning Regions coordinate the projections of sectoral strategies and documents at the regional level in economic development, health, education, science, social services, transport, water, energy, broadband tourism, and the environment and considers their regional specifics and territorial dimensions.

The plan for integrated development of the municipality determines the medium-term goals and priorities for sustainable development of the municipality and the relations with other municipalities following the integrated territorial strategy for developing the region for level 2 planning and the general development plan of the municipality. The document provides spatial, temporal, and factual coordination and integration of various policies and planning resources to achieve the defined goals for lasting improvement of the municipal territory's economic, social and environmental condition. The program for implementing the municipal plan for integrated development contains specific investment initiatives of the municipalities for sustainable local and regional development.

The obligatory elaboration of municipal plans for integrated development, regulated by the Law on Regional Development, is a good precondition for transforming the local authorities into a real partner of the government in the process of formation and implementation of the regional policy. This creates an opportunity to respond to one of the new challenges of the reform of European regional policy—the closer involvement of local authorities in preparing and implementing regional and local development policy.

The development of strategic documents combines both methodological approaches "top-down" to determine the framework of development and "bottom-up" in the inclusion of specific initiatives and development projects in the implementation program. The coordination of strategic and planning documents is an essential condition for implementing regional policy effectiveness. The general target orientation of the planned interventions to support regional development, concentrated in the priority areas, guarantees the efficiency of the invested financial resources.

28.5 Conclusion

The development of strategic documents for regional and local development until 2030 focuses on the full use of opportunities to integrate global goals for sustainable development in the process of regional development management, both at national and regional, and local levels. The governments are responsible for formulating and implementing the regional development policy, which will integrate the inclusion of the global goals for sustainable development in strategic development planning at the different territorial levels. The strategic documents for regional and local development of Bulgaria for the period 2021–2027 and the implementation of the future priorities and specific goals set in them could become a key mechanism for creating

the necessary conditions for the transition to sustainable development and mobilization of local potential. It would be crucial for regional and local authorities to adopt a regional and local agenda to transition to sustainable development. This will facilitate the identification of the regions and municipalities' contribution in implementing the concept of sustainable development and resource mobilization, including the participation of all stakeholders and the building of partnerships.

The integration of the global goals for sustainable development in the process of regional and local development, in the spatial development of the territory, can be achieved by strengthening the capacity at the national, regional, and local level to reflect the guidelines formulated in the UN Program and the European Consensus on Sustainable Development in regional and local planning and governance policies and practices. The concept of sustainable development sets the long-term vision for the movement of society. As an integrated concept, sustainable development includes all human activities from the global to the regional and local levels. The environment is the necessary basis for sustainable development. The economy is the tool for achieving sustainable development. A good harmonious and balanced life for all is the goal of sustainable development.

References

Development Program (2019) Bulgaria 2030 should be based on the UN Sustainable Development Goals, Bulgarian Platform for International Development. https://bpid.eu/?p=1606&lang=BG. Accessed 3 Apr 2019

Human rights and the goals of sustainable development. United Nations Society in Bulgaria, Sofia (2017)

Integrated Territorial Strategies for Development of the Level 2 Planning Regions (2021–2027) National Center for Territorial Development EAD. Section "Public Consultations" http://www.strategy.bg/. Accessed 25 Jan 2021

Methodical instructions for development and implementation of plans for integrated development of a municipality for the period 2021–2027, Ministry of Regional Development and Public Works. Section "Regional development/Methodical instructions, March 2020. www.mrrb.bg

Methodical instructions for preparation of integrated territorial strategies for development of the regions for planning from level 2 for the period 2021–2027, Ministry of Regional Development and Public Works. Section "Regional development/Methodical instructions", March 2020. www.mrrb.bg

Next steps towards a sustainable European future (2016) European Sustainability Action, Communication from the Commission to the European Parliament, the Council, the European Economic and Social Committee and the Committee of the Regions, COM (2016) 739 final, Strasbourg

Regulations for implementation of the Regional Development Act, prom. SG, no. 70/07 August 2020

Tanakov N (2018) Green growth and stimulating eco-innovation. In: Proceedings of scientific papers, contains from the international scientific conference-trends in regional development and security management, PC-UNWE 2018 Sofia BG, pp 69–79. ISBN 978-619-232-265-6

The Bulgarian Law on Regional Development was promulgated in the State Gazette No. 50 of May 30, 2008, and amended and supplemented in the State Gazette issue 28 of March 29, 2018

The new European consensus on development 'our World, our Dignity, our Future', EU document, BG Official Journal of the European Union, C 210/1, 30.06.2017

Transforming our world: the 2030 Agenda for Sustainable Development (2015) A document of the United Nations, adopted by Heads of State and Government and High Representatives, at a meeting at the UN headquarters in New York from 25 to 27 Sept 2015

Tsolov G (2018) Modern concepts for the development of regional management. In: Proceedings of scientific papers, contains from the international scientific conference-trends in regional development and security management, PC-UNWE 2018 Sofia BG, pp 188–193. ISBN 978-619-232-265-6

Velikova E (2019) Methodological guidelines for the sustainable development of the Bulgarian touristic resorts through reducing the harmful impact of transport. In: 10th international conference on environmental science and development (ICESD 2019), Milan, Italy. SCOPUS E3S web conference, vol 101, p. 01004. https://doi.org/10.1051/e3sconf/201910101004

Chapter 29
Study on the Model of Construction Safety Risk Evaluation Coupling Multiple Factors in Navigable Waters

Hui Sun, Yuchi Hao, Jiaming Qu, Ping Zhu, and Runli Tao

Abstract Construction safety risk assessment coupled with multiple factors is essential for the risk control in complex and changing navigable waters. Aiming at the characteristics of uncertainty, dynamics and fuzziness for engineering construction in navigable waters and the problems including incomplete risk index system, the risk-classification-quantification-standard unsuitable for real-time dynamic risk evaluation, and the empirical judgment for the current construction risk assessment, a general three-level safety risk index system was established based on the mutual influence and subordination of risk factors including the effect of human-related, equipment and environment factors. Taking the dredging project of a large trailing suction dredger as an example, the three-level quantitative standard of risk classification was established from the integration of objective evaluation mechanisms and subjective evaluation mechanisms, and the fuzzy comprehensive evaluation method was used to set up a comprehensive multifactor construction safety risk evaluation model. Finally the model was applied to the eighth phase of the Hengsha Dongtan silt promotion ring project successfully. The model of construction safety risk assessment coupled with multiple factors will provide effective reference and guidance for real-time dynamic construction risk assessment and control in navigable waters.

Keywords Construction safety · Navigable waters · Comprehensive safety risk evaluation · Fuzzy comprehensive evaluation method

29.1 Introduction

With the rapid development of water traffic industry in China and the trend of large scale and complicated construction for water traffic engineering, the construction region often inevitably overlaps with or intersects with channels, which is of significant influence for the safety of navigation vessels and engineering construction. Once

H. Sun · Y. Hao · J. Qu · P. Zhu · R. Tao (✉)
CCCC National Engineering Research Center Dredging Technology and Equipment CO., LTD., Shanghai 200082, China
e-mail: taorunli@cccc-drc.com

H.-Y. Jeon (ed.), *Sustainable Development of Water and Environment*,
Environmental Science and Engineering,
https://doi.org/10.1007/978-3-030-75278-1_29

a safety accident occurs, it will cause serious damage to engineering construction and life security (Fang 2019). On the one hand, the construction in navigable waters is affected by the dynamic changes of natural environment factors such as wind and wave. On the other hand, the passing vessels, changing navigation environment and construction schedule have an important impact on construction safety as the construction equipment needs to move continuously in the construction water region. The engineering construction is of complex construction environment, long cycle, great difficulty, and it has the characteristics of uncertainty, dynamics and fuzziness (Zhibao et al. 2017; Xuejun and Zhimin 2012; Akyildiz and Mentes 2017; Nuwen et al. 2013). Therefore, the safety of engineering construction in navigable waters is supposed to get highly emphasized, and it is necessary and of great engineering significance to study the construction risk prevention and control method in complex navigable waters with multiple factors.

Although the relevant management regulations and industry norms have been promulgated and the system of engineering construction safety is much mature, however, for the construction projects in navigable waters, the vital risk factors are still incomplete, the quantitative risk standard is not clear and the existing risk assessment is still mainly based on the empirical judgment of the construction workers due to the complex construction environment with dynamic changes. Once a single risk exceeds the allowable limit threshold, the corresponding safety management measures will be taken. However, there is no scientific and reasonable basis for the risk assessment of the multifactor not in excess of the limit threshold, which may lead to improper construction technology and low construction efficiency, and even lead to safety accidents. As a result, the use of scientific and standardized risk assessment method in the construction process is supposed to be utilized and it will provide effective guarantee for construction safety in navigable waters.

At present, the research on water construction risk could be mainly divided into qualitative research and quantitative research. The qualitative research is mainly to analyze and sort out the potential risk factors that affect the construction safety, and to remind the constructors to pay attention to and take necessary prevention actions. But it is not thoroughly discussed and studied for the influence degree of various risk factors on construction safety (Xuejun and Zhimin 2012; Akyildiz and Mentes 2017; Nuwen et al. 2013). The quantitative research is to evaluate the impact of the risk factors on construction safety, however the studies reported (Lei et al. 2019; Fang 2019; Chunhui et al. 2020; Jinngmin et al. 2003) are mostly periodic and static analysis. For example, for visibility factor, the number of days of fog within a year is used, which is unsuitable for real-time dynamic risk assessment during construction process, and cannot meet the real-time dynamic safety risk prevention and control requirement with the change of construction conditions.

In summary, this paper will focus on the construction safety risk evaluation coupling multiple factors in navigable waters, aiming to establish a multilevel index system suitable for the dynamic assessment of construction risk and a comprehensive risk assessment model based on fuzzy comprehensive evaluation method applied to the major engineering in navigable waters. The research achievement

could provide theoretical basis and technical support for safety risk identification, assessment and early warning of engineering construction in navigation waters.

29.2 Safety Risk Index System

The identification of safety risk factors and the establishment of index system are the basis of risk analysis and evaluation. Statistics and analysis of 41 domestic typical water construction safety accidents from 2012 to 2015,including collision accidents, equipment damage accidents, single ship damage accidents, industrial injury accidents, fire accidents and pollution accidents in 6 aspects, the results indicate that each accident is not caused by a single factor, but by a combination of multiple factors. The farther summary of the accident causes is shown in Table 29.1, 54% of the safety accidents are caused by human-related factors, mainly reflected in the insufficient staff energy, insufficient professional capacity and inadequate safety precautions, of which the insufficient professional capacity of staff is the main cause for safety incidents. The material factors account for 34% of the safety accidents mainly caused by the lack of safety control and maintenance of equipment which is the most important accident cause, excessive storage of special items such as inflammable and explosive materials, and incomplete safety facilities. The proportion of environment factors is 12%, which mainly consists of severe hydrological conditions, harsh meteorological conditions and limited navigation conditions. Especially in the harsh wind-wave-current condition, the change of regional construction environment can't be predicted in time due to the lack of local water environment monitoring means, which not only increases the difficulty of construction, but also brings severe test to the control of the construction vessel and the change of the construction technology. Once maloperation, it will easily lead to safety accidents.

Table 29.1 The risk causes and the proportion of typical water construction safety accidents from 2012 to 2015

Accident causes		Proportion (%)
Human-related factors	Insufficient staff energy	1.62
	Insufficient operational capacity	35.10
	Inadequate safety precautions	17.28
Material factors	Lack of safety control and maintenance of equipment	13.94
	Excessive storage of special items	8.16
	Incomplete safety facilities	11.90
Environment factors	Severe hydrological conditions	6.00
	Harsh meteorological conditions	3.96
	Limited navigation conditions	2.04

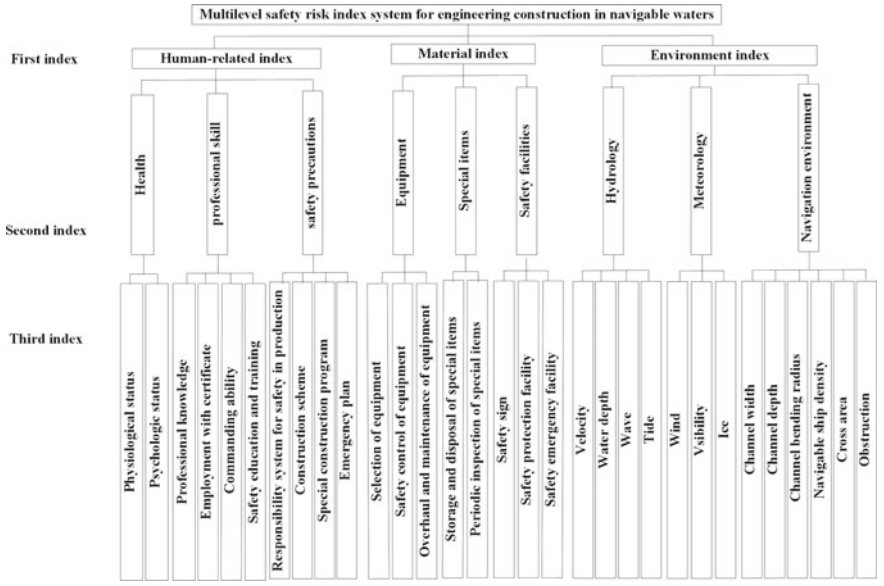

Fig. 29.1 Multilevel safety risk index system for engineering construction in navigable waters

Based on the above typical water construction safety accident case analysis, and combined with the characteristics of construction safety hazard sources in navigable waters, the safety risk index system for engineering construction in navigable waters is divided into three categories comprised of human-related, material and environment according to Classification and Code for the Hazardous and Harmful Factors in Process (GB/T 13861-2009). The human-related indexes are defined as relative indexes about artificiality and management. The material indexes include risk indexes for machinery, equipment, facilities and materials. The environment indexes refer to risk indexes in the construction environment.

In order to make the index system more refined and implementable, referring to the relevant industry specifications with major hazard identification of engineering construction accidents in navigable waters and collision accidents for sailing vessels, the three-level safety risk index system for engineering construction in navigable waters is established in Fig. 29.1 based on the mutual influence and subordination of risk factors.

29.3 Comprehensive Safety Risk Evaluation Model for Construction in Navigable Waters

The emphasis of construction safety risk assessment and prevention is different for diverse types of engineering. Taking the dredging project of large trailing suction

dredger as an example, environmental risk focused on, the fuzzy comprehensive evaluation method widely used in risk assessment was carried out to establish a comprehensive safety risk evaluation model coupling multiple factors to quantitatively evaluate the environmental risk of construction in navigable waters.

Fuzzy comprehensive evaluation method based on principle of fuzzy mathematics comprehensively analyzes the evaluation objects affected by multiple factors, and converts qualitative evaluation into quantitative evaluation (Weimin et al. 2009; Jun et al. 2018; Wei et al. 2019; Hui et al. 2005). The procedures are shown as follows:

(1) The set of factors U was established for evaluating the risk of construction environment in large trailing suction dredger engineering according to the integration of objective industry regulations and subjective experience of experts on the basis of the multilevel safety risk index system in Fig. 29.1.
(2) The set of the factor weight A was formed applied Analytic Hierarchy Process (AHP) method (Jun et al. 2018) to determine the weight distribution of each subfactor u_{ij} to the upper factor u_i in each layer.
(3) The set of risk assessment grade V for each factor was assigned and the quantitative threshold of each factor for different risk levels was confirmed reasonably by investigating experts using Delphi method (Elmer et al. 2009).
(4) The results of comprehensive safety risk evaluation in different cases were calculated. First, the membership matrix r_i of each subfactor u_{ij} for different risk levels v_i was calculated by membership function. Then the evaluation matrix B_i was obtained through multiplication operator to calculate the weight a_i and membership matrix r_i of each subfactor set u_i. The evaluation matrix B_i of the set participated in the calculation of the fuzzy comprehensive evaluation B for upper layer factor set U. Finally, the risk level evaluation result M of the whole construction environment was calculated by the weighted average method of defuzzification.

29.3.1 The Safety Risk Index System

As a result of a universal safety risk index system for engineering construction in navigable waters in Fig. 29.1, all or part of the indexes could be selected according to the feature of the specific engineering. Based on the environmental risk factors of trailing suction dredging engineering, a targeted safety risk index system was formed as shown in Fig. 29.2, of which the influence of tide is indirectly reflected by water depth.

Therefore, the environmental index set of trailing suction dredging engineering is U = (hydrology u_1, meteorology u_2, navigation environment u_3). The sub-index sets are hydrology u_1= (velocity u_{11}, water depth u_{12}, wave u_{13}), meteorology u_2= (wind u_{21}, visibility u_{22}, ice u_{23}), and navigation environment u_3= (channel width u_{31}, channel depth u_{32}, channel bending radius u_{33}, navigable ship density u_{34}, cross area u_{35}, obstruction u_{36}).

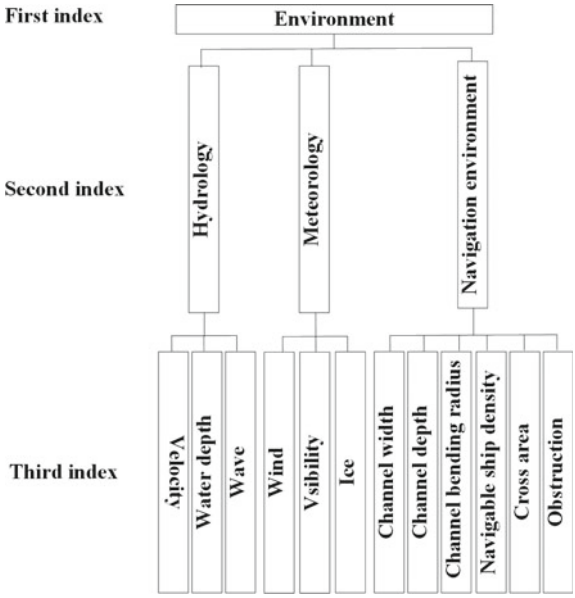

Fig. 29.2 Safety risk index system for construction environment of cutter suction dredger

29.3.2 The Weight Set of Index

Each index has different impacts on the comprehensive evaluation result of safety risk, so it is of great importance to quantify the weight of each index reasonably to improve the reliability of the comprehensive evaluation result. In this paper, the Analytic Hierarchy Process (AHP) (Jun et al. 2018) was applied to quantify the weight of each index by comparing the relative importance of each index with qualitative and quantitative analysis. Fifty experts in the fields of dredging engineering and safety risk prevention & control were invited marked all the index weights by themselves comparing the relative importance of the two indexes in the same level based on the 1–9 scale method of SAATY (Marie and Andrea 2017). Then all the results were integrated to form a judgment matrix and was published to the experts. If some experts disagree with the judgment matrix of index weight, they need to modify the relative weight results of the index and a new judgment matrix is reconstructed which is published to all members until all experts come to consistency. In the meantime, the comprehensive judgment matrix passed the consistency checking of single hierarchical arrangement and total hierarchical arrangement. The final weight set corresponding to the environmental safety risk indexes is $A = (0.258, 0.105, 0.637)$, the sub-index sets of weight include hydrology weight $a_1 = (0.637, 0.105, 0.258)$, meteorology weight $a_2 = (0.105, 0.637, 0.258)$, and navigation environment weight $a_3 = (0.040, 0.071, 0.065, 0.424, 0.228, 0.172)$, as shown in Table 29.2.

Table 29.2 The weight sets of different indexes

Second indexes	Weights	Third indexes	Weights
Hydrology u_1	a_1 0.258	Velocity u_{11}	a_{11} 0.637
		Water depth u_{12}	a_{12} 0.105
		Wave u_{13}	a_{13} 0.258
Meteorology u_2	a_2 0.105	Wind u_{21}	a_{21} 0.105
		Visibility u_{22}	a_{22} 0.637
		Ice u_{23}	a_{23} 0.258
Navigation environment u_3	a_3 0.637	Channel width u_{31}	a_{31} 0.040
		Channel depth u_{32}	a_{32} 0.071
		Channel bending radius u_{33}	a_{33} 0.065
		Navigable ship density u_{34}	a_{34} 0.424
		Cross area u_{35}	a_{35} 0.228
		Obstruction u_{36}	a_{36} 0.172

29.3.3 The Set of Risk Assessment Grade and the Quantitative Standard of Risk Classification

The quantitative standard of index risk classification is an important basis for risk assessment and early warning. In order to guarantee its practicability and rationality, the quantitative standards of risk classification for trailing suction dredger of various sizes are supposed to be different by the investigation and feedback of engineering construction. Aiming at large trailing suction dredging engineering, the risk assessment is divided into three levels, so the set of risk assessment grade can be written as $V =$ (high risk, average risk, low risk). Based on the cases in industry specifications, the rationality questionnaire about the quantitative standards of risk classification was preliminarily formulated, which was calibrated by many experts in relative fields. After reiterative anonymous verification according to the Delphi method (Elmer et al. 2009), the quantitative standard of risk classification of the environmental safety index system is shown in Table 29.3.

29.3.4 Comprehensive Multifactor Construction Safety Risk Evaluation Model

The two-layer fuzzy comprehensive evaluation method was used to evaluate the environmental risk of large trailing suction dredger in navigable waters. Firstly, the semi-gradient membership function is used to calculate the membership degree of each subfactor u_{ij} for the risk level v_i. If the risk of evaluation decreases with the

Table 29.3 Quantitative standard for the classification of environmental risks for large trailing suction dredger (9000–17,000 m^3)

Second indexes	Third indexes	Risk assessment grade		
		High risk	Average risk	Low risk
Hydrology	Velocity	$v \geq$ 5knots	2knots $\leq v <$ 5knots	$v <$ 2knots
	Water depth	$h \leq$ load draught + 0.5 m	load draught + 0.5 m$<h \leq$ load draught + 1.5 m	$h >$ load draught + 1.5 m
	Wave	$h_{wave} \geq$ 2.5 m	1.0 m $\leq h_{wave} <$ 2.5 m	$h_{wave} <$ 1.0 m
Meteorology	Wind	$v_{wind} \geq$ 17.1 m/s (>7 level)	5.5 m/s $\leq v_{wind} <$ 17.1 m/s (4–7 level)	$v_{wind} <$5.5 m/s (<4 level)
	Visibility	$H \leq$ 1000 m	1000 m $\leq H <$ 4000 m	$H >$ 4000 m
	Ice	$h_{ice} \geq$ 0.14 m	0.02 m$\leq h_{ice} <$ 0.14 m	$h_{ice} <$ 0.02 m
Navigation environment	Channel width	$B \leq$ ship length	ship length$\leq B <$ 2 times of ship length	$B >$ 2 times of ship length
	Channel depth	$h_{channel} \leq$ load draught + 0.5 m	load draught + 0.5 m$<h_{channel} \leq$ load draught + 2.0 m	$h_{channel} >$ load draught + 2.0 m
	Channel bending radius	$R \leq$ 3 times of ship length	3 times of ship length$\leq R <$ 4 times of ship length	$R >$ 4 times of ship length
	Navigable ship density	nonstop (1)	at times (0.5)	once a while (0)
	Cross area	$N \geq 2$	$N = 1$	$N = 0$
	Obstruction	$A_0 \geq$ 30%	10% $\leq A_0 <$ 30%	$A_0 <$ 10%

where v represents the vessel velocity, h represents water depth, h_{wave} represents wave height, v_{wind} represents wind velocity, H represents the distance of which can be identified for people from the background, h_{ice} represents ice thickness, B represents channel width, $h_{channel}$ represents channel depth, R represents channel bending radius, N represents the number of crossings between channel and construction area, A_0 represents the proportion of obstructions to construction area

increase of membership degree, the lift semi—trapezoidal membership function is adopted, otherwise lower semi—trapezoidal membership function is adopted.

Lift semi—trapezoidal membership function can be expressed as

$$r(x) = \begin{cases} 0, (x \le \alpha) \\ \dfrac{x-\alpha}{\beta-\alpha}, (\alpha < x < \beta) \\ 1, (x \ge \beta) \end{cases} \tag{29.1}$$

Lower semi—trapezoidal membership function can be expressed as

$$r(x) = \begin{cases} 1, (x \le \alpha) \\ \dfrac{\beta-x}{\beta-\alpha}, (\alpha < x < \beta) \\ 0, (x \ge \beta) \end{cases} \tag{29.2}$$

where x represents the measured data of index u_{ij}; α, β represent the lower and upper limits of the evaluation standard threshold corresponding to the risk grade v_i respectively.

So the evaluation matrix r_i of the subset of factors u_i can be expressed as

$$r_i = \begin{pmatrix} r_{i-11} & r_{i-12} & r_{i-13} \\ r_{i-21} & r_{i-22} & r_{i-23} \\ \cdots & \cdots & \cdots \\ r_{i-n1} & r_{i-n2} & r_{i-n3} \end{pmatrix} \tag{29.3}$$

where r_{i-n1}, r_{i-n2}, r_{i-n3} respectively represent the membership degree of the index u_{in} to high risk, average risk and low risk.

The evaluation matrix B_i of the subfactor set is calculated by multiplication operator to calculate the weight a_i and membership matrix r_i of each subfactor set u_i. So the evaluation matrix of hydrology, meteorology and navigation environment are as follows:

$$B_1 = a_1 \circ r_1 = \begin{pmatrix} 0.637 & 0.105 & 0.258 \end{pmatrix} \begin{pmatrix} r_{1-11} & r_{1-12} & r_{1-13} \\ r_{1-21} & r_{1-22} & r_{1-23} \\ r_{1-31} & r_{1-32} & r_{1-33} \end{pmatrix} \tag{29.4}$$

$$B_2 = a_2 \circ r_2 = \begin{pmatrix} 0.105 & 0.637 & 0.258 \end{pmatrix} \begin{pmatrix} r_{2-11} & r_{2-12} & r_{2-13} \\ r_{2-21} & r_{2-22} & r_{2-23} \\ r_{2-31} & r_{2-32} & r_{2-33} \end{pmatrix} \tag{29.5}$$

$$B_3 = a_3 \circ r_3 = \begin{pmatrix} 0.040 & 0.071 & 0.065 & 0.424 & 0.228 & 0.172 \end{pmatrix} \begin{pmatrix} r_{3-11} & r_{3-12} & r_{3-13} \\ \cdots & \ddots & \cdots \\ r_{3-61} & r_{3-62} & r_{3-63} \end{pmatrix} \tag{29.6}$$

Matrix operation is carried out of the set R composed of the above evaluation results B_i and the corresponding index weight set A to gain the fuzzy comprehensive evaluation B of the next layer of environmental factor set U.

$$B = A \circ R = (0.258\ 0.105\ 0.637)\begin{pmatrix} B_1 \\ B_2 \\ B_3 \end{pmatrix} = \begin{pmatrix} b_1\ b_2\ b_3\ b_4 \end{pmatrix} \tag{29.7}$$

The risk evaluation grade of the whole construction environment M can be calculated based on the weighted method, which the high risk corresponds to 3, the average risk corresponds to 2, and the low risk corresponds to 1, then M is written as

$$M = \frac{b_1 \times 3 + b_2 \times 2 + b_3 \times 1}{b_1 + b_2 + b_3} \tag{29.8}$$

If $M \geq 2.5$, the result is high risk; if $1.5 \leq M < 2.5$, it is average risk; if $M < 1.5$, it is low risk.

29.4 Engineering Applications

The total reclamation area of the eighth phase of the Hengsha Dongtan silt promotion ring engineering is about 43 km^2. The backfill sediment mainly consists of the dredged soil by the construction vessels from the deep water channel of the Yangtze River Estuary. With the rapid development of Shanghai Port and ports in the Yangtze River, more and more vessels sail through the deep water channel. Thus the construction safety of vessels in the deep water channel are not only affected by wind, waves and other environmental factors, but also by navigable ships. In order to analyze the safety risk degree of the complex environmental conditions during the construction of the Yangtze Estuary deep water channel, the measured data of a large trailing suction dredger were collected as shown in Table 29.4, and the above model was used to evaluate the degree of construction safety risk in different conditions.

The final risk evaluation results are shown in Table 29.5.

According to the defuzzification method in fuzzy comprehensive algorithm, the final evaluation results of risk grade in three cases are $M_1 = 1.9553$; $M_2 = 2.0543$; $M_3 = 2.5241$. It shows that the calculation results of Case (I) and Case (II) belong to average risk threshold, but Case (III) is close to the high risk threshold. So for Case (III), early warning measures should be carried out to prevent accidents, and the maritime meteorological conditions should be paid attention to momentarily, so as to stop the construction and return.

Table 29.4 Measured data

Third indexes	Velocity	Water depth	Wave	Wind	Visibility	Ice
Case (I)	2.5knots	load draught + 0.6 m	2.2 m	12 m/s	20 km	0.11 m
Third indexes	*Channel width*	*Channel depth*	*Channel bending radius*	*Navigable ship density*	*Cross area*	*Obstruction*
Case (I)	2 times of ship length	load draught + 0.6 m	3.5times of ship length	0.5	1	5%
Third indexes	*Velocity*	*Water depth*	*Wave*	*Wind*	*Visibility*	*Ice*
Case (II)	3.5knots	load draught + 1.4 m	2.3 m	15 m/s	2.5 km	0.1 m
Third indexes	*Channel width*	*Channel depth*	*Channel bending radius*	*Navigable ship density*	*Cross area*	*Obstruction*
Case (II)	2 times of ship length	load draught + 1.2 m	3.5times of ship length	0.5	1	10%
Third indexes	*Velocity*	*Water depth*	*Wave*	*Wind*	*Visibility*	*Ice*
Case (III)	4.9knots	load draught + 0.7 m	2.4 m	16.9 m/s	1 km	0.13 m
Third indexes	*Channel width*	*Channel depth*	*Channel bending radius*	*Navigable ship density*	*Cross area*	*Obstruction*
Case (III)	2 times of ship length	load draught + 1.1 m	3.8times of ship length	0.5	2	28%

Table 29.5 The risk evaluation grade results

Risk assessment grade	High risk	General risk	Low risk
Case (I)	0.1258	0.7037	0.1705
Case (II)	0.1673	0.7197	0.113
Case (III)	0.5678	0.3885	0.0437

29.5 Conclusions

Aiming at the construction safety risk problem of engineering construction in navigable waters, a comprehensive construction safety risk evaluation model coupling with diverse factors is established based on fuzzy comprehensive evaluation method,

and the application demonstration of major engineering is successfully carried out. The main conclusions are as follows:

A multilevel safety risk index system is established according to mutual influence and subordinate relationship among risk factors integrating suggestions of industry standards and construction experience based on the risk factor of typical water construction safety accidents.

The factor weight and the quantitative standard of risk classification are acquired from the integration of objective evaluation mechanisms such as industry norms and subjective evaluation mechanisms such as expert suggestions, which provides an important basis for risk assessment and risk early warning.

The comprehensive construction safety risk evaluation model coupling multiple factors for risk assessment of the construction environment in navigable waters has been established and successfully applied to the Hengsha Dongtan silt promotion ring engineering. The results show that the risk evaluation model has certain practical value and application prospect.

References

Akyildiz H, Mentes A (2017) An integrated risk assessment based on uncertainty analysis for cargo vessel safety. Saf Sci 92:34–43

Chunhui Z, Hongxun H, Shangding G, Run C, Yuanqiao W, Langxiong G (2020) Design and implementation of virtual warning buoy system for over-water construction. Navig China 43(1):62–66

Elmer F, Seifert-Dähmn I, Kreibich H, Thieken A (2009) A Delphi method expert survey to derive standards for flood damage data collection. Risk Anal 30(1):107–124

Fang Q (2019a) Research on ship navigation risk evaluation during construction period of waterway regulation project. Dalian Maritime University, Master's thesis

Fang L (2019b) Analysis of navigation hindrance of dredging construction in the inland waterway and discussion on precautions. China Water Transp 19(3):105–106

Hui X, Nan X, Zhenbang G, Jinying W (2005) Quantitative analysis of submarine pipeline routing risk based on AHP and grey-mode identification theory. Ocean Eng 23(4):105–110

Jinngmin Z, Weitao Y, Jianzeng H, Fan Y (2003) Methods for assessing safety in offshore construction of port works and their application. China Harb Eng 2:50–53

Jun H, Jie C, Zheng C, Junxing C, Quanfeng W, Libo Z, Hui Z, Bin X, Guodong C (2018) Risk assessment of seismic hazards in hydraulic fracturing areas based on fuzzy comprehensive evaluation and AHP method (FAHP): a case analysis of Shangluo area in Yibin City, Sichuan Province, China. J Pet Sci Eng 170:797–812

Lei W, Qing L, Shiyu D, Guedes S (2019) Effectiveness assessment of ship navigation safety countermeasures using fuzzy cognitive maps. Saf Sci 117:352–364

Marie M, Andrea Č (2017) The identification of crisis manager skills by using Saaty's method. Financ Environ Bus Dev 4:341–367

Nuwen X, Li T, Feng D (2013) Construction safety control and management on extra-large underwater caisson in Taizhou Bridge. Appl Mech Mater 361–363:1124–1128

Wei H, Zaiqiang Y, Lidong H, Chenxi S, Xiaojuan Y, Mengfan Z (2019) Fuzzy comprehensive evaluation of the effects of relative air humidity on the morpho-physiological traits of Pakchoi (Brassica chinensis L.) under high temperature. Sci Hortic 246:971–978

Weimin C, Shuxi D, Lirong W, Yanquan J, Wenqi Z (2009) Safety evaluation of over-sea construction based on the fuzzy-neural networks. J Saf Environ 5:170–174

Xuejun W, Zhimin Z (2012) Research on security-risk assessment system of coastal caisson wharf construction. J Chongqing Jiaotong Univ (Nat Sci) 31(4):885
Zhibao Z, Changfei M, Bo W, Guoqiang J (2017) Safety risk evaluation of construction of Pingtan straits rail-cum-road bridge. Bridg Constr 47(1):12–16

Chapter 30
Distribution Characteristics of Plastic Particles in Coastal and Beach of Hsinchu, Taiwan

Ying-Fang Hsu, Feng-Hsin Chang, Pei-Yi Feng, Hsiao-Chien Huang, Chi-Yu Chuang, Shinhao Yang, and Wei-Ting Liu

Abstract To know the situation of plastic particle concentration and distribution in Taiwan western costal, this study selects the sea area in Hsinchu County to conduct an analysis. Therefore, samples were taken in the beaches, beach junction sea area, estuaries and lower reaches of the river from Hsinchu County. And the thermal contact meth (NIEA M909.00C) for the detection of microplastics in water announced by Environmental Analysis Laboratory, Environmental Protection Administration, Executive Yuan is selected to investigate the concentration of plastic particles. At the same time, type of plastic particles under the microscope was recorded to further analyze the possible causes and sources of those plastic particles. The analysis results show that in terms of the distribution of plastic particles, the concentration of plastic particles on the beach is 25.3–53.3 items/kg; the concentration of plastic particles in the sea area is 1.6–8.0 items/L; the concentration of plastic particles in the estuaries and lower reaches of the river is 2.3–3.6 items/L. At each sampling location, the plastic particles are mainly long strips, and a few are round and flakes. The elongated plastic particles are mainly derived from discarded fishing nets or waste clothing; the main source of round plastic particles is cleaning agents; and the flake plastic particles are generated by plastic degradation. On the whole, the smallest appearance of plastic particles is round or spherical, which means that the occurrence rate of microbeads in the water bodies of Hsinchu County is low. It shows that the government has achieved remarkable results after banning the use of microbeads.

Keywords Plastic particles · Marine environment · Sustainable coast

Y.-F. Hsu · F.-H. Chang · P.-Y. Feng · H.-C. Huang · S. Yang (✉) · W.-T. Liu
Environmental Sustainability Lab, CTBC Business School, Center for General Education, Tainan, Taiwan, Republic of China
e-mail: shinhaoyang@ntu.edu.tw

C.-Y. Chuang
Department of Occupational Safety and Health, Chang Jung Christian University, Tainan, Taiwan, Republic of China

H.-Y. Jeon (ed.), *Sustainable Development of Water and Environment*,
Environmental Science and Engineering,
https://doi.org/10.1007/978-3-030-75278-1_30

30.1 Introduction

Microplastics refer to lumps, filaments, or spherical plastic particles with a diameter or length of less than 5 mm (Lusher 2015; Lusher et al. 2013). Compared with the immediate and direct impact of large and small plastic waste on marine organisms, microplastics are easily eaten by various marine organisms, causing different levels of impact on invertebrates to fish (Lusher et al. 2013).

Marine organisms may ingest microplastics in different ways. For example, organisms such as mussels, oysters, or sponges are filter feeders; fish or crabs eat by mouth. The basic consumer of filter feeders is not selective when filtering food, so they cannot distinguish microplastics. Other fish species that selective foraging will ingest microplastics by swallowing contaminated prey. According to the study, many kinds of plankton have been found in the body of plastic particles. These organisms at the bottom of the food chain are more likely to contact and eat plastic particles in the ocean due to their large number and small size (Cole et al. 2013). Plastic particles may be transferred to higher-order species due to the food chain; for example, fish, birds, marine or terrestrial mammals (do Sul et al. 2013). The organisms in the ocean include all kinds of plankton to fish at different growth stages (from juvenile to adult), have a record of ingested plastic particles. It can be seen that the micro-effects of plastic are quite extensive, and different trophic levels in the food chain may be ingested microplastic.

Marine organisms may ingest microplastics in different ways. Marine organisms may ingest microplastics in different ways. Moser and Lee (1992) surveyed 1,033 seabirds on the coast of North Carolina, and found that 55% of them accidentally ingested plastic pellets, and confirmed that some seabirds would choose plastic of specific shapes and colors, mistakenly believing them to be their prey (Moser and Lee 1992). Ryan (1988) used poultry as an experiment and used plastic pellets to understand the potential impact on seabirds (Ryan 1988). Finally, he found that when eating too many plastic pellets, their health would be harmed. Plastic pellets will reduce the food storage space in poultry's stomachs, reduce their appetite, and limit the ability of fat synthesis. Furthermore, if plastic particles further replace interconnection. It will also affect its normal physiological functions and eventually lead to death. Marine mammals are also hazarded. Tarpley and Marwitz (1993) found a dwarf sperm whale in the State of Texas, USA (Tarpley and Marwitz 1993). Its first two stomachs were filled with plastic waste. Also, toxic substances can enter the body due to eaten by mistake, causing death or loss of reproductive function (Moore et al. 2002), such as polychlorinated biphenyls (PCBs). In addition, studies have pointed out that because of the large overall surface area of microplastics, it is easy to adsorb toxic substances in seawater.

Besides, studies have pointed out that because of the large total surface area of microplastics, it is easy to adsorb toxic substances in seawater. Also, the plastic pellet is lipophilic and has a high affinity for persistent organic pollutants (POPs). Studies have found that the concentration of POP in plastic particles is one million times that of seawater (Le et al. 2016).

There is little research on marine plastic particles in Taiwan. Therefore, this study intends to survey the plastic particles on the sea area and beaches of Taiwan. The location is off the coast of Hsinchu, Taiwan.

30.2 Experimental Methods

30.2.1 Sampling Sites

In this study, plastic particles were collected in at least 20 locations in the sea, beaches, estuaries, or lower reaches of the river in Hsinchu County.

The following is a demonstration of sampling locations. Figure 30.1 shows the sampling points.

I. Beach and beach junction sea area

The selection is mainly based on the location of beach with artificial activities and the north and south shores of Xinfeng burial site. The following locations are the beach and the beach junction sea area where sampling is performed: Potou Fishing Port, Xinyue Beach, Xinfeng Mangrove Reserve, abandoned Fengkeng Fishing Port, and the north and south shores of Xinfeng Landfill.

II. Sea area

Discarded fishing nets are often found in artificial reef areas. Therefore, in order to find out whether the discarded fishing nets are the source of plastic particles in the sea area, the artificial reef area along the coast of Hsinchu County was investigated for the concentration of plastic particles in the sea area.

III. Estuaries and lower reaches of the river

This study has understood the possible sources of plastic particles in the sea, so the investigation of plastic particles at the estuary of Xinfeng River and its downstream is conducted.

30.2.2 The Thermal Contact Meth

Considering that the investigation of the concentration of plastic particles, and the executive team's desire to judge types of plastic particles from a morphological point of view, the thermal contact meth (NIEA M909.00C) for the detection of microplastics in water announced by Environmental Analysis Laboratory, Environmental Protection Administration, Executive Yuan in January 2020 is selected to conduct a survey of plastic particles.

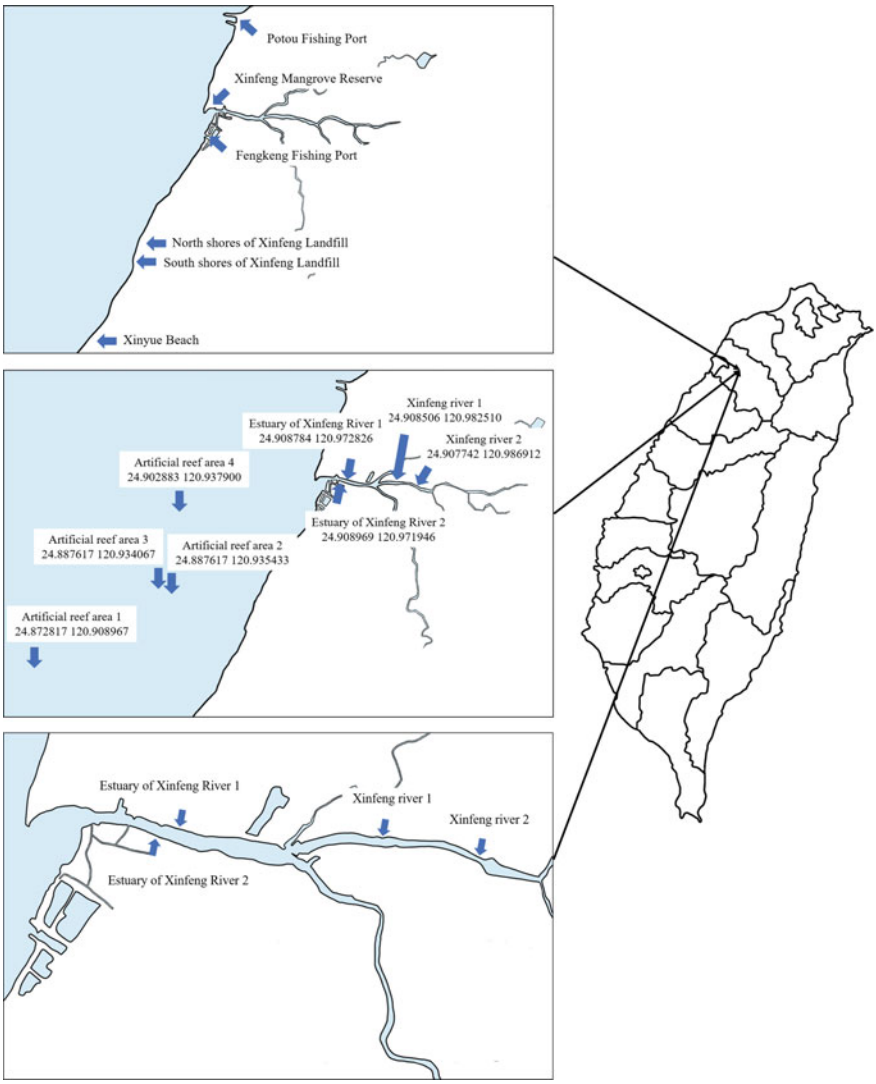

Fig. 30.1 Sampling locations

30.3 Results and Discussions

30.3.1 Analysis Results

Before conducted the analysis of the investigation of microplastic in the sea area, the study team tested the deionized water used in the project to detect plastic particles. After three times repeated experiments. The results showed that no plastic particles

were detected, indicating that the deionized water used in the analysis did not contain any plastic particles that would affect the subsequent experiments. The following is the characteristics of the plastic particle concentration and distribution.

I. Sea area

Table 30.1 is the consequence of plastic particle concentration analysis and the types of plastic particles in the sea area. Judging from the average number of three water samples, the concentration of plastic particles ranges from 1.6 to 8.0 items/L, and the average of 10 points is 3.68 ± 2.08. According to the survey report on plastic particles in the coastland of Taiwan from the Kuroshio Ocean Education Foundation (2018), the result of sampling at 17 places in the western sea area showed that the concentration of plastic particles was 4.00 ± 3.64 items/L. Compared with the results of this study, the two data are similar. The types of plastic particles are mainly long strip (especially in the artificial reef area), followed by round shapes and flakes.

II. Beach

Table 30.2 shows the analysis data of the concentration and the types of plastic particle on the beaches. Judging from the average number of three times beach

Table 30.1 Result of plastic particle concentration and shape types in the sea area

Location	Average concentration of Plastic particles (items/L)	Long strip shape	Round shape	Flake shape
Xinyue Beach	2.0	5	0	1
North shores of Xinfeng Landfill	6.3	5	4	10
South shores of Xinfeng Landfill	4.0	6	2	1
Fengkeng Fishing Port	3.0	1	4	4
Xinfeng Mangrove Reserve	3.0	3	2	4
Potou Fishing Port	1.6	2	2	1
Artificial reef area 1	8.0	17	4	3
Artificial reef area 2	4.3	11	0	2
Artificial reef area 3	3.0	8	1	3
Artificial reef area 4	1.6	2	2	1
Average	3.68±2.08			

Table 30.2 Result of plastic particle concentration and shape types on the beaches

Location	Average concentration of Plastic particles (items/kg)	Long strip shape	Round shape	Flake shape
Xinyue Beach	23.3	5	1	1
North shores of Xinfeng Landfill	53.3	14	1	1
South shores of Xinfeng Landfill	46.6	12	1	1
Fengkeng Fishing Port	40	12	0	0
Xinfeng Mangrove Reserve	50	14	0	1
Potou Fishing Port	43.3	10	1	2

gravel sampling and analysis, the concentration of plastic particles is between 23.3 and 53.3 items/kg. In the aspect of the types of plastic particles, they are mainly long strip plastic particles, and a few of them are flakes and round shapes.

III. Estuaries and lower reaches of the river

Table 30.3 shows the analysis data of the concentration and the types of plastic particles at the estuary of the river and the downstream of the river. From the average number of three water samples, the concentration of plastic particles is between 2.3 and 3.6 items/L. The types of plastic particles are mainly long strip plastic particles, and a few of them are flakes and round shapes.

Table 30.3 Result of plastic particle concentration and shape types at the estuary and lower reaches of the river

Location	Average concentration of Plastic particles (items/L)	Long strip shape	Round shape	Flake shape
Estuary of Xinfeng River 1	3.6	6	2	3
Estuary of Xinfeng River 1	2.6	7	0	1
Xinfeng River 1	2.3	5	1	1
Xinfeng River 2	2.3	5	0	2

30.3.2 Cause Analysis

In addition to understanding the concentration distribution of marine plastic particles in Hsinchu County, this study also explored the source of plastic particles. Therefore, this study records the plastic particles while analyzing the samples to confirm whether they are plastic particles. Then compare with the types of plastic particles mentioned in the literature, and analyze the possible causes and sources of plastic particles.

I. Literature related to plastic particles

Seawater sediment and plastic particles in the beach is very similar, mainly fibers, fragments (spheres and irregularities), and films. Among them, two-thirds of the particles are fibers, one-fifth of microplastic fragments, and one-tenth are plastic films, of which fibers are the most abundant (Desforges et al. 2014).

Fiber sources are diverse, including clothes, fishing nets, household washing sewage, etc. (De Falco et al. 2018). Every washing will produce ultra-fine plastic debris fibers. These fibers will go to the sewage treatment plant with the waste water, but because of their small size, they may eventually flow into the ocean through rivers and pollute the ecology. Some studies have identified microplastics in sewage effluents (Mintenig et al. 2017), which remain on beaches by waves beating.

Fragmented plastic particles are mainly degradation products of larger waste plastic products (Barnes et al. 2009). These plastic fragments mainly come from packaging materials. In addition, there are thousands of plastic particles per square kilometer, and most of these degraded plastic particles are irregular (Derraik 2002; Andrady 2003). In addition, small plastic fragments (usually no more than 0.5 mm) derived from hand cleansers, cosmetics and sprayed cleansers, most of the plastic particles in the personal care products are irregular shapes (Cheung and Fok 2017).

In cleaning preparations, polyethylene and polystyrene detergent particles were identified separately (Gregory 1996). Once discarded, they enter the sewage sanitation system. Although some of them may be filtered in the sewage treatment process, most of them are discharged into sea water.

Microbeads are a type of solid plastic particles with a diameter of less than 1 mm made through industrial production (Arthur et al. 2008). These particles are usually made of polyethylene, but some are also made of materials such as polypropylene and polystyrene. Such plastic particles have been observed in various water bodies.

Film plastic particles mainly include PE and PP types. When viewed under a microscope, samples made of PE have a certain degree of elasticity; while microplastics derived from PP are mainly derived from food packaging and are very brittle (Zhang et al. 2017).

Agricultural pollution is the main source of film plastic particles. In 2016, the global agricultural plastic film market was 4 million tons, and it is expected to grow at an annual rate of 5.6% by 2030 (Von Moos et al. 2012). Removal of these plastic mulches from fields is laborious and time-consuming, so plastic films or parts of them are often left in agricultural soil, intentionally or unintentionally, where they become brittle and decompose into micron-sized particles (Astner et al. 2019). However,

through the movement of irrigation water in agriculture, these plastic particles will eventually be discharged into the sea.

30.4 Summary

From the overall research results, the smallest appearance of plastic particles is round or spherical, which means that the occurrence rate of microbeads in the water of Hsinchu County is low. It shows that the government has achieved remarkable results after banning the use of microbeads. Taiwan imports 12 million metric tons of plastic raw materials each year, which is higher than that of other countries. In order to reduce the pollution of marine plastic particles, Taiwan has established a marine waste management platform to formulate strategies from four aspects: reduction at the source, prevention and removal, research and investigation, and expansion of cooperation. These strategies mainly include restricting the use of single-use plastic products and preventing Such practices as garbage entering the ocean, research and investigation, and environmental education.

Acknowledgements The authors would like to thank the HsinChu County Environmental Protection Bureau for financially supporting this research.

References

Andrady AL (2003) Plastics and the environment. Wiley

Arthur C, Baker J, Bamford H, Barnea N, Lohmann R, McElwee Kris, Morishige C, Thompson R (2008) Summary of the international research workshop on the occurrence, effects, and fate of microplastic marine debris. In: Proceedings of the international research workshop on the occurrence, effects, and fate of microplastic marine debris, 9–11 September 2008, University of Washington Tacoma, Tacoma, WA, USA, pp. 7–17

Astner AF, Hayes DG, O'Neill H, Evans BR, Pingali SV, Urban VS, Young TM (2019) Mechanical formation of micro-and nano-plastic materials for environmental studies in agricultural ecosystems. Sci Total Environ 685:1097–1106

Barnes DK, Galgani F, Thompson RC, Barlaz M (2009) Accumulation and fragmentation of plastic debris in global environments. Philos Trans R Soc Lond B Biol Sci 364(1526):1985–1998

Cheung PK, Fok L (2017) Characterisation of plastic microbeads in facial scrubs and their estimated emissions in Mainland China. Water Res 122:53–61

Cole M, Lindeque P, Fileman E, Halsband C, Goodhead R, Moger J, Galloway TS (2013) Microplastic ingestion by zooplankton. Environ Sci Technol 47(12):6646–6655

De Falco F, Gullo MP, Gentile G, Di Pace E, Cocca M, Gelabert L, Brouta-Agnésa M, Rovira A, Escudero R, Villalba R, Mossotti R, Montarsolo A, Gavignanoc S, Toninc C, Avellaa M (2018) Evaluation of microplastic release caused by textile washing processes of synthetic fabrics. Environ Pollut 236:916–925

Derraik JG (2002) The pollution of the marine environment by plastic debris: a review. Mar Pollut Bull 44(9):842–852

Desforges JPW, Galbraith M, Dangerfield N, Ross PS (2014) Widespread distribution of microplastics in subsurface seawater in the NE Pacific Ocean. Mar Pollut Bull 79(1–2):94–99
do Sul JAI, Costa MF, Barletta M, Cysneiros FJA (2013) Pelagic microplastics around an archipelago of the Equatorial Atlantic. Mar Pollut Bull 75(1–2):305–309
Gregory MR (1996) Plastic 'scrubbers' in hand cleansers: a further (and minor) source for marine pollution identified. Mar Pollut Bull 32(12):867–871
Le DQ, Takada H, Yamashita R, Mizukawa K, Hosoda J, Tuyet DA (2016) Temporal and spatial changes in persistent organic pollutants in Vietnamese coastal waters detected from plastic resin pellets. Mar Pollut Bull 109(1):320–324
Lusher A (2015) Microplastics in the marine environment: distribution, interactions and effects. In: Marine Anthropogenic Litter. Springer, Cham, pp 245–307
Lusher AL, Mchugh M, Thompson RC (2013) Occurrence of microplastics in the gastrointestinal tract of pelagic and demersal fish from the English Channel. Mar Pollut Bull 67(1–2):94–99
Mintenig SM, Int-Veen I, Löder MG, Primpke S, Gerdts G (2017) Identification of microplastic in effluents of waste water treatment plants using focal plane array-based micro-Fourier-transform infrared imaging. Water Res 108:365–372
Moore CJ, Moore SL, Weisberg SB, Lattin GL, Zellers AF (2002) A comparison of neustonic plastic and zooplankton abundance in southern California's coastal waters. Mar Pollut Bull 44(10):1035–1038
Moser ML, Lee DS (1992) A fourteen-year survey of plastic ingestion by western North Atlantic seabirds. Colon Waterbirds 83–94
Ryan PG (1988) Effects of ingested plastic on seabird feeding: evidence from chickens. Mar Pollut Bull 19(3):125–128
Tarpley RJ, Marwitz S (1993) Plastic debris ingestion by cetaceans along the Texas coast: two case reports. Aquat Mamm 19(2):93–98
Von Moos N, Burkhardt-Holm P, Köhler A (2012) Uptake and effects of microplastics on cells and tissue of the blue mussel Mytilus edulis L. after an experimental exposure. Environ Sci Technol 46(20):11327–11335
Zhang W, Zhang S, Wang J, Wang Y, Mu J, Wang P, Lin X, Ma D (2017) Microplastic pollution in the surface waters of the Bohai Sea, China. Environ Pollut 231:541–548